UNIVERSITÉ DE STRASBOURG

Ecole doctorale des Sciences de la Vie et de la Santé

Thèse présentée par :

Jiahao Ye
soutenue le 08 fév 2018

Pour obtenir le grade de : Docteur de l'Université de Strasbourg, Freiburg, Basel

Spécialité: Neurosciences

Etude anatomique de l'amygdale étendue centrale chez la souris : Connectivité générale et circuits cellule-spécifiques ; implications fonctionnelles dans la douleur.

(A study of mouse central extended amygdala: general connectivity and cell-type specific circuits; functional implications in pain)

Thèse dirigée par :

M. Pierre Veinante	Professeur à l'Université de Strasbourg, CNRS UPR 3212
M. Lutz Hein	Professeur à Albert Ludwig University of Freiburg Allemagne
M. Andreas Lüthi	Professeur à University of Basel, Suisse

RAPPORTEURS externe :

M. François Georges	Chargé de recherche – CNRS UMR 5293, Bordeaux
M. Cyril Herry	Directeur de recherche – CNRS UMR5293, Bordeaux

EXAMINATEUR interne :

Mme Anne. PEREIRA DE VASCONCELOS	Chargé de recherche – LNCA, Strasbourg

Jiahao Ye

Etude anatomique de l'amygdale étendue centrale chez la souris : Connectivité générale et circuits cellule-spécifiques ; implications fonctionnelles dans la douleur.

Résumé

L'amygdale centrale (EAc) est un macrosystème du cerveau antérieur qui joue un rôle important dans la peur, l'anxiété et la douleur. Les deux composants clés, le noyau latéral du lit de la strie terminale (STL) et l'amygdale centrale (CeA), possèdent des caractéristiques neurochimiques, hodologiques et fonctionnelles très similaires. En dépit de cette vision simplifiée du STL et du CeA, de nombreuses questions résident quant à l'organisation mésoscopiques des entrées et des sorties des subdivisions de l''EAc chez la souris. En outre, il reste à déterminer si ces similitudes de connexion sont également partagées au niveau cellulaire. Dans ce travail, nous avons abordé ces questions de manière comparative chez la souris. Nous avons trouvé de richesafférences et efférences préférentielles pour les différentes subdivisions de l'EAC, ainsi que des afférences convergentes et divergentes. Nous avons également mise en évidence deux groupes distincts de cellules exprimant la protéine kinase C delta (PKCδ) ou la somatostatine (SOM) qui sous-tendent des circuits neuronaux spécifiques parallèles dans le STL et le CeA, ainsi qu'entre les deux structures. Enfin, des données préliminaires suggèrent que les neurones exprimant la PKCδ dans le STL et le CeA pourraient être impliqués dans la douleur tonique. Ces organisations structurales parallèles, mais aussi différentielles, des circuits neuronaux dans le EAc pourraient sous-tendre des aspects fonctionnels similaires et dissociables de l'anxiété, de la peur et de la douleur.

Mots-clés :

Amygdale étendue centrale, noyau central de l'amygdale, Noyau du lit de la strie terminale, neurocircuits,

Abstract

Central extended amygdala (EAc) is a forebrain macrosystem that plays important roles in fear, anxiety and pain. The two key components, the lateral bed nucleus of stria terminalis (STL) and central nucleus of amygdala (CeA), are highly similar in their neurochemical, connectional, and functional features. Despite this simplified view of STL and CeA, much remains elusive of the mesoscopic inputs and outputs of EAc subdivisions in mouse model. Also, it is not known whether the connectional similarities are also shared at cellular level. Here, we addressed these question in comparative ways in mice. We found rich preferential inputs and outputs to different subdivisions of EAc, as well as convergent and divergent inputs. We also found two non-overlapping cell groups expressing either protein kinase C delta (PKCδ) or somatostatin (SOM) organize the parallel cell-type specific neuronal circuits in STL and CeA. Finally, preliminary data suggest that PKCδ in STL and CeA might be implicated in tonic pain. These parallel but also differential structural organizations of neuronal circuits in EAc might underlie similar and dissociable functional aspects of anxiety, fear and pain.

Key words:

central extended amygdala, central nucleus of the amygdala, bed nucleus of the stria terminalis, neurocircuit, protein kinase C delta, somatostatin

UNIVERSITE DE STRASBOURG

RESUME DE LA THESE DE DOCTORAT

Discipline :Sciences de la vie et de la santé

Spécialité : Neurosciences

Présentée par : YE Jiahao

Titre : Etude anatomique de l'amygdale étendue centrale chez la souris : Connectivité générale et circuits cellule-spécifiques ; implications fonctionnelles dans la douleur

Unité de Recherche : CNRS UPR3212, Institut des Neurosciences Cellulaires et Intégratives

Directeur de Thèse : VEINANTE Pierre, professeur

Co-Directeurs de Thèse (s'il y a lieu) : LUTHI Andeas, professeur ; HEIN Lütz, professeur

Localisation : 5 rue Blaise Pascal, 67000 Strasbourg

ECOLES DOCTORALES :

☐ ED - Sciences de l'Homme et des sociétés ☐ ED 99 – Humanités ☐ ED 101 – Droit, sciences politique et histoire ☐ ED 182 – Physique et chimie physique ☐ ED 221 – Augustin Cournot ☐ ED 222 - Sciences chimiques	☐ ED 269 - Mathématiques, sciences de l'information et de l'ingénieur ☐ ED 270 – Théologie et sciences religieuses ☐ ED 413 – Sciences de la terre, de l'univers et de l'environnement ☒ ED 414 – Sciences de la vie et de la santé

Résumé de thèse

Introduction

L'amygdale étendue centrale (EAc) est un macrosystème anatomofonctionnel du cerveau antérieur. Chez les rongeurs, comme chez les primates, elle forme un continuum de structures s'étendant de l'amygdale centrale, caudalement, au noyau du lit de la strie terminale (ST), rostralement (Alheid, 2003). L'EAc est impliquée dans les émotions, telles que la peur et l'anxiété, dans la douleur, la prise de nourriture, la motivation, l'addiction. Au sein de l'EAc, de nombreuses similitudes anatomiques, neurochimiques et fonctionnelles existent entre ses deux composantes principales, le ST latéral (STL) et le noyau central de l'amygdale (CeA) (Alheid 2003). Par exemple, les neurones principaux des deux noyaux sont GABAergiques, tout en coexprimant une grande variété de neuropeptides tels que les peptides opioïdes (enképhalines, dynorphines, endorphines), la somatostatine (SOM) ou le facteur de libération corticotrope (CRF) (Veinante et al. 2013). En terme de connectivité, le STL et le CeA reçoivent des afférences de, et envoient des efférences dans les mêmes structures cérébrales, en particulier le cortex insulaire, l'hypothalamus latéral, la substance grise périaqueducale (PAG) et le noyau parabrachial. Il existe de plus de très nombreuses connexions intrinsèques à l'EAc. Ces similitudes anatomofonctionnelles sont particulièrement flagrantes quand les subdivisions de ces noyaux sont comparées deux à deux. Ainsi la partie latérale et capsulaire du CeA (CeL/C) et la partie dorsale du STL (STLD) ont des caractéristiques très semblables, mais différent de la paire constituée de la partie médiane du CeA (CeM) et de la partie ventrale du STL (STLV). Fonctionnellement, le CeA et le STL participent aux réponses de peur et d'anxiété (De Bundel et al., 2016, Shackman et Fox 2016), et aux divers aspects de la douleur (Veinante et al., 2013).

Malgré ces notions simplifiées suggérant une homogénéité dans l'organisation mésoscopique de l'EAc, de nombreuses questions restent posées concernant les circuits neuronaux locaux et à longue distance. Plusieurs indices suggèrent des contributions fonctionnelles différentes de populations neuronales hétérogènes dans l'EAc. Par exemple, des approches pharmacologiques ou lésionnelles, ciblées sur des subdivisions précises de l'EAc, indiquent chez le rat des rôles différentiels du CeA et du STL dans les comportements de peur et d'anxiété, respectivement, éventuellement par une signalisation CRF spécifique (Walker et Davis, 2008). Par ailleurs, les manipulations optogénétiques cellule-spécifiques dans le CeA de la souris ont révélé les rôles critiques et opposés des neurones exprimant la protéine kinase C delta (PKCδ) et de ceux exprimant somatostatine (SOM), lors du conditionnement de peur

(Haubensak et al., 2010; Li et al., 2013). Enfin, l'activation du CeL/C module également les aspects sensoriels et affectifs de la douleur, en particulier lorsqu'elle est prolongée (Neugebauer et al., 2004), alors que le STL semble être impliqué surtout dans l'aspect affectif (Veinante et al., 2013). Pourtant, les travaux publiés à ce jour sur l'EAc n'ont que très rarement intégré les données relatives à la peur à celles concernant la douleur. Ainsi, notre compréhension de l'organisation et des rôles respectifs des différentes subdivisions de l'EAc reste largement incomplète, en particulier du fait de l'utilisation non complémentaire de rats et de souris, et d'études ne ciblant qu'une structure de l'EAc, dans une seule situation. Compte tenu des applications étendues des outils transgéniques et optogénétiques, une meilleure compréhension des connectivités spécifiques aux cellules dans les subdivisions de l'EAc semble plus urgente et nécessaire. Nous proposons l'hypothèse que le STL possède des circuits cellule-spécifiques et des projections longues qui peuvent être semblables à ceux du CeA, mais aussi distinctifs, ce qui sous-tendrait des fonctions proches mais pas complètement identiques.

Projet

Dans ce projet de doctorat, nous avons donc privilégié l'approche neuroanatomique pour identifier les substrats connectomiques et neurochimiques sous-tendant les rôles respectifs des subdivisions de l'EAc dans les émotions et la douleur. Les travaux ont été menés en utilisant des souris males C57BL6/J. Nous avons, dans un premier temps, examiné systématiquement la connectivité générale des principales subdivisions de l'EAc en caractérisant les entrées et les sorties avec des traceurs rétrogrades (c'est-à-dire fluorogold et sous-unité β de la toxine du choléra) et tracteurs antérogrades (c'est-à-dire la dextran amine biotinylé et la leucoagglutinine de *Phaseolus vulgaris*). Ceci a permis de comparer les subdivisions du CeA à celles du STL. Puis nous nous sommes concentrés sur la connectivité des neurones exprimant la PKCδ (PKCδ+) et de ceux exprimant la SOM (SOM+). En effet, ces populations neuronales sont spécifiquement présentes dans le CeL/C et le STLD (Lein et al., 2007; Haubensak et al., 2010) ; elles forment dans le CeA des circuits inhibiteurs locaux spécifiques (Haubensak et al., 2010; Li et al., 2013) et sont à l'origine des projections longues (Cai et al., 2014). Cependant, il n'existe aucune information sur les connexions de ces populations dans STL. Ainsi, nous avons combiné les expériences de traçage à la révélation par immunofluorescence de marques cellulaires pour disséquer les similitudes structurelles et les dissemblances des connexions du CeA et du STL.

Résultats

L'analyse du connectome général du STL et du CeA montre, comme attendu de nombreuses similitudes qualitatives, mais aussi des différences. Dans le cas des afférences, le STLD et le CeL/C sont fortement innervés par les cortex insulaire et entorhinal, des noyaux thalamiques (paraventriculaire en particulier), l'amygdale basolatérale (en particulier les noyaux basolatéral et basomédian), la zone de transition amygdalopiriforme, les régions hippocampiques ventrales (subiculum ventral) et le noyau parabrachial latéral. Des entrées plus modérées sont issues de l'hypothalamus latéral, l'aire tegmentale ventrale, la PAG ventrolatérale, le raphé dorsal et le noyau du tractus solitaire. Sur le plan quantitatif, il existe des différences puisque certaines structures innervent préférentiellement le CeL/C ou le STLD. Malgré les zones d'entrée partagées, le STLD et le CeL/C ne partagent qu'une proportion mineure à modérée de neurones de projection du cortex insulaire, du noyau paraventriculaire thalamique te du noyau parabrachial .Nous avons également identifié de nouvelles contributions du cortex préfrontal médian au STLD qui n'avaient pas été signalées chez le rat. Nous avons également observé des entrées similaires du cortex préfrontal, du thalamus, des noyaux amygdaloïdes et du noyau parabrachial au STL ventral (STLV) et au CeM, mais avec des innervations du cortex insulaire plus faibles vers le STLV et plus denses vers le CeM. Pour les efférences, le STLD et CeL/C projettent fortement au STLV, au CeM et à la région sublenticulaire de l'EAc, à l'hypothalamus latéral, la formation réticulée (mésencéphalique, pontique et bulbaire), le noyau parabrachial (latéral et médian) et le noyau du tractus solitaire Ils projettent également modérément au noyau accumbens et à la PAG latérale. Le CeL/C projette plus fortement que le STLD au noyau du tractus solitaire. Enfin, la projection du CeL/C vers le STLD est plus forte que dans l'autre direction.

En combinant des révélations histochimiques multiples, noua avons abordé la connectivité spécifique aux populations PKCδ+ et SOM+. Pour les entrées spécifiques au type cellulaire, nous avons observé que les terminaisons issues du noyau parabrachial, contenant le neuropeptide CGRP, ciblent principalement les neurones PKCδ+, mais peu les neurones SOM+, dans le STLD et le CeL/C dans une proportion similaire. De plus, les entrées sensorielles du cortex insulaire et les entrées polymodales de l'amygdale basolatérale peuvent converger vers des neurones PKCδ+ contactés par des terminaisons CGRP+. Dans le cas des connexions intra-EAc, nous avons observé que les projections du STLD et du CeL/C vers le STLV et le CeM étaient principalement médiées par les neurones PKCδ+, tandis qu'à la fois les neurones PKCδ+ et les neurones SOM+ peuvent être à l'origine des interconnexions STLD-CeL/C. Finalement, Les projections longues du STLD et du CeL/C vers des cibles

extra-EAc (noyau parabrachial, PAG...) reposent quant à elles essentiellement sur les neurones SOM+.

Conclusions

Nous avons caractérisé la connectivité générale STLD et CeL/C chez la souris. En effet, si ce connectome avait été décrit chez le rat, il n'avait jamais été analysé systématiquement chez la souris. De façon attendue, nous trouvons des résultats globalement similaires à ceux obtenus chez les rats, mais nous avons également noté une connectivité spécifique à la souris, en particulier sur le plan quantitatif.

Nous avons révélé une connectivité spécifique aux cellules du STLD et du CeL/C. De façon importante, les connexions spécifiques des deux-sous-populations neurochimiquement définies sont qualitativement identiques dans les deux noyaux. Nous avons montré que les entrées corticales et du tronc cérébral (véhiculant des informations nociceptives et intéroceptives convergent vers les neurones PKCδ+ du STLD et du CeL/C qui projettent vers les noyaux de sortie de l'EAc (STLV et CeM), tandis que les neurones SOM+ médient l'essentiel ces projections à longue distance vers des cibles à l'extérieur de l'EAc. En revanche, les deux sous-populations sont impliquées dans le dialogue entre le STLD et le CeL/C.

Ces résultats fournissent une vision détaillée des circuits neuronaux parallèles dans l'EAc. Ils montrent que l'essentiel de la structure des microcircuits du CeA se retrouve dans les microcircuits du STL, au moins sur le plan qualitatif. En revanche, il existe des différences subtiles dans les connexions extrinsèques de ces noyaux, ainsi qu'une asymétrie de leur interconnexion qui favorise la voie CeA-STL *vs* STL-CeA.

L'ensemble de ces résultats suggère que le STL et le CeA peuvent avoir des fonctions complémentaires dans les émotions et la douleur, basés sur les rôles complémentaires des neurones PKCδ+ et des neurones SOM+ dans le STL comme dans le CeA.

Références

Alheid GF (2003) Extended amygdala and basal forebrain. Ann N Y Acad Sci 985:185-205

Cai H, Haubensak W, Anthony TE, Anderson DJ (2014) Central amygdala PKC-delta(+) neurons mediate the influence of multiple anorexigenic signals. Nat Neurosci 17 (9):1240-1248. doi:10.1038/nn.3767

De Bundel D, Zussy C, Espallergues J, Gerfen CR, Girault JA, Valjent E (2016) Dopamine D2 receptors gate generalization of conditioned threat responses through mTORC1 signaling in the extended amygdala. Mol Psychiatry 21 (11):1545-1553. doi:10.1038/mp.2015.210

Haubensak W, Kunwar PS, Cai H, Ciocchi S, Wall NR, Ponnusamy R, Biag J, Dong HW, Deisseroth K, Callaway EM, Fanselow MS, Luthi A, Anderson DJ (2010) Genetic dissection of an amygdala microcircuit that gates conditioned fear. Nature 468 (7321):270-276. doi:10.1038/nature09553

Lein ES et al. (2007) Genome-wide atlas of gene expression in the adult mouse brain. Nature 445 (7124):168-176. doi:10.1038/nature05453

Li H, Penzo MA, Taniguchi H, Kopec CD, Huang ZJ, Li B (2013) Experience-dependent modification of a central amygdala fear circuit. Nat Neurosci 16 (3):332-339. doi: 10.1038/nn.3322
Neugebauer V, Li W, Bird GC, Han JS (2004) The amygdala and persistent pain. Neuroscientist 10 (3):221-234. doi:10.1177/1073858403261077
Veinante P, Yalcin I, Barrot M (2013) The amygdala between sensation and affect: a role in pain. Journal of Molecular Psychiatry 1 (9).
Shackman AJ, Fox AS (2016) Contributions of the Central Extended Amygdala to Fear and Anxiety. J Neurosci 36 (31):8050-8063. doi:10.1523/JNEUROSCI.0982-16.2016
Walker DL, Davis M (2008) Role of the extended amygdala in short-duration versus sustained fear: a tribute to Dr. Lennart Heimer. Brain Struct Funct 213 (1-2):29-42. doi:10.1007/s00429-008-0183-3

Production scientifique:

Manuscrits en écriture :

1. Jiahao Ye, Pierre Veinante. Cell-type specific parallel circuits in the bed nucleus of the stria terminalis and the central nucleus of the amygdala of the mouse. Preprint bioRxiv, 2017, doi: https://doi.org/10.1101/238493
2. Jiahao Ye, Pierre Veinante. Brain wide inputs/outputs of the mouse central extended amygdala: common and distinctive component. in preparation, submission in 2nd semester 2018

   (voir lettre d'accompagnement du DT)

Presentations:

1. Jiahao Ye, Pierre Veinante, Parallel neuronal circuits of the mouse central extended amygdala, (Poster) NeuroFrance 2017, international meeting of Société des Neurosciences, Bordeaux, 17-19 mai 2017.
2. Jiahao Ye, Pierre Veinante Cell-type specific parallel circuitries of central extended amygdala: a role in pain, (oral presentation) NeuroTime Annual Meeting 2017, 2017 April. 10-11; Amsterdam, Netherland.
3. Jiahao Ye, Pierre Veinante Cell-type specific connectivity in central extended amygdala, (oral presentation), NeuroTech Seminar, Spring 2016 sessions, 2016 April 19; Strasbourg, France.
4. Jiahao Ye, Pierre Veinante, Cell-type specific connectivity in central extended amygdala, (Poster) Doctoral school day 2016, École doctorale des sciences de la vie et de la santé, University of Strasbourg, France; 2016 Mars 14-15; Strasbourg, France
5. Jiahao Ye, Pierre Veinante Cell-type specific connectivity in central extended amygdala, (oral presentation) NeuroTime Annual Meeting 2016, 2016 Feb. 2-4; Strasbourg, France.
6. Jiahao Ye, Pierre Veinante, The central extended amygdala: between fear and pain, (oral presentation) NeuroTime Annual Meeting 2015, 2015 Jan. 20-22; Basal, Switzerland.

To the years lost in the darkness of stupidity.

2014 - 2017

ACKNOWLEDGEMENTS

I want to thank Prof. Dr. Pierre Veinante for creating this great PhD project. Without his first-rate supports, especially towards the end of my PhD, this thesis would be so much different. Without his insights and perseverance, I would have missed this great opportunity to take a refreshing look at the ancient techniques. I also want to thank him for his great kindness in translating part of the thesis into French.

I want to thank Prof. Lutz Hein for his advices on the attempted RNAseq project at different developing stages. I am particularly enjoyed that once-in-a-lifetime open discussion with him and Dr. Ralf Gilsbach in Freiburg.

I also want to thank Prof. Dr. Andreas Lüthi for being my cosupervisor and providing critical feedbacks to the project.

I want to thank Prof. Ilka Diester and Dr. Alexander Hanuschkin of Freiburg for accepting me as a tutor in their in-vivo electrophysiology practical course. It is forever a precious experience that kindles again my enthusiasm and confidence in doing good with an advanced academic degree in science.

I want to thank Prof. Dr. Michel Barrot for kindly hosting this project and constructive discussions in the lab. I want to thank Dr. Ipek Yalcin for her always kind helps in many of our discussions and experiments.

I want to thank Dr. Dominique Massotte for calretinin antibody and tutoring me in confocal microscopy; Prof. Dr. Paul Klosen for his pivotal help and generosities which enabled me to quickly hammer out staining protocols for somatostatin with the powerful tyramide signal amplification; Dr. Cristina Sandu for her marvelous help for setting up microdissection procedures; Prof. Dr. Paul Sawchenko from Salk Institute for his generously gift of an anti-CRF serum. These benevolent helps convince me the ancient old philanthropism in academia still exist here and there.

I want to thank Dr. Jim Sellmeijer for his wholeheartedly open discussions of science and life during our overlapping years. I want to thank Muris and Allessandro for being around, keeping me off the cliff by some heartless jokes and heartful beers. As I am generally not friendly, I am especially honored and grateful that they counted me as a friend.

I want to thank the funding agency and Dr. Paul Pevet and Dr. Domitille Boudard in organizing the Neurotime program. Long life to the EU!

Finally, thank God for his blessings that leading me through.

TABLE OF CONTENTS

COVER i

ABSTRACT iii

RÉSUMÉ DE THÈSE iv

ACKNOWLEDGEMENT xii

TABLE OF CONTENTS xiv

ABBREVIATIONS 1

CHAPTER I. INTRODUCTION 2

1. Central extended amygdala (EAc): a structural and functional macrosystem 3

1.1 What is EAc and why it bothers 3

1.2 Structural and functional organizations of EAc 5

1.2.1 Neuroanatomical structures 5

1.2.2 Neurochemistry 7

1.2.3 Morphology and electrophysiology 9

1.2.4 Mesoscopic circuits: structural organizations 11

1.2.5 Mesoscopic circuits: functional specifications 12

1.2.6 Microcircuits: structural organizations 14

1.2.7 Microcircuits: functional specifications 16

2. Research objectives 19

2.1 Ask the questions: what and why 20

2.2 Answer the questions: methodology 21

2.2.1 Tract-tracing technique 23

2.2.2 Immunohistochemistry 24

2.2.3 Experimental designs 24

CHAPTER II. RESULTS 26

1. Afferents to the central extended amygdala 27

2. Efferents of the central extended amygdala: preliminary comparative study 82

3. Parallel cell-type specific neuronal circuits in central amygdala 111
4. Functional implications of PKCδ-expressing neurons in tonic pain 163
CHAPTER III. DISCUSSIONS 172
1. Dissecting neural circuits: the best techniques wanted 173
1.1 Methodology of this study: pros and cons 173
1.2 Hunting the cell-types of EAc in functions: the alternative methods 174
2. Parallel and differential EAc neuronal circuits 176
2.1 Towards a synthetic view of EAc circuits 176
2.2 LPBE – EAc pathways 177
2.3 Convergent inputs to PKCδ+ neurons. 179
3. Miscellanies 182
3.1 Cell types of EAc-projecting LPBE neurons: alternative cell types 182
3.2 CRF immunoreactivity: discrepancy in STLD and CeA 182
REFERENCE 186

ABBREVIATIONS

5-HT: 5-hydroxytryptamine
AAV: adeno-associated virus
Arc: activity-regulated cytoskeleton-associated protein
BDA: biotin-dextran amine
BL: basolateral nucleus of amygdala
BLA: basolateral nucleus of amygdala, anterior
BLP: basolateral nucleus of amygdala, posterior
BM: basomedial nucleus of amygdala
CA1: field CA1 of the hippocampus
CARD: catalyzed reporter deposition
CeA: central nucleus of amygdala
CeC: central nucleus of amygdala, capsular part
CeL: central nucleus of amygdala, lateral part
CeL/C: central nucleus of amygdala, lateral and capsular part
CeM: central nucleus of amygdala, medial part
CGRP: calcitonin gene-related peptide
CGRPR: calcitonin gene-related peptide receptor
ChR2: channelrhodopsin-2
CPA: conditioned place aversion
CRF: corticotropin-releasing factor
CRF1R: corticotropin-releasing factor receptor type 1
CRF2R: corticotropin-releasing factor receptor type 2
CTb: cholera toxin subunit B
D2R: dopamine D2 receptor
DA: dopmaine
DAB: diaminobenzidine
DBH: dopamine beta hydroxylase
Drd1: dopamine receptor D1
DREAD: Designer Receptors Exclusively Activated by Designer Drugs
EA: extended amygdala
EAc: extended amygdala, central part
EAm: extended amygdala, medial part
ENK: enkephalin
eNpHR3.0: enhanced Natronomonas halorhodopsin, version 3.0
FG: fluorogold
Fu: fusiform nucleus
hM3Dq: Gq-DREAD
Htr2a: serotonin receptor 2A
ISH: in situ hybridization
KO: knockout
LC: locus coeruleus
LH: lateral hypothalamus
LPB: lateral parabrachial nucleus
LPBE: lateral parabrachial nucleus, external part
MeA: medial nucleus of amygdala
NPY: neuropeptide Y
NT: neurotensin
Pa: paraventricular nucleus of hypothalamus
PACAP: pituitary adenylate cyclase-activating polypeptide
PAG: periaqueductal gray
PBN: parabrachial nucleus
pERK: phosphorylated extracellular signal-regulated kinase
PHA-L: *phaseolus vulgaris*-leucoagglutinin
PKCδ: protein kinase C delta
PoT: posterior thalamic nuclear group, triangular part
PSTh: parasubthalamic nucleus
PV: paraventricular nucleus of thalamus
SLEA: sublenticular extended amygdala (SLEA)
SNL: substantia nigra, lateral part
SNR: substantia nigra, reticular part
Sol: solitary nucleus
SOM: somatostatin
ST: bed nucleus of stria terminalis
STL: bed nucleus of stria terminalis, lateral part
STLD: bed nucleus of stria terminalis, lateral dorsal part
STLJ: bed nucleus of stria terminalis, juxtacapsular part
STLP: bed nucleus of stria terminalis, lateral posterior part
STLV: bed nucleus of stria terminalis, lateral ventral part
STM: bed nucleus of stria terminalis, medial part
STMA: bed nucleus of stria terminalis, medial anterior part
STMV: bed nucleus of stria terminalis, medial ventral part
STS: bed nucleus of stria terminalis, supracapuslar part
Tac2: tachykinin 2
TH: tyrosine hydroxylase
Tu: olfactory tubercle
vgat: vesicular GABA transporter
VLPAG: ventrolateral periaqueductal gray
VPPC: ventral posterior nucleus of the thalamus, parvicellular
VS: ventral subiculum
VTA: ventral tegmental area

CHAPTER I. INTRODUCTION

In this chapter, we will introduce the concept of central extended amygdala, its basic elements of subdivisions, neuronal compositions, structural connectivities and functional neural circuit at mesoscopic or microscopic scales.

We then move to the questions that we tried to address with this study, and give an overview of the feasibility of the methods and experiments implemented for answering those questions.

1. Central extended amygdala (EAc): a structural and functional macrosystem

1.1 What is EAc and why it matters

The concept of extended amygdala (EA) was pioneered by J.B.Johnston almost one century ago (Johnston 1923) to emphasize the close relationship between the bed nucleus of stria terminalis (ST) and centromedial nucleus of amygdala, of which the later consists of central nucleus (CeA) and medial nucleus (MeA). This concept was confirmed and developed later by discovering two distinct continuous cell columns connecting ST and CeA/MeA (de Olmos and Heimer 1999; de Olmos et al. 2004; Alheid and Heimer 1988; Heimer et al. 1997b). Although the initial efforts focused on rats, the EA has been consistently confirmed in many species including mouse, cat, rabbit, dog, non-human primate and human with multiple evidence from cytoarchitecture, neurochemistry, tract-tracing connectivity and imaging study (Heimer et al. 1997a; de Olmos and Heimer 1999; Heimer et al. 1999; de Olmos et al. 2004; Fox and Shackman 2017; Gorka et al. 2017).

The EA is composed of ST, CeA, MeA, supracapuslar bed nucleus of stria terminalis (STS) and sublenticular extended amygdala (SLEA), which together formed a ring-like structural continuum spanning in the rostral to caudal direction (Fig. 1). STS and SLEA are two cells columns that run dorsally along the stria terminals and ventrally along the ventral amygdalofugal pathway, respectively (Fig. 1).

In fact, the EA can be further divided into a central part (EAc) and a medial part (EAm) (de Olmos and Heimer 1999; Alheid 2003), which are basically two parallel structural system composed of the central and medial parts of each EA element respectively (Fig. 1). In a nutshell, the EAc is composed of CeA, central part of STS, lateral ST (STL) and lateral part of SLEA, while EAm consists of MeA, medial part of STS, medial ST (STM) and medial part of SLEA (Fig. 1). In this thesis, we focused on the EAc.

It is worth noting that, the concept of extended amygdala denotes a structural extension of centromedial nuclei group of amygdala to ST,, but does not include the cortical or basolateral amygdaloid nuclei (see Fig 1 - 2) (de Olmos and Heimer 1999; Alheid 2003), even though EA received major inputs from other amygdaloid nuclei such as basolateral (BL) and basomedial (BM) nuclei (Pitkanen et al. 1997; Cassell et al. 1999; Sah et al. 2003). It has been clear that EA and non-EA amygdaloid nuclei are structurally and functionally different (McDonald 1982; Cassell et al. 1999; Moga et al. 1989; Walker and Davis 1997; Daniel and Rainnie 2016).

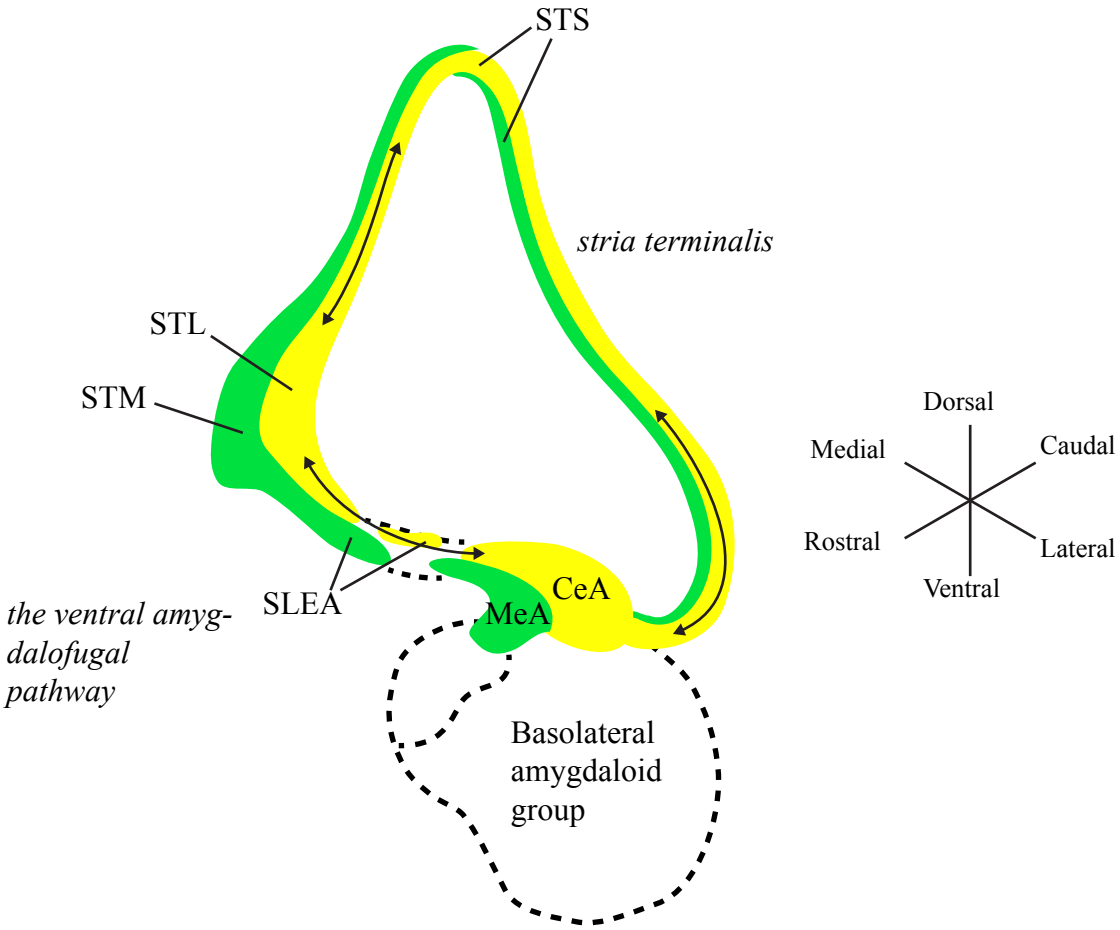

Fig. 1 A 3D model of extended amygdala (EA). The extended amygdala (EA) is composed of a central part (EAc) (yellow) and a medial part (EAm) (green), which are both bidirectionally connected (arrowed lines) dorsally via the stria terminalis and ventrally via the ventral amygalofugal pathway. The two cell columns that situtated dorsally is STS, and ventrally the SELA. In short, the EAc is composed of CeA, central component of STS, STL and central part of SLEA; while the EAm consists of MeA, medial part of STS, STM, and medial part of SLEA.. Figure is adpated from Heimer et al. 1999. Abbreviations: see the list.

With years of efforts, the EAc has been revealed to participate in many physiological and behavioral functions including cardiovascular function, stress hormone response, fear, anxiety and pain in normal and disorder conditions (Kim et al. 2013; Davis et al. 2009; Fox et al. 2015; De Bundel et al. 2016; Lebow and Chen 2016; Tovote et al. 2015; Shackman and Fox 2016; Neugebauer et al. 2004; Veinante et al. 2013). The surprising functional diversity of EAc, however, is somehow contrasted by a limited knowledge of the organization of its neural circuits, especially in the mouse model, of which neuronal circuits are amenable to study, largely due to a rich number of transgenic mouse line and optogenetic/chemogenetic tools that became available (Madisen et al. 2010; Gerfen et al. 2013; Harris et al. 2014; Taniguchi 2014; Deisseroth 2015; Kim et al. 2017a; Roth 2016).

1.2 Structural and functional organizations of EAc

A detailed review of the structural and functional organization is out of the scope of this short introduction. As in most of the researches, as well as in this study, the CeA and STL are the main focuses when it comes to EAc. Hence, we will briefly outline some of the key profiles of what we know of the EAc at the mesoscopic and microscopic levels, as well as its association and causal relationship with certain behavioral and emotional outputs.

In general, the EAc subdivisions have long been known to haunt neuroscientists with their rich diversities in molecular, cellular morphological, electrophysiological and neuronal connectional properties.

1.2.1 Neuroanatomical structures

Lateral bed nucleus of stria terminalis

The STL can be divided according to different schemes, which basically exploit all the three axis (Dong et al. 2001a; Gungor and Pare 2016). In our study, we take reference from the Paxinos and Franklin's mouse brain atlas (Paxinos and Franklin 2012). Basically, STL is divided dorsally into dorsal part (STLD) and a surrounding posterior part (STLP), which also extends caudally; and ventrally into a ventral part (STLV) and the small distinct fusiform nucleus (Fu) (Fig. 2a – b, in yellow). A short summary of STL subnuclei and their acronyms is summarized (see Table 1) (Paxinos and Franklin 2012; Moga et al. 1989; Ju et al. 1989; Dong et al. 2001a; Oler et al. 2017; Schwaber et al. 1980; de Olmos and Heimer 1999; Cassell et al. 1999).

Central nucleus of amygdala

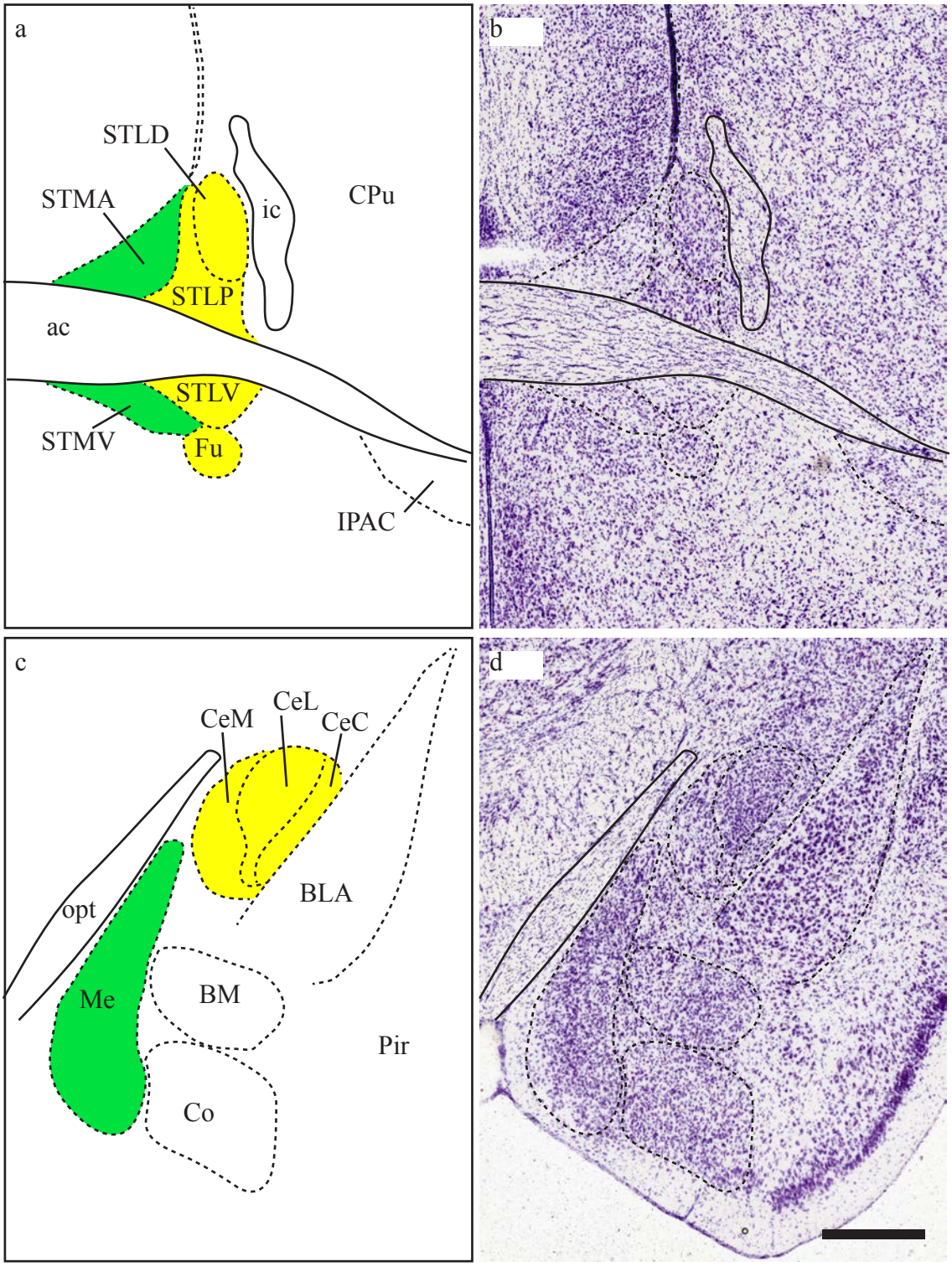

Fig. 2 Main subdivisions of EAc in mouse brain. The EAc subdivisions (in yellow) are depicted at a STL level (a - b) and CeA level (c - d), while EAm components are also shown (in green). **a - b** The main components of STL: STLD and STLP at its dorsal part, STLV and Fu at its ventral part, are shown in a diagram (**a**) and the Nissl staining (**b**). **c - d** The main subdivisions of CeA: from lateral to medial, CeC ,CeL and CeM, are displayed in the diagram (**c**) and the Nissl staining (**d**). Nissl staining images are taken from Allen Brain Atlas (Lein and et al. 2007) and delineated according to the Paxinos and Franklin's mouse brain atlas (Paxinos and Franklin 2012). Abbreviations: see the list. Scale bars: **b**, 500 μm; **d**, 500 μm.

Compared to STL, there are more agreements on the parcellations and nomenclatures of CeA subdivisions. Generally speaking, three main subdivisions are consistently named in studies of different species (Paxinos and Franklin 2012; McDonald 1982; Cassell et al. 1986; Sun and Cassell 1993; Chieng et al. 2006; Haubensak et al. 2010; Oler et al. 2017). These CeA subdivisions are capsular (CeC), lateral (CeL) and medial part (CeM) (Fig. 2c – d), accompanied by multiple variations in the acronyms or additional neuroanatomical substructures (see Table 2). In this study, we also adhere to the nomenclature from the Paxinos and Franklin's mouse brain atlas (Paxinos and Franklin 2012).

1.2.2 Neurochemistry

In both rat and mouse, EAc subdivisions are predominantly occupied by intrinsic GABAergic neurons (Sun and Cassell 1993; Poulin et al. 2009; Cassell et al. 1999), while some scattered glutamatergic neurons are observed in ST areas (i.e. STMA, STLV) (Kaufling et al. 2017; Poulin et al. 2009; Kudo et al. 2012; Jennings et al. 2013b), but absent from CeA (Poulin et al. 2008).

Despite this simple glutamate-GABA dichotomy, EAc is well-known to be composed of heterogeneous neuronal populations expressing a repertoire of neurochemical molecules including neuromodulators, neuropeptides, receptors, transcription factors and kinases (Roberts et al. 1982; Cassell and Gray 1989; Cassell et al. 1999; Moga et al. 1989; Lein and et al. 2007) (also see Table 3). For a specific cellular marker, there is some degree of congregation in one subdivision of EAc against another one. For example, CeL is densely enriched in neurotensin (NT), corticotropin-releasing factor (CRF), enkephalin (ENK), somatostatin (SOM) neurons; CeC is moderately enriched in ENK and NT neurons; CeM is enriched in SOM and, exclusively, substance P neurons (Cassell et al. 1986). In STLD, enrichment of neurons expressing CRF or NT are observed, while the ventral Fu is enriched with CRF neurons but displays a very sparse expression of NT neurons if any (Ju et al. 1989). Among these known molecular markers, protein kinase C delta (PKCδ) and SOM are of our interest. Both PKCδ and SOM are specifically expressed in STLD and lateral/capsular part of CeA (CeL/C) (Haubensak et al. 2010; Li et al. 2013; De Bundel et al. 2016) (also see Table 3), and they mediate cell-type specific circuits with distinct functions (Haubensak et al. 2010; Li et al. 2013; De Bundel et al. 2016). In CeL/C, PKCδ and SOM labels two non-overlapping neuronal populations and they together constitute a majority of GABAergic neurons in CeL/C (Haubensak et al. 2010; Li et al. 2013; Kim et al. 2017b). For example, in mouse CeL, 95% of

Table 1: Comparison of nomenclatures of STL from different studies.

		(Paxinos and Franklin 2012)	(Moga et al. 1989)	(Ju and Swanson 1989)	(Dong et al. 2001a)	Oler et al. 2017)
Whole nuclei		ST	BST	BST	BST	BST
Lateral division		STL	BSTL	-[1]	-	BSTL
subdivisions	dorsal lateral	STLD	BSTDL	Ov (oval)	BSTov (oval)	BSTLcn (central)
	anterior lateral	STLP	BSTAL	AL	BSTal	BSTLP
	juxtacapsular	STLJ	BSTJXC	Ju	BSTju	BSTLJ
	supracapsular	STS	BSTSC	SE (striatal extension)	BSTse (striatal extension)	-
	ventral lateral	STLV	BSTVL	Fu	BSTsc (subcommissural) & BSTav (anteroventral)	-
	fusiform	Fu			BSTfu	-
Species		mouse	rat	rat	rat	monkey
Methods		Nissl	Thionin	Cyto- & Chemoarchitecture	Cyto- & Chemoarchitecture	AChE

[1] A minus sign (-) means the name corresponding to that division is not found.

Table 2: Comparison of CeA nomenclatures from different studies.

		(Paxinos and Franklin 2012)	(McDonald 1982)	(Cassell et al. 1986)	(Sun and Cassell 1993)	(Chieng et al. 2006)	(Haubensak et al. 2010)	(Oler et al. 2017)
Whole Nucleus		CeA	CN	CNA	Ce	CeA	CEA	Ce
Subdivisions	**capsular**	CeC	CLC	CLC	CeLC	CeC [1]	CEl	CeLc
	lateral	CeL	CL	CL	CeL	CeL		CeLcn [2]
	medial	CeM	CM	CM	CeM	CeM	CeM	CeM
	intermediate	-	CI	-	-	-	-	-
	ventral	-	-	CV	CeV	-	-	-
Species		mouse	rat	rat	rat	rat	mouse	primate
Method		Nissl	Nissl, Golgi	Nissl (quantitative)	Golgi, GABA	DAPI, ENK, TH	PKCδ-cre	AChE, SOM, ENK

[1] CeC: includes the lateral capsular, the ventral capsular part and the amygdalostriatal transition area (AStr) area (Chieng et al. 2006).

2 CeLcn: includes the capsular division and lateral amygdalostriatal transition zone (Oler et al. 2017).

glutamate decarboxylase 1 positive (Gad1+) neurons can be attributed to PKCδ, SOM, and tachykinin 2 (Tac2) expressing populations (Kim et al. 2017b).

Like other neuropeptidergic EAc neurons, PKCδ and SOM neurons also have multiple neurochemical identities. PKCδ and SOM neurons can express calcitonin gene-related peptide receptor (CGRPR), although more than 50% PKCδ cells are CGRPR positive (CGRPR+), while only less than 20% SOM cells are CGRPR+ (Han et al. 2015). A recent study on mouse also revealed that more than 70% PKCδ cells in CeL/C and STLD expressed dopamine D2 receptor (D2R), using Drd2-cre-EGFP mouse (De Bundel et al. 2016). More than 70% of ENK cells express PKCδ, while only about 40% PKCδ cells express ENK in mouse (Haubensak et al. 2010).

Apart from the endogenous molecules expressed by EAc neurons, they also receive axonal inputs of various neurochemical natures, including glutamate, GABA, dopamine, serotonin, noradrenaline, CRF, calcitonin gene-related peptide (CGRP) and pituitary adenylate cyclase-activating polypeptide (PACAP) (Lopez de Armentia and Sah 2004; Turesson et al. 2013; Lu et al. 2015; Han et al. 2015; Phelix et al. 1992; Krawczyk et al. 2011; Bienvenu et al. 2015; Missig et al. 2017; Missig et al. 2014). Often than not, axonal projections show preferential distributions in different EAc subdivisions.

Recently, a number of studies have been carried out to characterize the preferential gene expression patterns in EAc nuclei (Zirlinger et al. 2001; Becker et al. 2008; Garcia-Lopez et al. 2008; Bupesh et al. 2011; Partin et al. 2013). We also find it is interesting to list the expression levels of dozens of genes, which related to GABAergic, glutamatergic, neuropeptidergic, monoaminergic transmissions, from the online Allen Brain Atlas (Lein and et al. 2007) (Table 3). The differential expression in EAc subnuclei of these different genes might shade lights on effects of corresponding neurotransmissions or neuromodulations. We also noted that the gene expressed in EAm subnuclei are not shown.

1.2.3 Morphology and electrophysiology

The majority of EAc neurons display medium spiny neuron like morphology, which are distinctive from the lateral amygdala principal neurons which closely resemble the cortical pyramidal neurons (Moga et al. 1989; Cassell et al. 1986; Cassell et al. 1999; Rodriguez-Sierra et al. 2013).

In both CeA and STL, there are three major types of neurons defined by their membrane electrophysiological properties and their responses hyperpolarizing and depolarizing current injection (Schiess et al. 1999; Amano et al. 2012; Hammack et al. 2007; Rodriguez-Sierra et

Table 3. Semi-quantitative gene expression in EAc[1].

Groups	Gene	Exp.	STLD	STLP	STLV	Fu	CeLC	CeM
GABA	*Gad1*	79556706	++++	++++	++++	++++	++++	++++
	Gad2	79591669	++++	++++	++++	++++	++++	++++
Glutamate	*Grm1*	79591723	-/+	+/++	+/++	++++	-	-/+
	Grm2	79591611	-	-/+	-/+	-	-	-
	Grm5	73512423	++++	++++	++	+	++++	++++
	Slc17a6	73818754	-	-	-/+	-	-	-
	Slc17a7	75081210	-	-	-	-	-	-
Neuropeptide	*Adcyap1*	74511882	-	-	-	-	-	-
	Adcyap1r1	74988667	+++	+++	+++	+++	+++	+++
	Calcr	75080999	-	-	-/+	-	++	-
	Crf	292	+/++	++/+++	++/+++	++/+++	+++	+/++
	Crfr1	297	-	+	+	-/+	-	+
	Npy	717	-	+	+	-/+	-	+
	Nts	73788032	++++	+	++	-	++++	+
	Penk	74881286	++++	+++	++	++	++++	++++
	Sst	1001	++++	++	+	-/+	++++	++
	Sstr2	77371821	-/+	-/+	-/+	-	NA	NA
	Sstr4	73636037	+	+	-	-	++	-
	Tac1	1038	-/+	+	+	-	-/+	+
	Tac2	72339556	++++	++	+	-	++++	++/+++
Monoamine	*Drd1*	352	-/+	+	+	-/+	-/+	+
	Drd2	357	-/+	+	+	+	+	+
	Drd3	75038431	NA	NA	NA	NA	++/+++	-/+
	Htr1a	79556616	-/+	++	+	+	NA	NA
	Htr2c	73636098	++	++	+/++	-/+	+++	+
	Ppp1r1b	73732146	++++	+	+	-	++++	+
Others	*Foxp2*	72079884	-	+	+	-	-	+
	Prkcd	70301274	++++	-	-	-	++++	-

[1] Manual assessment of gene expression in EAc, based on selected genes from the Allen Mouse Brain Atlas ISH database (Lein and et al. 2007) and the neuroanatomical delineations of Paxinos and Franklin's mouse brain atlas (Paxinos and Franklin 2012). Scales: -, absence; -/+, very sparse; +, light; ++, moderate; +++, strong; ++++, dense.

[2] NA: not available, due to the poor signal/noise ratio.

al. 2013; Daniel et al. 2017). The type I neurons display regular spiking patterns, and can be found as PKCδ

negative (PKCδ-) neurons in mouse CeL (Haubensak et al. 2010; Li et al. 2013) and in all STL subdivisions of rats (Rodriguez-Sierra et al. 2013). The type II neurons show low-threshold bursting and can be found as PKCδ- cells in the CeL of mice (Haubensak et al. 2010) and in the whole STL of rat (Rodriguez-Sierra et al. 2013). Type III neurons can show either late-firing or inward-rectification and can be found as the PKCδ+ neurons or SOM+ neurons in CeL of mice (Haubensak et al. 2010; Li et al. 2013) and only in anterolateral ST (roughly corresponding to STLD and STLP) (Rodriguez-Sierra et al. 2013). Some species difference between rat versus mouse are observed (Dumont et al. 2002; Amano et al. 2012). For example, type III late-firing neurons are distributed mostly in CeL and CeM of Guinea pigs, but sparsely in CeA of rat and rarely in CeM of cat (Dumont et al. 2002).

1.2.4 Mesoscopic circuits: structural organizations

EAc subdivisions are extensively and similarly connected with many brain areas, including EAc itself, amygdala, thalamus, hypothalamus, ventral tegmental area (VTA), periaqueductal gray (PAG) and pontine parabrachial nucleus (PBN) (Holstege et al. 1985; Cassell et al. 1999; Dong et al. 2001a; McDonald et al. 1999; Jolkkonen and Pitkanen 1998; Petrovich and Swanson 1997; Krettek and Price 1978; Shammah-Lagnado et al. 1999).

There seems to be several common themes of mesoscopic connectivity of EAc subnuclei. First, there are often reciprocal connections between an EAc subnucleus and its afferent or efferent areas. This can be applied to intra-EAc connections as well as extra-EAc connections. Within EAc, for example, STLV and Fu are heavily innervated by its dorsal part, especially oval-shaped STLD, while only moderate projection from Fu to STLD was observed (Dong et al. 2001b). Fu and STLD also project strongly to CeA (Dong et al. 2001b), while CeA can also send intense projections to STLD, STLV, and Fu (Krettek and Price 1978; Sun et al. 1991). Among extra-EAc connections, for instance, the PBN strongly projects to both STL and CeA, in reverse, strong EAc projections to PBN have also been observed (Saper and Loewy 1980; Veening et al. 1984; Krukoff et al. 1993; Moga et al. 1989).

Second, some EAc connections are unidirectional. For example, while CeL strongly project to CeM, projection from CeM to CeL/C is absent (Jolkkonen and Pitkanen 1998). A mostly unidirectional connection from ventromedial prefrontal cortical areas to CeA has also been reported (McDonald 1998; McDonald et al. 1999; Majak et al. 2004).

Third, different EAc subnuclei can be connected to the same nuclei in different strength, which contribute to the distinct connectivity profiles of individual EAc subarea. For example, the paraventricular nucleus of hypothalamus (Pa) is targeted lightly by STLD but strongly by the Fu (Dong et al. 2001b). CeM and STLV can receive common as well as distinct inputs from areas like basolateral amygdaloid group and solitary nucleus (Sol) (Bienkowski and Rinaman 2013). There is a lack of systematic comparisons of the common and distinct connections of EAc subnuclei in mouse. With these three features, we are by no means comprehensively describe the connectivity patterns of EAc subnuclei.

1.2.5 Mesoscopic circuits: functional specifications

Function of EAc mesoscopic connections have been studied in various ways including immunohistochemistry of neuronal activity markers (Sarhan et al. 2013; De Bundel et al. 2016), lesion (chemical or electrolytic) (Sullivan et al. 2004), local pharmacological manipulations (De Bundel et al. 2016), and optogenetic interrogation at the soma of a nucleus (Mazzone et al. 2016). Usually, the functional effects are examined without specifying a specific neuronal pathway, thus any effects likely reflect the combined impact of manipulating the whole inputs and/or outputs of that particular EAc subdivision. Depending on the type of interrogation techniques, a correlational or caudal role of an EAc subdivision can be revealed.

Different EAc mesoscopic pathway can carried out different functions. For example, lesion studies demonstrated that three CeA output targets, the LH, PAG, and ST, revealed preferential roles in automatic, behavioral and no effect in the conditioned fear responses (LeDoux et al. 1988). Here, we summarize some of the studies on STL and CeA, as well as ST as a whole (Table 4), which together revealed various functional roles of EAc subnuclei in anxiety behavior, fear learning, affective pain and feeding behavior. This list is not meant to be a comprehensive review of researches on dissecting functions of EAc subnuclei, but insightful reviews can be found (Gungor and Pare 2016; Shackman and Fox 2016).

We noticed that there seems to be at least two kinds of functional relationships between EAc nuclei. The first one consists in coordinate or synchronized functions, for example, between STLD and CeL/C. Application of fluoxetine, a selective serotonin reuptake inhibitor, after fear conditioning, can significantly enhance the expressions of neuronal Arc (activity-regulated cytoskeleton-associated protein) in STLD and CeL/C, but not in basal or lateral amygdala (Ravinder et al. 2013). Morphine can also induce robust c-fos expression in STLD and CeL/C in rats and mice (Sarhan et al. 2013; Xiu et al. 2014). Systematic application of

Table 4: Region-specific functions

Region[1]	Treatment	Results[2]	Reference
ST	*Vgat-cre*:hM3Dq; DREAD activation	GABAergic neurons => Anxiogenic↑; Activity of LC & LPB↑	(Mazzone et al. 2016)
ST	Electrolytic lesion	Lesion => Fear learning↓ HPA response (context)↓	(Sullivan et al. 2004)
ST	Pre-training lesion of BLA && post-training lesion of ST	Fear expression (context)↓	(Zimmerman and Maren 2011)
ST(dorsolateral)	CRF1R/CRF2R antagonist;	Inactivation CRF signaling => Pain-induced CPA↓;	(Ide et al. 2013)
ST(dorsolateral)	CRF infusion	Induce CPA↑ without pain stimulation	(Ide et al. 2013)
ST(dorsolateral)	Neuropeptide Y infusion	Suppress pain induced-CPA↓	(Ide et al. 2013)
ST(dorsolateral)	*GAD670-cre* ; ChR2	Immediate arousal from sleep state↑	(Kodani et al. 2017)
ST(posterior)	*CRFR2-cre*: Optogenetic activation	CRFR2 neurons => Anxiolytic↑, HPA response↓, stress↓	(Henckens et al. 2016)
STLD	*Drd1a-cre*: eNpHR3.0	Drd1a+ neurons => open arm time↑, respiratory rate↓	(Kim et al. 2013)
STLD & CeA	D2R agonist/antagonist	D2 signaling =>Promote fear generalization↑	(De Bundel et al. 2016)
CeA	Electrolytic lesion	Lesion => Fear learning↓ HPA response (cue/context)↓	(Sullivan et al. 2004)
CeA	*Htr2a-cre*: DREAD or optogenetic inactivation	Htr2a+ neurons => Inactivation => innate fear↑, learned fear↓	(Isosaka et al. 2015)
CeA	*Htr2a-cre*: DREAD & optogenetics	Htr2a+ neurons => food intake↑, positive enforcement↑	(Douglass et al. 2017)
CeA	*Tac2-cre*:ChR2	Tac2+ neurons => Fear learning↑	(Andero et al. 2016)
CeA	AAV1-Cre: CeA in *Crf-lox/lox* mouse Or cre-mediated TeTx inactivation	KO CRF in CeA => Fear learning of weak threat↓	(Sanford et al. 2017)
CeL/C	*SOM-cre*:DREAD inhibition	Fear learning (cue)↓	(Li et al. 2013)
CeL/C	*SOM-cre*:optogenetic manipulation, TeTx inactivation	SOM+ neurons => active avoidance↓, passive defensive behavior↑	(Yu et al. 2016)
CeL/C	*PKCδ-cre*: DREAD/ optogenetic inactivation	Inactivation PKCδ+ neurons => Anorexigenic behavior↓, food intake↑	(Cai et al. 2014)
CeL/C	*PKCδ-cre*: ChR2	Food intake↓	(Cai et al. 2014)
CeL/C	Cre-dependent knock out α5-$GABA_AR$ in PKCδ:CeL/C	KO GABAaR in CeA => Fear generalization↑	(Botta et al. 2015)
CeM	rAAV-ChR2	Freezing behavior↑	(Ciocchi et al. 2010)

[1] The nomenclatures of the regions are adapted either from the original research paper or Paxinos and Franklin's mouse brain atlas (Paxinos and Franklin 2012) to reflect smallest identifiable structures that manipulated in that paper.

[2] Unless explicitly mentioned, the results are summarized as the consequences of activations of a particular region, cell population or signaling pathway.

D2R agonist increased the neuronal activations in STLD and CeL/C (De Bundel et al. 2016). Moreover, only blocking D2R signaling in contralateral STLD and CeL/C can block the contextual fear overgeneralization in fear learning paradigm (De Bundel et al. 2016)

On the other hand, dissociable roles can be attributed to different EAc subdivisions. For example, local infusions of AMPA receptor antagonist in ST (including STL), but not in CeA, blocked the light-induced startle responses; whereas infusions into CeA, but not ST, blocked the fear-potentiated startle responses (Walker and Davis 1997). This type of preferential role of CeA in phasic, associative fear responses and ST(L) in a sustained, anxiety-like responses gained its importance through many more rat and human studies (Walker et al. 2003; Walker and Davis 2008; Davis et al. 2009; Walker et al. 2009).

1.2.6 Microcircuits: structural organizations

Here, we classify the EAc microcircuits into three groups: the intrinsic local connections are confined in a local area (i.e. between different STLD neurons), the intrinsic long range connections connect distal elements of EAc (i.e. between STLD and CeA) and the external connections deal with long-range connections between EAc and extra-EAc brain regions (i.e. CeA and PBN).

The neuronal microcircuits of EAc have been explored in different animal models with various techniques. Traditional approaches of combining retrograde tact-tracing with immunofluorescent staining have successfully revealed cellular identities of long range connections. For example, in CeA, PBN-projecting neurons can express CRF, NT, SOM, but not ENK (Moga and Gray 1985); in anterolateral ST, ENK or neuropeptide Y (NPY) neurons can project to CeA (Poulin et al. 2006; Wood et al. 2016). Recent advances in techniques including transgenic mouse lines, virus tracing, channelrhodopsin 2 (ChR2) assisted circuit mapping make it possible to systematically map the afferents or efferents to a specific cell type in EAc nuclei (see Table 5). We list only some of CeA neuronal microcircuits defined by genetic labeling of specific cell types including PKCδ, SOM, CRF and serotonin receptor 2A (Htr2a). Although many of these cell types can also be found in STL (Potter et al. 1994; Chen et al. 2015; Xu et al. 2016b), most of the researches focused on CeA.

Often, one neuronal population can give rise to multiple type of projections or receive different types of inputs (Table 5). For example, in CeL PKCδ+ neurons can synapse onto PKCδ- neurons, and also to CeM and lateral PBN (LPB) (Haubensak et al. 2010; Cai et al. 2014; Oh et al. 2014). Also, multiple cell-types can participate the same pathway. For

Table 5. Cell-type specific neuronal circuits in EAc

Cell-type	Pathways	References
PKCδ		
Intrinsic.local	$CeL^{PKCδ\text{-}cre:ChR2}$ →$CeL^{PKCδ-}$	(Haubensak et al. 2010)
	$CeL^{PKCδ\text{-}cre:rabies}$ ← $CeL^{PKCδ-}$ (few $CeL^{PKCδ+}$)	(Douglass et al. 2017)
	CeL: PKCδ-→CeL: PKCδ- (homotypical > heterotypical)	(Hunt et al. 2017)
Intrinsic.long	$CeL^{PKCδ\text{-}cre:ChR2}$ →CeM →$PAG^{CTb/retrobeads}$	(Haubensak et al. 2010)
	CeL→$CeM^{HSV\text{-}GFP}$	(Ciocchi et al. 2010)
	$CeL^{PKCδ\text{-}cre:ChR2\text{-}EGFP}$ →CeM/ STLV/ STLP	(Cai et al. 2014)
	CeL/C $^{PKCδ\text{-}cre:rabies}$→$CeM^{neurotensin}$	(Kim et al. 2017b)
	$STLD^{PKCδ\text{-}cre:EGFP}$ →CeM/CeL	(Oh et al. 2014)
	$CeL^{PKCδ:rabies}$ ←STLD	(Cai et al. 2014)
	$CeL^{PKCδ\text{-}cre:EGFP}$ →STLV/STLP/STLD/CeM	(Oh et al. 2014)
External	$CeL^{PKCδ:rabies}$ ←BLA/LPB/Insular/PV/PoT/CA1/VS/EnT	(Cai et al. 2014)
	CeL $^{PKCδ\text{-}cre:ChR2\text{-}EGFP}$→ STMV/LPB	(Cai et al. 2014)
	$STLD^{Prckd\text{-}cre:EGFP}$ →STMA/STMV	(Oh et al. 2014)
SOM		
Intrinsic.local	CeL: SOM+→CeL: SOM+ (homotypical > heterotypical)	(Hunt et al. 2017)
Intrinsic.long		
External	$CeL^{SOM\text{-}cre:Ai14}$, not PKCδ+ → PAG/PVT:CTb injection	(Penzo et al. 2014)
	$CeL^{SOM\text{-}cre:Ai14}$ ← $PV^{AAV\text{-}ChR2\text{-}YFP}$	(Penzo et al. 2015)
CRF		
Intrinsic.local	$CeL^{CRF\text{-}cre:ChR2}$ → CeL: SOM+/PKCδ+	(Fadok et al. 2017)
	$CeL^{SOM\text{-}cre:ChR2}$ → CeL: CRF+/ PKCδ+	(Fadok et al. 2017)
Intrinsic.long	$CeL^{CRF\text{-}cre:ChR2\text{-}eYFP}$ (rat) →CeL/CeM: CRF-negative	(Pomrenze et al. 2015)
	$CeL^{CRF\text{-}cre:ChR2\text{-}eYFP}$ (rat) →STLV & STLP	(Pomrenze et al. 2015)
External	$CeL^{CRF\text{-}cre:ChR2\text{-}eYFP}$ (rat) → MPB, LPB, LC, SNr, VTA, LH	(Pomrenze et al. 2015)
	ST:CRF ←$DR^{Sert\text{-}cre:ChR2\text{-}eYFP}$	(Marcinkiewcz et al. 2016)
Htr2a		
Intrinsic.local	$CeL^{Htr2a\text{-}cre:rabies}$ ← $CeL^{Htr2a+/-}$ (also strong IPSC)	(Douglass et al. 2017)
Intrinsic.long	$CeL^{Htr2a\text{-}cre:rabies\text{-}eGFP}$ ← ST	(Douglass et al. 2017)
External	$CeL^{Htr2a\text{-}cre:rabies\text{-}eGFP}$ ← Insular/VPPC/PSTh/ Tu/SNL	(Douglass et al. 2017)
	$CeL^{Htr2a:AAV\text{-}synaptophysin}$ →STLD/STLV/LH/PAG/NTS	(Douglass et al. 2017)
	$CeL^{Htr2a:ChR2\text{-}eYFP}$ →LPB	(Douglass et al. 2017)
NPY		
Intrinsic.long	ST ←→CeA, by Flurogold tracing in NPY-GFP mouse	(Wood et al. 2016)

instance, both PKCδ+ and SOM+ neurons in CeL are innervated by paraventricular nucleus of thalamus (PV) (Cai et al. 2014; Penzo et al. 2015).

Although there is no any unified picture on EAc microcircuits currently, some interesting patterns appears in different studies. In CeL, an asymmetric connection exists between PKCδ+ and PKCδ- cells in CeL/C, with much stronger functional inhibition from PKCδ- to PKCδ+ (Ciocchi et al. 2010). In a synthetic effort, Hunt and colleagues found that CeL local connections between the same cell types (i.e. PKCδ- → PKCδ- and SOM+ →SOM+) are the most common, while optogenetic activation SOM+ activate almost all CeL neurons (Hunt et al. 2017).

1.2.7 Microcircuits: functional specifications

Many researches have been delved into the functional interrogations of cell-type specific microcircuits of EAc, especially in CeA. Often, a specific neuronal circuit need to be activated or inhibited at its axonal terminal areas, rather than at the cell bodies. Manipulation of specific EAc microcircuit can modulate many behaviors including fear, anxiety, respiratory function, feeding behavior and reward seeking (Kim et al. 2013; Carter et al. 2013; Penzo et al. 2015; Tovote et al. 2015; Jennings et al. 2013b). We list a handful of such works (Table 6) and illustrate some of the features of EAc functional microcircuits.

Several different microcircuits can affect the same behavior, and different behaviors can be affected by one pathway. For example, LPB CGRP+ projections to CGRP receptor expressing CeL/C neurons can modulate freezing behavior, threat memory and pain response (Han et al. 2015). Serotonergic neurons of dorsal raphe nucleus activate CRF+ neurons in ST, promoting fear and anxiety (Marcinkiewcz et al. 2016); while ST glutamatergic outputs to VTA can similarly potentiate anxiety behavior (Jennings et al. 2013b).

A single EAc microcircuit can also achieve bidirectional controls on one type of behavior. For example, glutamatergic inputs from basolateral nucleus of amygdala to STLP can cause anxiolytic effects when activated, but anxiogenic effects when inhibited (Kim et al. 2013). The bidirectional regulation can also be achieved by intrinsic local connections. Fadok and colleagues took a synthetic approach combining cre mouse line, optogenetics, *in vivo* and *in vitro* electrophysiology, to elucidate competing roles of a CeL reciprocal inhibitory circuits formed by CRF+ and SOM+ neurons, in active fear and passive freezing behavior (Fadok et al. 2017).

Table 6. Functions of cell-type specific neuronal circuits in EAc.

	Treatment	Results	Reference
Afferent pathway			
AAV5-*CaMKIIa*: BLA → STLP	ChR2 or eNpHR3.0	Activation => axiolytic Inhibition =>anxiogenic	(Kim et al. 2013)
AAV5-*hSyn*: LH → STLP	ChR2	Open arm time↑	(Kim et al. 2013)
Sert-cre:DR → CRF: ST	Optogenetic, DREAD	fear↑,anxiety↑	(Marcinkiewcz et al. 2016)
CRF-*cre*:CeL → SOM-ir:CeL	ChR2, electrophysiology	Activate CRF+ cells=>active fear↑;	(Fadok et al. 2017)
SOM-cre:CeL →CRF-ir:CeL	ChR2, electrophysiology	Activate SOM+ cells => passive freezing↑;	(Fadok et al. 2017)
PV →CeLC:SOM	DREAD	Inactivation => Fear conditioning↓	(Penzo et al. 2015)
Calca-cre:LPB →CeL	Optogenetic, DREAD	Activation => Appetite↓	(Carter et al. 2013)
Ppp1r1b-cre: BLA →*D1R*-ISH: CeA	optogenetics, genetic tracing, ISH	Appetite↑	(Kim et al. 2017b)
Rspo2-cre: BLA →*D2R*-ISH:CeA	optogenetics, genetic tracing, ISH	Appetite↓	(Kim et al. 2017b)
Calca-cre: LPB → *calcr1-cre* : CeL/C	Cre-dependent lesion, optogenetic manipulation	Activation => Freezing ↑, threat memory↑; Inactivation => pain signal↓	(Han et al. 2015)
Efferent pathways			
AAV5-*hSyn*: dorsal ST → VTA	ChR2	Place preference↑	(Kim et al. 2013)
Vglut2-cre: STLV+STMV →VTA	ChR2	Aversion & anxiety↑	(Jennings et al. 2013b)
Vgat-cre: STLV+STMV →VTA	ChR2	Reward seeking↑, anxiety↓	(Jennings et al. 2013b)
Vgat-cre: ST (lateral and medial) → LH	ChR2 or eArch3.0	Activation => Food intake↑; Inactivation => Food intake↓.	(Jennings et al. 2013a)
AAV5-*hSyn*: dorsal ST → LPB	ChR2	Respiratory rate↓	(Kim et al. 2013)
Ventral hippocampus →CeA: PAG/Sol-projecting neurons	ArchT-GFP inactivation	contextual fear renewal↓	(Xu et al. 2016a)

Again, there seems hardly a rule for a strict functional relationship between one EAc microcircuit and behavior. The EAc microcircuits are structurally diverse and functional heterogeneous.

2. Research objectives

In this part, we will introduce the questions we wanted to ask and explain the rationale of choosing the feasible methods to answer them. Therefore, we brief some theoretical backgrounds of the techniques and give an overview of the experimental designs for answering the questions.

2.1 Ask the questions: what and why

We are interested in three aspects of structural organizations of EAc neural circuits. First, what are the general and differential features of afferents and efferents of EAc subdivisions? Even though the basic picture of afferents and efferents has already been known by study of rats, there is a lack of direct comparison of connectivity strength between different EAc nuclei. On the other hand, even armed with the remarkable database of mesoscale connectome of mouse brain (Oh et al. 2014), we cannot identify enough cases which have confined and strong local injection for a comparative study on efferents of all the main EAc subdivisions. More importantly, accumulating evidences have been revealing more and more functional heterogeneities between different subdivisions of EAc in mouse model (Walker et al. 2009; Haubensak et al. 2010; Cai et al. 2012; Kim et al. 2013; Tovote et al. 2015), while the connectivity of EAc nuclei in mouse is still elusive.

Second, are the EAc subdivisions innervated by the same neuron pools in a common afferent region? As EAc nuclei share many afferents, one might expect that a certain common input area equally affects all the innervated EAc subdivisions. However, if several distinct neuron groups in the shared input area contribute differentially to the corresponding pathways to different EAc subdivisions, then one would reasonably expect differential functions are played by the shared input area. For instance, CeL/C and its counterpart STLD, both receive strong inputs from the exteral LPB (LPBE) (Alden et al. 1994; Bernard et al. 1993), but it is not known whether and how much EAc-projecting LPBE neurons send collaterals to CeL/C and STLD.

Third, what are the cellular identities of EAc microcircuits? Are there cell-type specific neuronal circuits that exist in STL and CeA in parallel? The general connectivity of the rat EAc is largely known, but the cell-types of these circuits are less clear (Cassell et al. 1999). Among the reported neurochemical identities of EAc neurons, there are two molecular markers which particularly interesting. The PKCδ and SOM are expressed in two complementary GABAergic neuronal populations in the CeL/C (Haubensak et al. 2010; Ciocchi et al. 2010), and they are critically involved in a variety of associative learning and emotion responses (Ciocchi et al. 2010; Haubensak et al. 2010; Cai et al. 2014; Botta et al. 2015; De Bundel et al. 2016; Douglass et al. 2017; Sanford et al. 2017; Li et al. 2013; Penzo et al. 2015; Fadok et al. 2017). On the other hand, a similar specific expression of PKCδ and SOM in STLD, an EAc counterpart of CeL/C, was observed. Thus, it possible that, similar neuronal circuits might exist in STL as that in CeL/C.

In addition, we would like to investigate possible functional roles of the cell-type specific neuronal circuits. Among many of functional studies of EAc, one captured our attention. Carrasquillo and Gereau found a particularly dense pERK induction in CeL/C in a formalin pain rat model (Carrasquillo and Gereau 2007). Interestingly, the same CeL/C area is concentrated with PKCδ-expressing neurons. Thus, it is likely some of the pERK-expression neurons are also PKCδ-positive. Considering the similarity between STLD and CeL/C, the PKCδ+ neurons in STLD are also worth to be probed. Thus, we carried out primitive association study of EAc PKCδ+ neurons in formalin pain model.

2.2 Answer the questions: methodology

In order to answer the questions related to patterns and neurochemical identities of the afferents and efferents, we turned to the classic approaches of dissecting neuronal circuits. We took advantage of highly sensitive tract-tracing techniques with anterograde tracers and retrograde tracers to indiscriminately label the afferents and efferents, respectively. Subsequently, we applied sensitive immunostaining techniques to reveal the tracers and identify the cell-types of interest.

In general, this combined tract-tracing and immunostaining method consist of two steps. In the first step, we applied stereotaxic injection of tracers into individual EAc subdivision and labeled its corresponding afferents or efferents depending on the nature of that tracer (Fig. 3). The efferents of the injection nucleus will be labeled with an anterograde tracer, which is supposed to be transported from axon terminals to soma (hence it is anterograde). On the other hand, the afferents of injection areas will be labeled by a retrograde tracer (Fig. 3), which is presumably to be transported from soma to axonal terminals (hence it is retrograde).

In the second step, the tracer molecules or/and the cellular markers of interest were revealed by different immunostaining protocols, depending on the purpose of that experiment. Generally, we applied DAB immunohistochemistry (see 2.2.2 for more details) to reveal patterns of afferents or efferents across the brain. We also employed traditional multi-color immunofluorescent staining to reveal several molecules, usually for confirming possible somatic colocalizations and axonal appositions.

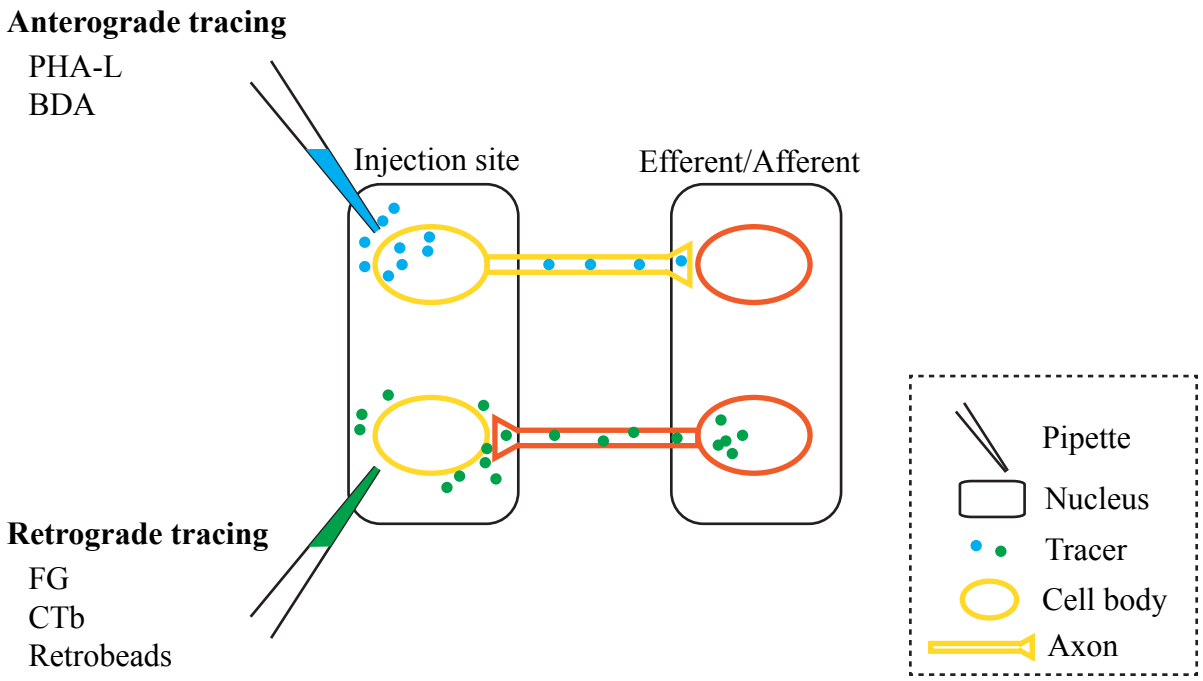

Fig. 3 Anterograde tracing and retrograde tracing. Injection of anterograde tracers (i.e. PHA-L, BDA) will label cell body and its distal axonal terminals in the efferents, thus called anterograde tracing. Injection of retrograde tracers (i.e. FG, CTb, and retrobeads) will result in uptake of tracers by the axonal terminals in the injection site, and subsequent transportation of tracers to the distal cell bodies of afferents, resulting in retrograde tracing.

2.2.1 Tract-tracing technique

Stereotaxic injection offers a stable way to target any brain area given that its coordinates is known. We based all our coordinates on the widely accepted Paxinos and Franklin's mouse brain atlas (Paxinos and Franklin 2012). Here, we briefly review the tracing properties and uptake mechanisms of the tracers used in this study.

The widely used biotin-dextran amine (BDA) is taken up by dendrites and cell bodies, and predominantly transported in the anterograde direction (Lanciego and Wouterlood 2011). To make it fixable by aldehyde based fixatives, a lysine conjugated form is used (Lanciego and Wouterlood 2011). BDA conjugates can homogeneously fill the long-range projecting axons, revealing the fine morphology of boutons or en-passant terminals (Brandt and Apkarian 1992). A recent study systematically compared the quality and quantity of the anterograde tracing by BDA and adeno-associated virus (AAV) tracing in mouse, revealing a comparable sensitivity between the two tracers.

Another well applied anterograde tracer, the *phaseolus vulgaris*-leucoagglutinin (PHA-L) (Gerfen and Sawchenko 1984), is a lectin extracted from kidney bean (*phaseolus vulgaris*). It can be taken up by neuronal soma by receptor mediated endocytosis and exclusively transported in the anterograde direction (Gerfen and Sawchenko 1984; Lanciego and Wouterlood 2011). Similar to BDA, PHA-L is excellent in labeling axonal collaterals and terminals.

As a non-toxic protein fragment, cholera toxin subunit B (CTb) is primary used as a anterograde tracers, despite it also anterogradely fill axon terminals (Luppi et al. 1990). It can be taken up by axonal terminals and damaged fibers of passage (Luppi et al. 1990), which presumably transported from cell surface to cytosol via glycolipid receptors mediated endocytosis (Montecucco et al. 1994; Sandvig and van Deurs 2002; Lencer and Tsai 2003).

Fluorogold (FG) or by its official name, 2-hydroxy-4,4'-diamidinostilbene (hydroxystilbamidine) is a well-characterized retrograde tracer of small molecular weight (Schmued and Fallon 1986; Wessendorf 1991). The tracer is presumably able to cross the membrane and taken up by lysosomes and endosomes (Wessendorf 1991), which usually ends in cytoplasmic puncta-like structures. It can emit intrinsic fluorescence under UV light (Lanciego and Wouterlood 2011).

Retrobeads, or fluorescent latex microspheres, are sensitive retrograde tracers (Katz and Iarovici 1990) which usually result in fluorescent labeling of cytoplasmic granules in the neuronal soma (Katz and Iarovici 1990; Apps and Ruigrok 2007).

2.2.2 Immunohistochemistry

Immunofluorescent staining

The immunofluorescent staining usually take advantages of specific affinity binding between antibody and antigens. As a routine techniques to detect biomolecules, a workable and efficient protocol is often tailed to individual researchers. In our study, we applied an unlabeled primary antibody first to recognize a specific antigen, and subsequently a fluorophore conjugated secondary antibody to visualize the cellular localization of the primary antibody.

DAB immunohistochemistry

The DAB immunohistochemistry refers to immunoperoxidase detection of epitopes with chromogenic products from diaminobenzidine (DAB) reaction catalyzed by peroxidase. We employed a highly sensitive avidin-biotin-peroxidase complex (ABC) system, which provides a simple and robust way to amplify immunohistochemical signals in formalin fixed tissues (Hsu et al. 1981). Further, the product of DAB reaction can be modified by different metal ions, for example, to give a darker colored product by adding of nikel (Hsu and Soban 1982).

The catalyzed reporter deposition (CARD) method

The catalyzed reporter deposition (CARD), also known as tyramide-signal amplification (TSA) is based on peroxidase enzymatic reaction and can deposit tyramide conjugates to protein residues in close vicinity to the peroxidase (Adams 1992; Hunyady et al. 1996; Faget and Hnasko 2015). With fluorophore conjugated tyramide, it can achieve 10 to 100 fold sensitivity than conventional immunofluorescent staining (Hunyady et al. 1996; Bobrow and Moen 2001). Additionally, the combination of CARD and conventional immunofluorescent staining can enable double immunostaining with antibodies from same species (Hunyady et al. 1996).

2.2.3 Experimental designs

To trace the inputs and outputs, we injected single tracer into an EAc nucleus in the right hemisphere. To better meet “Three Rs” ethic guides, we usually injected an anterograde tracer in one EAc subdivision, and subsequently injected a retrograde tracer in another one. Then subsequent immunohistochemistry procedures were tailored to needs. For general connectivity, single DAB immunohistochemistry was used. For cellular identification of projection neurons, multi-color immunofluorescent staining was carried out after tract-tracing.

To explore the convergent inputs to STLD and CeL/C, we injected fluorogold into STLD and CTb into the ipsilateral CeL/C. The collateral input neurons were then revealed with double immunofluorescent staining and fluorescent microscopy.

CHAPTER II. RESULTS

1. Afferents to central extended amygdala

In this part, we will look at the general afferents (or inputs) to four major subdivisions of EAc, as well as convergent inputs to STLD and CeL/C.

We thus implemented retrograde tracing in distinct subdivisions of STL (STLD, STLV) and CeA (CEL/C, CeM) to label the projection neurons across the brain. The results are presented with graphic illustrations, semi-quantitative scoring of the afferent strength, and statistical comparisons of the collateral inputs and preferential ones. We also include a concise summary of comparative view of the afferents.

The results of this whole part is formatted as a preliminary manuscript which will be completed for submission to *Brain Structure and Functions*.

Afferents of central extended amygdala: general connectivity and collateral inputs

Jiahao Ye[1,2], Pierre Veinante*[1,2]

[1]Institut des Neurosciences Cellulaires et Intégratives, Centre National de la Recherche Scientifique;
[2]Université de Strasbourg, Strasbourg, France.

***Corresponding author**:
Pierre Veinante
Institut des Neurosciences Cellulaires et Intégratives, CNRS UPR3212, 5 rue Blaise Pascal, 67084, Strasbourg, France
Tel: +33 388 456 609
E-mail: veinantep@inci-cnrs.unistra.fr

Abstract

Lateral bed nucleus of stria terminalis (STL) and central nucleus of amygdala (CeA) are the two key components of central extended amygdala (EAc), which is a forebrain macrosystem that participates in fear, anxiety and pain. The STL and CeA display highly similar mesoscopic connectivities and neurochemical compositions, but also show dissociated roles in, for example, anxiety and fear. However, it is still not clear what the preferential afferents to different EAc subdivisions are. Here, we compared inputs to four major EAc subareas with sensitive retrograde tracers and focused on several collateral inputs to dorsal STL (STLD) and lateral/capsular part of CeA (CeL/C). We found that, for any pair of EAc subdivisions, common inputs of similar strength outnumbers preferential ones of differential strength. Some areas such as posterior basolateral nucleus of amygdala (BLP) and external lateral part of parabrachial nucleus (LPBE) innervate all four EAc subdivisions similarly. Surprisingly, at cellular level, there are major BLP collateral inputs, but very limited LPBE collateral ones to STLD and CeL/C. These results indicate that, while EAc nuclei are more likely to receive inputs from the same source, these inputs are also likely to be arisen from different neuron pools. The functional significance of distinct neuronal inputs to EAc nuclei from shared mesoscopic brain regions remains to be explored.

Key words: central extended amygdala, preferential input, tract-tracing

Abbreviations

5-HT: 5-hydroxytryptamine
A24a: cingulate cortex, area 24a
A25: cingulate cortex, area 25
A32: cingulate cortex, area 32
ac: anterior commissure
Acb: accumbens nucleus, core region
AcbC: accumbens nucleus, core region
AcbSh: accumbens nucleus, shell region
ACo: anterior cortical amygdaloid nucleus
AHA: anterior hypothalamic area
AHi: amygdalohippocampal area
AI: agranular insular cortex, anterior part
AIP: agranular insular cortex, posterior part
APir: amygdalopiriform transition area
Arc: arcuate hypothalamic nucleus
ASt: amygdalostriatal transition area
BLAc: basolateral amygdaloid nucleus, anterior part, caudal
BLAr: basolateral amygdaloid nucleus, anterior part, rostral
BLPc: basolateral amygdaloid nucleus, posterior part, caudal
BLPr: basolateral amygdaloid nucleus, posterior part, rostral
BLV: basolateral amygdaloid nucleus, ventral part
BMA: basomedial amygdaloid nucleus, anterior part
BMP: basomedial amygdaloid nucleus, posterior part
CA1: field CA1 of the hippocampus
CeC: central amygdaloid nucleus, capsular part
CeL: central amygdaloid nucleus, lateral part
CeL/C: lateral/capsular part of CeA
CeM: central amygdaloid nucleus, medial part
CGRP: calcitonin gene-related peptide
CGRP: calcitonin gene-related peptide
cl: claustrum
CLi: caudal linear nucleus of the raphe
CMc: central medial thalamic nucleus, caudal
CMr: central medial thalamic nucleus, rostral
CR: calretinin
CRF: corticotropin-releasing factor
CTb: cholera toxin subunit B
CxA: cortex-amygdala transition zone
DEn/IEn: dorsal/intermediate endopiriform nucleus
DI: dysgranular insular cortex
DIEnt: dorsal intermediate entorhinal cortex
DLEnt: dorsolateral entorhinal cortex
DMH: dorsomedial hypothalamic nucleus
DPAG: dorsal periaqueductal gray
DRC: dorsal raphe nucleus, caudal part
DRD: dorsal raphe nucleus, dorsal part
DRL: dorsal raphe nucleus, lateral part
DRV: dorsal raphe nucleus, ventral part
DTT: dorsal tenia tecta
EAc: central extended amygdala
EAm: medial extended amygdala
Ect/PRh: ectorhinal/perirhinal cortex
EW: Edinger-Westphal nucleus
FG: flurogold
Fu: bed nucleus of stria terminalis, fusiform part
GI: granular insular cortex
HDB: nucleus of the horizontal limb of the diagonal band
I: intercalated nuclei of the amygdala
IM: intercalated amygdaloid nucleus, main part
IMD: intermediodorsal thalamic nucleus
IPAC: interstitial nucleus of the posterior limb of the anterior commissure
isRt: isthmic reticular formation
KF: Kolliker-Fuse nucleus
KLH: Keyhole limpet hemocyanin
La: lateral amygdaloid nucleus
LaDL: lateral amygdaloid nucleus, dorsolateral part
LaVL: lateral amygdaloid nucleus, ventrolateral part
LaVM: lateral amygdaloid nucleus, ventromedial part
LC: locus coeruleus
LH: lateral hypothalamic area
LO: lateral orbital cortex
LOT: nucleus of the lateral olfactory tract
LPAG: lateral periaqueductal gray
LPBC: lateral parabrachial nucleus, central part
LPBCr: lateral parabrachial nucleus, crescent part
LPBD: lateral parabrachial nucleus, dorsal part
LPBE: lateral parabrachial nucleus, external part
LPBEc: lateral parabrachial nucleus, external central part
LPBV: lateral parabrachial nucleus, ventral part
LPBW: lateral parabrachial nucleus, waist part
LPO: lateral preoptic area
LSD: lateral septal nucleus, dorsal part
LSV: lateral septal nucleus, ventral part
MCLH: magnocellular nucleus of the lateral hypothalamus
MDM: mediodorsal thalamic nucleus, medial part
Me: medial amygdaloid nucleus
MeAD: medial amygdaloid nucleus, anterodorsal
MePD: medial amygdaloid nucleus, posterodorsal part
MePV: medial amygdaloid nucleus, posteroventral part
MGM: medial geniculate nucleus, medial part
MiTg: microcellular tegmental nucleus
MM: medial mamillary nucleus, medial part
MnPO: median preoptic nucleus
MnR: median raphe nucleus
MPA: medial preoptic area
MPB: medial parabrachial nucleus
MPBE: medial parabrachial nucleus, external part
MPO: medial preoptic nucleus
mRt: mesencephalic reticular formation
MTu: medial tuberal nucleus
NeuN: neuronal nuclei
opt: optic tract
Pa: paraventricular hypothalamic nucleus
PaF: parafascicular thalamic nucleus

PAGr: periaqueductal gray, rostral
PB: posphate buffer
PBP: parabrachial pigmented nucleus of the ventral tegmental area
PeF: perifornical nucleus
PFA: paraformaldehyde
PH: posterior hypothalamic nucleus
PHA-L: phaseolus vulgaris-leucoagglutinin
PIL/PoT: posterior intralaminar thalamic nucleus/posterior thalamic nuclear group, triangular part
Pir: piriform cortex
PKCδ: protein kinase C delta type
PLCo: posterolateral cortical amygdaloid area
PMCo: posteromedial cortical amygdaloid area
PoMn: posteromedian thalamic nucleus
PR: prerubral field
PSTh: parasubthalamic nucleus
PT: paratenial thalamic nucleus
PTe: pararetere nucleus
PTg: pedunculotegmental nucleus
PV: paraventricular thalamic nucleus
PVA: paraventricular thalamic nucleus, anterior part
PVG: periventricular gray
PVP: paraventricular thalamic nucleus, posterior part
RAPir: rostral amygdalopiriform area
RCh: retrochiasmatic area
Re: reuniens thalamic nucleus
REth: retroethmoid nucleus
RLi: rostral linear nucleus
RML: retromamillary nucleus, lateral part
RMM: retromamillary nucleus, medial part
RRF: retrorubral field
scp: superior cerebellar peduncle
SFO: subfornical organ
SHy: septohypothalamic nucleus
SIB: substantia innominata, basal part
SLEA: sublenticular extended amygdala
SNCD: substantia nigra, compact part, dorsal tier
SolM: solitary nucleus, medial part
SOM: somtatostatin
SPF: subparafascicular thalamic nucleus
ST: medial bed nucleus of stria terminalis
STIA: bed nucleus of the stria terminalis, intraamygdaloid division
STL: lateral bed nucleus of stria terminalis
STLD: bed nucleus of the stria terminalis, lateral division, dorsal part
STLJ: bed nucleus of the stria terminalis, lateral division, juxtacapsular part
STLP: bed nucleus of the stria terminalis, lateral division, posterior part
STLV: bed nucleus of the stria terminalis, lateral division, ventral part
STM: medial bed nucleus of stria terminalis
STMA: bed nucleus of the stria terminalis, medial division, anterior part
STMP: bed nucleus of the stria terminalis, medial division, posterior part
STMV: bed nucleus of the stria terminalis, medial division, ventral part
STS: bed nucleus of stria terminalis, supracapsular division
SubCV: subcoeruleus nucleus, ventral part
TeA: temporal association cortex
TH: tyrosine hydroxylase
Tu: olfactory tubercle
VLPAG: ventrolateral periaqueductal gray
VMH: ventromedial hypothalamic nucleus
VP: ventral pallidum
VPPC: ventral posterior nucleus of the thalamus, parvicellular
VS: ventral subiculum
VTAR: ventral tegmental area, rostral part
Xi: xiphoid thalamic nucleus

Introduction

Central extended amygdala (EAc) is a forebrain macrosystem that critically involved in a variety of psychiatric conditions such as anxiety, stress and chronic pain (Alheid and Heimer 1988; Heimer 2003; Waraczynski 2006; Shackman and Fox 2016; Waraczynski 2016; Lebow and Chen 2016; Neugebauer et al. 2004; Veinante et al. 2013; Neugebauer 2015). The two major components of EAc, the lateral bed nucleus of stria terminalis (STL) and central nucleus of amygdala (CeA), share high degree of structural similarity in cell types, neuron physiology and mesoscopic connectivity (Alheid and Heimer 1988; Sun and Cassell 1993; Veinante and Freund-Mercier 1998; Cassell et al. 1999). The overall mesoscopic connectivity of STL and CeA are well-studied based on different animal models including rats, cats and non-human primate (Jolkkonen and Pitkanen 1998; Price 2003; Dong et al. 2001a; Krettek and Price 1978a; Martin et al. 1991; Oler et al. 2017). For example, in rats both two structures receive inputs from insular cortex (InsCtx) (Saper 1982; McDonald 1998), lateral parabrachial nucleus (LPB) (Shimada et al. 1989; Krukoff et al. 1993) and paraventricular nucleus of the thalamus (PV) (Li and Kirouac 2008; Kirouac 2015). A comparative study on the shared afferents between EAc subdivisions of mouse is still lacking.

Consistent with mesoscopic common inputs, collateral neurons to EAc subdivisions have been reported in prefrontal cortical areas, hypothalamus, paraventricular nucleus of thalamus (PV) (Reynolds and Zahm 2005; Bienkowski and Rinaman 2013; Reichard et al. 2016; Dong et al. 2017). On the other hand, STL and CeA are functionally dissociable, for example, in fear and anxiety (Davis et al. 2009; Walker and Davis 2008). Preferential afferents that favor one EAc subdivision over another were also observed (Bienkowski and Rinaman 2013; Dong et al. 2017). A recent study on rat revealed significant amount of collateral inputs from caudal PV to dorsal part of STL (STLD) and lateral/capsular part of CeA (CeL/C) (Dong et al. 2017). PV also displays strong preferential innervations to medial CeA (CeM) and ventral STL (STLV) in rat (Bienkowski and Rinaman 2013). However, the preferential inputs and common inputs to STLD and CeL/C in mouse at cellular level remains elusive.

In this study, we took advantage of the sensitive retrograde tract-tracing techniques to label the projection neurons to four EAc subdivisions. We found differential strength of afferents from EAc nuclei, amygdala, medial prefrontal cortex, thalamus, hypothalamus, brain stem and the pons to different EAc subdivisions. However, common inputs of any two of EAc subdivisions outnumbers their preferential ones. We then went further to investigate the proportion of convergent and divergent inputs to STLD and CeL/C from the same brain areas, such as external lateral parabrachial nucleus (LPBE), paraventricular nucleus of thalamus

(PV) and posterior part of basolateral nucleus of amygdala (BLP). We also demonstrated collateral inputs from PV and BLP express calretinin (CR), a calcium-binding protein known to express in amygdala and thalamus (Arai et al. 1994; McDonald and Mascagni 2001).

METHODS

Animal

6 – 9 week-old adult male C57BL/6J mice (Charles River®, L'Arbresle, France) were raised in the standard housing cages for 3 - 5 weeks before experiments. Food and water were allowed for ad libitum access with a normal light-dark cycle (12/12-hour, 7 PM off). All the experimental procedures were implemented according to the regulations of European Communities Council Directive and were approved by the local ethical committee (CREMEAS under reference AL/61/68/02/13).

Anterograde tract-tracing

Animals were deeply anesthetized with a mixture of ketamine (87 mg/kg) and xylazine solution (13 mg/kg) via intraperitoneal (i.p.) injection. After that, metacam (2 mg/kg, subcutaneous, or s.c.) and bupivacaine (2 mg/kg, s.c.) were applied to reduce inflammatory response and induce local analgesia. The animal was then mounted onto a stereotaxic frame (Model 900, David Kopf Instrument) and a local craniotomy above the injection site was carried out with a surgical drill. Throughout the surgery, the eyes were moisturized with Ocry-gel (Laboratoire TVM, France) and monitored constantly.

A glass pipette (tip diameter 15-35 μm) was used to load tracer solutions and was positioned according to the coordinates (see Table 1). In this study, two different tracers had been used for retrograde tracing via iontophoresis (Midgard Model 51595, Stoelting Co.). The hydroxystilbamidine methanesulfonate (2% in 0.9% NaCl) (cat. #A22850, Molecular Probes®) as the fluorogold (FG) was injected for 10 min (+2 μA, 3 s ON/OFF cycle); and the cholera toxin B subunit (CTb; 0.25% in 0.1 M Tris buffer and 0.1% NaCl; cat. #C9903, Simga®) for 15 min (+4 - 5 μA, 3 s ON/OFF cycle). The pipette was left in place for 5 - 10 min before withdrawing, then a second injection at the ipsilateral side was made for the paired injection. For paired injection, FG and CTb were injected into STLD and CeL/C, respectively, via sequential iontophoresis.

After that, the lidocaine spray was applied near the wound and the scalp was sutured. The animal recovered from anesthesia and returned to the home cage with regular feeding

conditions. To get optimal labeling, a survival time of 7 - 14 days was allowed before sacrificing the animal.

Tissue preparation

Animals were euthanized with pentobarbital (273 mg/kg, i.p.) or Dolethal (300 mg/kg, i.p.). The loss of toe-pinch reflex was confirmed before surgery. Transcardial perfusion was performed with the ice-cold phosphate buffer (PB) (0.1 M, pH 7.4; 10 ml) and paraformaldehyde (PFA) (2%, in 0.1 M PB, pH 7.4; 150 ml). The brain was dissected out and post-fixed overnight (4 °C). Depending on the usages, brains were either sectioned immediately or stored in sodium azide solution (0.02%, in phosphate-buffered saline or PBS) for one week before sectioning.

Coronal sections (30 μm thickness) were cut with a vibratome (VT1000S, Leica Biosystem). Slices were sorted (120 μm apart, except 160 μm for Fig. 1) in PBS and kept in PBS or in sodium azide solution (0.02%, in PBS) depending on the needs.

Primary Antibody

In total, primary antibodies against the following antigens were used: neuronal nuclei (NeuN), corticotropin-releasing factor (CRF), tyrosine hydroxylase (TH), calcitonin gene-related peptide (CGRP), protein kinase C delta (PKCδ), somatostatin (SOM), calretinin (CR), CTb and FG. The specificity of primary antibodies are summarized in the Table 2 and were checked by omitting the primary antibody in immunostaining.

Immunostaining

Depending on the case, the molecules of interest were revealed either by immunohistochemistry (IHC) with chromogenic detection or immunofluorescent (IHF) labeling for multiple targets. All procedures were carried out on floating brain slices.

The IHC detection was performed as following. Slices were washed in PBS (3 x 5 min) and intrinsic peroxidase was inactivated by H_2O_2 (1% in 50% ethanol; Cat. #: H1009, Sigma™) for 20 min. Then, the non-specific binding sites were saturated by the blocking buffer (0.3% Triton X-100, 5% normal donkey serum in PBS). Then slices were incubated with primary antibody (see Table 2) overnight. The peroxidase was introduced with subsequent incubation of biotinylated secondary antibody (1.5 hr) and ABC-HRP system (1: 500; Cat. #: PK-6100, Vector Laboratories™). The following biotinylated secondary antibodies were used depending on the host species of primaries: the biotinylated horse-anti-goat secondary

antibody (1:400; Cat. #: BA-9500, Vector Laboratories ™), the biotinylated donkey-anti-mouse (1:500; Cat. #: 715-065-150, Jackson Immunoresearch ™) and the biotinylated rabbit donkey-anti-rabbit (1:500, Cat. #: RPN-1004, GE Healthcare UK Limited ™). For single chromogenic revelation, substrate solution of 3,3'-diaminobenzidine (DAB) (0.05%; Cat. #: D8001, Simag™), H_2O_2 (0.015%) in Tris-Cl buffer (50 mM, pH 7.5; adjusted from Tris-base, Ref. #: 26-128-3094-B, Euromedex ™, France) was applied for 5 – 10 min at room temperature. Slices were then left air-dried on Superfrost® plus slides (Thermo Fisher Scientific™) and cleaned in sequential ethanol or limonene solution (Roti®-Histol, Carl Roth™). Subsequently, slices were mounted in EUKITT® mounting medium (O. Kindler, ORSAtec GmbH, Germany) and coverslipped.

Double IHF labeling was performed to reveal FG and CTb, while triple IHF labeling to reveal FG- CTb-CR or CTb-CR-CGRP. The general procedures were as the following. Slice were washed in PBS and non-specific binding sites blocked by blocking buffer (as above). Slices were incubated in a mixture of primary antibodies overnight (see Table 2). After that, a mixture of fluorophore-conjugated secondary antibodies were incubated for 3 – 4 hrs at room temperature. Overall, the following secondary antibodies were used: donkey-anti-mouse, Cy3 conjugate (1:400; Cat. #: 715-165-150, Jackson Immunoresearch™); donkey-anti-rabbit, Cy5 conjugate (1:300; Cat. #: 711-175-152, Jackson Immunoresearch™); donkey-anti-goat, Alexa-488 conjugate (1:500, Cat. #A-11055, Invitrogen™). Nuclear counter staining with 4',6-Diamidino-2-Phenylindole, Dihydrochloride (DAPI, 300 nM; Cat.# D1306, Invitrogen™) was performed for 5 – 7 min at room temperature. The slices were then mounted in aqueous mounting medium (Fluoromount-G®, SouthernBiotech™).

Imaging and Data analysis

In general, bright-field microscopy was used for cases with IHC staining, and fluorescent microscopy (either epifluorescent or confocal microscopy) was used for cases with multiple IHF staining.

Bright-field images were acquired by Neurolucida 10.0 software (MBF Bioscience ™) on a Nikon Eclipse 80i microscope equipped with a MBF CX9000 digital camera (MBF Bioscience ™). Depending on the needs, different objectives (4x, 10x, 20x) were used. Contrast adjustment and image stitching (by the grid/collection stitching plugin) were performed in FIJI software (Preibisch et al. 2009; Schindelin et al. 2012). The semi-quantitative assessment were then carried out on brain sections of comparable bregma levels

for a given neuroanatomical region, according to the mouse brain atlas (Paxinos and Franklin 2012).

Epifluorescent images were taken either with a Leica DM R (Leica microsystem ™) or Axio Imager 2 system (Carl Zeiss™) equipped with optical filters for DAPI, FITIC, Cy3 and Cy5. Percentage of collateral inputs were done on epifluorescent images acquired at 10x objective, after confirming the colocalization at 20x and 40x objectives in principle. The subdivisions were delineated according to the cytoarchitecture (by DAPI) and manually mapped to the matched level of standard mouse brain atlas (Paxinos and Franklin 2012). The number of CTb-positive (CTb+), CTb and FG positive (CTb+FG+), FG-positive (FG+) neurons in each areas were then counted from two or three consecutive slices. The percentage of each category was determined for the every checked area in each injection case.

Confocal images of were taken with a Leica TCS SP5II confocal microscope (Leica Biosystem™). To demonstrate somatic colocalization of triple labeling (i.e. CTb-CR-CGRP), single-plane images were acquired at 2.5x Nyquist sampling rate under 20x objectives.

Statistics

For analysis of collateral inputs, mean value and the standard of the mean (SEM) were computed by R program (©The R Foundation), and reported accordingly. Unpaired Student's *t*-test was performed to reveal statistical difference between the means of group pairs.

RESULTS

Neurochemical features of subdivisions of central extended amygdala

Immunoreactivity of six molecular markers including NeuN, CGRP, PKCδ, SOM, CRF, TH were revealed on successive coronal sections containing STL and CeA (Fig. 1). And a semi-quantitative assessment of the relative intensity of immunoreactivities is summarized in Table 3.

In general, the EAc components (i.e. STL and CeA) were more strongly stained than medial extended amygdala (EAm) subdivisions (i.e. medial ST (STM) and medial nucleus of amygdala (Me)) (see Table 3). Within EAc, differential expressions were observed across subdivisions of STL and CeA.

The STLD had a lighter staining of NeuN, compared with the STLV and fusiform nucleus (Fu) (Fig. 1a2). In contrast, the STLD was specifically enriched with CGRP, PKCδ and CRF (Fig. 1b2, c2, e2), which at the same time outlined its oval shape of STLD. In addition, SOM+ (SOM-positive) soma and fibers were also abundant in STLD (Fig. 1d2), while TH+ axonal

terminals were light to moderate (Fig. 1f2). It worth to note that, the TH+ fiber seems to spread in patches, with much lighter density was observed in dorsal or ventral poles of STLD (Fig. 1f2). The STLV is just below the anterior commissure (ac), and is very close to the much smaller, amorphous Fu. The STLV was stained strongly in NeuN, moderately in CRF and TH, lightly in CGRP and SOM (Fig. 1a2 – f2). Similar to STLD, the Fu was stained faintly in NeuN and strong in CGRP, but rather light in SOM+ signal. Comparatively, the CRF and CGRP immunoreactivity was higher in Fu than medial STM (STMV) or STLV. Similar to STL, CeA also stands out obviously with strong staining of most of molecular markers that we tested. The CeA is situated ventrally to the caudate putamen and sandwiched by the optic tract (opt) and lateral nucleus of amygdala (Fig. 1g – l). Similar to STLD, lateral CeA (CeL) and capsular part of CeA (CeC) was especially abundant in PKCδ+ cells and CGRP+ axonal field, which largely traced out the shape of CeL/C (CeL and CeC) in a similar way. The CeLC were also weaker in NeuN staining (Fig. 1i2) than CeM, basolateral nucleus of amygdala (BLA) or Me. Among CeA subdivisions, the lateral part (CeL) has the densest SOM, CRF and TH signals comparing to the CeM or CeC (Fig. 1j2, k2, l2). The CeC harbors the highest expression levels in CGRP (Fig. 1b2), less intense in SOM and CRF, and very faint in TH staining.

Injection sites of general tract-tracing

An overview neuroanatomical locations of the CTb injection sites are shown (Fig. 2) by aligning them to the matched bregma level of the mouse brain atlas (Paxinos and Franklin 2012).

In this study, an eligible case for STLD injection can be located from bregma levels from +0.25 mm to +0.01 mm (Fig.2a1 – a2), which resulted in injection core located dorsally to anterior commissure and formed an apparent oval-shape with the diffusive labeling (Fig. 2a3). A good injection site for STLV(Fu) can be located from +0.25 mm to +0.01 mm, which featured by an inverted triangle-like diffusive background labeling ventrally to the anterior commissure (Fig. 2b3). The injection site of STLV(Fu) usually limited to the characteristic inverted triangular-like areas ventral to the horizontal ac fiber bundle, often with probably significant encroachment into the Fu, but not extended to STMV as evidenced by a lack of labeling in the Me subdivisions.

Similarly, a case with CeL/C can be found at bregma levels from -1.23 mm to -1.55 mm (Fig. 2c1 – c2), and the local diffusive labeling was usually restricted to the borders of capsular and lateral part of CeA, as this diffusive labeling was shapely reduced medially in the adjacent

CeM, laterally in BLA, and dorsally in the amygdalostriatal transition area (ASt) (Fig. 2c3). But due to its compact size, it is difficult to locate the CTb injection sites clearly to either CeC or CeL, thus we termed them together as CeL/C in the subsequent analysis.

Finally, for CeM, we targeted the rostral part from -0.83 mm to -1.23 mm (Fig. 2d1 – d2), and the injection usually led to dense diffusive labeling in caudal levels of CeM, but very lightly in caudal CeL/C.

In some cases with CTb injection in CeL/C or CeM, however, the presumed pipette track or a few neurons in ASt or globus pallidus were obvious with CTb immunoreactivity, but we rarely found retrograde labeled neurons from those leakage sites. We conclude that these leakages likely marginally contribute to the retrograde somatic labeling across the brain and cases like that were included into the analysis.

Inputs to EAc subdivisions

Overview of brain-wide mesoscopic inputs to EAc subdivisions

Overall, the inputs to STLD, CeL/C, STLV, or CeM are distributed from the caudal to rostral levels of brain. The main inputs come from cerebral cortical areas, hippocampal formation, telencephalonic nuclei, the thalamus, hypothalamus and brain stem nuclei. Among them, the heaviest inputs come from non-cortical telencephalonic areas such as basal ganglia, septum, amygdala, and extended amygdala, as well as from visceral and gustatory related insular cortical areas and pontine parabrachial nucleus.

To compare input strengths from the same source area, an arbitrary scoring system of six scales was used to semi-quantify a given input by its retrograde labeling. We applied this semi-quantification to all input areas to the four EAc subdivisions (Fig. 3). In total, most of the brain areas (total number = 139) send light or stronger inputs to EAc subdivisions, while 20 out of them projects to EAc very sparsely or absently.

We defined an input as a preferential one when the pairwise scoring difference of equal or greater than two scales is found (including the pair with intensities of ++ and -/+), otherwise a common input of light and greater intensity is defined. The numbers of preferential versus common inputs were summarized in the Table 4. We found 23 out them (16.5%) displayed preferential inputs to one EAc subdivision not others, while 113 of them (83.1%) projected similarly to at least two of the EAc nuclei. We also found common inputs outnumbered preferential inputs to any specific EAc subdivision in every comparison scheme (Table 4). In another words, common mesoscopic inputs to EAc are more likely than unique preferential

ones when inputs to any two of them compared. Here, we will start to describe some of the key comparative features of EAc afferents.

Inputs from EAc and EAm

The projection neurons were distributed heterogeneously within EAc subdivisions. In STL, very strong STLD inputs to STLV(Fu), light inputs to CeM, but very sparse inputs to CeL/C were observed (Fig. 4a, d, g, j). This intra-EAc projections was mirrored by the strong CeL/C inputs to CeM (Fig. 4l), but not in the opposite direction. However, as the major output nucleus of STL, STLV and especially the Fu, show very limited inputs to the rest EAc nuclei (Fig. 4 g – l). In contrast, as the output nucleus of CeA, CeM sent a moderate input to STLD and a strong one to STLV(Fu) (Fig. 4c, f, j, l). Besides, CeA →STL pathway was also mediated by strong inputs from CeL/C to STLD and to STLV(Fu) (Fig. 4c, f). The cell corridors of IPAC and SLEA both can provide strong input to CeM, weaker to STLV, light to STLD and Cel/C (Fig. 4b, e, h, k). In addition, the supracapsular part of ST (STS) also lightly innervate the STLD, CeL/C, STLV(Fu), but very sparsely the CeM.

Most EAm nuclei innervated EAc sparsely or lightly. The rostral to dorsal levels of STM innervate lightly or moderately the STLV(Fu), but o nly STMP project lightly the STLD and CeL/C. The caudal and rostral levels of Me can gives rise to light projection to CeM, sometimes to CeL/C.

Inputs from non-EA telencephalonic groups

Several of non-EA telencephalonic nuclei groups in basal ganglia, amygdala, and preoptic areas provided considerable inputs to EAc subdivisions.

In basal ganglia, the accumbens nucleus (Acb) had a strong projection to STLV(Fu), but very sparse or light ones to the rest divisions. The retrograde labeling from STLV(Fu) mainly was distributed in the dorsal part of shell region of Acb (AcbSh) which laterally bordered with AcbC, as well as medial and ventral part of core region of Acb (AcbC) that neighbored along the border with AcbSh.

Amygdaloid nuclei such as its basolateral nucleus, and cortical amygdaloid nucleus provided prominent driving forces to EAc. At its rostral levels, lateral nucleus of amygdala (La) provided moderate input to CeM only, with sparse/light input to others (Fig. 5a, d, g, j); in contrast, at more caudal level, light La inputs to STLD and CeL/C were observed. The anterior part of BLA also showed differential innervations at different rostral level and caudal level, which featured a strong rostral BLA (BLAr) (Fig. 5a, d, g, j) input innervating CeM and

a strong caudal BLA (BLAc) one innervating STLD (Fig. 5b, e, h, k). By contrast, the posterior part of basolateral nucleus of amygdala (BLP) at its rostral (BLPr) and caudal (BLPc) levels gave a more or less strong inputs to all the four EAc subdivisions (Fig. 5c, f, i, l), except only light innervations from BLPr was observed in CeL/C injection. The basomedial nucleus of amygdala at its anterior portion (BMA) innervated strongly to all four EAc nuclei, with less prominent innervations from its posterior portion (BMP).

Rostral levels of intercalated nucleus or the main nucleus (IM), which is located just ventrally to the BLA, sent strong inputs to CeM, light ones to STLV(Fu), but very sparse ones to STLD or CeL/C. However, its dorsomedial part (I) at more posterior levels, whose location was similar to that was described by Pinard and colleagues (Pinard et al. 2012), sent light inputs to CeL/C. Other amygdaloid nuclei such as cortical amygdaloid area and amygdalopiriform transition area, also provided differential inputs to EAc subdivisions. The cortical amygdaloid area at its anterior part (ACo) strongly innervated CeM, moderately to STLD, and lightly to CeL/C and STLV(Fu). By contrast, its posterior lateral part (PLCo) gave rise to moderate input to STLD, but very sparse one or absent to the rest three EAc divisions. The amygdalopiriform transition area also showed preferential strong innervations from its posterior part (APir) (Fig. 6c, f, i, l), rather than its rostral part (RAPir).

Other telencephalonic nuclei such as dorsal tenia tecta (DTT) of the ventral medial prefrontal cortex and the dorsal/intermediate endopiriform nucleus (DEn/IEn) also sent obvious inputs to CeM, but very sparse ones to other three. Also the basal part of substantia innominate (SIB) favored stronger inputs to STLV(Fu) and CeM, rather than STLD and CeL/C. We also observed light to sparse labeling in the subfornical organ (SFO) to STLV(Fu) and CeM.

Inputs from cortex and hippocampus

Ventromedial prefrontal cortical areas such as the area 24a (A24a), area 25 (A25), area 32 (A32) of cingulate cortex differentially innervated the STL and CeA subdivisions (Fig. 6a, d, g, j). Strong A25 inputs to STLV(Fu) and CeM were observed, presumably from the layer 6 and layer 5 respectively (Fig. 6g, j), which was reported to host projecting neurons in prefrontal cortex (Gabbott et al. 2005). Strong A24a inputs (mainly from layer 5) to STLV(Fu), moderate ones to STLD and CeM, sparse ones to CeL/C were observed. A32 had a moderate input STLD, but light one to STLV(Fu) and CeM, very sparse one to CeL/C (Fig. 6a, d, g, j). In addition, lateral orbital cortex (LO) also strongly projected to STLV(Fu), and lightly to STLD and CeM, but very sparsely to CeL/C.

Insula also sent prominent inputs to the EAc nuclei. The anterior part of agranular insular cortex (AI) strongly innervated CeM, while lightly or sparsely to others; in comparison, its posterior part (AIP) innervated CeM as well as CeL/C strongly. The dysgranular insular cortex (DI) and granular insular cortex (GI) both provided strong input to CeL/C and CeM, moderate ones to STLD, but only light or very sparse ones to STLV(Fu) (Fig. 6b, e h, k). Other cortical inputs such as piriform cortex (Pir), entorhinal cortex (Ent), ectorhinal/perirhinal cortex (Ect/PRh), favored stronger inputs to CeM while largely avoid STLV(Fu), and leaves mostly lighter inputs to STLD and CeL/C.

Hippocampal inputs to EAc subdivisions mainly came from the ventral pole of ventral subiculum (VS) and, to a lesser extent, the ventral part of field CA1 of the hippocampus (CA1) (Fig. 7a – d). Interestingly, heavier inputs from VS to STLD and to CeL/C were observed comparing to STLV(Fu) and CeM. On the other hand, the CA1 inputs to STL seems to be stronger than that to CeA.

Inputs from thalamus

Thalamic inputs to EAc nuclei mainly came from its midline nuclei group and posterior nuclei group. Among the midline thalamic nuclei, the paraventricular thalamic nucleus at its rostral (PVA), middle (PV) and rostral (PVP) levels displayed differential inputs to EAc subdivisions. Both STLD and STLV(Fu) received very strong inputs from PVA (Fig. 8a, c) but moderate or light ones from PV and PVP (Fig. 9a, c); by contrast, CeL/C and CeM received strong inputs from PVA (Fig. 8b, d) and PVP (Fig. 9b, d) respectively, moderate or light ones from the rest parts. Inputs from the paratenial thalamic nucleus (PT) was comparatively stronger in STLD than STLV(Fu), and in CeL/C than CeM (Fig. 8a – d). It worth noting that the xiphoid thalamic nucleus (Xi), which lined along the midline of the brain, sent a modest number of inputs to CeM, light ones to STLD and CeL/C (Fig. 8e – f). The parvicellular part of the ventral posterior nucleus of the thalamus (VPPC), the posterior intralaminar thalamic nucleus (PIL) and triangular part of posterior thalamic nuclear group (PoT), all provided notable amount of inputs to EAc nuclei, especially to CeA. The VPPC innervated CeM strongly, CeL/C moderately, but STLV lightly and STLD very sparsely (Fig. 9b – k). Significant inputs from retroethmoid nucleus (REth) and PIL/PoT to CeA, especially to CeM were also observed (Fig. 9c – l).

Inputs from hypothalamus

Hypothalamic inputs to EAc nuclei are distributed in its different compartments, including the anterior, tuberal, posterior and lateral parts. In general, STL and CeM were more innervated when comparing with the often sparsely innervated STLV(Fu).

The CeM, to a less extent STLV(Fu), received light inputs from the paraventricular hypothalamic nucleus (Pa) and anterior hypothalamic area (AHA) of anterior hypothalamus. In the tuberal group, dorsomedial hypothalamic nucleus (DMH) and ventromedial hypothalamic nucleus (VMH) innervated moderately or strongly the STLV(Fu) (Fig. 10a, d, g, j), and the medial tuberal nucleus (mTu) project moderately to both divisions of STL. The inputs from retrochiasmatic area (RCh) and the arcuate hypothalamic nucleus (Arc) were mostly sparse or light. Inputs from the posterior group were also very limited. It is worth noting that, light inputs from retromamillary nucleus to STLV were observed. In the lateral group, the lateral hypothalamus (LH) gave strong input to STLV and light ones to CeM, but very sparse to STLD and CeL/C (Fig. 10b, e, h, k). The more prominent source to all the EAc nuclei was the parasubthalamic nucleus (PSTh), which strongly projected to CeM and moderately to all the rest three (Fig. 10c, f, i, l).

Inputs from brain stem

Brain stem inputs come in several different levels including in the midbrain, pons and medulla. In midbrain, the periaqueductal gray (PAG) sent light input to STLV(Fu) but very sparse ones to the rest from its rostral part (PAGr); while at its rostral portion, the ventrolateral PAG (VLPAG) seemed equally innervated all the four EAc areas (Fig. 11b, e, h, k). Dopaminergic groups in dorsal tier of the compact part of substantia nigra (SNCD) and ventral tegmental area (VTA) largely avoided inputs to CeL/C, but gave light or moderate input to the rest three EAc subdivisions (Fig. 11a, d, g, j). The retrorubral field (RRF), however, provided light inputs to CeL/C, including light to moderate ones to the rest. Inputs from different subdivisions of raphe nuclei and reticular formation were mostly very sparse or light. At pontine levels, major inputs from LPBE were observed (Fig. 11c, f, i, j). The STLV and CeM, unlike the STLD and CeL/C, received light or moderate inputs from the waist part (LPBW) and the medial parabrachial nucleus (MPB). The locus coeruleus (LC), however, gave very sparse inputs to CeM, while stronger ones to the rest three. Finally, the solitary nucleus of medulla sent stronger input to STL than to CeA.

CGRP+ and CR+ neurons of LPBE project to EAc

As we showed previously that LPBE sends strong inputs to EAc nuclei, including STLV(Fu), there is still doubt of whether these retrogradely labeled neurons were indeed in LPBE as scattered CGRP-immunoreactive terminal and light LPBE projections had been reported in rat (Shimada et al. 1989; Alden et al. 1994). To further confirm a specific LPBE innervation to EAc nuclei including STLV and Fu, we performed triple immunofluorescent labeling of CTb (in green), calcitonin gene-related peptide (CGRP, in red) and calretinin (CR, in blue) to reveal the cellular identity of those retrogradely labeled LPB neurons. In LPB, both CGRP-expressing neurons and CR-expressing ones primarily aggregated in the LPBE subdivision (Fig. 12a3, a4), which largely overlapped the areas where retrograde labeled CTb+ neurons from STLV(Fu) was concentrated (Fig. 12a). Subsequent confocal imaging analysis revealed colocalization of CTb and CGRP (Fig. 12b, indicated by the arrows) in many LPBE neurons, most of which were also CR+. A similar colabeling of CTb and CGRP was also observed in LPBE subdivisions after retrograde labeling from STLD (Fig. 12c), CeM (Fig. 12d) and CeL/C (Fig. 12e). Thus, we confirmed prominent LPBE afferents, which were CGRP+ or CR+, projected to EAc subdivisions including STLV/Fu.

Collateral inputs to STLD and CeL/C

In our hands, about 30 (21.6%) brain areas are common inputs that sending light or stronger inputs to both the STLD and CeL/C (Table 4). But it is not clear how much divergent these common inputs can arise from the same group of cells. Therefore, we carried out double tract-tracing experiments from ipsilateral injection of two retrograde tracers, FG and CTb, into STLD and CeL/C, respectively, and revealed the collateral projection neurons by double immunofluorescent staining.

Injection sites of paired tract-tracing

After triple labeling of FG, CTb and DAPI, the injection sites (n = 3) were checked on successive slices and registered manually onto a matched level from the mouse brain atlas (Paxinos and Franklin 2012). Generally, injection sites of FG laid in the anterior to middle portion of STLD (Fig. 14a1 – a2), and the ones of CTb in middle to caudal levels of CeL/C (Fig. 14b1 – b2). Unlike to CTb injection, the FG injection in STLD usually resulted in substantial diffusive labeling in nearby areas such as STLP, but not any significant encroachment into STMA as evidenced by a lack of retrograde labeling other EAm subdivisions.

Convergent and divergent inputs to STLD and CeL/C

Although collateral neurons have been observed in several dozens of areas, we selected several prominent afferents including GI/DI, PV, BLPc, VLPAG, dorsal raphe nucleus (DR), and LPBE, to quantify the input convergence and divergence to STLD and CeL/C.

In GI and DI, projection neurons to STLD or CeL/C can be found in layer 4 – 6 (Fig. 14a1), and double-labeled ones mostly in layer 4-5 (Fig. 14a2, indicated by short arrows). In GI, the CeL/C-only projecting neurons (71.6% ± 1.7%) was significantly denser than that STLD-projecting ones (19.6% ± 1.4%; CeL/C-only vs. STLD-only, p = 0.0023, n = 3, Student's unpaired *t*-test) (Fig. 14a3). By contrast, 8.9% ± 0.4% projection neurons provided collaterals to both STLD and FG (Fig. 14a3). The difference between mean of each group in GI were statistically significant (CeL/C-only vs. Both, p = 0.00135; CeL/C-only vs. STLD-only, p = 0.002299, n = 3; STLD-only vs. Both, p = 0.03548, n = 3) (Fig. 14a3). Similarly, the DI had a similar strong projection to CeL/C (64.4% ± 1.7%), compared to that to STLD (23.5% ± 1.5%), while a similar portion (12.1% ± 0.4%) projected to both (Fig. 14a3). Similar to GI, statistical significance also existed between each pairs of DI projection neurons (CeL/C-only vs. Both, p = 0.001765, n = 3; CeL/C-only - STLD-only, p =0.00048, n = 3; STLD-only vs. Both, p = 0.03868, n = 3) (Fig. 14a3).

Depending on the rostral to caudal levels, the percentage of PV projection neurons to STLD and CeL/C could be quite varied (Fig. 14b). The anterior part, that is PVA, sent much higher proportion only to STLD (60.0% ± 2.6%) than that only to CeL/C (28.3% ± 2.7%, p = 0.008363), with a much lower level of collateralization (11.6% ± 0.6%, p = 0.006184) (Fig. 14b3). In contrast, the middle level of PV projected roughly similarly to STLD (43.8% ± 3.9%) and CeL/C (35.7% ± 4.7%), but had a much higher proportion of collateral neurons (20.4% ± 0.8%) (Fig. 14b3).

In the caudal level of BLP (bregma -2.45 mm), a large proportion of neurons (45.6% ± 1.1%) projected collaterally to STLD and CeL/C (Fig. 14c1). This subdivision also harbored a comparable large portion of STLD-only projecting neurons (41.5% ± 2.4%, Student's unpaired *t*-test, p = 0.4339 for Both vs. STLD-only, n = 3) (Fig. 14c3). Suprisingly, only marginal CeL/C-only projection neurons (12.9% ± 1.5%; p = 0.0067 for CeL/C-only vs. Both, p = 0.0072 for CeL/C-only vs. STLD-only) was found (Fig. 14c3). In other words, among all the BLP projection neurons to CeL/C, 89.4% of them was shared with STLD; and this portion is 81.0% for STLD-projecting BLP neurons.

The projection neurons from VLPAG and DR tended to be divided comparably between the three categories (Fig. 14d1 – d2). In VLPAG, 30.7% ± 4.1% are CeL/C-only projection

neurons, 39.6% ± 4.7% were STLD-only ones, while 29.7% ± 2.9% were collateral ones(Fig. 14d3). In DR, 21.6% ± 2.3% were CeL/C-only projection neurons, 40.9% ± 5.4% were STLD-only ones, while 37.5% ± 3.6% were collateral projecting ones (Fig. 14d3). This means a major proportion of STLD-projecting DR neurons is shared by CeL/C, and vice versa.
In LPBE, however, a very low level of collateral inputs were observed, while strong inputs to STLD or CeL/C existed (Fig 14e1 – e2). The CeL/C-only and STLD-only projection neurons took up 43.7% ± 0.8% and 49.0% ± 0.2%, respectively (Fig. 14e3). Each of two groups of projection neurons outnumbers that of collateral ones (7.3% ± 0.8%) significantly ($p = 5.30E-05$ for CeL/C-only vs. Both, and $p = 0.00065$ for STLD-only vs. Both, Student's unpaired *t*-test) (Fig. 14e3). This implies two distinctive pools of LPBE projection neurons that preferentially target either STLD or CeL/C.

Collateral inputs from CR+ neurons

As we showed before, a substantial percentage of projection neurons in PV and BLP sent collaterals to both STLD and CeL/C, but the cellular identities of those neurons were not known. We carried out triple labeling of FG (red), CTb (green), and CR (blue) in slices containing PV (Fig. 16a – b) and caudal BLP (Fig. 16c – d). Confocal images showed specific expression of CR in both PV and caudal BLP (Fig. 16a, c). Further, we found many collateral projection neurons (STLD-only and CeL/C-only) also colocalized with CR in PV (Fig. 16b; indicated by arrow heads) and in caudal BLP (Fig. 16d; indicated by arrow heads). Thus, we provided the evidences showing that CR+ neurons in PV and BLP could send collaterals to both STLD and CeL/C.

DISCUSSIONS

In this study, we addressed mainly three aspects of afferents to EAc nuclei of mouse. First, afferents between STL and CeA subdivisions were compared to reveal preferential and common inputs. Second, divergent and convergent inputs to STLD or CeL/C were examined by double retrograde tracing. Third, cellular identity of input neurons in PV, BLP and LPBE were checked with triple straining of CTb, CR and CGRP.

Technical considerations

Injection sites

In this study, the accurate and non-confounding injection sites are the key steps towards comparative analysis of the inputs to the four EAc areas. For each animal, the injection sites

were checked on successive coronal sections containing the target nucleus. In general, we chose eligible cases based on the following rules of thumbs. First, in any cases there was only one dense injection core with the most intense diffusive labeling, and it was centered around a slight local lesion. Second, the injection core was restricted to local nucleus defined by its neuroanatomical shape (i.e. typical borders of CeL/C in Fig. 2a3, d3). Third, there was minimal confounding tracing from the leakage of tracers, which was checked case by case against known EAc and non-EAc input/output connections. Usually cases that match these criteria were also cross checked with injections in different nucleus. For instance, a CTb injection in STLD or in CeL/C could led to similar, characteristic axonal field in areas around the STLV, indicating a good agreement of projection patterns among the selected tracing cases. Due to a lack of strong anatomical boundary of rostral CeM, CTb injection site at this level usually impeded a direct judgement on the exact location. We combined indirect evidences either by confirming the confinement of diffusive CTb signal within CeM at the more caudal levels, but not extent to CeL/C or nearby areas, or by cross-checking the same with DAPI staining separately. However, in the case of STLV injection, it is highly possible that the retrograde labeling reflected the inputs of a combination of STLV and Fu.

Immunohistochemistry

In this study, the primary antibodies can be monoclonal or polyclonal depending on the sources. The specificity of antibodies were reported previously (see Table 2), and also tested against the negative control experiments. In our hands, all the antibodies resulted in specific characteristic labeling in known areas. For example, PKCδ+ signal was mostly abundant in thalamic nuclei, second by STLD and CeA, which was consistent with previous report on PKCδ-cre mouse line (Haubensak et al. 2010; Cai et al. 2014). We also detected dense CGRP+ signal in non-EAc areas, such as ASt, ventral striatum, which is also in line with previous report on rat (Dobolyi et al. 2005). Occasionally, strong but sparse somatic labeling was seen in hippocampus CA1 areas, most likely due to the intrinsic IgG expression in mouse tissue.

For the double or triple immunofluorescent labeling, the cross-reactions of different primary antibodies were mostly ruled out by checking against the negative control and known patterns of each antigen.

Delineations and nomenclatures

All the delineation and nomenclature are adapted from the Franklin & Paxinos brain atlas (Paxinos and Franklin 2012), except in this study we use sublenticular extended amygdala (SLEA) instead of extended amygdala (EA) and delineate additional two structures in LPB. To better delineate EAc subdivisions, we chose six molecular markers to reveal different aspects of neurochemical architectures of EAc subdivisions, including the cytoarchitectural organization (NeuN), intrinsic neuronal populations (PKCδ, SOM, CRF), exogenous neuropeptidergic input (CGRP) and monoaminergic innervations (TH) in STL and CeA (Fig. 1).

In bed nucleus of stria terminalis (ST), subdivisions usually are divided in two axis: the anterior-posterior axis and dorsal-ventral axis (Gungor and Pare 2016). But exactly how many divisions are there is debatable and usually is defined by individual study according to the use (Dong et al. 2001a; Gungor and Pare 2016). In this study, to make it simple, we divided the ST at its rostral level into five divisions, based on the microscopic distribution of the cytoplasm and salient neuronal markers (i.e. PKCδ or CGRP shows salient oval-shaped STLD, fusiform nuclei and CeL/C), with the reference to the Franklin & Paxinos brain atlas (Paxinos and Franklin 2012). We used STMA to stand for the combined divisions of STMA and STMAL in Franklin & Paxinos atlas (Paxinos and Franklin 2012). The borders of STLP and STMA were drawn based on a combination of NeuN staining and the prominent presence of TH+ fibers in STLP. Other subdivisions of dorsal STL, such as STLJ or STMP in its more posterior level were defined as that by Paxinos and Franklin (Paxinos and Franklin 2012).

In comparison, there are more consensus in how to delineate CeA than ST. It is well accepted that three major divisions exist in CeA, and that are CeC, CeL, and CeM in rat and mouse (Cassell et al. 1999; Calhoon and Tye 2015), even though other subdivisions were proposed occasionally (McDonald 1982; Cassell et al. 1986). To make it clear, we chose caudal levels of CeA to illustrate the neurochemical profiles of subdivisions because at these levels all the three subdivisions of CeA are relatively easy to tell. But their expression patterns were conserved in the rostral and more caudal sections. In particular, both STLD and CeL are characterized by specific expression of PKCδ, CGRP+ fibers, and lighter NeuN. The CeC area was traditionally well-defined in rat (McDonald 1982) but less clear in mouse as seen by different delineations in several publications (Haubensak et al. 2010; Li et al. 2013; Kim et al. 2016; Kim et al. 2017b). In our serial staining, we found a narrow strip of cells sandwiched by CeL and BLA, displaying quite distinct features, including fainter NeuN staining, strongest CGRP and almost a lack of TH, comparing to its neighbors such as CeL, BLA and Me. These features of CeC were maintained in its rostral levels as well.

Finally, we defined the waist areas of parabrachial nucleus (PBW), which was interweaved with the superior cerebellar peduncle (scp) and has been well-defined on rats (Bernard et al. 1993; Bester et al. 1997). In our study, PBW has stronger inputs to STLV and CeM, but very sparse ones to STLD or CeL/C (Fig. 3). We also assigned a central external part of LPB (LPBEc), which is a thin lamina-like cell groups that course along the lateral border of scp (Fig. 11c – l). This area is largely overlapping with the central part (LPBC) (Paxinos and Watson 2007) or the ventral lateral part (PBvl) in rat (Bernard et al. 1993). They also stained distinctively in NeuN (unpublished data), and Nissl. In addition, we found a light retrograde labeling from CeM but only very sparse one from the rest EAc nuclei that we tested.

Differential inputs and functional implications

Inputs from extended amygdala

On the whole, EAc subdivisions are likely more intensely innervated by EAc nuclei than by EAm (Fig. 3), which is consistent with the classic view of distinction between central and medial divisions of extended amygdala (Alheid 2003). EAc subdivisions are extensively interconnected (Fig. 16), while only STMP of EAm gives significant inputs to all but CeL/C in our hands.

Intra-EAc afferents to STLV(Fu) and CeM tends to be bidirectionally connected, while those to STLD and CeL/C tends to be unidirectionally linked (Fig. 16). This unidirectional information flow within STL and CeA has also been reported in rats and mice (Dong et al. 2001b; Ciocchi et al. 2010; Haubensak et al. 2010; Li et al. 2013). In our data, we also observed preferential innervation from CeL/C to STLV(Fu), which was in line with previous study on rats (Dong et al. 2001a). The unidirectional projection EAc partly contributed to the heavily innervated STLV(Fu) and CeM, comparing to STLD or CeL/C (Fig. 16), while STLV(Fu) is likely under strong influence of CeM.

Inputs from amygdala

Amygdaloid nuclei have long been known to innervate subdivisions of CeA (Krettek and Price 1978b; Smith and Pare 1994; Pare et al. 1995; Savander et al. 1995; Pitkanen et al. 1997; Jolkkonen and Pitkanen 1998; McDonald 1991) and of STL (Krettek and Price 1978a; Dong et al. 2001a; McDonald 1991). We found similarly strong inputs from basal nuclei group and amygdalopiriform area amygdala to all four EAc subdivision, which are in line with previous reports (McDonald 1991; Pare et al. 1995; Reichard et al. 2016; Jolkkonen et al. 2001).

On the other hand, we also noticed some discrepancies in our study. Dong and colleagues reported light to moderate inputs to STLD and Fu, while absence of inputs from BMP in rats (Dong et al. 2001a). Petrovich and colleagues showed light axonal projections from BMA to CeL/C and STL, only moderate to strong ones to CeM in rats (Petrovich et al. 1996). In our study, we observed very intense BMA inputs and less strong BMP inputs to all the four EAc subdivisions (Fig. 3, Fig. 16). This discrepancy might be attributed to the species difference, or likely by different properties of anterograde versus retrograde tracers.

There are evidences suggesting different groups of BLA projection neurons that innervate different targets. Optogenetic activation of BLA→ CeL projection induce anxiolytic effect while no effect was observed with direct optogenetic manipulation on BLA soma (Tye et al. 2011). Distinctive roles of BLA→ CeM pathway versus BLA→STL in acute, phasic fear response versus sustained ones have been proposed (Walker and Davis 2008). More recently, Kim and colleagues revealed two distinctive principle neuronal populations expressing either *Rspo2* or *Ppp1r1b* in basolateral group of amygdala, mediated opposing roles in fear, reward and appetitive behavior (Kim et al. 2016; Kim et al. 2017b). Even though the author did not specify BLA versus BLP in their study, they noticed spatial segregations of *Rspo2*-expressing and *Ppp1r1b*-expressing neurons along the rostral-caudal axis basolateral amygdala, which correspond to the anterior, magnocellular part and the posterior, parvocellular part respectively (Kim et al. 2016). Our data suggests that, there are preferential projections to different EAc nuclei from BLA versus BLP. We also observed robust inputs from caudal BLP, to all four EAc subareas, while strong BLA inputs to STLD and CeM. As different compartment of STL and CeA can also play opposing roles, partly through the local inhibitory control, one can image BLP → CeL/C pathway and BLP → CeM pathway might exert opposing role in controlling the same behavior.

Inputs from thalamus

We observed light to moderate amount of retrograde labeling in the xiphoid thalamic nucleus (Xi). However, considering the total size of the Xi, this light or modest inputs reflect strong density and proportion of EAc-projecting neurons, especially to CeM. The function role of Xi → EAc pathway remains to be explored.

Input from ventral hippocampus

The ventral hippocampal pathway to EAc were unveiled with anterograde and retrograde tract-tracing in rat (Pitkanen et al. 2000; Kishi et al. 2006; Canteras and Swanson 1992). But

there are some inconsistency reported. For example, STLD was largely avoided by PHA-L injection in ventral hippocampus (Cenquizca and Swanson 2006) while caudal CeL/C was strongly innervated (Canteras and Swanson 1992). With both anterograde and retrograde tracing, little ventral hippocampal retrograde labing to CeA were found in rats (Kishi et al. 2006), by contrast strong VS projection to CeA was observed (Pitkanen et al. 2000). Here, we observed strong ventral hippocampal inputs to EAc nuclei, especially the STLD and CeL/C. The different results might come from the subtle differences of injection sites in ventral subiculum areas in different studies, as in our study, EAc-projecting hippocampal neurons tended to locate dispersedly along the septal-ventral axis. It is also possible that there is species difference in this pathway. For example, Xu and colleagues demonstrated functional role of ventral hippocampal to CeA projection neurons in memory retrieval in mice (Xu et al. 2016). As ventral hippocampal network is implicated in affective behaviors and fear responses (Fanselow and Dong 2010; Xu et al. 2016; Sierra-Mercado et al. 2011; Adhikari 2014), it is likely strong ventral hippocampal inputs to EAc might be involved in these functions as well.

Common and region-specific inputs to STLD and CeL/C

We chose 8 out of the 30 shared inputs of similar strength to STLD and CeL/C, and observed three types of afferents (Fig. 14). The first type has dominant preferential inputs and limited collateral (i.e. insula and LPBE); the second one shows strong collaterals (i.e. BLP); the third one display more or less equal strength of preferential inputs and collaterals (i.e. VLPAG, DR).

By double tract-tracing using two different CTb Alexa Fluor conjugates (CTb-488 and CTb-594), Dong and colleagues reported more region-specific than collateral projection neurons from paraventricular nucleus of hypothalamus to CeL or STLD in rats (Dong et al. 2017). Our results revealed a similar dominance of region-specific projection neurons in rostral and caudal part, but significantly more STLD-projecting neurons in the rostral portion. Interestingly, a much lower portion of PV collaterals to STLV and CeM was found in rats (Bienkowski and Rinaman 2013).

We reported 7.3% of LPBE projection neurons to STLD and CeL/C made collaterals. A similar proportion of LPBE projection neurons to CeM and STLV was reported in rats (Bienkowski and Rinaman 2013). Thus, there are likely two distinct projection neuron pools in LPBE that project to STLD and CeL/C in rodents.

The functional implications of distinctive LPBE projection neuron pools are extensive. There could be functional segregations in STLD-projecting versus CeL/C projecting CGRP+ neurons. Functional manipulations of LPBE CGRP+ neurons or $LPBE^{CGRP+}$ → CeL/C pathway critically affect fear learning and pain signaling (Han et al. 2015). Optogenetic activation of either CGRP+ neurons in LPBE, or CGRP+ axons in CeL/C reduce food intake (Carter et al. 2013). The $LPBE^{CGRP+}$ → STLD pathway might play a different role other than feeding behavior. The LPBE-EAc is an important component of pain pathway (Gauriau and Bernard 2002) and optogenetic activation of LPBE neurons could replace electric shock as a unconditioned stimulus for associative fear learning (Sato et al. 2015). Considering CeA and ST were proposed to be critical for phasic fear and sustained fear respectively (Davis et al. 2009), STLD-projecting and CeL/C-projecting neurons in LPBE might be differently activated by different stimuli.

Cell-types of afferent neurons to EAc

In this study, we found CR+ (calretinin positive) neurons and CGRP+ ones projected to all four EAc subdivisions. In particular, retrograde tracing from STLV(Fu) also labeled many CGRP+ neurons in LPBE. The functional roles of LPBE → STLV/Fu pathway is not clear. We also found collateral afferent neurons in PV and BLP expressed CR. CR+ neurons in dorsal horn are implicated in pain processing (Smith et al. 2015). A major portion of GABAergic interneurons in basolateral amygdala express CR (McDonald and Mascagni 2001). It is possible some of the CR+ EAc-projecting BLP neurons are GABAergic.
There are other well-known monoaminergic afferents to EAc. For example, dopamine neurons in PAG and DR specifically target STLD and CeL/C (Li et al. 2016). It is likely some of the collateral neurons in VLPAG and DR could be dopaminergic.

CONCLUSIONS

The STL and CeA have been well known to mediate various behaviors including fear and anxiety. While they each can be conceptualized as a whole functional unit (Walker et al. 2003; Davis et al. 2009; Wilensky et al. 2006; Tovote et al. 2015), functional antagonisms by different subdivisions of STL and CeA were reported more recently (Kim et al. 2013; Jennings et al. 2013; Tovote et al. 2015; Ciocchi et al. 2010). In this study, we revealed two seemingly puzzling features of EAc inputs. At one hand, common inputs of similar strength, not of differential strength, are more likely to be encountered between any pair of EAc subdivision. On the other hand, a common input to EAc subdivisions can be arisen from

distinctive pathway-specific neuron pools. These convergent and divergent pathways from one afferent area might differentially regulate functions of EAc macrosystem. By taking advantage of the well-developed transgenic and optogenetic toolsets (Tovote et al. 2015; Kim et al. 2017a) and molecular profiling of novel cell-types (Nectow et al. 2015; Usoskin et al. 2015), future studies of dissecting the differential function roles of path-specific inputs to EAc nuclei can be very promising.

REFERENCES

Adhikari A (2014) Distributed circuits underlying anxiety. Front Behav Neurosci 8:112. doi:10.3389/fnbeh.2014.00112

Alden M, Besson JM, Bernard JF (1994) Organization of the efferent projections from the pontine parabrachial area to the bed nucleus of the stria terminalis and neighboring regions: a PHA-L study in the rat. J Comp Neurol 341 (3):289-314. doi:10.1002/cne.903410302

Alheid GF (2003) Extended amygdala and basal forebrain. Ann N Y Acad Sci 985:185-205. doi:10.1111/j.1749-6632.2003.tb07082.x

Alheid GF, Heimer L (1988) New perspectives in basal forebrain organization of special relevance for neuropsychiatric disorders: the striatopallidal, amygdaloid, and corticopetal components of substantia innominata. Neuroscience 27 (1):1-39

Arai R, Jacobowitz DM, Deura S (1994) Distribution of calretinin, calbindin-D28k, and parvalbumin in the rat thalamus. Brain Res Bull 33 (5):595-614

Bernard JF, Alden M, Besson JM (1993) The organization of the efferent projections from the pontine parabrachial area to the amygdaloid complex: a Phaseolus vulgaris leucoagglutinin (PHA-L) study in the rat. J Comp Neurol 329 (2):201-229. doi:10.1002/cne.903290205

Bester H, Besson JM, Bernard JF (1997) Organization of efferent projections from the parabrachial area to the hypothalamus: a Phaseolus vulgaris-leucoagglutinin study in the rat. J Comp Neurol 383 (3):245-281

Bienkowski MS, Rinaman L (2013) Common and distinct neural inputs to the medial central nucleus of the amygdala and anterior ventrolateral bed nucleus of stria terminalis in rats. Brain Struct Funct 218 (1):187-208. doi:10.1007/s00429-012-0393-6

Cai H, Haubensak W, Anthony TE, Anderson DJ (2014) Central amygdala PKC-delta(+) neurons mediate the influence of multiple anorexigenic signals. Nat Neurosci 17 (9):1240-1248. doi:10.1038/nn.3767

Calhoon GG, Tye KM (2015) Resolving the neural circuits of anxiety. Nat Neurosci 18 (10):1394-1404. doi:10.1038/nn.4101

Canteras NS, Swanson LW (1992) Projections of the ventral subiculum to the amygdala, septum, and hypothalamus: a PHAL anterograde tract-tracing study in the rat. J Comp Neurol 324 (2):180-194. doi:10.1002/cne.903240204

Carter ME, Soden ME, Zweifel LS, Palmiter RD (2013) Genetic identification of a neural circuit that suppresses appetite. Nature 503 (7474):111-114. doi:10.1038/nature12596

Cassell MD, Freedman LJ, Shi C (1999) The intrinsic organization of the central extended amygdala. Ann N Y Acad Sci 877:217-241

Cassell MD, Gray TS, Kiss JZ (1986) Neuronal architecture in the rat central nucleus of the amygdala: a cytological, hodological, and immunocytochemical study. J Comp Neurol 246 (4):478-499. doi:10.1002/cne.902460406

Cenquizca LA, Swanson LW (2006) Analysis of direct hippocampal cortical field CA1 axonal projections to diencephalon in the rat. J Comp Neurol 497 (1):101-114. doi:10.1002/cne.20985

Chen Y, Molet J, Gunn BG, Ressler K, Baram TZ (2015) Diversity of Reporter Expression Patterns in Transgenic Mouse Lines Targeting Corticotropin-Releasing Hormone-Expressing Neurons. Endocrinology 156 (12):4769-4780. doi:10.1210/en.2015-1673

Chung EK, Chen LW, Chan YS, Yung KK (2008) Downregulation of glial glutamate transporters after dopamine denervation in the striatum of 6-hydroxydopamine-lesioned rats. J Comp Neurol 511 (4):421-437. doi:10.1002/cne.21852

Ciocchi S, Herry C, Grenier F, Wolff SB, Letzkus JJ, Vlachos I, Ehrlich I, Sprengel R, Deisseroth K, Stadler MB, Muller C, Luthi A (2010) Encoding of conditioned fear in central amygdala inhibitory circuits. Nature 468 (7321):277-282. doi:10.1038/nature09559

Davis M, Walker DL, Miles L, Grillon C (2009) Phasic vs sustained fear in rats and humans: role of the extended amygdala in fear vs anxiety. Neuropsychopharmacology 35 (1):105-135. doi:10.1038/npp.2009.109

Dobolyi A, Irwin S, Makara G, Usdin TB, Palkovits M (2005) Calcitonin gene-related peptide-containing pathways in the rat forebrain. J Comp Neurol 489 (1):92-119. doi:10.1002/cne.20618

Dong HW, Petrovich GD, Swanson LW (2001a) Topography of projections from amygdala to bed nuclei of the stria terminalis. Brain Res Brain Res Rev 38 (1-2):192-246

Dong HW, Petrovich GD, Watts AG, Swanson LW (2001b) Basic organization of projections from the oval and fusiform nuclei of the bed nuclei of the stria terminalis in adult rat brain. J Comp Neurol 436 (4):430-455

Dong X, Li S, Kirouac GJ (2017) Collateralization of projections from the paraventricular nucleus of the thalamus to the nucleus accumbens, bed nucleus of the stria terminalis, and central nucleus of the amygdala. Brain Struct Funct. doi:10.1007/s00429-017-1445-8

Fanselow MS, Dong HW (2010) Are the dorsal and ventral hippocampus functionally distinct structures? Neuron 65 (1):7-19. doi:10.1016/j.neuron.2009.11.031
Franke-Radowiecka A (2011) Immunohistochemical characterisation of dorsal root ganglia neurons supplying the porcine mammary gland. Histol Histopathol 26 (12):1509-1517. doi:10.14670/HH-26.1509
Furmanski O, Gajavelli S, Lee JW, Collado ME, Jergova S, Sagen J (2009) Combined extrinsic and intrinsic manipulations exert complementary neuronal enrichment in embryonic rat neural precursor cultures: an in vitro and in vivo analysis. J Comp Neurol 515 (1):56-71. doi:10.1002/cne.22027
Gabbott PL, Warner TA, Jays PR, Salway P, Busby SJ (2005) Prefrontal cortex in the rat: projections to subcortical autonomic, motor, and limbic centers. J Comp Neurol 492 (2):145-177. doi:10.1002/cne.20738
Gauriau C, Bernard JF (2002) Pain pathways and parabrachial circuits in the rat. Exp Physiol 87 (2):251-258. doi:EPH_2357 [pii]
Gungor NZ, Pare D (2016) Functional Heterogeneity in the Bed Nucleus of the Stria Terminalis. J Neurosci 36 (31):8038-8049. doi:10.1523/JNEUROSCI.0856-16.2016
Han S, Soleiman MT, Soden ME, Zweifel LS, Palmiter RD (2015) Elucidating an Affective Pain Circuit that Creates a Threat Memory. Cell 162 (2):363-374. doi:10.1016/j.cell.2015.05.057
Haubensak W, Kunwar PS, Cai H, Ciocchi S, Wall NR, Ponnusamy R, Biag J, Dong HW, Deisseroth K, Callaway EM, Fanselow MS, Luthi A, Anderson DJ (2010) Genetic dissection of an amygdala microcircuit that gates conditioned fear. Nature 468 (7321):270-276. doi:10.1038/nature09553
Heimer L (2003) A new anatomical framework for neuropsychiatric disorders and drug abuse. Am J Psychiatry 160 (10):1726-1739. doi:10.1176/appi.ajp.160.10.1726
Jennings JH, Sparta DR, Stamatakis AM, Ung RL, Pleil KE, Kash TL, Stuber GD (2013) Distinct extended amygdala circuits for divergent motivational states. Nature 496 (7444):224-228. doi:10.1038/nature12041
Jhou TC, Geisler S, Marinelli M, Degarmo BA, Zahm DS (2009) The mesopontine rostromedial tegmental nucleus: A structure targeted by the lateral habenula that projects to the ventral tegmental area of Tsai and substantia nigra compacta. J Comp Neurol 513 (6):566-596. doi:10.1002/cne.21891
Jolkkonen E, Miettinen R, Pitkanen A (2001) Projections from the amygdalo-piriform transition area to the amygdaloid complex: a PHA-l study in rat. J Comp Neurol 432 (4):440-465
Jolkkonen E, Pitkanen A (1998) Intrinsic connections of the rat amygdaloid complex: projections originating in the central nucleus. J Comp Neurol 395 (1):53-72
Kim CK, Adhikari A, Deisseroth K (2017a) Integration of optogenetics with complementary methodologies in systems neuroscience. Nat Rev Neurosci 18 (4):222-235. doi:10.1038/nrn.2017.15
Kim J, Pignatelli M, Xu S, Itohara S, Tonegawa S (2016) Antagonistic negative and positive neurons of the basolateral amygdala. Nat Neurosci 19 (12):1636-1646. doi:10.1038/nn.4414
Kim J, Zhang X, Muralidhar S, LeBlanc SA, Tonegawa S (2017b) Basolateral to Central Amygdala Neural Circuits for Appetitive Behaviors. Neuron 93 (6):1464-1479 e1465. doi:10.1016/j.neuron.2017.02.034
Kim SY, Adhikari A, Lee SY, Marshel JH, Kim CK, Mallory CS, Lo M, Pak S, Mattis J, Lim BK, Malenka RC, Warden MR, Neve R, Tye KM, Deisseroth K (2013) Diverging neural pathways assemble a behavioural state from separable features in anxiety. Nature 496 (7444):219-223. doi:10.1038/nature12018
Kirouac GJ (2015) Placing the paraventricular nucleus of the thalamus within the brain circuits that control behavior. Neurosci Biobehav Rev 56:315-329. doi:10.1016/j.neubiorev.2015.08.005
Kishi T, Tsumori T, Yokota S, Yasui Y (2006) Topographical projection from the hippocampal formation to the amygdala: a combined anterograde and retrograde tracing study in the rat. J Comp Neurol 496 (3):349-368. doi:10.1002/cne.20919
Krettek JE, Price JL (1978a) Amygdaloid projections to subcortical structures within the basal forebrain and brainstem in the rat and cat. J Comp Neurol 178 (2):225-254. doi:10.1002/cne.901780204
Krettek JE, Price JL (1978b) A description of the amygdaloid complex in the rat and cat with observations on intra-amygdaloid axonal connections. J Comp Neurol 178 (2):255-280. doi:10.1002/cne.901780205
Krukoff TL, Harris KH, Jhamandas JH (1993) Efferent projections from the parabrachial nucleus demonstrated with the anterograde tracer Phaseolus vulgaris leucoagglutinin. Brain Res Bull 30 (1-2):163-172
Lebow MA, Chen A (2016) Overshadowed by the amygdala: the bed nucleus of the stria terminalis emerges as key to psychiatric disorders. Mol Psychiatry 21 (4):450-463. doi:10.1038/mp.2016.1
Li C, Sugam JA, Lowery-Gionta EG, McElligott ZA, McCall NM, Lopez AJ, McKlveen JM, Pleil KE, Kash TL (2016) Mu Opioid Receptor Modulation of Dopamine Neurons in the Periaqueductal Gray/Dorsal Raphe: A Role in Regulation of Pain. Neuropsychopharmacology 41 (8):2122-2132. doi:10.1038/npp.2016.12
Li H, Penzo MA, Taniguchi H, Kopec CD, Huang ZJ, Li B (2013) Experience-dependent modification of a central amygdala fear circuit. Nat Neurosci 16 (3):332-339. doi:10.1038/nn.3322

Li S, Kirouac GJ (2008) Projections from the paraventricular nucleus of the thalamus to the forebrain, with special emphasis on the extended amygdala. J Comp Neurol 506 (2):263-287. doi:10.1002/cne.21502
Martin LJ, Powers RE, Dellovade TL, Price DL (1991) The bed nucleus-amygdala continuum in human and monkey. J Comp Neurol 309 (4):445-485. doi:10.1002/cne.903090404
McDonald AJ (1982) Cytoarchitecture of the central amygdaloid nucleus of the rat. J Comp Neurol 208 (4):401-418. doi:10.1002/cne.902080409
McDonald AJ (1991) Topographical organization of amygdaloid projections to the caudatoputamen, nucleus accumbens, and related striatal-like areas of the rat brain. Neuroscience 44 (1):15-33
McDonald AJ (1998) Cortical pathways to the mammalian amygdala. Prog Neurobiol 55 (3):257-332
McDonald AJ, Mascagni F (2001) Colocalization of calcium-binding proteins and GABA in neurons of the rat basolateral amygdala. Neuroscience 105 (3):681-693
Nectow AR, Ekstrand MI, Friedman JM (2015) Molecular characterization of neuronal cell types based on patterns of projection with Retro-TRAP. Nat Protoc 10 (9):1319-1327. doi:10.1038/nprot.2015.087
Neugebauer V (2015) Amygdala pain mechanisms. Handb Exp Pharmacol 227:261-284. doi:10.1007/978-3-662-46450-2_13
Neugebauer V, Li W, Bird GC, Han JS (2004) The amygdala and persistent pain. Neuroscientist 10 (3):221-234. doi:10.1177/1073858403261077
Oler JA, Tromp DP, Fox AS, Kovner R, Davidson RJ, Alexander AL, McFarlin DR, Birn RM, B EB, deCampo DM, Kalin NH, Fudge JL (2017) Connectivity between the central nucleus of the amygdala and the bed nucleus of the stria terminalis in the non-human primate: neuronal tract tracing and developmental neuroimaging studies. Brain Struct Funct 222 (1):21-39. doi:10.1007/s00429-016-1198-9
Pare D, Smith Y, Pare JF (1995) Intra-amygdaloid projections of the basolateral and basomedial nuclei in the **cat:** Phaseolus vulgaris-leucoagglutinin anterograde tracing at the light and electron microscopic level. Neuroscience 69 (2):567-583
Paxinos G, Franklin K (2012) Paxinos and Franklin's The mouse brain in stereotaxic coordinates. Fourth edition. edn. Academic Press, Amsterdam
Paxinos G, Watson C (2007) The Rat Brain in Stereotaxic Coordinates. In: 123Library. 6 edn. Academic Press,
Petrovich GD, Risold PY, Swanson LW (1996) Organization of projections from the basomedial nucleus of the amygdala: a PHAL study in the rat. J Comp Neurol 374 (3):387-420. doi:10.1002/(SICI)1096-9861(19961021)374:3<387::AID-CNE6>3.0.CO;2-Y
Pinard CR, Mascagni F, McDonald AJ (2012) Medial prefrontal cortical innervation of the intercalated nuclear region of the amygdala. Neuroscience 205:112-124. doi:10.1016/j.neuroscience.2011.12.036
Pitkanen A, Pikkarainen M, Nurminen N, Ylinen A (2000) Reciprocal connections between the amygdala and the hippocampal formation, perirhinal cortex, and postrhinal cortex in rat. A review. Ann N Y Acad Sci 911:369-391
Pitkanen A, Savander V, LeDoux JE (1997) Organization of intra-amygdaloid circuitries in the rat: an emerging framework for understanding functions of the amygdala. Trends Neurosci 20 (11):517-523
Preibisch S, Saalfeld S, Tomancak P (2009) Globally optimal stitching of tiled 3D microscopic image acquisitions. Bioinformatics 25 (11):1463-1465. doi:10.1093/bioinformatics/btp184
Price JL (2003) Comparative aspects of amygdala connectivity. Ann N Y Acad Sci 985:50-58
Reichard RA, Subramanian S, Desta MT, Sura T, Becker ML, Ghobadi CW, Parsley KP, Zahm DS (2016) Abundant collateralization of temporal lobe projections to the accumbens, bed nucleus of stria terminalis, central amygdala and lateral septum. Brain Struct Funct. doi:10.1007/s00429-016-1321-y
Reynolds SM, Zahm DS (2005) Specificity in the projections of prefrontal and insular cortex to ventral striatopallidum and the extended amygdala. J Neurosci 25 (50):11757-11767. doi:10.1523/JNEUROSCI.3432-05.2005
Saper CB (1982) Convergence of autonomic and limbic connections in the insular cortex of the rat. J Comp Neurol 210 (2):163-173. doi:10.1002/cne.902100207
Sato M, Ito M, Nagase M, Sugimura YK, Takahashi Y, Watabe AM, Kato F (2015) The lateral parabrachial nucleus is actively involved in the acquisition of fear memory in mice. Mol Brain 8:22. doi:10.1186/s13041-015-0108-z
Savander V, Go CG, LeDoux JE, Pitkanen A (1995) Intrinsic connections of the rat amygdaloid complex: projections originating in the basal nucleus. J Comp Neurol 361 (2):345-368. doi:10.1002/cne.903610211
Schindelin J, Arganda-Carreras I, Frise E, Kaynig V, Longair M, Pietzsch T, Preibisch S, Rueden C, Saalfeld S, Schmid B, Tinevez JY, White DJ, Hartenstein V, Eliceiri K, Tomancak P, Cardona A (2012) Fiji: an open-source platform for biological-image analysis. Nat Methods 9 (7):676-682. doi:10.1038/nmeth.2019
Shackman AJ, Fox AS (2016) Contributions of the Central Extended Amygdala to Fear and Anxiety. J Neurosci 36 (31):8050-8063. doi:10.1523/JNEUROSCI.0982-16.2016

Shimada S, Inagaki S, Kubota Y, Kito S, Funaki H, Takagi H (1989) Light and electron microscopic studies of calcitonin gene-related peptide-like immunoreactive terminals in the central nucleus of the amygdala and the bed nucleus of the stria terminalis of the rat. Exp Brain Res 77 (1):217-220
Sierra-Mercado D, Padilla-Coreano N, Quirk GJ (2011) Dissociable roles of prelimbic and infralimbic cortices, ventral hippocampus, and basolateral amygdala in the expression and extinction of conditioned fear. Neuropsychopharmacology 36 (2):529-538. doi:10.1038/npp.2010.184
Smith KM, Boyle KA, Madden JF, Dickinson SA, Jobling P, Callister RJ, Hughes DI, Graham BA (2015) Functional heterogeneity of calretinin-expressing neurons in the mouse superficial dorsal horn: implications for spinal pain processing. J Physiol 593 (19):4319-4339. doi:10.1113/JP270855
Smith Y, Pare D (1994) Intra-amygdaloid projections of the lateral nucleus in the cat: PHA-L anterograde labeling combined with postembedding GABA and glutamate immunocytochemistry. J Comp Neurol 342 (2):232-248. doi:10.1002/cne.903420207
Sun N, Cassell MD (1993) Intrinsic GABAergic neurons in the rat central extended amygdala. J Comp Neurol 330 (3):381-404. doi:10.1002/cne.903300308
Tovote P, Fadok JP, Luthi A (2015) Neuronal circuits for fear and anxiety. Nat Rev Neurosci 16 (6):317-331. doi:10.1038/nrn3945
Tye KM, Prakash R, Kim SY, Fenno LE, Grosenick L, Zarabi H, Thompson KR, Gradinaru V, Ramakrishnan C, Deisseroth K (2011) Amygdala circuitry mediating reversible and bidirectional control of anxiety. Nature 471 (7338):358-362. doi:10.1038/nature09820
Usoskin D, Furlan A, Islam S, Abdo H, Lonnerberg P, Lou D, Hjerling-Leffler J, Haeggstrom J, Kharchenko O, Kharchenko PV, Linnarsson S, Ernfors P (2015) Unbiased classification of sensory neuron types by large-scale single-cell RNA sequencing. Nat Neurosci 18 (1):145-153. doi:10.1038/nn.3881
Veinante P, Freund-Mercier MJ (1998) Intrinsic and extrinsic connections of the rat central extended amygdala: an in vivo electrophysiological study of the central amygdaloid nucleus. Brain Res 794 (2):188-198. doi:S0006-8993(98)00228-5 [pii]
Veinante P, Yalcin I, Barrot M (2013) The amygdala between sensation and affect: a role in pain. J Mol Psychiatry 1 (1):9. doi:10.1186/2049-9256-1-9
Walker DL, Davis M (2008) Role of the extended amygdala in short-duration versus sustained fear: a tribute to Dr. Lennart Heimer. Brain Struct Funct 213 (1-2):29-42. doi:10.1007/s00429-008-0183-3
Walker DL, Toufexis DJ, Davis M (2003) Role of the bed nucleus of the stria terminalis versus the amygdala in fear, stress, and anxiety. Eur J Pharmacol 463 (1-3):199-216. doi:S0014299903012822 [pii]
Wang TW, Stromberg GP, Whitney JT, Brower NW, Klymkowsky MW, Parent JM (2006) Sox3 expression identifies neural progenitors in persistent neonatal and adult mouse forebrain germinative zones. J Comp Neurol 497 (1):88-100. doi:10.1002/cne.20984
Waraczynski M (2016) Toward a systems-oriented approach to the role of the extended amygdala in adaptive responding. Neurosci Biobehav Rev 68:177-194. doi:10.1016/j.neubiorev.2016.05.015
Waraczynski MA (2006) The central extended amygdala network as a proposed circuit underlying reward valuation. Neurosci Biobehav Rev 30 (4):472-496. doi:10.1016/j.neubiorev.2005.09.001
Wilensky AE, Schafe GE, Kristensen MP, LeDoux JE (2006) Rethinking the fear circuit: the central nucleus of the amygdala is required for the acquisition, consolidation, and expression of Pavlovian fear conditioning. J Neurosci 26 (48):12387-12396. doi:10.1523/JNEUROSCI.4316-06.2006
Xu C, Krabbe S, Grundemann J, Botta P, Fadok JP, Osakada F, Saur D, Grewe BF, Schnitzer MJ, Callaway EM, Luthi A (2016) Distinct Hippocampal Pathways Mediate Dissociable Roles of Context in Memory Retrieval. Cell 167 (4):961-972 e916. doi:10.1016/j.cell.2016.09.051

TABLES

Table 1. Stereotaxic coordinates for retrograde tract-tracing

Areas	Coordinates		
	AP (mm)	ML (mm)	DV (mm)
STLD	+0.20	+0.90	-3.30
STLV	+0.20	+0.90	-4.00
CeL/C	-1.43	+2.35	-3.75
CeM(rostral)	-1.07	+2.20	-4.00

Abbreviations, see the list. The stereotaxic coordinates are taken according to the Paxinos and Franklin's mouse brain atlas (Paxinos and Franklin 2012), with the bregma point as the origin for anterior – posterior (AP) and middle – lateral (ML) axis. The dorsal – ventral (DV) distance was referred to its cortical surface above the corresponding AP, ML location.

Table 2. Primary antibodies that used in this study

Name	Species, Poly/mono-	Dilution	Antigen	Source, catalog etc.	Reference
NeuN	Mouse, monoclonal	1:10k	Purified nuclei (mouse)	Cat. #: MAB377; Millipore™	(Furmanski et al. 2009)
CRF	Rabbit, antiserum	1:15k	CRF coupled to α-globulins	Code PBL rC68; Dr. P. Sawchenko, Salk Institute	(Chen et al. 2015)
TH	Mouse, monoclonal	1:10k (IHC); 1:1k (IHF)	Purified TH from PC12 cells	Cat. #: MAB318; Millipore™	(Chung et al. 2008)
CGRP	Rabbit, polyclonal	1:10k	CGRP peptide (rat)	Cat. #: RPN1842, Amersham	(Franke-Radowiecka 2011)
PKCδ	Mouse, polyclonal	1:1k	Human PKCδ aa. 114-289	Cat. #: 610398, BD Biosciences	(Haubensack et al; 2010)
SOM	Rabbit, polyclonal	1:4k	KLH-conjugated synthetic somatostatin (AGCKNFFWKTFTSC)	Cat. #20067, Immunostar	(Jhou et al. 2009)
CR	Mouse, monoclonal	1:1500 (IHF)	Recombinant calretinin (rat)	Cat. #: MAB1568, Millipore™	(Wang et al. 2006)
CTb	Goat, antiserum	1:50k (IHC); 1:1.5k (IHF)	choleragenoid	Cat. #: 703; List Biological Laboritories™	(Thompson and Swanson 2010)
FG	Rabbit, polyclonal	1:750	KLH-conjugated Fluorescent Gold	Cat. #AB153-I, Millipore	(Thompson and Swanson 2010)

Table 3. Intensity of immunoreactivities in anterior STL and CeA

Group	Area	Molecular markers					
		NeuN*	CGRP**	PKCδ*	SOM*	CRF**	TH**
STL	STLD	++	++++	+++	++	++++	+/++++
	STLP	++++	+	-/+	+	++/+++	+++/++++
	STLJ	++++	-/+	-	+	+	++++
	STLV	++++	+	-	+	++	++
	Fu	+	+++	-	+	+++	++
CeA	CeC	+/++	++++	+++	++	+++	+
	CeL	++	++/+++	++/+++	+++	++++	++++
	CeM	++	-/+	-/+	+/++	++	+++
EAm	STMA	++++	+	-	-/+	++	+/++
	STMV	++++	+	+**	+	+	+/++
	MeAD	++++	++	-	+	++	+
	MePD	+++/++++	+	-	+	+/++	+
	MePV	++++	-/+	-	+	-/+	-/+
amygdala	LA	++++	+/++	-	+	-/+*	-/++
	BLA	+++/++++	-/+	-	+	+*	+/++
	BLP	++++	-/+	-	+	+*	++/+++

Notes: 1).The intensity of individual molecular marker was assessed based on its primary type of labeling (either somatic or fibrous). The CRF+ somas in EAc was not available due to the intensive axonal fibers. Notation: *, soma; **, fiber.
2). Intensity of immunoreactivity was manually assessed based on the relative intensity of bright-field images of DAB product. The intensity scales: -, few or not observable; +, light; ++, moderate; +++, intense; ++++, very intense.
3) In cases where heterogeneous intensity were observed in individual subdivision, the expression level was denoted as a range (i.e. +/++++, means light to very dense expression).

Table 4. Number of afferents that show preferential or common inputs

Pairwise comparison	Preferential inputs				Common inputs	
	STLD	CeL/C	STLV	CeM	Pair #1	Pair #2
Any two pair	2	0	7	9	12	
Pair #1: STLD-CeL/C; Pair #2: STLV-CeM	11	2	10	18	30	44
Pair #1: STLD-STLV; Pair #2: CeL/C-CeM	4	2	8	16	42	28
Pair #1: STLD-CeM; Pair #2: CeL/C-STLV	5	3	13	15	39	29

Note: A preferential input is counted when the scoring difference of equal or greater than two scales (including ++ versus -/+) found, otherwise a common input of light and greater intensity is counted.

Legends

Fig. 1 Subdivisions of STL and CeA revealed by neurochemical features. Expression of NeuN (**a**, **g**), CGRP (**b**, **h**), PKCδ (**c**, **i**), SOM (**d**, **j**), CRF (**e**, **k**), and TH (**f**, **l**) in STL levels (**a1- f1**, **a2 – f2**; bregma +0.25 mm to +0.07 mm) and CeA levels (**g1 – l1**, **g2 – l2**; bregma -1.43 mm to -1.61 mm, except that **l2** is anterior to **g2**) of wild-type mouse were revealed in successive coronal sections (thickness = 30 μ m). In the rostral-caudal axis (pictures in left to right), subdivisions of STL, STM, and CeA show differential expressions of the six molecular markers. High magnification images (insert of **g1 – l1**) showed cellular distribution of individual molecular marker. Notably, several markers (i.e. CGRP, PKCδ, SOM, CRF) were enriched in the STLD and CeL/C in a similar way. Abbreviation: see list. Scale bar: **a1 – f1**, 1000 μm; **a2 – f2**, 200 μm; **g1 – l1**, 1000 μm; **g2 – l2**, 200 μm; inserts of **g2 – l2**, 20 μm.

Fig. 2 CTb injection sites. Following the CTb immunostaining on STL and CeA sections, injection sites were checked on successive sections of rostral to caudal STL (**a, b**) and CeA (**c, d**). The injections in STLD (**a1 – a2**; bregma level +0.25 to +0.13 mm), STLV(Fu) (**b1 – b2**; bregma level +0.25 to +0.13 mm), CeL/C (**c1 – c2**; bregma level -1.43 to -1.67 mm) and rostral CeM (**d1 – d2**; bregma level -0.95 to -1.07mm) are coded in different colors for individual case, with injec- tion site circled in the same color at the corresponding bregma level. Brightfield images of case 1703F (**a3**), case 1703N (**b3**), case 1608D (**c3**), and case 1703H (**d3**) are illustrated. Abbreviation: see list. Scale bar: **a3**, 500 μm; **b3**, 500 μm; **c3**, 500 μm; **d3**, 500 μm.

Fig. 3 Heatmap of the inputs to STLD, CeL/C, STLV and CeM. Following iontophoresis of CTb into STLD, CeL/C, STLV(Fu) or CeM(r), retrograde CTb+ somas in a given brain region were counted on two or three consecu- tive slices and converted into a semi-quantitative assessment by an arbitrary scale. Scales: NA, not available; -, absence; -/+, sparse; +, light; ++, moderate; +++, strong; ++++, very strong; +++++, densest.

Fig. 4 Differential inputs from EAc subdivisions. Coronal brain slices were immunostained for CTb following iontophoresis injection of CTb in STLD (**a – c**; case 1701E), CeL/C (**d – f**; case 1608D), STLV(Fu) (**g – i**; case 1703N) and CeM (**j – l**; case 1703H and 1703D). Images show similar levels of STL (**a, d, g, j**; bregma +0.13 to +0.01 mm), SLEA and IPAC (**b, c, h,**

k; bregma -0.59 mm), and caudal CeA (**c, f, i, l**; bregma -1.43 to -1.55 mm). High-magnification (20x objective) of the insets in **a1**, **d1**, **g1**, and **j1** show retrograde somatic labeling (indicated by the arrow heads) in corresponding subdivisions of ST. Abbreviations: see the list. Scale bars: **a1, d1**, **g1**, **j1**, 200 μm; **a2 – a3**, **d2 – d3**, **g2 – g3**, **j2 – j3**, 100 μm; **b**, **e**, **h**, **k**, 200 μm; **c**, **f**, **i**, **l**, 200 μm.

Fig. 5 Differential inputs from the basolateral group of the amygdala. Amygdala sections containing rostral to caudal levels of LA, BLA and BLP were immunostained for CTb, following iontophoresis of CTb in STLD (**a – c**; case 1701E), CeL/C (**d – f**; case 1608D), STLV(Fu) (**g – i**; case 1703N) and CeM (**j – l**; case 1703H). Bright field images show CTb+ labeling in LA and BLA at rostral level (**a**, **d**, **g**, **j**; bregma -0.95 to -1.07 mm), middle level of BLA and rostral level of BLP (**b**, **e**, **h**, **k**; bregma -1.43 to -1.55 mm), and rostral level of BLP (**c**, **f**, **i**, **l**; bregma -2.45 to -2.53 mm). Abbreviations: see the list. Scale bars: **a – l**, 200 μm.

Fig. 6 Differential inputs from cerebral cortex and cortico-amygdaloid regions. Coronal brain sections contai- ning mPFC, middle level of InsCx, and APir were immunostained for CTb with inject site in STLD (**a – c**; case 1701E), CeL/C (**d – f**; case 1608D), STLV(Fu) (**g – i**; case 1703N) and CeM (**j – l**; case 1703H). Images were taken from similar levels of mPFC areas (**a**, **d**, **g**, **j**; bregma +1.93 mm), middle level InsCx areas (**b**, **e**, **h**, **k**; bregma +0.13 mm) and caudal level of APir areas (**c**, **f**, **i**, **l**; bregma - 3.07 mm). Abbreviations: see the list. Scale bars: **a**, **d**, **g**, **j**, 500 μm; **b** – **c**, **e – f**, **h – i**, **k – j**, 500 μm.

Fig. 7 Differential inputs from ventral hippocampus areas. Coronal brain sections (bregma -3.07 mm) containing VS and ventral CA1 areas were immunostained for CTb, following the iontophoresis of CTb in STLD (**a**, case 1701E), CeL/C (**b**, case 1608D), STLV(Fu) (**c**, case 1608C) and CeM (**d**, case 1703D). The location of VS and CA1 were assigned according to the overall neuroanatomical structures in that corresponding whole section. Abbrevia- tions: see the list. Scale bars: **a – d**, 500 μm.

Fig. 8 Differential inputs from the anterior midline thalamic nuclei. Coronal sections containing PVA or Re/Xi were immunostained for CTb following iontophoresis injection of CTb in STLD (**a**, **e**; case 1701E), CeL/C (**b**, **f**; case 1608D), STLV(Fu) (**c**, **g**; case 1703N) and CeM (**d**, **h**; case 1703H). Images were chosen to illustrate retrograde labeling at the anterior level of PV (**a – d**; bregma -0.35 to -0.47 mm) and Re (**e – h**; bregma -0.95 to -1.07 mm).

Abbreviations: see the list. Scale bars: **a – d**, 200 μm; **e – h**, 200 μm.

Fig. 9 Differential inputs from posterior thalamus. CTb positive somatic labeling was revealed by immunostaining of CTb, following iontophoresis of CTb in STLD (**a – c**; case 1701E), CeL/C (**d – f**; case 1608D), STLV(Fu) (**g – i**; case 1703N) and CeM (**j – l**; case 1703H). Images were chosen to illustrate retrograde somatic labeling at the caudal level of PVP (**a**, **d**, **g**, **j**; bregma -1.79 to -1.91 mm), SPF/VPPC (**b**, **e**, **h**, **k**; bregma -2.15 to -2.27 mm), and PoT/PIL (**c**, **f**, **i**, **l**; bregma -2.91 to -3.07 mm). Abbreviations: see the list. Scale bars: **a - l**, 200 μm.

Fig. 10 Differential inputs from hypothalamus. CTb positive somatic labeling was revealed by immunostaining of CTb, following iontophoresis of CTb in STLD (**a – c**; case 1701E), CeL/C (**d – f**; case 1608D), STLV(Fu) (**g – i**; case 1703N) and CeM (**j – l**; case 1703H). Images were chosen to illustrate retrograde somatic labeling at VMH (**a**, **d**, **g**, **j**; bregma -1.43 to -1.55 mm), LH (**b**, **e**, **h**, **k**; bregma -1.43 to -1.55 mm) and PSTh (**c**, **f**, **i**, **l**; bregma -2.15 to -2.27 mm). Abbreviations: see the list. Scale bars: **a – l**, 200 μm.

Fig. 11 Differential inputs from midbrain and pons. CTb positive somatic labeling was revealed by immunostai- ning of CTb, following iontophoresis of CTb in STLD (**a – b**, case 1701E), CeL/C (**c – d**, case 1608D), STLV(Fu) (**e – f**, case 1703N) and CeM (**g – h**, case 1703H). Images were taken from VTA areas (**a**, **d**, **g**, **j**; bregma, -3.07 to -3.27 mm), caudal PAG areas (**b**, **e**, **h**, **k**; bregma -4.47 to -4.59 mm) and middle level of LPB (**c**, **f**, **i**, **l**; bregma -5.19 to
-5.33 mm). Among these differential inputs, it is particularly noticable that CTb from STLD and CeL/C resulted in intense fiber labeling in LPBE, where most of EAc-projecting neurons resides. Abbreviations: see the list. Scale bars: **a**, **d**, **g**, **j**, 200 μm; **b**, **e**, **h**, k, 200 μm; **c**, **f**, **i**, **l**, 200 μm.

Fig. 12 CGRP+ neurons project to subdivisions of EAc. Triple immunofluorescent staining of CTb (in green), CGRP (in red), and CR(in blue) was performed following single retrograde tracing from STLV(Fu) (**a – b**, case 1703N), STLD (**c**, case 1703F), CeM (**d**, case 1703H), and CeL/C (**e**, case 1703B). **a1-a4** Retrograde CTb+ labeling from STLV was concentrated in a LPBE section (bregma -5.33 mm), where densest CGRP+ cells and CR+ cells were found. **b1 – b4** High magnification confocal images showing somatic CGRP-CTb colocalizations

(indicated by arrow heads) in the insert of **a1**. Similarly, LPBE neurons projecting to STLD (**c1 – c4**), or to CeM (**d1 – d4**), or to CeL/C (**e1 – e4**) can colocalize with CGRP (arrow heads). In all the tracing from the four subdivisions, the CGRP+CTb+ neurons are almost always CR+. Scale bars: **b1 – b4**, 200 μm; **b1 – b4**, 50 μm; **c1 – c4**, 50 μm; **d1 – d4**, 50 μm; **e1 – e4**, 50 μm.

Fig. 13 Injection sites of paired retrograde tracing from ipsilateral STLD and CeL/C. The injection sites were revealed by immunofluorescent staining of FG (in red), CTb (in green) and DAPI (in blue), following ipsilateral paired injection of FG into STLD (**a**) and CTb into CeL/C (**b**; n = 3). The contour of each injection area is depicted in one unique color. **a1 - a2** The injection sites of FG in STLD at different levels, case 1609B in **a1**, case 1608F and 1607B in **a2**. **a3** An epifluorescent image of case 1608F at the corresponding STLD level, stained with FG and DAPI. **b1 - b2** Injection sites of CTb at different levels of CeA, from the same cases as that in **a1 – a2**. **b3** An epifluorescent image of case 1608F at CeL/C section with double staining of CTb and DAPI. Abbreviations: see the list. Scale bars: **a3**, 200 μm; **b3**, 200 μm.

Fig. 14 Collateral inputs to ipsilateral STLD and CeL/C. Double immunofluorescent staining of FG (in red) and CTb (in green), together with the counter staining by DAPI (in blue) was performed after injection of FG into STLD and CTb into CeL/C. Epifluorescent images showing collateral inputs from insular cortex (**a1- a2**; bregma +0.13 mm), PVA (**b1 – b2**; bregma -0.83 mm), caudal BLP (**c1 – c2**; bregma, -2.53 mm), VLPAG and DR (**d1 – d2**; bregma -4.59 mm), and LPBE (**e1 – e2**, bregma -5.19 mm). Cells that project to both STLD and CeL/C (indicated by short arrows) were found in all the above areas. **a3 – e3** Comparison of means of percentage (n = 3, Student's unpaired *t*-test) of projection neurons that projected to CeL/C only, to STLD only and to both areas, were performed for GI and DI (**a3**), PVA and PV (**b3**), BLP (**c3**), VLPAG and DR (**c3**), and LPBE (**e3**). Scale of significance: *, <0.05; **, <0.01; ***, <0.001. Abbreviations: see the list. Scale bars: **a1**, **b1**: 250 μm; **a2**, **b2**: 50 μm; **c1**, **d1**, **e1**: 200 μm; **c2**, **d2**, **d3**, **e3**: 100 μm.

Fig. 15 Individual calretinin+ neurons in PV and BLP can project collaterally to STLD and CeL/C. Triple immu- nofluorescent staining of CTb (in green), FG (in red), and CR (in blue) was performed following ipsilateral injection of FG into STLD and CTb into CeL/C (case 1608F). **a** Overall distribution of FG, CR, and CTb somatic labeling in a PV section

(bregma – 1.43 mm). **b1 – b7** Confocal images showing the same CR+ neurons (indicated by arrow heads) can provide collaterals to STLD and CeL/C. **c** Overall distribution of FG, CR, and CTb somatic labeling in a BLP section (bregma – 2.53 mm). **d1 – d7** Confocal images showing individual CR+ neurons (indicated by arrow heads) innervate both STLD and CeL/C. Scale bars: **a**, 100 μm; **b1 – b7**, 50 μm; **c**, 200 μm; **d1 – d7**, 50 μm.

Fig. 16 Schematic summary of the differential inputs of STLD, STLV, CeL/C and CeM. The main inputs were reorganized to display the preferential afferents of each EAc nuclei. The relative strength of intra-EAc inputs are repre- sented by sized sharp arrow heads (filled), and that of extra-EAc inputs by sized triangular heads (empty). The STL nuclei and their preferential afferents (defined by socre difference of equal or more than two scoring levels, see Fig. 3) are highlighted with green shapes (left side), while CeA nuclei and their preferential afferents with red shapes (right side). Extra-EAc afferents receiving equal or minor differential projections (defined by score difference of less than two scoring levels) are highlighted in yellow shapes (middle side). Abbreviation: see the list.

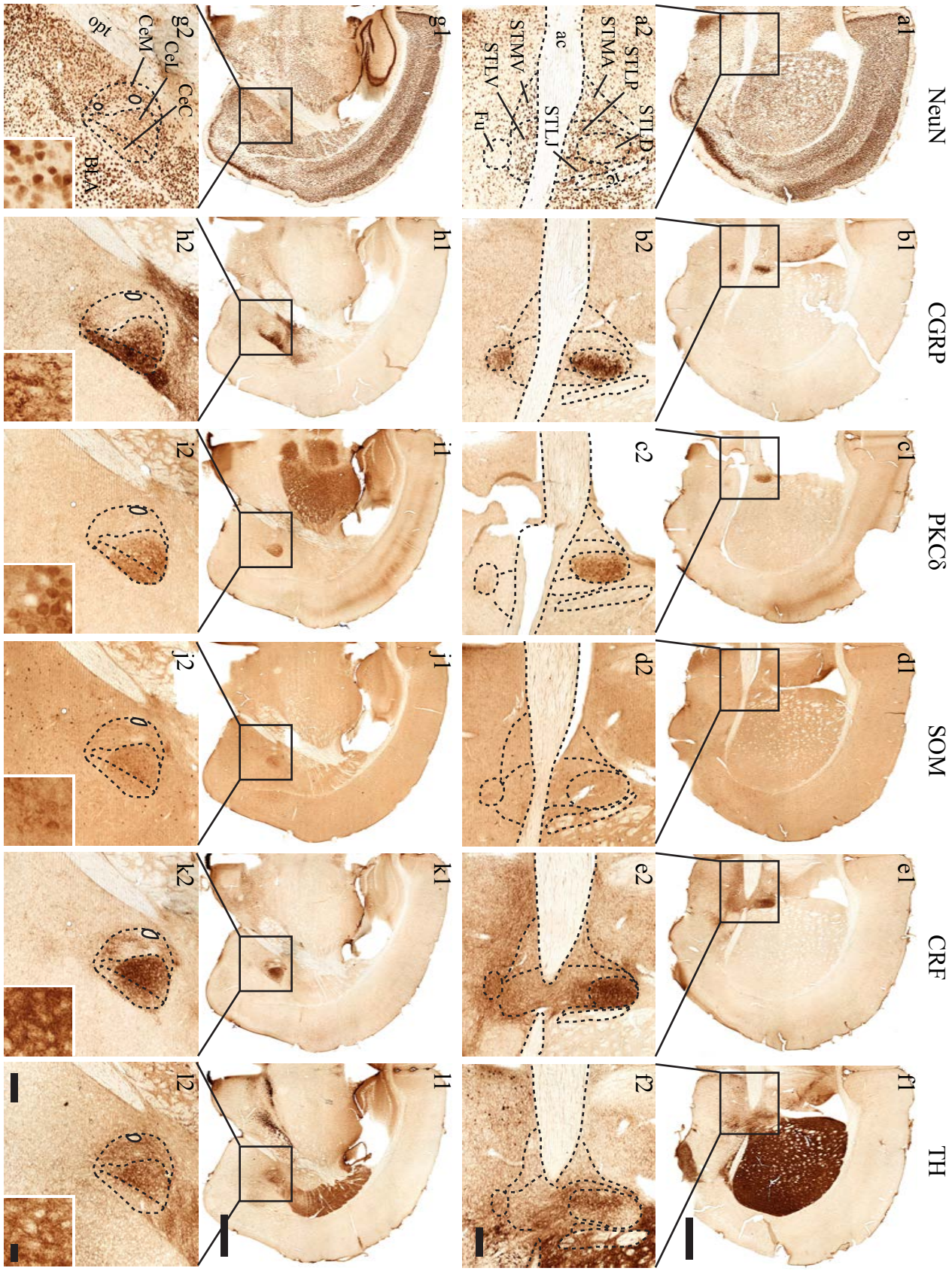
NeuN
CGRP
PKCδ
SOM
CRF
TH
a1
a2
STLD
STLP
STMA
ac
STLJ
STMV
STLV
Fu
ce
b1
b2
c1
c2
d1
d2
e1
e2
f1
f2
g1
g2
CeL
CeC
CeM
opt
BLA
h1
h2
i1
i2
j1
j2
k1
k2
l1
l2

Fig. 1

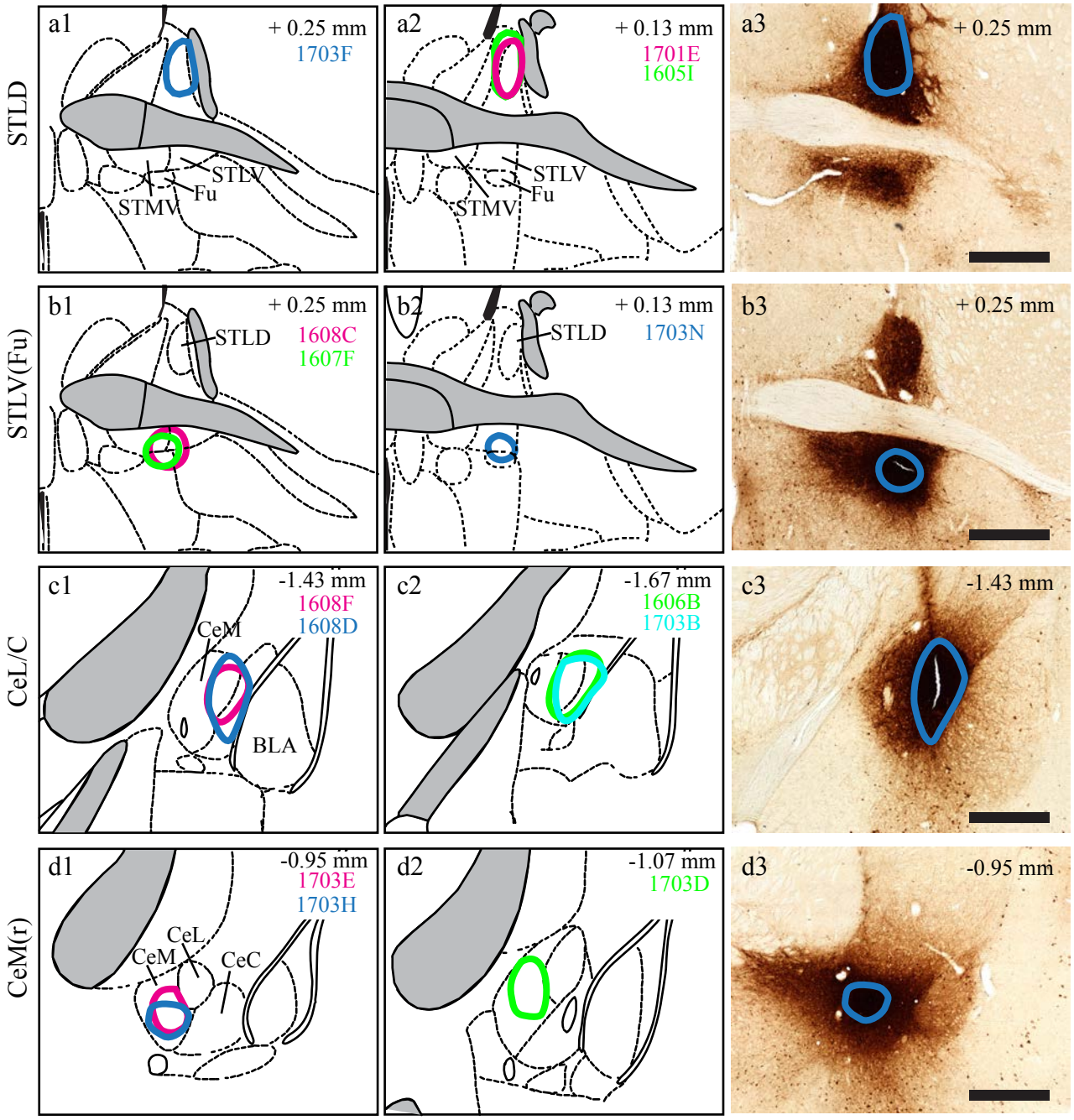
STLD
STLV(Fu)
CeL/C
CeM(r)
a1
+ 0.25 mm
1703F
STLV
Fu
STMV
a2
+ 0.13 mm
1701E
1605I
STLV
Fu
STMV
a3
+ 0.25 mm
b1
+ 0.25 mm
STLD
1608C
1607F
b2
+ 0.13 mm
STLD
1703N
b3
+ 0.25 mm
c1
-1.43 mm
1608F
1608D
CeM
BLA
c2
-1.67 mm
1606B
1703B
c3
-1.43 mm
d1
-0.95 mm
1703E
1703H
CeL
CeM
CeC
d2
-1.07 mm
1703D
d3
-0.95 mm

Fig. 2

Area	STLD	CeL/C	STLV	CeM
Cerebral cortex				
LO	+	-/+	+++	+
A25	+	+	+++	+++
A32	++	-/+	+	+
A24a	++	-/+	+++	++
AI	+	+	-/+	++++
AIP	+	+++	-/+	+++
DI	++	++++	+	+++
GI	++	+++	-/+	+++
Pir	+	+	-/+	+++
DIEnt	+	+	+	++
DLEnt	-/+	+	-/+	+
Ect/PRh	+	+	-/+	+++
TeA	+	+	-/+	+
Hippocampal formation				
CA1	++	-/+	+	-/+
VS	+++	+++	++	+
Telencephalon				
Basal ganglia				
AcbC	-/+	-/+	++++	-/+
AcbSh	+	-/+	+++	-/+
Tu	+	-	-/+	+
VP	-/+	-/+	-/+	-/+
Septum				
LSD	-/+	-	+	-/+
LSV	-/+	-	-/+	-
SHy	-/+	-	-/+	-
Amygdala				
LaDL	-/+	-/+	-/+	++
LaVL	-/+	+	-/+	++
LaVM	+	+	-/+	+
BLAr	+	-/+	-/+	+++
BLAc	+++	+	+	+
BLPr	+++	+	+++	+++
BLPc	+++++	++++	+++	++++
BLV	+	-/+	-/+	+
BMA	+++++	+++	++++	+++++
BMP	+++	+	++	+++
RAPir	++	+	-/+	++
APir	+++++	++++	++++	++++
CxA	+	+	-/+	+++
ACo	++	+	+	+++
PLCo	++	-/+	-	-/+
PMCo	-/+	-	-/+	-/+
AHi	++	-/+	-/+	+
LOT	-	-/+	-	+
IM	-/+	-/+	+	+++
I	-/+	+	-/+	+
ASt	-	+	-	-/+

Area	STLD	CeL/C	STLV	CeM
Central extended amygdala				
STLD	NA	-/+	++++	+
STLJ	NA	-/+	+	-/+
STLP	NA	++	+++	++
STLV	-/+	-/+	NA	+
Fu	-/+	-/+	NA	-/+
STS	+	+	+	-/+
CeC	++	NA	+++	+++
CeL	+++	NA	++++	+++
CeM	++	-/+	+++	NA
IPAC	+	+	++	+++
SLEA	+	+	+	++
Medial extended amygdala				
STMA	-/+	-/+	+	-/+
STMP	+	-/+	++	+
STMV	-/+	-	+	-/+
STIA	-/+	-/+	+	+
MeAD	-/+	+	-/+	+
MePD	-/+	-/+	-/+	-/+
MePV	-/+	-/+	-/+	+
Preoptic area				
LPO	+	-/+	++	-/+
MPA	+	-	+++	-/+
MPO	+	-	++	+
MnPO	-/+	-	+	-/+
Other telencephalic				
DTT	-/+	-/+	-/+	++
DEn/IEn	-/+	-/+	-/+	+
cl	-/+	-/+	-/+	-/+
HDB	-/+	-	-/+	-/+
SIB	+	+	++	++
SFO	-	-	+	-/+
Thalamus				
Midline & intralaminar nuclei				
PVA	++++	+++	++++	+
PV	++	++	+	+
PVP	++	++	++	+++
PT	+	-/+	++	+
Re	-/+	-/+	+	-/+
PoMn	-/+	-/+	-/+	+
Xi	+	-/+	+	++
IMD	-/+	-	-/+	-/+
CMr	+	-/+	+	+
CMc	+	-/+	-/+	++
PaF	-/+	-/+	+	+
Mediodorsal nucleus				
MDM	-/+	-/+	-/+	+
Posterior nuclei				
VPPC	-/+	++	+	+++

Fig. 3 *(to be continued)*

Area	STLD	CeL/C	STLV	CeM
Posterior nuclei				
SPF	-	-	-	-/+
REth	-/+	+	-/+	++
PIL/PoT	-/+	-/+	-/+	++
MGM	-	-	-	+
Hypothalamus				
Anterior				
AHA	-/+	-	+	-
Pa	-/+	-/+	+	+
Tuberal				
RCh	+	-/+	+	+
Arc	-/+	-/+	+	-
DMH	+	-	+++	-/+
VMH	+	-/+	++	+
MTu	++	-/+	++	+
Posterior				
PH	+	-	-/+	-/+
MM	-	-	-/+	-/+
RML	-/+	-/+	+	+
RMM	-	-/+	+	-/+
Lateral				
LH	-/+	-/+	+++	+
MCLH	-/+	+	+	++
PTe	-/+	-	-/+	-/+
PeF	-/+	-/+	+	-
PSTh	++	++	++	+++
Brainstem				
Midbrain				
PVG	-/+	-/+	+	++
PAGr	-/+	-/+	+	-/+
DPAG	-	-	-/+	-
LPAG	+	-/+	-/+	-/+
VLPAG	+	+	+	+
SNCD	+	-/+	+	+

Area	STLD	CeL/C	STLV	CeM
Brainstem				
Midbrain				
VTAR	+	-/+	+	+
PBP	+	-/+	++	+
RRF	+	+	+	++
EW	-/+	-/+	-/+	+
RLi	-/+	-/+	-/+	-/+
CLi	+	-/+	+	-/+
MnR	-/+	-	-/+	-/+
DRL	-/+	-/+	-/+	-/+
DRV	-	+	-/+	+
DRD	+	+	+	-/+
DRC	+	+	+	-/+
PR	-	-	-/+	-/+
mRt	-	-	-	+
isRt	+	+	+	-/+
PTg	-	-/+	-/+	-/+
MiTg	-/+	-	-/+	-
Pons				
LPBC	-/+	+	+	-/+
LPBCr	-/+	-/+	-/+	-/+
LPBD	-	-/+	-/+	-/+
LPBEc	-/+	-/+	-/+	+
LPBE	++	+++	+++	+++
LPBV	-/+	-/+	-/+	-/+
LPBW	-/+	-/+	+	+
MPB	-/+	-/+	+	++
MPBE	-	-/+	-/+	-/+
KF	-	-	-/+	-/+
LC	+	+	+	-/+
SubCV	-	-	-	-/+
Medulla				
SolM	+	-/+	++	-/+

Fig. 3 *(continued)*

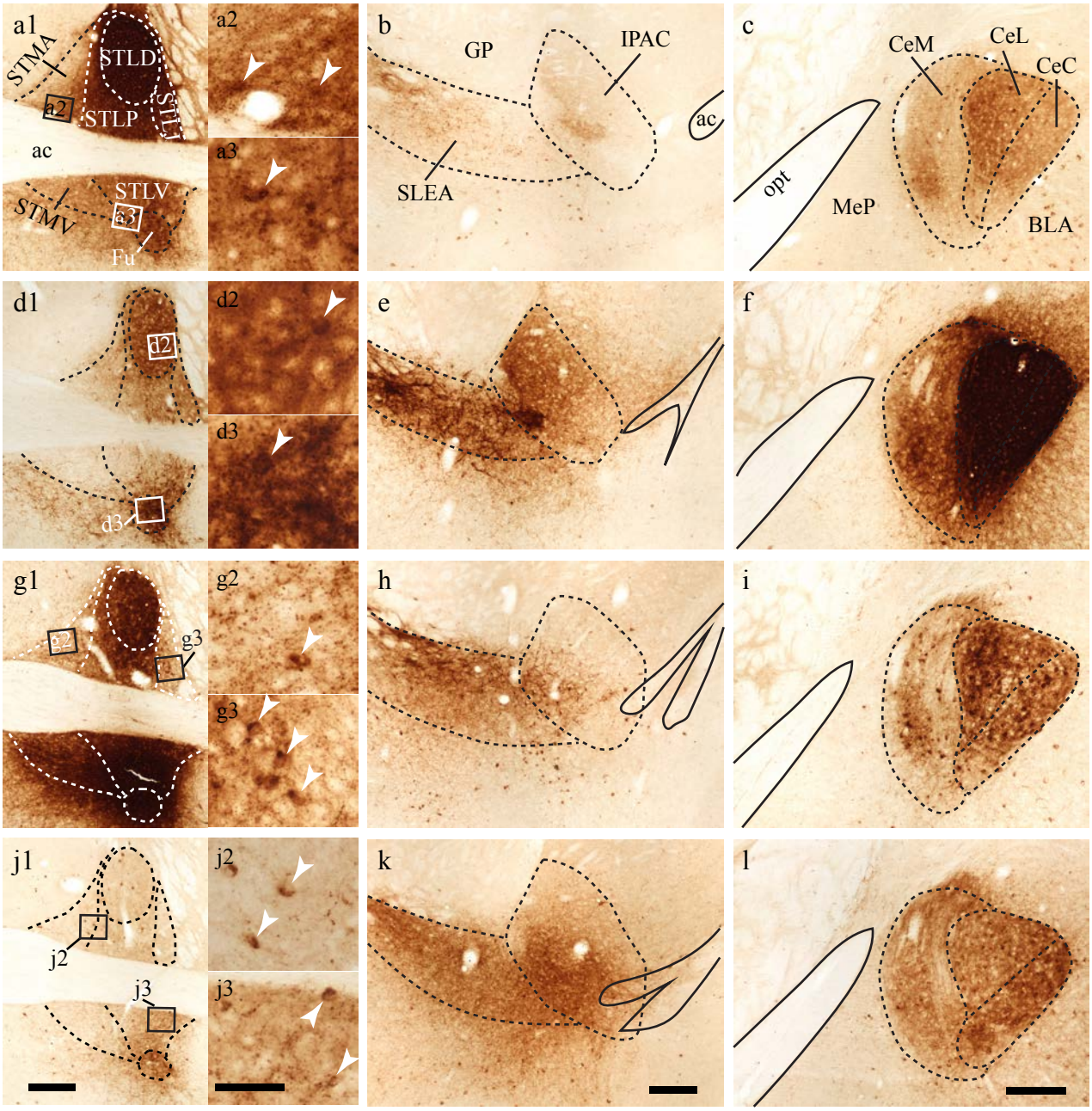
a1
STMA
STLD
STLV
a2
STLP
ac
STMV
STLV
a3
Fu
a2
a3
b
GP
IPAC
ac
SLEA
c
CeM
CeL
CeC
opt
MeP
BLA
d1
d2
d3
d2
d3
e
f
g1
g2
g3
g3
h
i
j1
j2
j3
j2
j3
k
l

Fig. 4

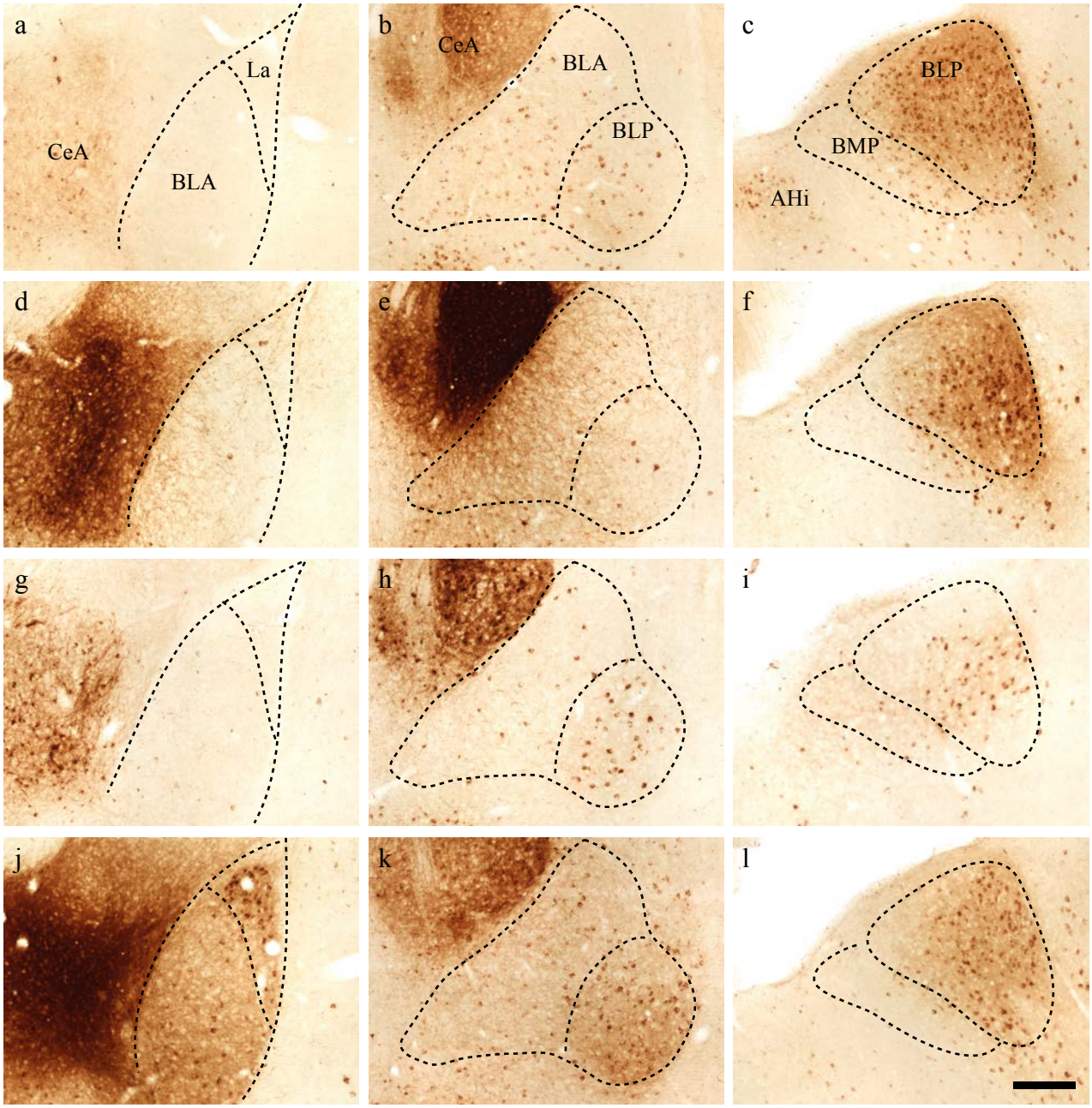

Fig. 5

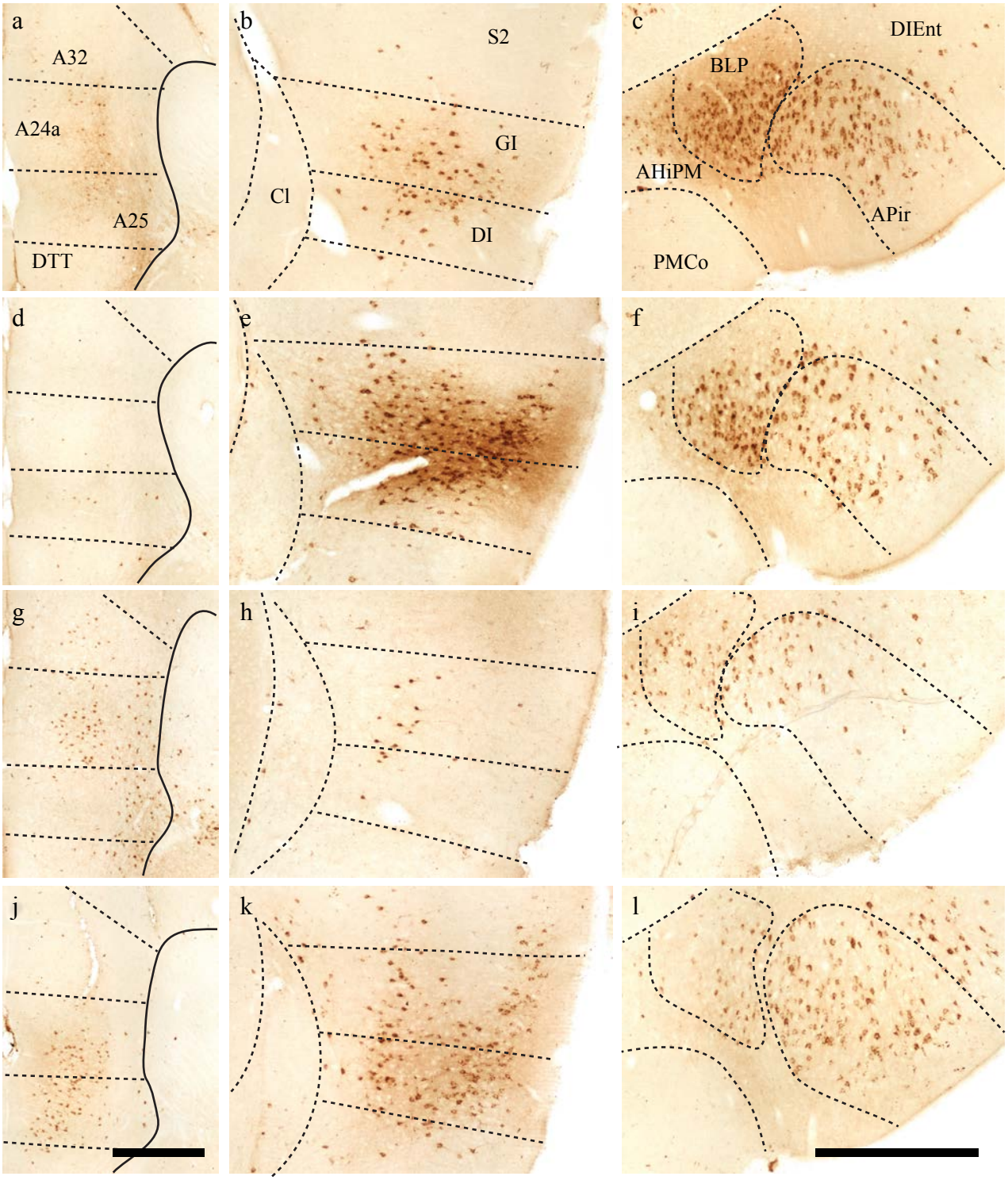
a
A32
A24a
A25
DTT
b
S2
GI
Cl
DI
c
DIEnt
BLP
AHiPM
APir
PMCo
d
e
f
g
h
i
j
k
l

Fig. 6

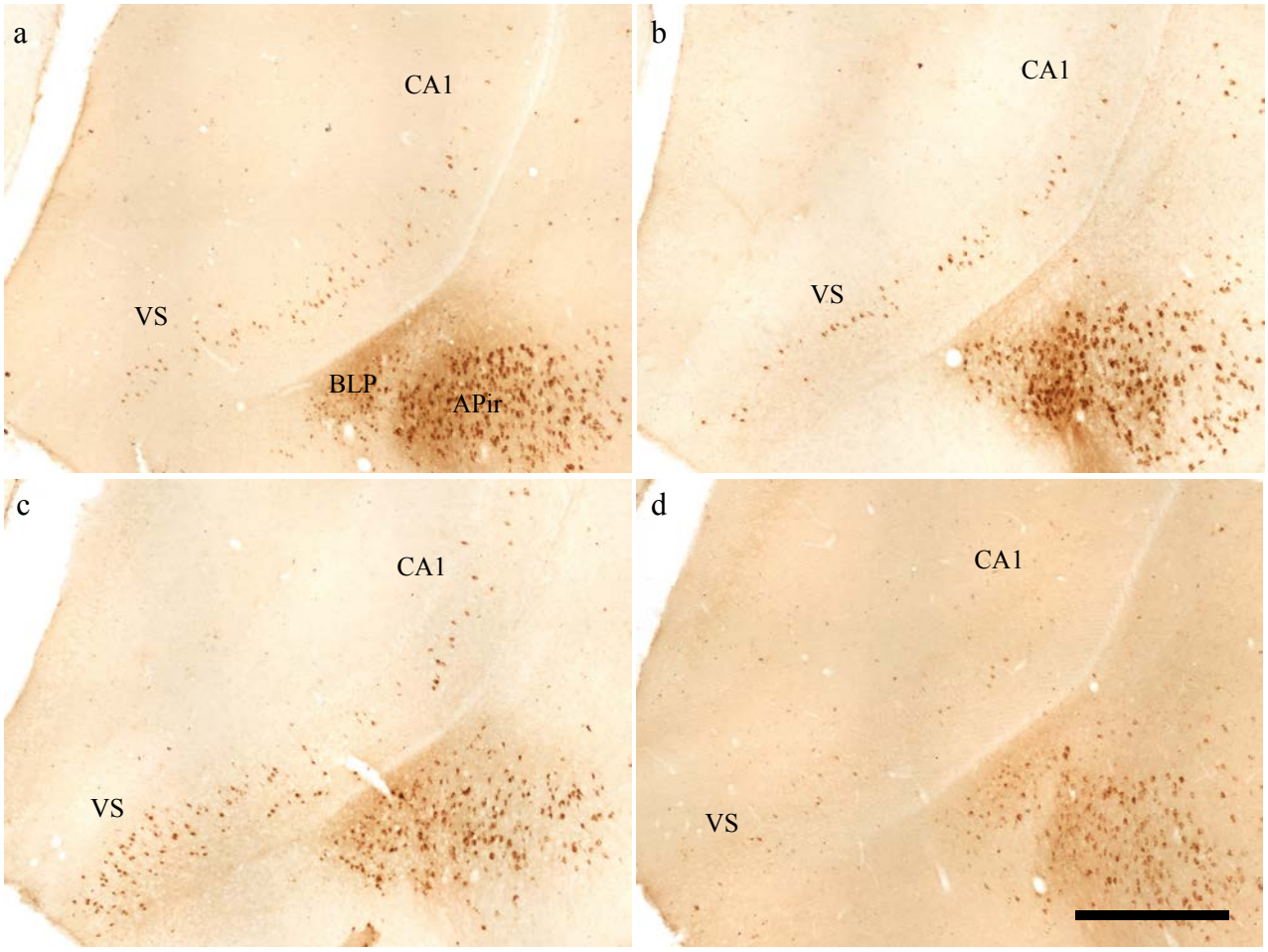

Fig. 7

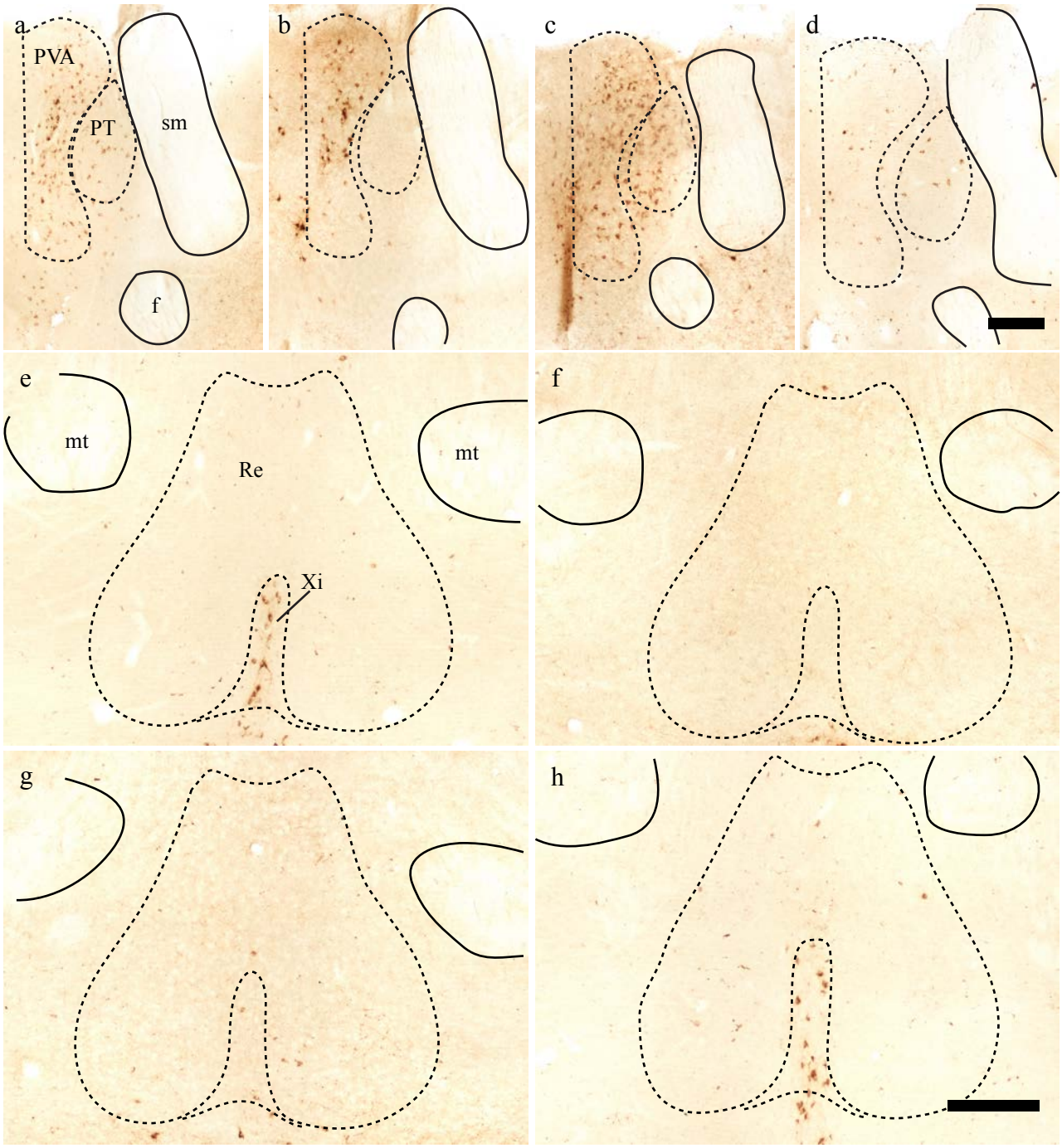

Fig. 8

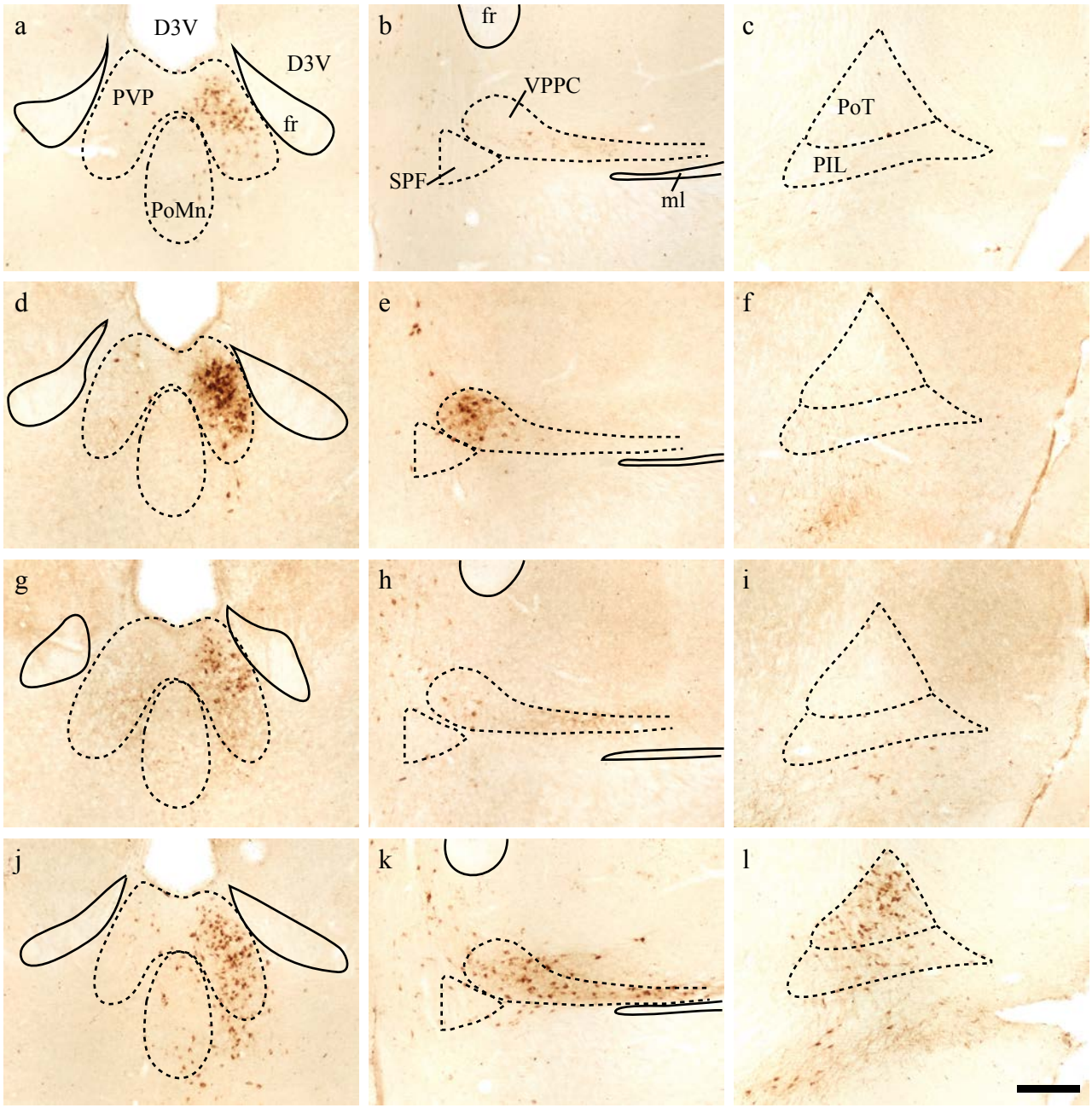

Fig. 9

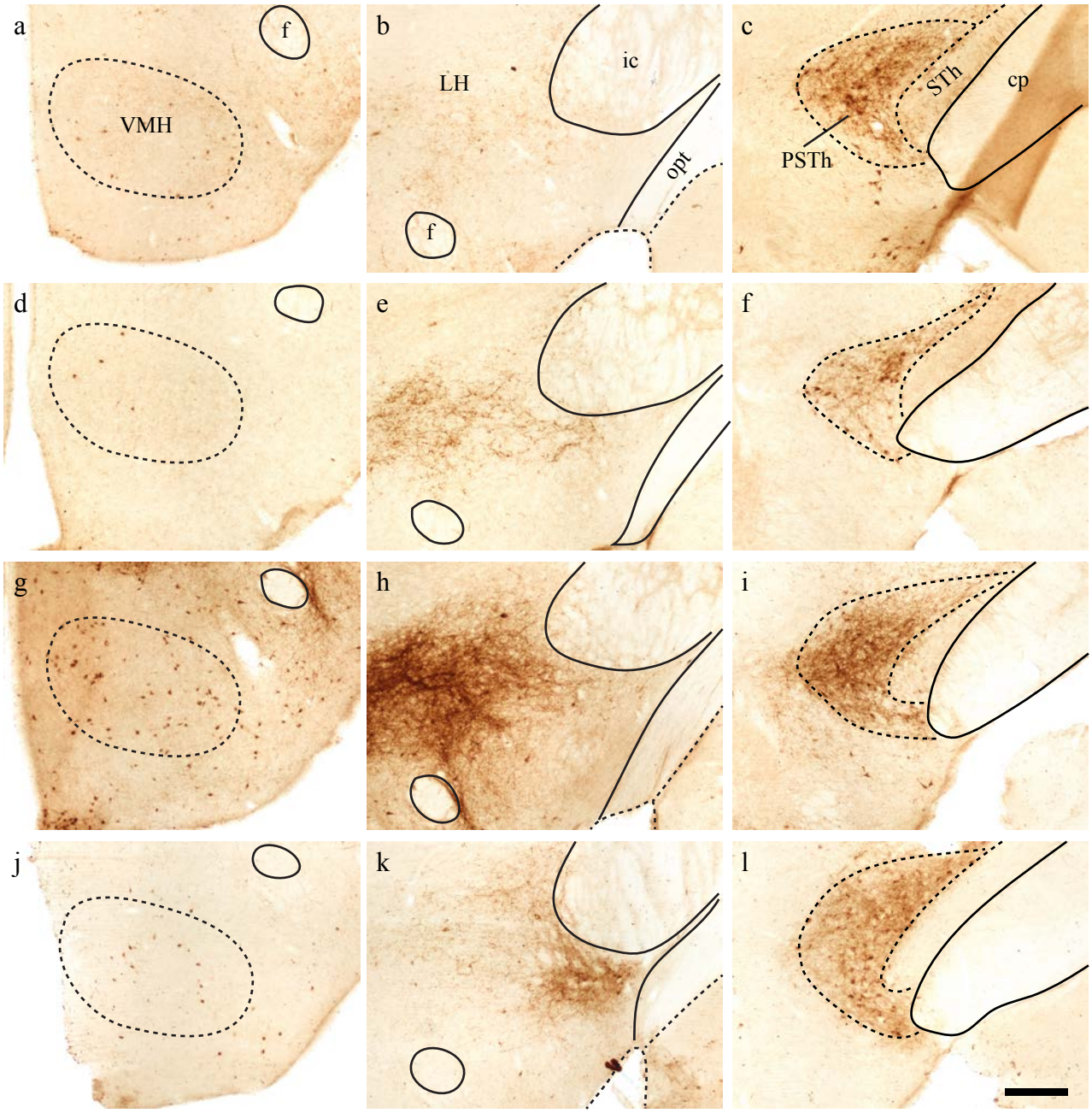

Fig. 10

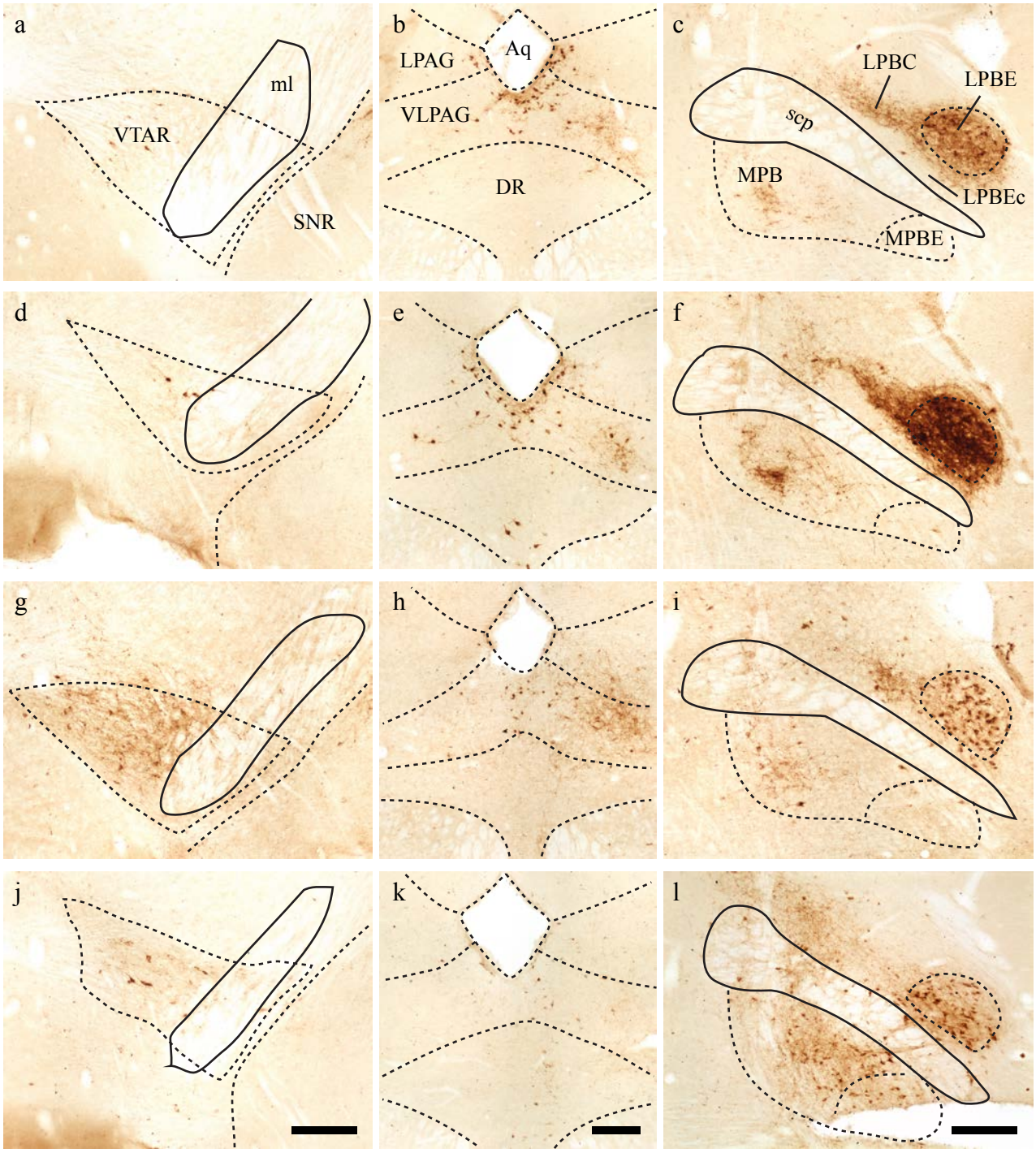
a
ml
VTAR
SNR
b
LPAG
Aq
VLPAG
DR
c
LPBC
LPBE
scp
MPB
LPBEc
MPBE
d
e
f
g
h
i
j
k
l

Fig. 11

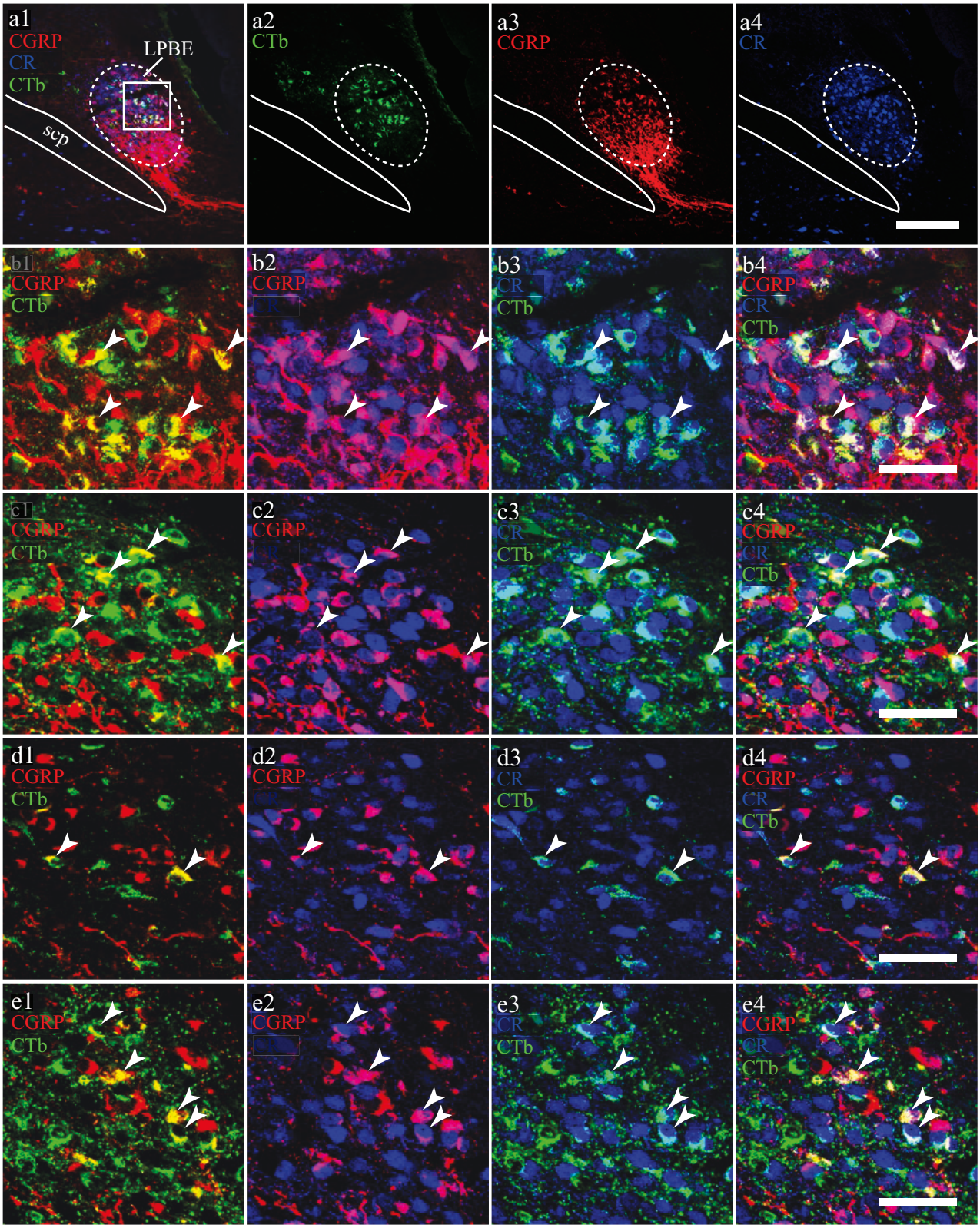
a1
CGRP
CR
CTb
LPBE
scp
a2
CTb
a3
CGRP
a4
CR
b1
CGRP
CTb
b2
CGRP
CR
b3
CR
CTb
b4
CGRP
CR
CTb
c1
CGRP
CTb
c2
CGRP
CR
c3
CR
CTb
c4
CGRP
CR
CTb
d1
CGRP
CTb
d2
CGRP
CR
d3
CR
CTb
d4
CGRP
CR
CTb
e1
CGRP
CTb
e2
CGRP
CR
e3
CR
CTb
e4
CGRP
CR
CTb

Fig. 12

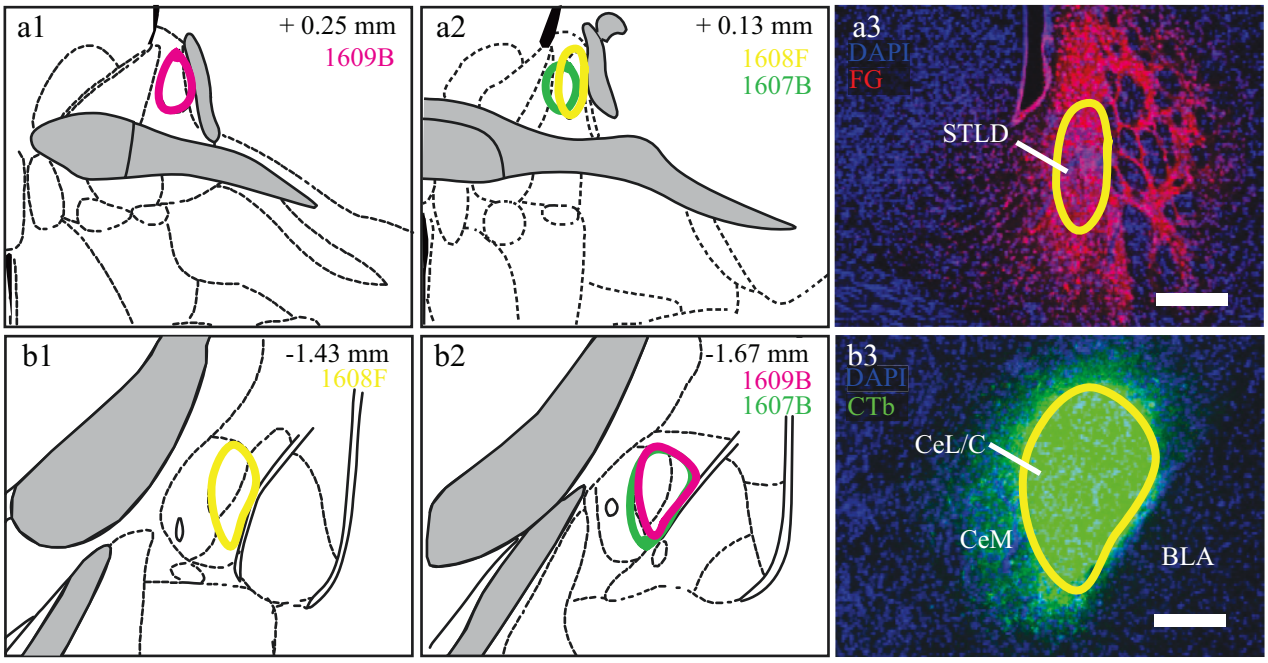
a1
+ 0.25 mm
1609B
a2
+ 0.13 mm
1608F
1607B
a3
DAPI
FG
STLD
b1
-1.43 mm
1608F
b2
-1.67 mm
1609B
1607B
b3
DAPI
CTb
CeL/C
CeM
BLA

Fig. 13

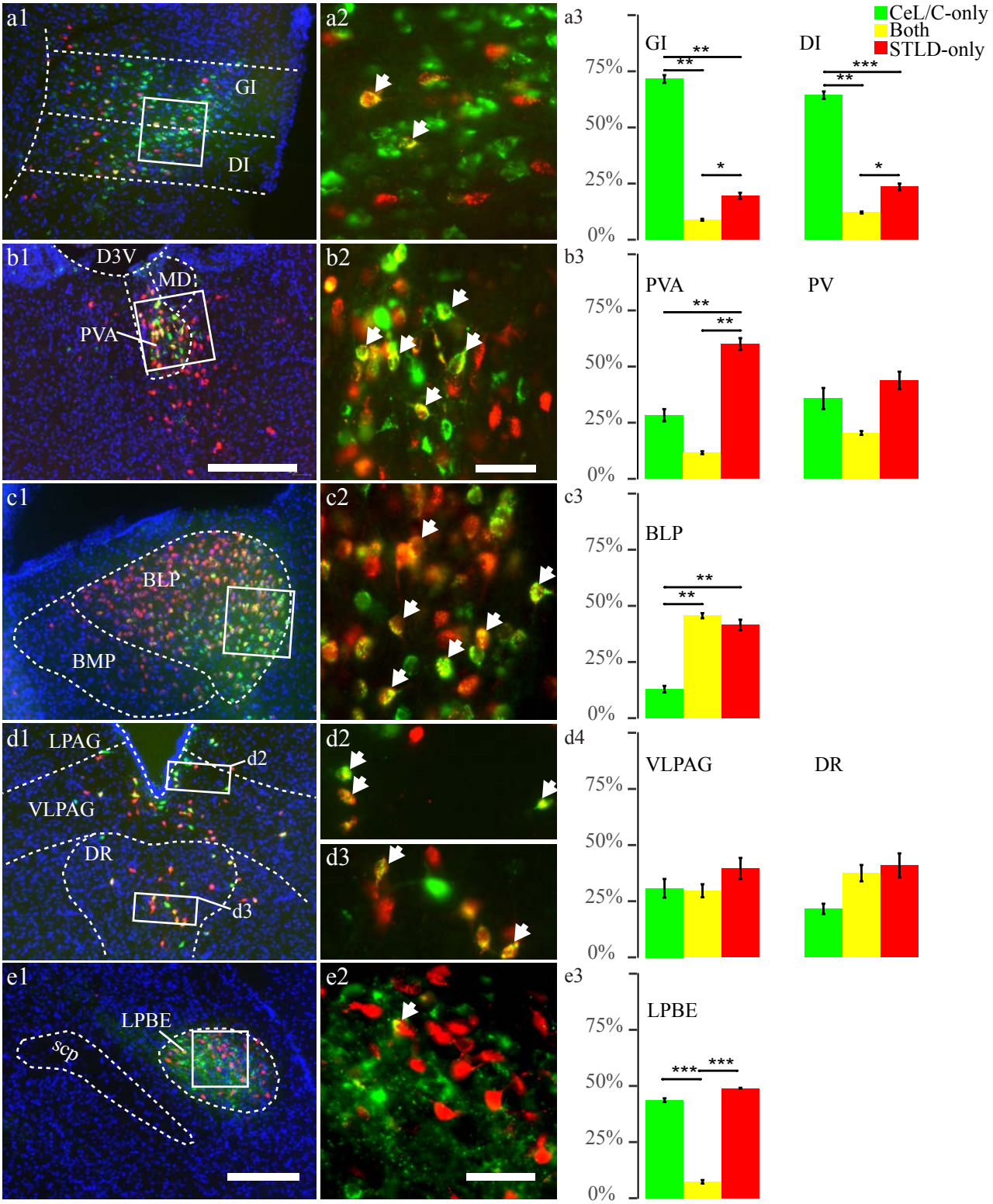
a1
GI
DI
a2
a3
CeL/C-only
Both
STLD-only
GI
DI
75%
50%
25%
0%
b1
D3V
MD
PVA
b2
b3
PVA
PV
c1
BLP
BMP
c2
c3
BLP
d1
LPAG
d2
VLPAG
DR
d3
d2
d3
d4
VLPAG
DR
e1
LPBE
scp
e2
e3
LPBE

Fig. 14

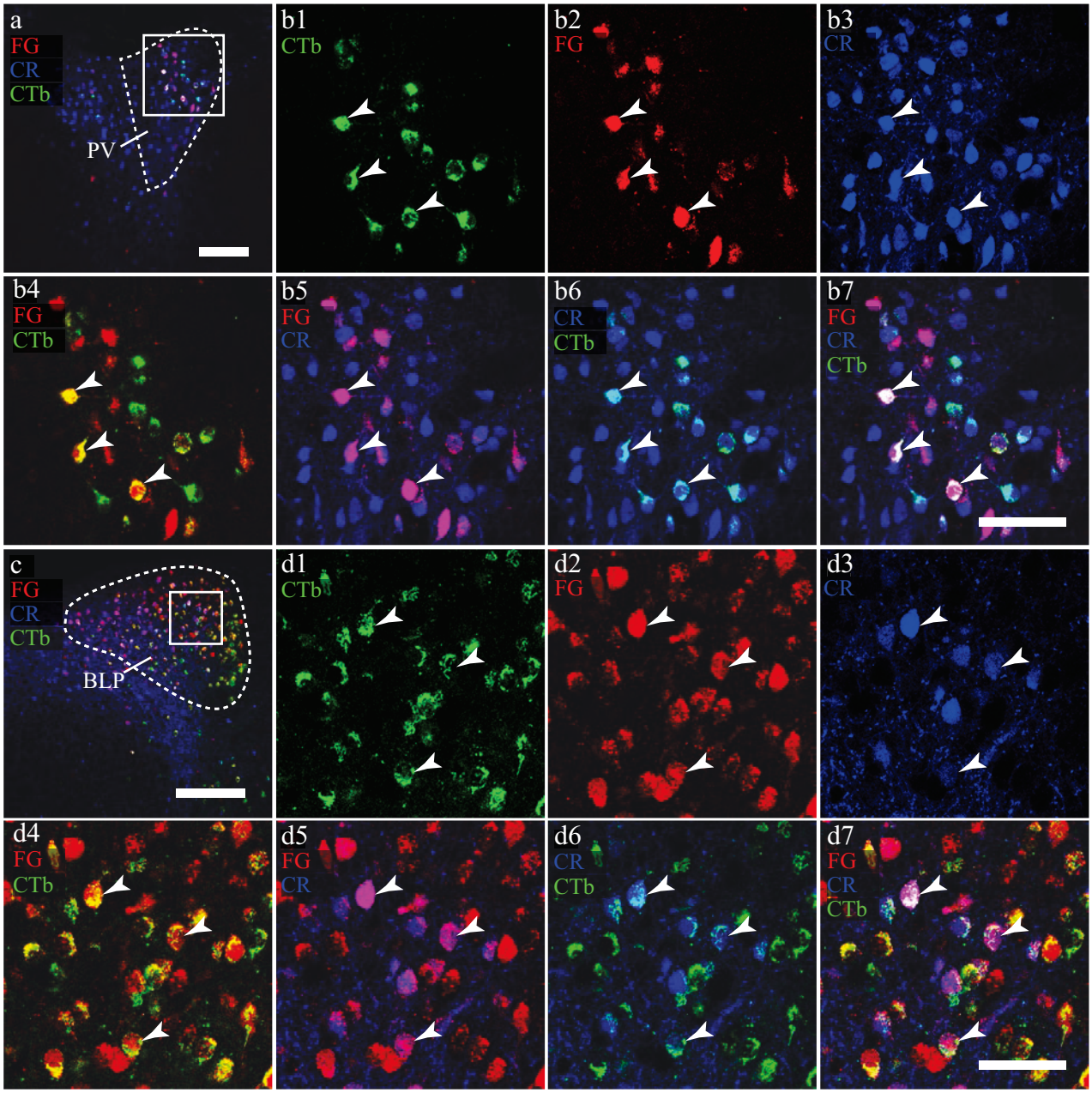
a
FG
CR
CTb
PV
b1
CTb
b2
FG
b3
CR
b4
FG
CTb
b5
FG
CR
b6
CR
CTb
b7
FG
CR
CTb
c
FG
CR
CTb
BLP
d1
CTb
d2
FG
d3
CR
d4
FG
CTb
d5
FG
CR
d6
CR
CTb
d7
FG
CR
CTb

Fig. 15

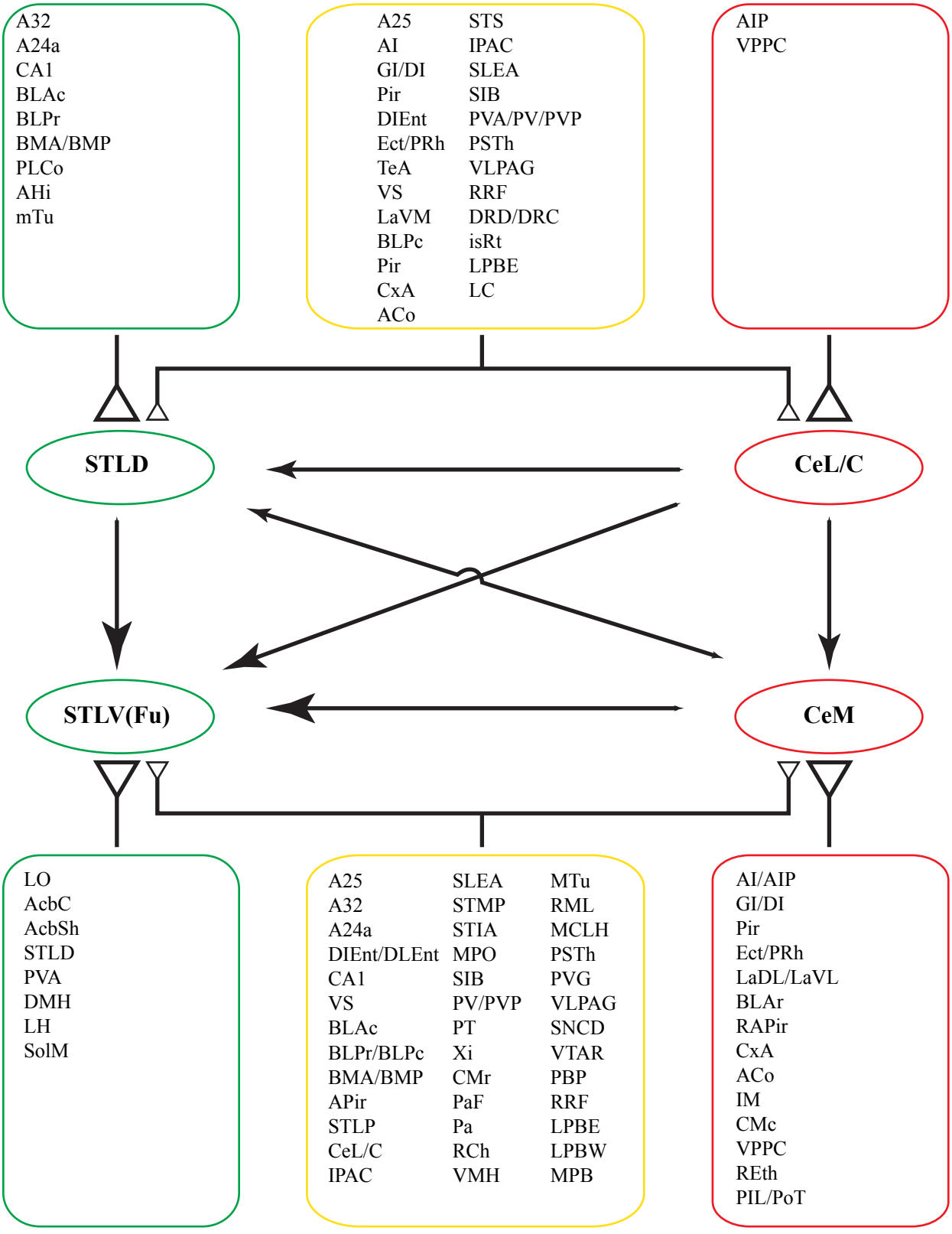
A32
A24a
CA1
BLAc
BLPr
BMA/BMP
PLCo
AHi
mTu
A25
AI
GI/DI
Pir
DIEnt
Ect/PRh
TeA
VS
LaVM
BLPc
Pir
CxA
ACo
STS
IPAC
SLEA
SIB
PVA/PV/PVP
PSTh
VLPAG
RRF
DRD/DRC
isRt
LPBE
LC
AIP
VPPC
STLD
CeL/C
STLV(Fu)
CeM
LO
AcbC
AcbSh
STLD
PVA
DMH
LH
SolM
A25
A32
A24a
DIEnt/DLEnt
CA1
VS
BLAc
BLPr/BLPc
BMA/BMP
APir
STLP
CeL/C
IPAC
SLEA
STMP
STIA
MPO
SIB
PV/PVP
PT
Xi
CMr
PaF
Pa
RCh
VMH
MTu
RML
MCLH
PSTh
PVG
VLPAG
SNCD
VTAR
PBP
RRF
LPBE
LPBW
MPB
AI/AIP
GI/DI
Pir
Ect/PRh
LaDL/LaVL
BLAr
RAPir
CxA
ACo
IM
CMc
VPPC
REth
PIL/PoT

Fig. 16

2. Efferents of central extended amygdala: preliminary comparative study

In this section, we will look at the mesoscopic outputs from subdivisions of EAc, following the previous part on inputs (or afferents). Anterograde tracers like BDA and PHA-L were injected into major EAc subdivisions including STLD, STLV (including Fu), CeLC and CeM. In the following section, we will present a preliminary report regarding the differential outputs of STLD vs. CeL/C, and of STLV(Fu) versus CeM based on a partial analysis of our experimental data.

Summary

Central nucleus of amygdala (CeA) and lateral bed nucleus of stria terminalis (STL) are two major elements of central extended amygdala (EAc), which has been studied as structural and functional macrosystem in mediating various psychiatric conditions. Mesoscopic efferents of EAc nuclei have been studies intensively in rats, but a comparative study of the differential and common EAc efferents in mouse is missing. In this study, we focused on the efferents of four major subdivisions of EAc, by using anterograde tract-tracing techniques. With available preliminary data, we found two salient structural patterns of EAc efferents. The intra-EAc efferents are often unidirectional and tends to be converged to ventral part of STL (STLV)/fusiform nucleus (Fu) and medial part of CeA (CeM). On the other hand, extra-EAc efferents are mainly mediated by STLV(Fu) and CeM to a more-or-less equal extent, as well as display unique sets of common and preferential outputs.

Keywords

Central nucleus of amygdala (CeA), lateral bed nucleus of stria terminalis (STL), extend amygdala, efferents, anterograde tract-tracing

Abbreviations

3V: 3rd ventricle
ac: anterior commussure
AcbC: accumbens nucleus, core region
AcbSh: accumbens nucleus, shell region
AHA: anterior hypothalamic area
Aq: aqueduct
BDA: biotin dextran amine
BLA: basolateral nucleus of amygdala, anterior part
BMP: basomedial amygdaloid nucleus, posterior part
cc: corpus callosum
CeA: central extended amygdala
CeLC: central nucleus of amygdala, lateral and capsular part
CeM: central amygdaloid nucleus, medial part
CLi: caudal linear nucleus of the raphe
D3V: dorsal 3rd ventricle
DAB: 3,3'-diaminobenzidine
DR: dorsal raphe nucleus
DMPAG: dorsomedial periaqueductal gray
EAc: extended amygdala, central part
EAm: extended amygdala, medial part
f: fornix
fr: fasciculus retroflexus
Fu: bed nucleus of stria terminalis, fusiform part
ic: internal capsule
IPAC: interstitial nucleus of the posterior limb of the anterior commiscommissure
IRt: intermediate reticular nucleus
LH: lateral hypothalamic area
LPAG: lateral periaqueductal gray
LPB: lateral parabrachial nucleus
LPBE: lateral parabrachial nucleus, external part
LPBV: lateral parabrachial nucleus, ventral part
LS: lateral septal nucleus
LV: lateral ventricle
MePD: medial amygdaloid nucleus, posterodorsal part
MPB: medial parabrachial nucleus
opt: optic tract
Pa: paraventricular hypothalamic nucleus
PAG: periaqueductal gray
PBN: parabrachial nucleus
PHA-L: *Phaseolus* vulgaris-leucoagglutinin
PoMn: posteromedian thalamic nucleus
PSTh: parasubthalamic nucleus
PT: paratenial thalamic nucleus
PV: paraventricular thalamic nucleus
PVA: paraventricular thalamic nucleus, anterior part
PVP: paraventricular thalamic nucleus, posterior part
RRF: retrorubral field
SIB: substantia innominata, basal part
SLEA: sublenticular extended amygdala
Sol: solitary nucleus
SolDL: solitary nucleus, dorsolateral part
SolDM: solitary nucleus, dorsomedial part
SolIM: solitary nucleus, intermediate part
SolL: solitary nucleus, lateral part
SolM: solitary nucleus, medial part
SolV: solitary nucleus, ventral part
STh: subthalamic nucleus
STL: lateral bed nucleus of stria terminalis
STLD: bed nucleus of the stria terminalis, lateral division, dorsal part
STLP: bed nucleus of the stria terminalis, lateral division, posterior part
STLV: bed nucleus of the stria terminalis, lateral division, ventral part
STMA: bed nucleus of the stria terminalis, medial division, anterior part
STMV: bed nucleus of the stria terminalis, medial division, ventral part
VLPAG: ventrolateral periaqueductal gray
VMH: ventromedial hypothalamic nucleus
VTAR: ventral tegmental area, rostral part

INTRODUCTION

The central extended amygdala (EAc) is a structural and functional macrosystem that is distinct from amygdala (Cassell et al. 1999; de Olmos and Heimer 1999; Alheid 2003; Heimer 2003; Shackman and Fox 2016). Its two principal elements, the central nucleus of amygdala (CeA) and the lateral bed nucleus of stria terminalis (STL) are critically involved in various emotion response such as fear and anxiety (Walker et al. 2009; Cai et al. 2012; Ravinder et al. 2013; Butler et al. 2016; De Bundel et al. 2016; Lange et al. 2016; Gungor and Pare 2016; Lebow and Chen 2016).

Multiple evidences suggest distinctive and often complex functional roles (i.e. opposing, complementary) of different EAc subdivisions. Though being treated as a main amygdaloid output nucleus (Pitkanen et al. 1997), CeA has been unveiled to exert differential functions via its different subdivisions (Tye et al. 2011; Ciocchi et al. 2010; Tovote et al. 2015). On the other hand, the STL, as a counterpart of CeA in the EAc macrosystem, also displays divergent, sometimes opposing functional roles in threat-related behavior responses (Jennings et al. 2013; Kim et al. 2013; Beyeler et al. 2016; Daniel and Rainnie 2016; Gungor and Pare 2016). The underlying structural heterogeneity of EAc efferents of mouse, particularly at its mesoscopic level, however, are not clear.

Mesoscopic efferents of STL have been extensively studied in rats (Holstege et al. 1985; Cassell et al. 1999; Dong et al. 2000; Dong et al. 2001b; Dong and Swanson 2003, 2004) and CeA (Krettek and Price 1978; Petrovich and Swanson 1997; Jolkkonen and Pitkanen 1998; Zahm et al. 1999). Within STL, its dorsal part (STLD) project very densely to its ventral part (STLV) and fusiform nucleus (Fu), but the reciprocal projection is much less strong (Dong et al. 2001b). In CeA, its lateral part (CeL) intensely project to its medial part (CeM), but there is an absence of projection in the reverse direction (Petrovich and Swanson 1997; Jolkkonen and Pitkanen 1998). Comparatively, the efferents of CeM tend to be denser and more complex than that of CeL (Petrovich and Swanson 1997; Jolkkonen and Pitkanen 1998), and a similar situation for STLV/Fu versus STLD was reported (Dong et al. 2001b). Some common output areas are also been reported across different studies. For instance, all the compartments of EAc project to the periaqueductal gray (PAG) and the parabrachial nucleus (PBN) (Petrovich and Swanson 1997; Zahm et al. 1999; Dong et al. 2001b). While these information has been essentially accumulated in rats, much less is known about the comparative EAc outputs in mice.

In this study, we injected the high sensitive anterograde tracers, the *Phaseolus* vulgaris-leucoagglutinin (PHA-L) (Gerfen and Sawchenko 1984; Wouterlood and Groenewegen 1985)

and biotin dextran amine (BDA) (Brandt and Apkarian 1992) into four subdivisions of EAc. While our preliminary work only concerned the main targets of EAc and that other prominent outputs remains to be analyzed, a concise view of EAc efferents is proposed which includes some of the salient patterns that consistently occur both for STL and CeA. First, intra-EAc projections originate in all the subdivisions, and often unidirectional and tend to converge to STLV(Fu) and CeM,. Second, compared to STLD and CeL/C, the STLV(Fu) and CeM tend to mediate the majority of extra-EAc outputs, either preferentially or similarly to a target area. These results indicate a comparable position of STLV(Fu) and CeM as the convergent point of intra-EAc circuits to mediating the extra-EAc outputs.

METHODS

Animal

6 – 9 week-old adult male C57BL/6J mice were purchased (Charles River®, L'Arbresle, France) and kept in a normal light-dark cycle (12/12-hour, 7 PM off) for 3 - 5 weeks before experiments. Food and water were available ad libitum. All the experimental protocols complied with the regulations of European Communities Council Directive and approved by the local ethical committee (CREMEAS under reference AL/61/68/02/13).

Anterograde tract-tracing

Anterograde tract-tracing was performed similarly to that retrograde tracing reported in the previous section. Briefly, animals were anesthetized with ketamine (87 mg/kg) and xylazine solution (13 mg/kg) (intraperitoneal injection, or i.p.). Animal care to prevent inflammation and drying of eyes were taken. A local craniotomy right above the area of interest was performed after the animal being mounted onto a stereotaxic frame (Model 900, David Kopf Instrument). Individual tracer solution was loaded into a glass pipette (tip diameter 15-35 μm) and positioned following the desired stereotaxic coordinates (see Table 1). Biotin dextran amine (BDA, 10000 MW; cat. #D1956, Molecular Probe®) was prepared as 4% solution in phosphate buffer saline, and the *Phaseolus vulgaris* leucoagglutinin (PHA-L; cat. #L-1110, Vector Laboratories®) as 2.5% solution in phosphate buffer. Subsequent iontophoresis was carried out via +3-5 μA (7 s ON/OFF cycle) (Midgard Model 51595, Stoelting Co.) for 10-15 min. The pipette was left in place for 5 - 10 min before withdrawing and wounds were taken care of. Then animal was monitored for recovery from the anesthesia and returned to their home cages. Survival time for both BDA and PHA-L is 7 - 14 days.

Tissue Preparations

The euthanasia of animal were done by pentobarbital (273 mg/kg, i.p.) or Dolethal (300 mg/kg, i.p.). After confirming the loss of toe-pinch reflex, transcardial perfusion was carried out with sequential the phosphate buffer (PB) (0.1 M, pH 7.4; 10 ml) and paraformaldehyde (PFA) (2%, in 0.1 M PB, pH 7.4; 150 ml). The brain was dissected out and post-fixed overnight (4 °C). Coronal brain sections (30 μm thick) were cut with a vibratome (VT1000S, Leica Biosystem) and sorted into a 12-well plate.

Primary Antibody

A goat-anti-PHA-L primary antibody (1:50000; Cat. #AS-2224, Vector Laboratories™) and the biotin-avidin system (1: 500; Cat. # PK-6100, Vector Laboratories™) was used for revealing BDA.

DAB Immunohistochemistry (IHC)

The IHC by peroxidase substrate, the 3,3'-diaminobenzidine (DAB), was used to reveal axonal fibers labeled by PHA-L and BDA. The procedures similar to previous section was carried out on floating brain slices. Briefly, slices were rinsed in PBS (3 x 5 min) and treated with H_2O_2 (1% in 50% ethanol; Cat. #: H1009, Sigma™) for 20 min. Then, slices were incubated with the blocking buffer (0.3% Triton X-100, 5% normal donkey serum in PBS) before being incubated with primary antibody (room temperature). A biotinylated horse-anti-goat secondary antibody (1:400; Cat. #: BA-9500, Vector Laboratories ™) and avidin-biotin-complex system (ABC-HRP kit, 1:400; Cat. #: PK-6100, Vector Laboratories ™) were each applied for 1.5 hr sequentially. Peroxidase DAB reaction were developed for 5 – 10 min with the following solution (1 ml): 900 μl Tris-Cl (50 mM, pH 7.5), 100 μl DAB (0.025%, Cat. #: D8001, Sigma™), 1.5 mg Nickel Ammonium Sulfate (0.15%), 0.25 mg CoCl (0.025%), 0.0006% H_2O_2. was applied at room temperature. Slices were mounted onto Superfrost® plus slides (Thermo Fisher Scientific™) and left for air-drying. Then slices were cleared in Roti®-Histol (Carl Roth™) and coverslipped with EUKITT® mounting medium (O. Kindler, ORSAtec GmbH, Germany).

Imaging and Data analysis

Images of the black reaction product from DAB IHC were acquired by Neurolucida 10.0 software (MBF Bioscience ™) on a brightfield microscope (Nikon Eclipse 80i, 4x). Images

cropping, stitching and contrasts were adjusted in FIJI (Preibisch et al. 2009; Schindelin et al. 2012).

RESULTS

Injection sites

The quality of injection sites were checked on the successive brain sections containing the regions of interest. Thirteen cases displayed injection sites centered in the target EAc subdivision (Table 2). Depending on the nature of tracers and target structures, the injection sites often encroached into nearby areas, which we terms as the secondary injection sites (Table 2). These secondary injections sites (i.e. ventral medial ST, or STMV in Fig. 1 b) displayed diffuse somatic labeling laying outside the primary targets including STLD (Fig. 1a), STLV (possibly also containing Fu, Fig. 1b), CeL/C (Fig. 1c) and CeM (Fig. 1d). In all the 8 cases that qualified for the analysis of outputs, the concerns of confounding projections from these secondary structures seem negligible, as the descriptive patterns and semi-quantifications remained quite consistent across the cases. Hence, we describe the outputs from subdivisions of EAc in a comparative manner.

Major outputs from subdivisions of EAc

The major outputs from the four subdivisions of EAc were distributed across the brain, including mainly subcortical nuclei. These targets can be grouped into several categories, such as the extended amygdala, telencephalon, hypothalamus, thalamus, midbrain, pons, and medulla. The intensity of the projection field were assessed in a four grade scales (Table 3), with the absence (denoted as "-") as the lowest intensity and densest (denoted as "++++") as the highest one. This semiquantitative assessment revealed the differences of projection strength from the four nuclei of EAc.

In general, all four nuclei can project to intra-EAc targets, either faintly or strongly depending on the output subdivisions. On the other hand, the major extra-EAc outputs come from STLV(Fu) and CeM, while STLD and CeL/C innervate significantly only a few nuclei (i.e. parasubthalamic nucleus or PSTh, the external part of lateral PBN or LPBE and the solitary nucleus or Sol) (see Table 3).

Outputs to the extended amygdala

Anterograde tract tracing from the four areas unveiled strong projections within EAc, as well as to STMA and STMV, the ST areas belonging to medial extended amygdala (EAm), but not the amygdaloid components of the EAm (i.e. medial nucleus of amygdala).
Within EAc, moderate to strong axonal projections can be found in all the subdivisions. STLD was innervated strongly by CeL/C and CeM, but only very sparsely by STLV (Fig. 2). In comparison, its neighbouring STLP received strong projections from all the three areas (Fig. 2). The fusiform nucleus (Fu) got the strongest inputs from the rest of EAc, especially from STLD and CeL/C. On the other hand, CeL/C was only lightly or moderately innervated by STLD and barely by the CeM or STLV (Fig. 3). Comparatively, the CeM received moderate to strong inputs from STLD, STLV and CeL/C (Fig. 3). Finally, the IPAC received a significant input from CeM, along with a lighter one from STLV/Fu.
Projections from EAc to EAm were also observed. In particular, STMA and STMV received strong inputs from CeM, and likely from STLV (Fig. 2). The STLD and CeL/C, in a similar way, moderately project to STMV, and less to STMA (Fig. 2).
Overall, several projection patterns were unfolded. First, both bidirectional and unidirectional connections were ubiquitously found within EAc. Strong bidirectional projections were obvious in pairs including STLD – CeL/C, STLD – CeM and STLV – CeM, while projections like CeL/C→STLV, CeL/C→CeM and, STLD→ STLV were preferentially unidirectional. In a similar way to CeM, STLD and CeL/C also strongly projected to Fu, lesser to STLV. However, unlike CeM, STLV projected poorly to STLD or CeL/C. Second, the CeM, Fu, to a less extent the STLV are the most innervated nuclei within EAc. While CeL/C was only significantly targeted by STLD, the latter was under strong influence of both CeL/C and CeM.

Outputs to other telencephalic structures

Beside extended amygdala, a few other structures in telencephalon received outputs from EAc. Both shell and core portions of nucleus accumbens (AcbSh and AcbC respectively) were significantly innervated by STLV/Fu, but appear relatively deprived of projections from STLD and CeL/C (Fig. 4). CeM injections produced light labeling in the AcbSh, but very few in the AcbC. The basal part of substantia innominata (SIB), however, was substantially innervated by the output nuclei (i.e. STLV and CeM), but sparsely by STLD and CeL/C (Fig. 2).

Outputs to thalamus

The paraventricular thalamic nucleus is a major thalamic target of EAc and is innervated differentially by these four EAc subdivisions depending on the rostrocaudal level. The anterior part (PVA) was innervated by light to moderate density of STLV axons, but very sparsely by others subdivisions (Fig. 5a, d, g, j). Its middle part (PV) was strongly innervated by STLV and CeM, lightly by CeL/C, but very sparsely by STLD (Fig. 5b, e, h, k). In comparison, the posterior portion (PVP) received only a light innervation, even from STLV and CeM, while STLD and CeL/C provided a very sparse input (Fig. 5c, f, i, l). Thus, the STLV/Fu, and to a less extent CeM, projected most intensely to PV; the STLD barely projected to PV, but CeL/C lightly innervated the middle level of PV. At rostral level, STLV and CeM also strongly innervated the posteromedian thalamic nucleus (PoMn) (Fig. 5c, f, i, l).

Outputs to the hypothalamus

EAc provided strong inputs to several hypothalamic nuclei, including the paraventricular hypothalamic nucleus (Pa), lateral hypothalamic area (LH), and PSTh. The Pa was most densely innervated by STLV/Fu, lightly by CeM, but very sparsely by STLD or CeL/C (Fig. 6a, c, e, g). The lateral Pa (or the magnocellular Pa) was the most frequent target of EAc nuclei, but equally strong axon field was observed along the medial Pa (or the parvocellular Pa) when injection was placed in STLV/Fu.

Similarly, the strongest inputs to LH came from STLV/Fu, while less intense inputs from CeM, but very sparse from STLD or CeL/C (Fig. 6a, c, e, g). The STLV/Fu also strongly innervated areas around the fornix and the ventral part of hypothalamus. In contrast, PSTh received substantial inputs from STLD and CeL/C, even though stronger inputs originated from STLV and CeM (Fig. 6b, d, f, h).

Outputs to the brainstem

Several brainstem regions, including rostral part of ventral tegmental area (VTAR), PAG, dorsal raphe nucleus (DR), retrorubral field (RRF), PBN, sol and pontomedullary reticular formation were strongly innervated by EAc outputs.

In the midbrain, the VTAR was most strongly innervated by STLV/Fu, moderately by CeM, lightly by CeL/C, but very sparsely by STLD (Fig. 7a, d, g, j). STLV/Fu axonal projections to the ventral poles of VTAR, as well as to the retromamillary nucleus were also quite strong. The ventrolateral PAG (VLPAG) was strongly innervated by STLV and CeM (Fig.7). By contrast, both STLD and CeL/C projected very sparsely to the rostral or caudal LPAG (Fig.

7b, e, h, k; c, f, i, l), but lightly or moderately to VLPAG (Fig. 7c, f, i, l). The STLV/Fu and CeM injection also resulted in light axon labeling in dorsomedial PAG (DMPAG), which was not the case for STLD or CeL/C injections. Besides PAG, STLV/Fu and CeM provided the most intense inputs to raphe nuclei, including caudal linear nucleus and DR. Interestingly, the RRF was significantly innervated by all four areas. However, the strongest inputs came from STLV/Fu and CeM, while those from STLD and CeL/C were light to moderate (Fig. 7b, e, h, k).

In the pons, the PBN was among the major targets of EAc nuclei. The LPBE was strongly innervated by STLD, CeL/C and CeM, but only lightly by STLV/Fu (Fig. 8a, c, e, g). The STLV/Fu projection sparsely distributed in the ventral and dorsal part of LPB, and took a different fiber pathway than that of the other EAc subdivisions. It is also worth noting that STLV and CeM also projected strongly to the ventral part of LPB. In comparison, medial PBN (MPB) was mostly innervated by CeM, while lightly to moderately by other EAc subdivisions.

The Sol of medulla, especially its ventral, medial and dorsomedial parts, was most strongly innervated by CeM, moderately by CeL/C and STLV/Fu and lightly by STLD. The projection to intermediate reticular nucleus (IRt) came in a similar fashion, with strongest to weakest projections from CeM, STLV/Fu, CeL/C, and STLD respectively (Fig 8b, d, f, h).

DISCUSSION

In this study, we investigated the efferents of four EAc nuclei with anterograde tract-tracing. As a preliminary effort, the analysis was limited to some prominent EAc efferents, including the EAc, pontine and medulla, forebrain areas, hypothalamus and thalamus. There are several features stay quite consistent under the analysis.

Overview of intra-EAc and extra-EAc efferents

First, all EAc nuclei display strong intra-EAc projections, whereas extra-EAc innervations are mainly come from STLV(Fu) and CeM. The strong intrinsic connectivities between EAc subdivisions and predominant roles of STLV and CeM in mediating outputs in mouse are consistent with previous reports on rats (Cassell et al. 1999; de Olmos and Heimer 1999; Alheid 2003; Dong et al. 2001a; Dong et al. 2001b; Jolkkonen and Pitkanen 1998). Second, the intra-EAc projection patterns favor a unidirectional information flow from STLD and CeL/C to STLV and CeM respectively, which are in line with previous reports (Krettek and Price 1978; Jolkkonen and Pitkanen 1998). While a moderate Fu projection to STLD was

observed in rat (Dong et al. 2001b), we found little in mouse. This discrepancy in our results might reflect a species difference. Finally, between CeM and STLV(Fu), we observed very often innervations of similar strength, as well as preferential innervations to many extra-EAc targets (Fig. 9). The PSTh, VLPAG, RRF are among the common targets of STLV(Fu) and CeM, Acb and VTAR are preferential efferents of STLV(Fu), and Sol is preferential one of CeM.

The first two patterns put STLV(Fu) at a similar position as that of CeM, by serving a major role in sending out information that processed by EAc. A significant innervations of STLV(Fu) by CeM was also observed.

Differential efferents to Acb

The AcbSh, not AcbC, has been reported to closely related to elements of EAc, especially the rostral levels of STL (Alheid and Heimer 1988). The AcbSh is reciprocally connected with EAc (Nauta et al. 1978; Heimer et al. 1991; Brog et al. 1993; Heimer et al. 1997). For example, retrograde tracing with fluorogold from its dorsomedial extremity resulted in strong labeling in STL, sublenticular extended amygdala (SLEA), and CeA (Brog et al. 1993). In our hands, we observed intense axonal projections to the ventromedial portion of AcbSh from STLV(Fu), but very sparse or light one from other three nuclei (Fig 4), which are in line with a previous study (Dong et al. 2001b). We also found a less intense labeling in ventral AcbC, which could due to a possible encroachment of nearby lateral preoptic area or ventral pallidum that project to both AchSh and AcbC (Brog et al. 1993). Therefore, future retrograde tracing experiments from dorsomedial part of AcbSh are needed to confirm Acb-projecting neurons in STL.

Differential efferents to PV

The paraventricular nucleus of thalamus, especially its posterior part (PVP) strongly projects to EAc nuclei such as STL, SLEA and CeA (Li and Kirouac 2008; Kirouac 2015). On the other hand, EAc also projects back to PV (Otake and Nakamura 1995; Penzo et al. 2014; Dong et al. 2017b). In this study, we looked at EAc projections to paraventricular nucleus of thalamus at its different rostral-caudal levels. Overall, its middle levels were most heavily innervated, primarily by STLV(Fu), less by CeM, while often not or sparsely by STLD and CeL/C. As PV plays roles both in appetitive behavior and fear learning (Penzo et al. 2015; Dong et al. 2017a), a stronger STLV(Fu) → PV pathway can potentially modulate effects of CeL/C → PV pathway.

Differential efferents to Pa

Retrograde tracing from Pa shows moderate labeling in the ventral STL, but light one in its dorsal part (Cullinan et al. 1993). In line with this, our results showed dense axonal labeling in Pa after PHA-L injection in STLV(Fu).

As a whole structure, ST has been regarded as a hub in mediating hypothalamic-pituitary-adrenal (HPA) (Sullivan et al. 2004; Lebow and Chen 2016). For instance, lesion of ST impaired HPA response to contextual fear conditioning (Sullivan et al. 2004) and lesion of STLV (Fu) reduced HPA response to acute stress (Choi et al. 2007). It is possible that STLV(Fu) is the major EAc nucleus that modulate the HPA response to stress and anxiety, possibly via CRF neurons (Moga and Saper 1994).

Differential efferents to parabrachial nucleus

EAc subdivisions are strongly innervated by LPBE (Saper and Loewy 1980; Bernard et al. 1991; Yasui et al. 1991; Bernard et al. 1993; Krukoff et al. 1993; Alden et al. 1994). On the other hand, STL and CeA project strongly back to parabrachial nucleus, including the LPBE (Veening et al. 1984; Moga and Gray 1985; Moga et al. 1989; Moga et al. 1990; Petrovich and Swanson 1997; Tokita et al. 2009; Panguluri et al. 2009). In our study, we observed similar mutual connections between LPBE and EAc subdivisions, except the STLV(Fu) which only projected back lightly. This indicates a stronger direct LPBE influence on STLV(Fu) than the opposite direction.

On the other hand, strong density of axonal terminals from STLD, CeL/C, and CeM can significantly influence the activity of LPBE neurons. Considering the intrinsic control of CeM by CeL/C projection neurons (Sun and Cassell 1993; Veinante and Freund-Mercier 1998; Cassell et al. 1999), we could expected a bidirectional modulation of LPBE activity by EAc nuclei.

Differential efferents to solitary nucleus

CeM forms the one of the densest axonal terminal fields in Sol, while only sparse or moderate innervations from other parts of EAc. This dominant CeM output to Sol in mouse stands well in line with what has been reported in cat (Hopkins and Holstege 1978), rat (Higgins and Schwaber 1983), and rabbit (Schwaber et al. 1980). Although the posterior STL can strongly project to Sol (Schwaber et al. 1980; Holstege et al. 1985), STLD and STLP lightly innervated Sol.

CONCLUSION

In this study, we looked at the comparative aspects of mesoscopic efferents from four major EAc nuclei. Many of our preliminary results stand in line with previous reports on rat studies, however, we also present evidences of parallel, primary roles of STLV(Fu) and CeM in mediating the EAc outputs to brain centers in generating autonomic and emotional responses (Hopkins and Holstege 1978; Holstege et al. 1985; Gray and Magnuson 1987, 1992). On the other hand, we saw certain limitations in this study. For example, in most of our descriptions and discussions, we use STLV(Fu) refer to STLV and Fu collectively, both which not equally projected by STLD or CeA. Of course, further researches are needed to delve into specific aspects of these afferents.

While the functional neuronal circuits of CeM have been a hot research topics (Ciocchi et al. 2010; Haubensak et al. 2010; Calhoon and Tye 2015; Han et al. 2015; Tovote et al. 2015), its counterpart, the STLV(Fu), has only been sporadically addressed (Jennings et al. 2013; Kim et al. 2013; Daniel and Rainnie 2016; Gungor and Pare 2016). Our results revealed coexistence of distinctive set of common efferents and preferential efferents from STLV(Fu) and CeM, which might guide future efforts in dissecting functional roles of these distinct and shared efferents.

REFERENCES

Alden M, Besson JM, Bernard JF (1994) Organization of the efferent projections from the pontine parabrachial area to the bed nucleus of the stria terminalis and neighboring regions: a PHA-L study in the rat. J Comp Neurol 341 (3):289-314. doi:10.1002/cne.903410302

Alheid GF (2003) Extended amygdala and basal forebrain. Ann N Y Acad Sci 985:185-205. doi:10.1111/j.1749-6632.2003.tb07082.x

Alheid GF, Heimer L (1988) New perspectives in basal forebrain organization of special relevance for neuropsychiatric disorders: the striatopallidal, amygdaloid, and corticopetal components of substantia innominata. Neuroscience 27 (1):1-39

Bernard JF, Alden M, Besson JM (1993) The organization of the efferent projections from the pontine parabrachial area to the amygdaloid complex: a Phaseolus vulgaris leucoagglutinin (PHA-L) study in the rat. J Comp Neurol 329 (2):201-229. doi:10.1002/cne.903290205

Bernard JF, Carroue J, Besson JM (1991) Efferent projections from the external parabrachial area to the forebrain: a Phaseolus vulgaris leucoagglutinin study in the rat. Neurosci Lett 122 (2):257-260

Beyeler A, Namburi P, Glober GF, Simonnet C, Calhoon GG, Conyers GF, Luck R, Wildes CP, Tye KM (2016) Divergent Routing of Positive and Negative Information from the Amygdala during Memory Retrieval. Neuron 90 (2):348-361. doi:10.1016/j.neuron.2016.03.004

Brandt HM, Apkarian AV (1992) Biotin-dextran: a sensitive anterograde tracer for neuroanatomic studies in rat and monkey. J Neurosci Methods 45 (1-2):35-40. doi:0165-0270(92)90041-B [pii]

Brog JS, Salyapongse A, Deutch AY, Zahm DS (1993) The patterns of afferent innervation of the core and shell in the "accumbens" part of the rat ventral striatum: immunohistochemical detection of retrogradely transported fluoro-gold. J Comp Neurol 338 (2):255-278. doi:10.1002/cne.903380209

Butler RK, Oliver EM, Sharko AC, Parilla-Carrero J, Kaigler KF, Fadel JR, Wilson MA (2016) Activation of corticotropin releasing factor-containing neurons in the rat central amygdala and bed nucleus of the stria terminalis following exposure to two different anxiogenic stressors. Behav Brain Res 304:92-101. doi:10.1016/j.bbr.2016.01.051

Cai L, Bakalli H, Rinaman L (2012) Yohimbine anxiogenesis in the elevated plus maze is disrupted by bilaterally disconnecting the bed nucleus of the stria terminalis from the central nucleus of the amygdala. Neuroscience 223:200-208. doi:10.1016/j.neuroscience.2012.08.008

Calhoon GG, Tye KM (2015) Resolving the neural circuits of anxiety. Nat Neurosci 18 (10):1394-1404. doi:10.1038/nn.4101

Cassell MD, Freedman LJ, Shi C (1999) The intrinsic organization of the central extended amygdala. Ann N Y Acad Sci 877:217-241

Chen Y, Molet J, Gunn BG, Ressler K, Baram TZ (2015) Diversity of Reporter Expression Patterns in Transgenic Mouse Lines Targeting Corticotropin-Releasing Hormone-Expressing Neurons. Endocrinology 156 (12):4769-4780. doi:10.1210/en.2015-1673

Choi DC, Furay AR, Evanson NK, Ostrander MM, Ulrich-Lai YM, Herman JP (2007) Bed nucleus of the stria terminalis subregions differentially regulate hypothalamic-pituitary-adrenal axis activity: implications for the integration of limbic inputs. J Neurosci 27 (8):2025-2034. doi:10.1523/JNEUROSCI.4301-06.2007

Chung EK, Chen LW, Chan YS, Yung KK (2008) Downregulation of glial glutamate transporters after dopamine denervation in the striatum of 6-hydroxydopamine-lesioned rats. J Comp Neurol 511 (4):421-437. doi:10.1002/cne.21852

Ciocchi S, Herry C, Grenier F, Wolff SB, Letzkus JJ, Vlachos I, Ehrlich I, Sprengel R, Deisseroth K, Stadler MB, Muller C, Luthi A (2010) Encoding of conditioned fear in central amygdala inhibitory circuits. Nature 468 (7321):277-282. doi:10.1038/nature09559

Cullinan WE, Herman JP, Watson SJ (1993) Ventral subicular interaction with the hypothalamic paraventricular nucleus: evidence for a relay in the bed nucleus of the stria terminalis. J Comp Neurol 332 (1):1-20. doi:10.1002/cne.903320102

Daniel SE, Rainnie DG (2016) Stress Modulation of Opposing Circuits in the Bed Nucleus of the Stria Terminalis. Neuropsychopharmacology 41 (1):103-125. doi:10.1038/npp.2015.178

De Bundel D, Zussy C, Espallergues J, Gerfen CR, Girault JA, Valjent E (2016) Dopamine D2 receptors gate generalization of conditioned threat responses through mTORC1 signaling in the extended amygdala. Mol Psychiatry 21 (11):1545-1553. doi:10.1038/mp.2015.210

de Olmos JS, Heimer L (1999) The concepts of the ventral striatopallidal system and extended amygdala. Ann N Y Acad Sci 877:1-32

Dong H, Petrovich GD, Swanson LW (2000) Organization of projections from the juxtacapsular nucleus of the BST: a PHAL study in the rat. Brain Res 859 (1):1-14

Dong HW, Petrovich GD, Swanson LW (2001a) Topography of projections from amygdala to bed nuclei of the stria terminalis. Brain Res Brain Res Rev 38 (1-2):192-246

Dong HW, Petrovich GD, Watts AG, Swanson LW (2001b) Basic organization of projections from the oval and fusiform nuclei of the bed nuclei of the stria terminalis in adult rat brain. J Comp Neurol 436 (4):430-455
Dong HW, Swanson LW (2003) Projections from the rhomboid nucleus of the bed nuclei of the stria terminalis: implications for cerebral hemisphere regulation of ingestive behaviors. J Comp Neurol 463 (4):434-472. doi:10.1002/cne.10758
Dong HW, Swanson LW (2004) Organization of axonal projections from the anterolateral area of the bed nuclei of the stria terminalis. J Comp Neurol 468 (2):277-298. doi:10.1002/cne.10949
Dong X, Li S, Kirouac GJ (2017a) Collateralization of projections from the paraventricular nucleus of the thalamus to the nucleus accumbens, bed nucleus of the stria terminalis, and central nucleus of the amygdala. Brain Struct Funct. doi:10.1007/s00429-017-1445-8
Dong X, Li S, Kirouac GJ (2017b) Collateralization of projections from the paraventricular nucleus of the thalamus to the nucleus accumbens, bed nucleus of the stria terminalis, and central nucleus of the amygdala. Brain Struct Funct 222 (9):3927-3943. doi:10.1007/s00429-017-1445-8
Franke-Radowiecka A (2011) Immunohistochemical characterisation of dorsal root ganglia neurons supplying the porcine mammary gland. Histol Histopathol 26 (12):1509-1517. doi:10.14670/HH-26.1509
Furmanski O, Gajavelli S, Lee JW, Collado ME, Jergova S, Sagen J (2009) Combined extrinsic and intrinsic manipulations exert complementary neuronal enrichment in embryonic rat neural precursor cultures: an in vitro and in vivo analysis. J Comp Neurol 515 (1):56-71. doi:10.1002/cne.22027
Gerfen CR, Sawchenko PE (1984) An anterograde neuroanatomical tracing method that shows the detailed morphology of neurons, their axons and terminals: immunohistochemical localization of an axonally transported plant lectin, Phaseolus vulgaris leucoagglutinin (PHA-L). Brain Res 290 (2):219-238
Gray TS, Magnuson DJ (1987) Neuropeptide neuronal efferents from the bed nucleus of the stria terminalis and central amygdaloid nucleus to the dorsal vagal complex in the rat. J Comp Neurol 262 (3):365-374. doi:10.1002/cne.902620304
Gray TS, Magnuson DJ (1992) Peptide immunoreactive neurons in the amygdala and the bed nucleus of the stria terminalis project to the midbrain central gray in the rat. Peptides 13 (3):451-460
Gungor NZ, Pare D (2016) Functional Heterogeneity in the Bed Nucleus of the Stria Terminalis. J Neurosci 36 (31):8038-8049. doi:10.1523/JNEUROSCI.0856-16.2016
Han S, Soleiman MT, Soden ME, Zweifel LS, Palmiter RD (2015) Elucidating an Affective Pain Circuit that Creates a Threat Memory. Cell 162 (2):363-374. doi:10.1016/j.cell.2015.05.057
Haubensak W, Kunwar PS, Cai H, Ciocchi S, Wall NR, Ponnusamy R, Biag J, Dong HW, Deisseroth K, Callaway EM, Fanselow MS, Luthi A, Anderson DJ (2010) Genetic dissection of an amygdala microcircuit that gates conditioned fear. Nature 468 (7321):270-276. doi:10.1038/nature09553
Heimer L (2003) A new anatomical framework for neuropsychiatric disorders and drug abuse. Am J Psychiatry 160 (10):1726-1739. doi:10.1176/appi.ajp.160.10.1726
Heimer L, Alheid GF, de Olmos JS, Groenewegen HJ, Haber SN, Harlan RE, Zahm DS (1997) The accumbens: beyond the core-shell dichotomy. J Neuropsychiatry Clin Neurosci 9 (3):354-381. doi:10.1176/jnp.9.3.354
Heimer L, Zahm DS, Churchill L, Kalivas PW, Wohltmann C (1991) Specificity in the projection patterns of accumbal core and shell in the rat. Neuroscience 41 (1):89-125
Higgins GA, Schwaber JS (1983) Somatostatinergic projections from the central nucleus of the amygdala to the vagal nuclei. Peptides 4 (5):657-662
Holstege G, Meiners L, Tan K (1985) Projections of the bed nucleus of the stria terminalis to the mesencephalon, pons, and medulla oblongata in the cat. Exp Brain Res 58 (2):379-391
Hopkins DA, Holstege G (1978) Amygdaloid projections to the mesencephalon, pons and medulla oblongata in the cat. Exp Brain Res 32 (4):529-547
Jennings JH, Rizzi G, Stamatakis AM, Ung RL, Stuber GD (2013) The inhibitory circuit architecture of the lateral hypothalamus orchestrates feeding. Science 341 (6153):1517-1521. doi:10.1126/science.1241812
Jhou TC, Geisler S, Marinelli M, Degarmo BA, Zahm DS (2009) The mesopontine rostromedial tegmental nucleus: A structure targeted by the lateral habenula that projects to the ventral tegmental area of Tsai and substantia nigra compacta. J Comp Neurol 513 (6):566-596. doi:10.1002/cne.21891
Jolkkonen E, Pitkanen A (1998) Intrinsic connections of the rat amygdaloid complex: projections originating in the central nucleus. J Comp Neurol 395 (1):53-72
Kim SY, Adhikari A, Lee SY, Marshel JH, Kim CK, Mallory CS, Lo M, Pak S, Mattis J, Lim BK, Malenka RC, Warden MR, Neve R, Tye KM, Deisseroth K (2013) Diverging neural pathways assemble a behavioural state from separable features in anxiety. Nature 496 (7444):219-223. doi:10.1038/nature12018
Kirouac GJ (2015) Placing the paraventricular nucleus of the thalamus within the brain circuits that control behavior. Neurosci Biobehav Rev 56:315-329. doi:10.1016/j.neubiorev.2015.08.005

Krettek JE, Price JL (1978) Amygdaloid projections to subcortical structures within the basal forebrain and brainstem in the rat and cat. J Comp Neurol 178 (2):225-254. doi:10.1002/cne.901780204
Krukoff TL, Harris KH, Jhamandas JH (1993) Efferent projections from the parabrachial nucleus demonstrated with the anterograde tracer Phaseolus vulgaris leucoagglutinin. Brain Res Bull 30 (1-2):163-172
Lange MD, Daldrup T, Remmers F, Szkudlarek HJ, Lesting J, Guggenhuber S, Ruehle S, Jungling K, Seidenbecher T, Lutz B, Pape HC (2016) Cannabinoid CB1 receptors in distinct circuits of the extended amygdala determine fear responsiveness to unpredictable threat. Mol Psychiatry. doi:10.1038/mp.2016.156
Lebow MA, Chen A (2016) Overshadowed by the amygdala: the bed nucleus of the stria terminalis emerges as key to psychiatric disorders. Mol Psychiatry 21 (4):450-463. doi:10.1038/mp.2016.1
Li S, Kirouac GJ (2008) Projections from the paraventricular nucleus of the thalamus to the forebrain, with special emphasis on the extended amygdala. J Comp Neurol 506 (2):263-287. doi:10.1002/cne.21502
Moga MM, Gray TS (1985) Evidence for corticotropin-releasing factor, neurotensin, and somatostatin in the neural pathway from the central nucleus of the amygdala to the parabrachial nucleus. J Comp Neurol 241 (3):275-284. doi:10.1002/cne.902410304
Moga MM, Herbert H, Hurley KM, Yasui Y, Gray TS, Saper CB (1990) Organization of cortical, basal forebrain, and hypothalamic afferents to the parabrachial nucleus in the rat. J Comp Neurol 295 (4):624-661. doi:10.1002/cne.902950408
Moga MM, Saper CB (1994) Neuropeptide-immunoreactive neurons projecting to the paraventricular hypothalamic nucleus in the rat. J Comp Neurol 346 (1):137-150. doi:10.1002/cne.903460110
Moga MM, Saper CB, Gray TS (1989) Bed nucleus of the stria terminalis: cytoarchitecture, immunohistochemistry, and projection to the parabrachial nucleus in the rat. J Comp Neurol 283 (3):315-332. doi:10.1002/cne.902830302
Nauta WJ, Smith GP, Faull RL, Domesick VB (1978) Efferent connections and nigral afferents of the nucleus accumbens septi in the rat. Neuroscience 3 (4-5):385-401. doi:10.1016/0306-4522(78)90041-6
Otake K, Nakamura Y (1995) Sites of origin of corticotropin-releasing factor-like immunoreactive projection fibers to the paraventricular thalamic nucleus in the rat. Neurosci Lett 201 (1):84-86
Panguluri S, Saggu S, Lundy R (2009) Comparison of somatostatin and corticotrophin-releasing hormone immunoreactivity in forebrain neurons projecting to taste-responsive and non-responsive regions of the parabrachial nucleus in rat. Brain Res 1298:57-69. doi:10.1016/j.brainres.2009.08.038
Paxinos G, Franklin K (2012) Paxinos and Franklin's the Mouse Brain in Stereotaxic Coordinates. Academic Press
Penzo MA, Robert V, Li B (2014) Fear conditioning potentiates synaptic transmission onto long-range projection neurons in the lateral subdivision of central amygdala. J Neurosci 34 (7):2432-2437. doi:10.1523/JNEUROSCI.4166-13.2014
Penzo MA, Robert V, Tucciarone J, De Bundel D, Wang M, Van Aelst L, Darvas M, Parada LF, Palmiter RD, He M, Huang ZJ, Li B (2015) The paraventricular thalamus controls a central amygdala fear circuit. Nature. doi:10.1038/nature13978
Petrovich GD, Swanson LW (1997) Projections from the lateral part of the central amygdalar nucleus to the postulated fear conditioning circuit. Brain Res 763 (2):247-254
Pitkanen A, Savander V, LeDoux JE (1997) Organization of intra-amygdaloid circuitries in the rat: an emerging framework for understanding functions of the amygdala. Trends Neurosci 20 (11):517-523
Preibisch S, Saalfeld S, Tomancak P (2009) Globally optimal stitching of tiled 3D microscopic image acquisitions. Bioinformatics 25 (11):1463-1465. doi:10.1093/bioinformatics/btp184
Ravinder S, Burghardt NS, Brodsky R, Bauer EP, Chattarji S (2013) A role for the extended amygdala in the fear-enhancing effects of acute selective serotonin reuptake inhibitor treatment. Transl Psychiatry 3:e209. doi:10.1038/tp.2012.137
Saper CB, Loewy AD (1980) Efferent connections of the parabrachial nucleus in the rat. Brain Res 197 (2):291-317
Schindelin J, Arganda-Carreras I, Frise E, Kaynig V, Longair M, Pietzsch T, Preibisch S, Rueden C, Saalfeld S, Schmid B, Tinevez JY, White DJ, Hartenstein V, Eliceiri K, Tomancak P, Cardona A (2012) Fiji: an open-source platform for biological-image analysis. Nat Methods 9 (7):676-682. doi:10.1038/nmeth.2019
Schwaber JS, Kapp BS, Higgins G (1980) The origin and extent of direct amygdala projections to the region of the dorsal motor nucleus of the vagus and the nucleus of the solitary tract. Neurosci Lett 20 (1):15-20
Shackman AJ, Fox AS (2016) Contributions of the Central Extended Amygdala to Fear and Anxiety. J Neurosci 36 (31):8050-8063. doi:10.1523/JNEUROSCI.0982-16.2016
Sullivan GM, Apergis J, Bush DE, Johnson LR, Hou M, Ledoux JE (2004) Lesions in the bed nucleus of the stria terminalis disrupt corticosterone and freezing responses elicited by a contextual but not by a

specific cue-conditioned fear stimulus. Neuroscience 128 (1):7-14. doi:10.1016/j.neuroscience.2004.06.015
Sun N, Cassell MD (1993) Intrinsic GABAergic neurons in the rat central extended amygdala. J Comp Neurol 330 (3):381-404. doi:10.1002/cne.903300308
Tokita K, Inoue T, Boughter JD, Jr. (2009) Afferent connections of the parabrachial nucleus in C57BL/6J mice. Neuroscience 161 (2):475-488. doi:10.1016/j.neuroscience.2009.03.046
Tovote P, Fadok JP, Luthi A (2015) Neuronal circuits for fear and anxiety. Nat Rev Neurosci 16 (6):317-331. doi:10.1038/nrn3945
Tye KM, Prakash R, Kim SY, Fenno LE, Grosenick L, Zarabi H, Thompson KR, Gradinaru V, Ramakrishnan C, Deisseroth K (2011) Amygdala circuitry mediating reversible and bidirectional control of anxiety. Nature 471 (7338):358-362. doi:10.1038/nature09820
Veening JG, Swanson LW, Sawchenko PE (1984) The organization of projections from the central nucleus of the amygdala to brainstem sites involved in central autonomic regulation: a combined retrograde transport-immunohistochemical study. Brain Res 303 (2):337-357
Veinante P, Freund-Mercier MJ (1998) Intrinsic and extrinsic connections of the rat central extended amygdala: an in vivo electrophysiological study of the central amygdaloid nucleus. Brain Res 794 (2):188-198. doi:S0006-8993(98)00228-5 [pii]
Walker DL, Miles LA, Davis M (2009) Selective participation of the bed nucleus of the stria terminalis and CRF in sustained anxiety-like versus phasic fear-like responses. Prog Neuropsychopharmacol Biol Psychiatry 33 (8):1291-1308. doi:10.1016/j.pnpbp.2009.06.022
Wang TW, Stromberg GP, Whitney JT, Brower NW, Klymkowsky MW, Parent JM (2006) Sox3 expression identifies neural progenitors in persistent neonatal and adult mouse forebrain germinative zones. J Comp Neurol 497 (1):88-100. doi:10.1002/cne.20984
Wouterlood FG, Groenewegen HJ (1985) Neuroanatomical tracing by use of Phaseolus vulgaris-leucoagglutinin (PHA-L): electron microscopy of PHA-L-filled neuronal somata, dendrites, axons and axon terminals. Brain Res 326 (1):188-191
Yasui Y, Saper CB, Cechetto DF (1991) Calcitonin gene-related peptide (CGRP) immunoreactive projections from the thalamus to the striatum and amygdala in the rat. J Comp Neurol 308 (2):293-310. doi:10.1002/cne.903080212
Zahm DS, Jensen SL, Williams ES, Martin JR, 3rd (1999) Direct comparison of projections from the central amygdaloid region and nucleus accumbens shell. Eur J Neurosci 11 (4):1119-1126

TABLES

Table 1. Stereotaxic coordinates for retrograde tract-tracing

Areas	Coordinates		
	AP (mm)	ML (mm)	DV (mm)
STLD	+0.20	+0.90	-3.30
STLV	+0.20	+0.90	-4.00
CeL/C	-1.43	+2.35	-3.75
CeM(rostral)	-1.07	+2.20	-4.00

Notes: Abbreviations, see the list. The stereotaxic coordinates are taken according to the Paxinos and Franklin's mouse brain atlas (Paxinos and Franklin 2012), with the bregma point as the origin for AP and ML axis. The DV distance was referred to its cortical surface above the corresponding AP, ML location.

Table 2: Summary of injection site of anterograde tracing.

Category	Case	Tracers	Injection site (primary)	Injection site (secondary)
STLD	1607G	PHA-L	STLD	STLP
	1603G	BDA	STLD	-
	1701C	BDA	STLD	STLP
CeL/C	1607F	BDA	CeL/C	CeM
	1701N	PHA-L	CeL/C	CeM, BLA
	1605I	PHA-L	CeL/C	CeM
	1602D	BDA	CeL/C	CeM
STLV	1609K	PHA-L	STLV/ Fu	STMV, LPO
	1705I	PHA-L	STLV	STMV, Fu
	1601E	BDA	STLV	Fu, STMV, LPO
CeM	1701M	PHA-L	CeM	CeC, CeL
	1705B	BDA	CeM	-
	1705D	PHA-L	CeM	CeL

Note: 1). The primary injection sites were confirmed by the intensity of somatic labeling in the targeted areas and the consistency of projection patterns within the same category.
2). A secondary injection sites were assigned to the confounding areas nearby the primary ones. In general, projections arising from these secondary injection sites contribute minorly to the overall projection pattern and intensity of a given case.
3). The minus sign (-) denotes absence of confounding secondary injection site.

Table 3. Semiquantitative assessments of projections from subdivisions of EAc.

Group	Area	Injection sites			
		STLD	CeL/C	STLV(Fu)	CeM
EAc	STLD	NA	++/+++	-/+	++/+++
	STLP	+/++	++	+++	++++
	Fu	++++	++++	NA	++++
	STLV	+/++	++	NA	++++
	IPAC	-/+	-/+	+	++/+++
	CeLC	+/++	NA	-/+	-/+
	CeM	+/++	+++	+++	NA
EAm	STMA	-/+	+	+++	+++/++++
	STMV	++	++	NA	+++/++++
Telencephalon	AcbSh	-/+	-	+++	+
	AcbC	-/+	-	++/+++	-/+
	SIB	-/+	-/+	+/++	+++
Thalamus	PVA	-	-/+	+/++	-/+
	PT	-	-	++	-/+
	PV	-/+	+	++/+++	++
	PVP	-/+	-/+	+	+
	PoMn	-	-/+	++/+++	++/+++
Hypothalamus	Pa	-/+	-/+	++++	+
	LH	-/+	-/+	+++/++++	++/+++
	PSTh	++	+++	++++	++++
Midbrain	DMPAG	-	-	+	+
	LPAG	-/+	-/+	+++	+++
	VLPAG	++	+/++	++++	+++/++++
	VTAR	-/+	+	++++	++
	RRF	+/++	++	+++	+++
	CLi	-/+	-/+	++++	-/+
	DR	+	-/+	+++	++
Pons	LPBE	++++	++++	+	++++
	MPB	+	+/++	++	++++
Medulla	IRt	-/+	+	+/++	++/+++
	SolM	-/+	+/++	+	++++
	SolV	-/+	++	++	++++
	SolDM	-/+	++	+	++++
	SolIM	-	-	-	-/+
	SolL	-	-	-	-/+

Note: Scales of semi-quantifications: NA, not available; -, absence; -/+, sparse; +, light; +/++, light to moderate; ++, moderate; ++/+++, moderate to strong; +++, strong; +++/++++, strong to densest; ++++, densest.

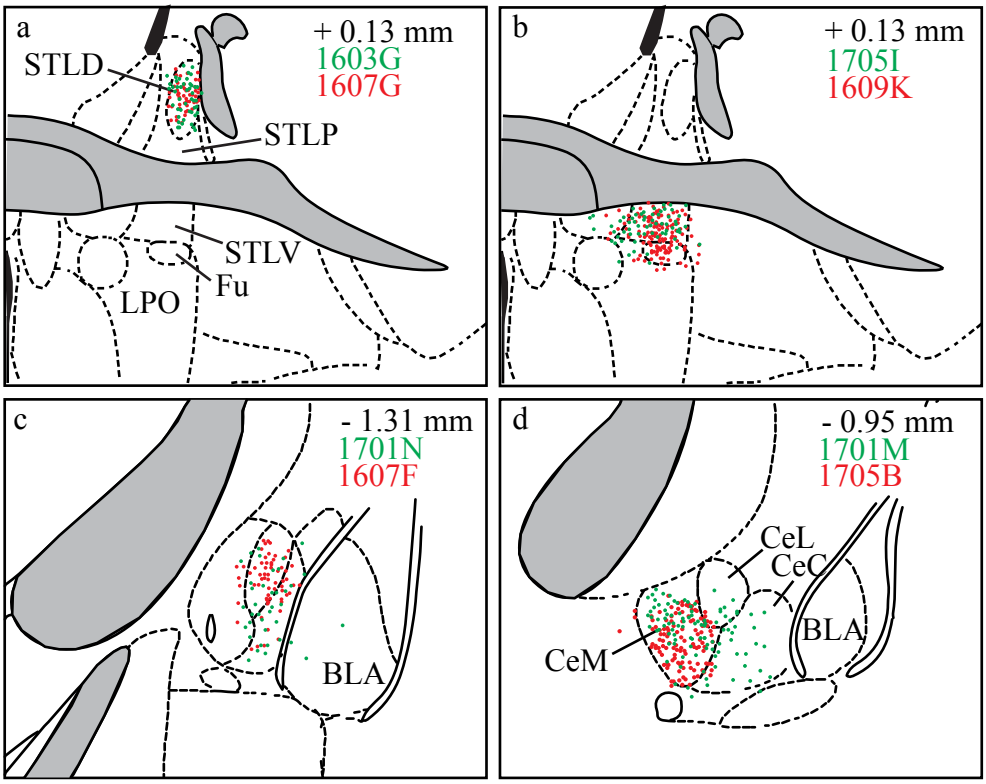

Fig. 1 Injection sites from the anterograde tracing cases used in the study. Following iontophoresis injection of BDA or PHA-L into subdivisions of EAc, injection sites were checked on successive sections of STL and CeA. Injection sites for STLD (**a**; case 1607G and 1607G, bregma level +0.13 mm), STLV (**b**; case 1705I and 1609K, bregma level +0.13 mm), CeL/C (**c**; case 1607F and 1701N, bregma level -1.31 mm) and rostral CeM (**c**; case 1701M and 1705B, bregma level -0.95 mm) were shown in which PHAL+ or BDA+ cells are represented by the dots. Distributions of soma were traced and mapped manually to a matched level of mouse brain atlas. Abbreviation: see list.

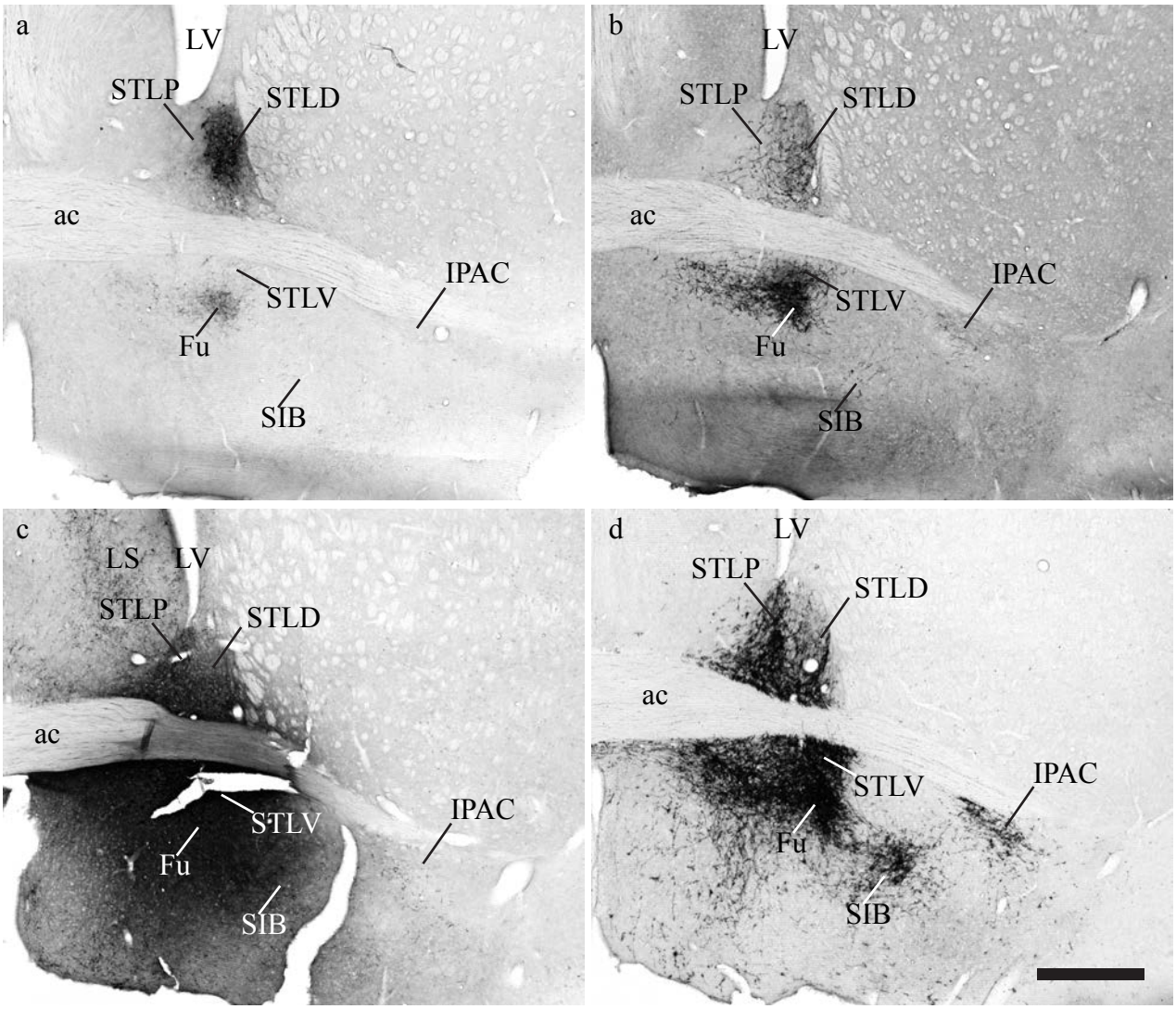

Fig. 2 Differential outputs to bed nucleus of stria terminalis from subdivisions of EAc. Bright field images show outputs to ST (bregma level +0.13 mm) from STLD (**a**; case 1603G), CeL/C (**b**; case 1607F), STLV (**c**; case 1609K) and rostral CeM (**d**; case 1701M), following the iontophoresis injection of BDA or PHA-L into corresponding areas. Abbreviation: see list. Scale bar: **a, b, c, d**, 500 μm.

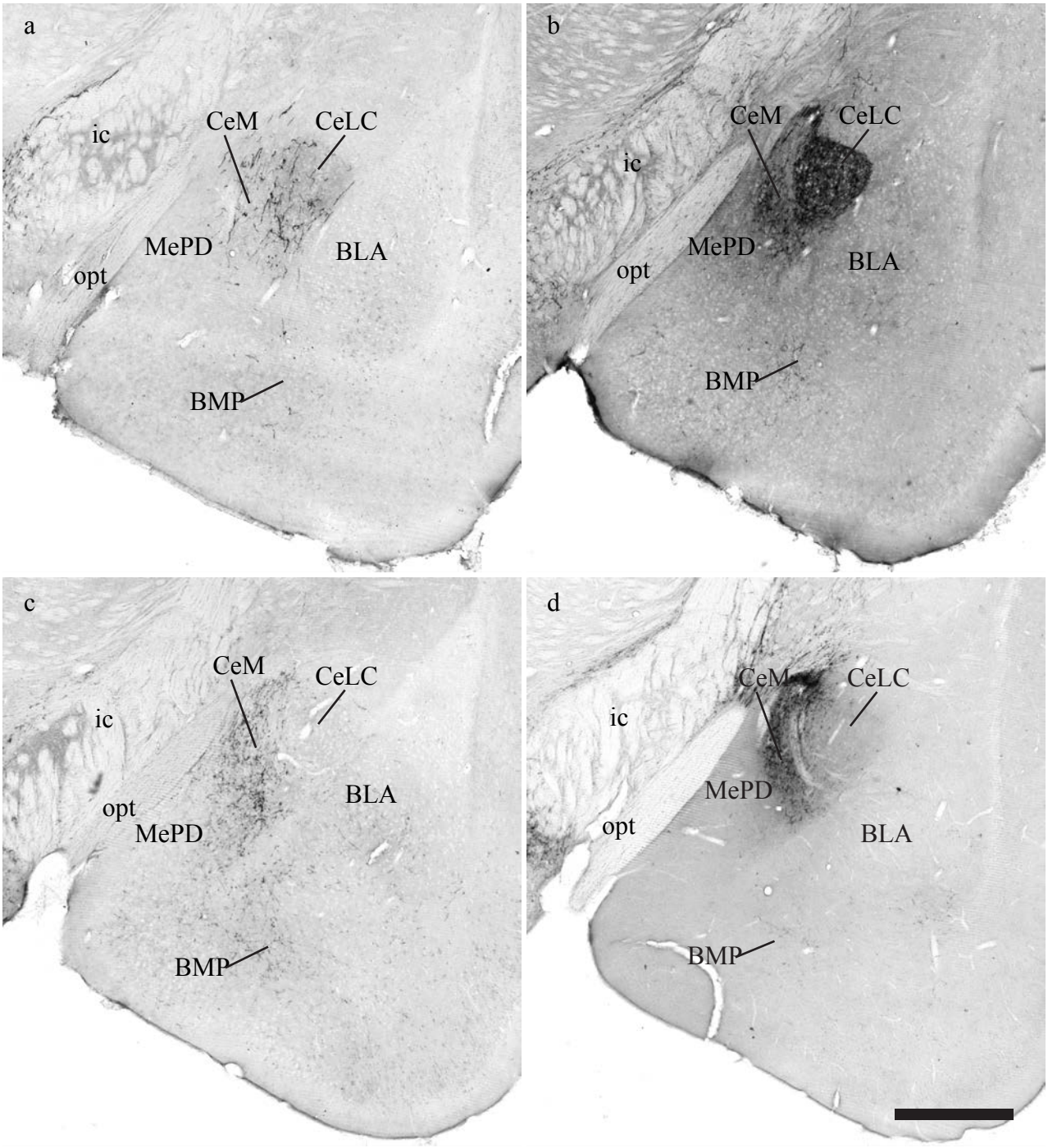

Fig. 3 Differential outputs to central nucleus of amgydala from subdivisions of EAc. After iontophoresis injection of BDA or PHA-L, outputs to caudal CeA (bregma level -1.55 mm) from STLD (**a**; case 1607G), CeL/C (**b**; case 1607F), STLV (**c**; case 1609K) and rostral CeM (**d**; case 1705B) were shown in bright field images. Abbreviation: see list. Scale bar: **a, b, c, d**, 500 μm.

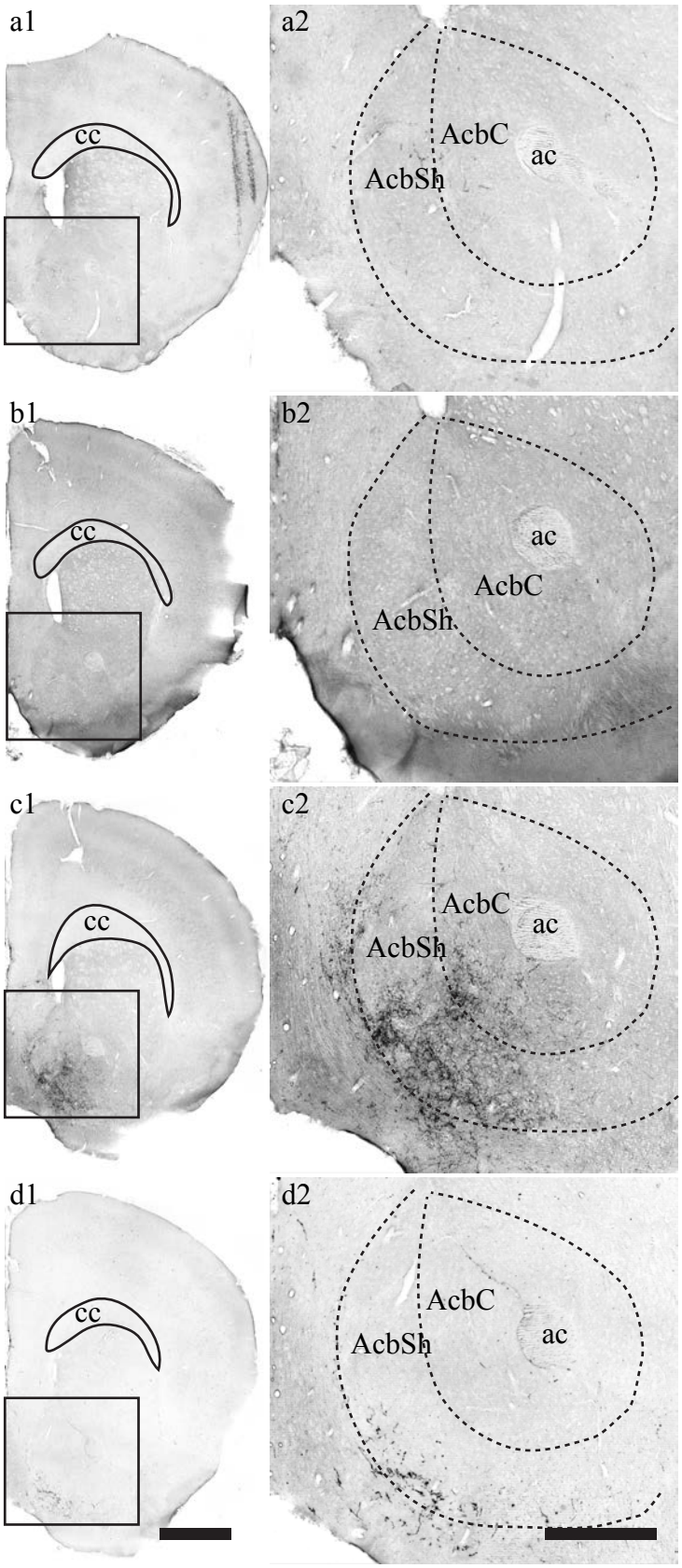

Fig. 4 Differential outputs to nucleus accumbens from subdivisions of EAc. Bright field images show outputs from STLD (**a1 – a2**; case 1607G), CeL/C (**b1 – b2**; case 1607F), STLV (**c1 – c2**; case 1609K) and rostral CeM (**d1 – d2**; case 1701M) to subdivisions of nucleus accumbens (bregma level -1.21 mm), after iontophoresis injection of BDA or PHA-L into corresponding nucleus. Abbreviation: see list. Scale bar: **a1**, **b1**, **c1**, **d1**, 1000 μm; **a2**, **b2**, **c2**, **d2**, 500 μm.

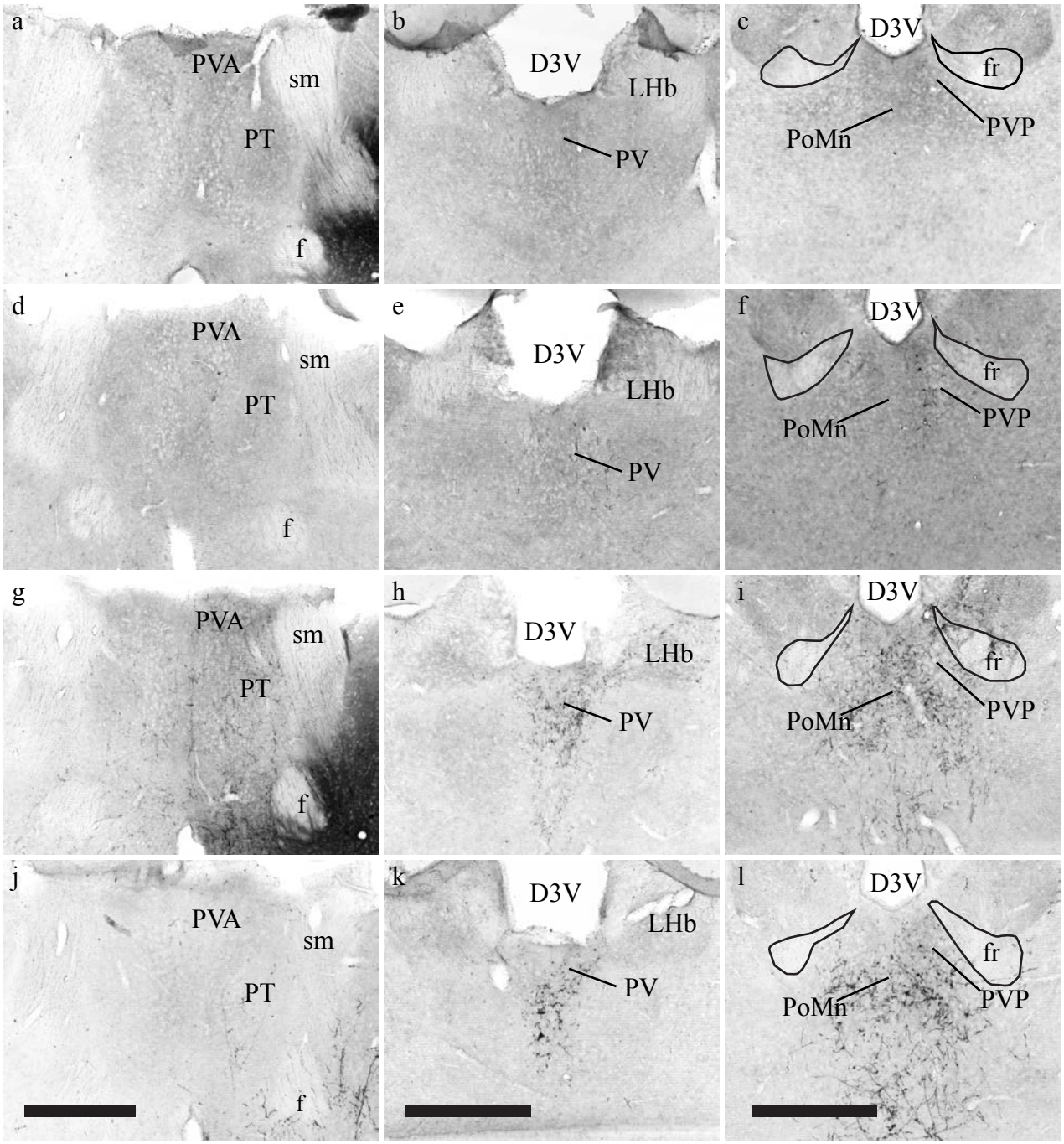

Fig. 5 Differential outputs to paraventricular thalamic nucleus from subdivisions of EAc. Bright field images show outputs to rostral to caudal paraventricular thalamic areas, including PVA (bregma level -0.35 mm), PV (bregma level -1.07 mm) and PVP (bregma level -1.91 mm), following iontophoresis injection of BDA or PHAL into STLD (**a – c**; case 1607G), CeL/C (**c – f**; case 1607F), STLV (**g – i**; case 1609K) and rostral CeM (**j – l**; case 1701M). Abbreviation: see list. Scale bar: **a, d, g, j,** 500 μm; **b, e, h, k**, 500 μm; **c, f, i, l**, 500 μm.

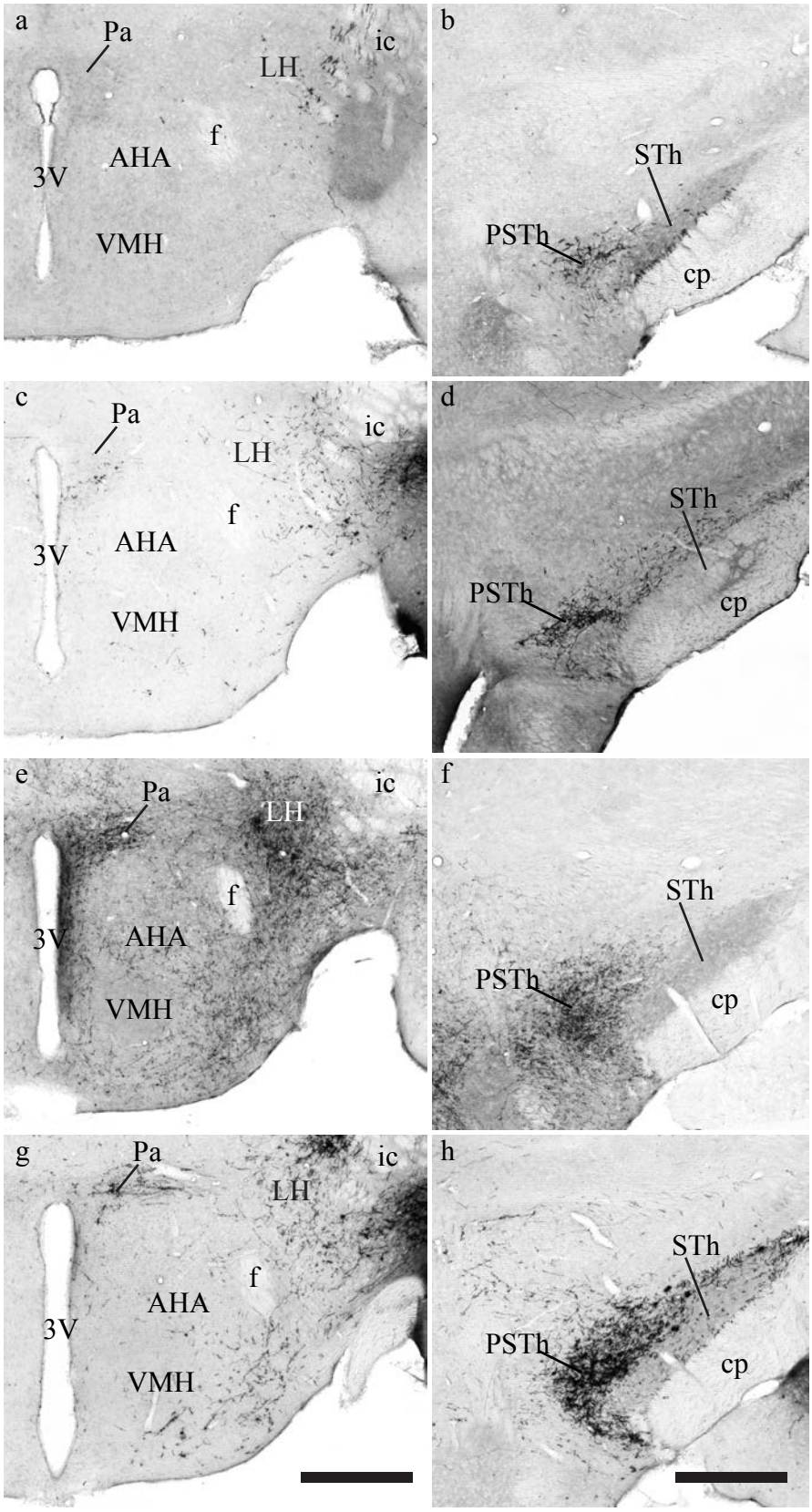

Fig. 6 Differential outputs to hypothalamic nuclei from subdivisions of EAc. Bright field images show outputs to LH (bregma level -1.07 mm) and PSTh (bregma level -2.27 mm), following iontophoresis injection of BDA or PHA-L into STLD (**a, b**; case 1607G), CeL/C (**c, d**; case 1701N and 1607F respectively), STLV (**e, f**; case 1609K) and rostral CeM (**g, h**; case 1701M) to, after corresponding areas. Abbreviation: see list. Scale bar: **a, c, e, g,** 500 μm; **b, d, f, h,** 500 μ m.

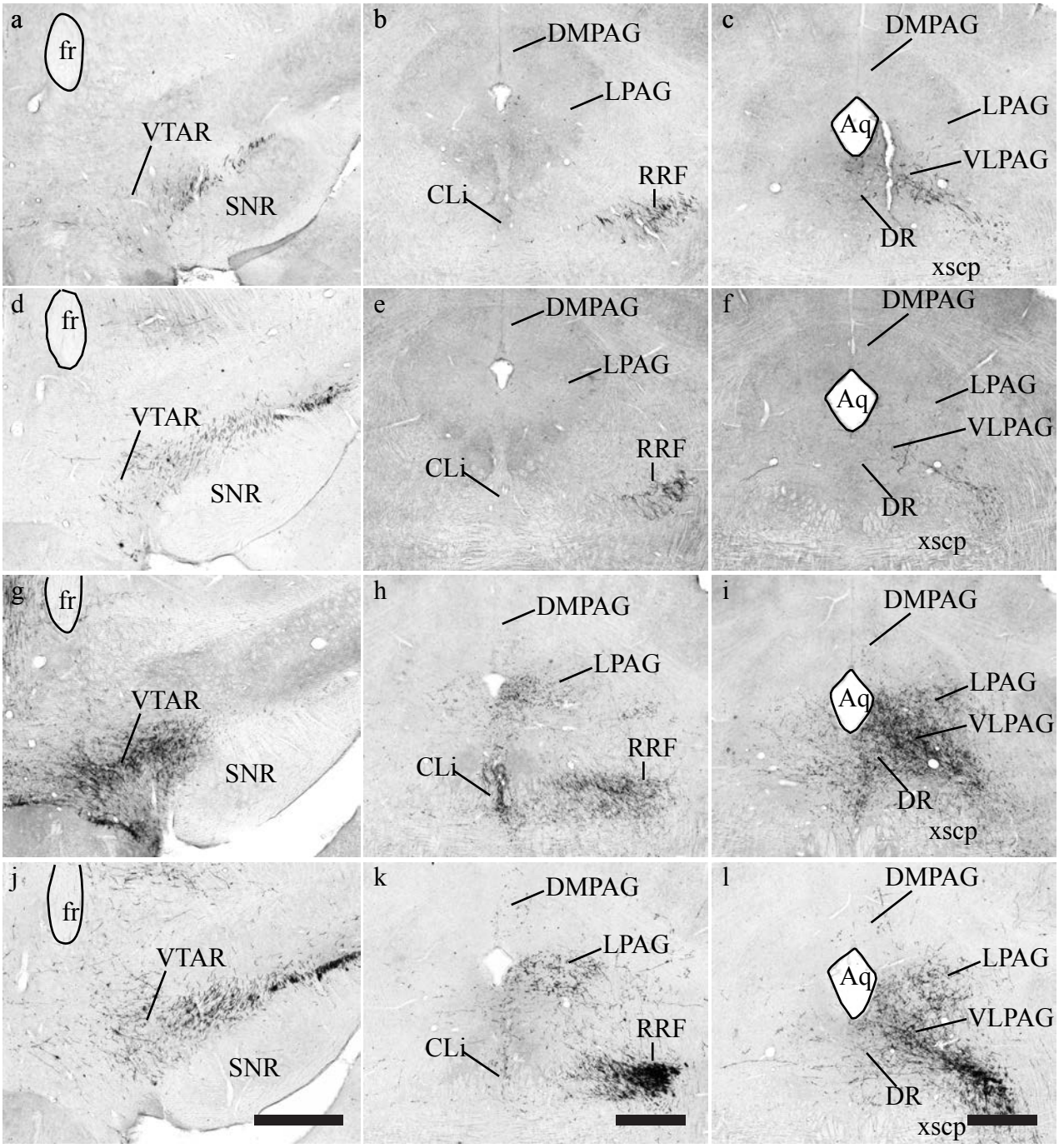

Fig. 7 Differential outputs to VTAR and PAG from subdivisions of EAc. Bright field images show outputs to VTAR (bregma level -2.91 mm), rostral PAG (bregma level -4.03 mm) and rostral PAG (bregma level -4.59 mm), after iontophoresis injection of BDA or PHAL into STLD (**a – c**; case 1607G), CeL/C (**c – f**; case 1701N and 1607F respectively), STLV (**g – i**; case 1609K) and rostral CeM (**j – l**; case 1701M). Abbreviation: see list. Scale bar: **a, d, g, j,** 500 μm; **b, e, h, k,** 500 μm; **c, f, i, l,** 500 μm.

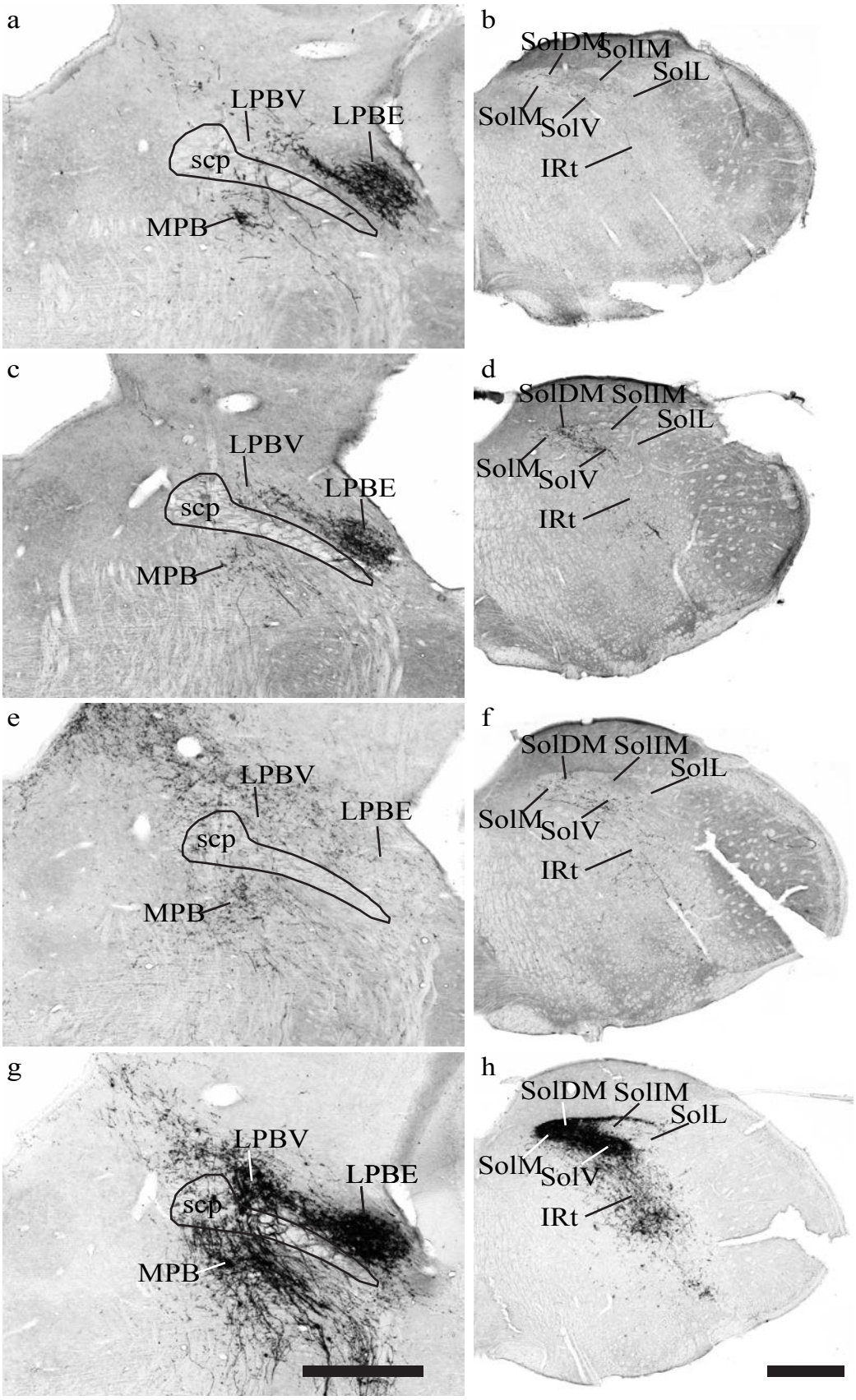

Fig. 8 Differential outputs to parabrachial nucleus and solitary nucleus from subdivisions of EAc. Bright field images show outputs to PBN (bregma level -5.19 mm) and Sol (bregma level -6.83 mm), following iontophoresis injection of BDA or PHAL into STLD (**a, b**; case 1607G), CeL/C (**c, d**; case 1607F), STLV (**e, f**; case 1609K) and rostral CeM (**g, h**; case 1701M). Abbreviation: see list. Scale bar: **a, c, e, g**, 500 μm; **b, d, f, h**, 500 μm.

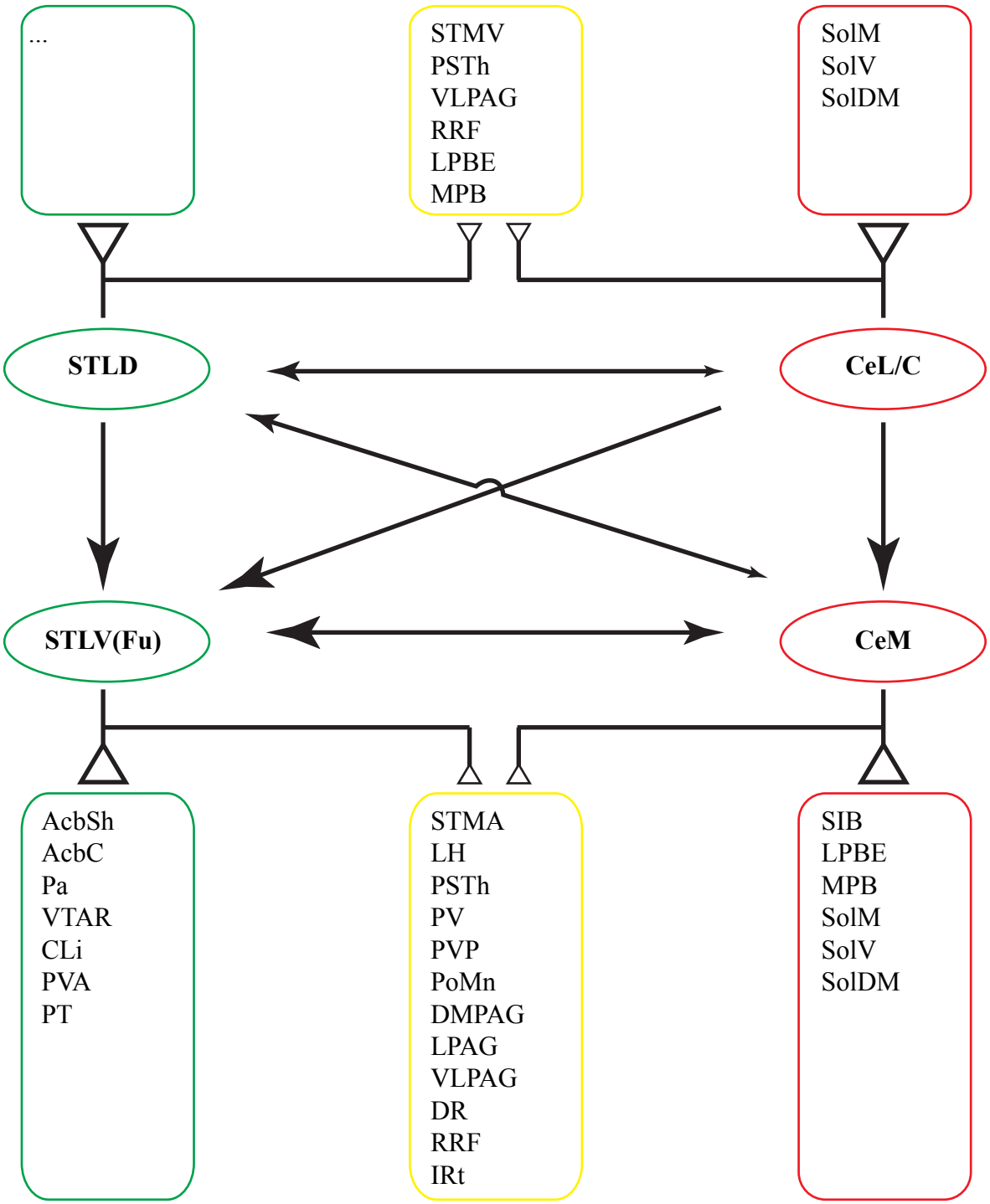

Fig. 9 Schematic summary of the differential outputs of STLD, STLV, CeL/C and CeM. The main outputs were reorganized to display the preferential target of each EAc nuclei. The relative strength of intra-EAc outputs are represented by sized sharp arrow heads (filled), and that of extra-EAc outputs by sized triangular heads (empty). The STL nuclei and their preferential targets (defined by socre difference of equal or more than two scoring levels, see Table. 3) are highlighted with green shapes (left side), while CeA nuclei and their preferential targets with red shapes (right side). Extra-EAc targets receiving equal or minor differential projections (defined by score difference of less than two scoring levels) are highlighted in yellow shapes (middle side). Abbreviation: see the list.

3. Parallel cell-type specific neuronal circuits in central amygdala

In this part, we will look at the cell-type specificity of EAc circuits, particularly focusing on two non-overlapping cell-types in STLD and CeL/C: the protein kinase C delta type (PKCδ)-expressing neurons and somatostatin (SOM)-expressing ones.
Dependent on cases, we implemented anterograde and retrograde tracing, together with immunofluorescent staining to reveal the identity of labeled neurons or axonal terminals.The results are mainly presented with graphic illustrations and statistical comparisons of projection neurons between pathways. At the end, we briefly illustrate the main conclusions on cell-type specific microcircuits in STLD and CeL/C.
The part is formatted as a manuscript that has been submitted to the preprint server bioRxiv (https://www.biorxiv.org/), and will be submitted to *Brain Structure and Function* later.

Cell-type specific parallel circuits in bed nucleus of the stria terminalis and central nucleus of amygdala of mouse

Jiahao Ye[1,2], Pierre Veinante*[1,2]

[1]Institut des Neurosciences Cellulaires et Intégratives, Centre National de la Recherche Scientifique;

[2]Université de Strasbourg, Strasbourg, France.

***Corresponding author**:

Pierre Veinante

Institut des Neurosciences Cellulaires et Intégratives, CNRS UPR3212, 5 rue Blaise Pascal, 67084, Strasbourg, France

Tel: +33 388 456 609

E-mail: veinantep@inci-cnrs.unistra.fr

Abstract

The central extended amygdala (EAc) is a forebrain macrosystem which has been widely implicated in fear, anxiety and pain. The two key structures of EAc, lateral bed nucleus of the stria terminalis (STL) and central nucleus of amygdala (CeA), share similar mesoscale connectivity. However, it is not known whether they also share similar cell-type specific neuronal circuits. We addressed this question using tract-tracing and immunofluorescence to reveal the connectivity of two neuronal populations expressing either protein kinase C delta type (PKCδ) or somatostatin (SOM). PKCδ and SOM are expressed predominantly in the dorsal part of STL (STLD) and in the lateral/capsular parts of CeA (CeL/C). We found that, in both STLD and CeL/C, PKCδ+ cells are the main recipient of extra-EAc inputs from the external lateral part of the parabrachial nucleus (LPB), while SOM+ cells are the sources of long-range projections to extra-EAc targets including LPB and periaqueductal gray. PKCδ+ cells can also integrate inputs from posterior basolateral nucleus of amygdala or insular cortex. Within EAc, PKCδ+, but not SOM+ neurons, serve as the major source of projections to ventral part of STL and to medial part of CeA. However, both cell types mediate interconnections between STLD and CeL/C, although a stronger connection from CeL/C to STLD is observed than the other direction. These results unveil the pivotal positions of PKCδ and SOM neurons in organizing the parallel cell-type specific neuronal circuits of CeA and STL, which further support the idea of EAc as a structural and functional macrostructure.

Keywords

Central extended amygdala; protein kinase C delta type; somatostatin; neuronal tracing; microcircuit

Abbreviations

ac: anterior commissure
ASt: amygdalostriatal transition area
BDA: biotin dextran amine, 10000 MW
BL: basolateral nucleus of the amygdala
BLA: basolateral nucleus of the amygdala, anterior
BLP: basolateral nucleus of the amygdala, posterior
BMP: basomedial nucleus of the amygdala, posterior
Calcrl: calcitonin receptor-like
CARD: combined catalyzed reporter deposition
CeA: central nucleus of amygdala
CeC: central nucleus of amygdala, capsular part
CeL: central nucleus of amygdala, lateral part
CeL/C: central nucleus of amygdala, lateral and capsular part
CeM: central nucleus of amygdala, medial part
CGRP: calcitonin gene-related peptide
CGRPR: calcitonin gene-related peptide receptor
CPu: caudate putamen
CRF: corticotrophin-releasing factor
cst: commissural stria terminalis
CTb: cholera toxin B subunit
D2R, dopamine receptor D2
DAPI: 4',6-Diamidino-2-Phenylindole, Dihydrochloride
DMPAG: dorsomedial periaqueductal gray
DR: dorsal rahpe nucleus
EAc: central extended amygdala
ENK: enkephalin
FG: Fluorogold
Fu: fusiform nucleus
GI/DI: granular and dysgranular insular cortex
GP: globus pallidus
Htr2a: serotonin receptor 2a
i.p.: intraperitoneal injection
InsCx: insular cortex
KLH: keyhole limpet hemocyanin
LaVM: lateral nucleus of amygdala, ventromedial
LPAG: lateral periaqueductal gray
LPB: lateral parabrachial nucleus
LPBE: external lateral parabrachial nucleus
MPB: medial parabrachial nucleus
NPY: neuropeptide Y
PAG: periaqueductal gray
PB: phosphate buffer
PBS: phosphate-buffered saline
PHA-L: *Phaseolus vulgaris* leucoagglutinin
Pir: piriform cortex
PKCδ: protein kinase C, delta type
Ppp1r1b: phosphatase 1 regulatory subunit 1B positive
Rspo2: R-spondin 2 positive
s.c.: subcutaneous injection
S2: secondary somatosensory cortex
scp: superior cerebellar peduncle
SEM: standard error of the mean
SOM: somatostatin
ST: bed nucleus of the stria terminalis
STL: lateral bed nucleus of the stria terminalis
STLD: dorsal lateral bed nucleus of the stria terminalis
STLP: posterior lateral bed nucleus of the stria terminalis
STLV: ventral lateral bed nucleus of the stria terminalis
STMA: anterior medial bed nucleus of the stria terminalis
STMV: ventral medial bed nucleus of the stria terminalis
VLPAG: ventral lateral periaqueductal gray

INTRODUCTION

The central extended amygdala (EAc) is a forebrain macrosystem which contributes to diverse functions and disorders including pain, associated learning behavior and emotion in animal models (Neugebauer et al. 2004; Shackman and Fox 2016; Veinante et al. 2013; Alheid 2003; de Olmos and Heimer 1999). The concept of EAc is also increasingly gaining importance as an fundamental structure underlying psychiatric disorders such anxiety and post-traumatic stress disorder in human (Shackman and Fox 2016), but the organization of its neuronal microcircuits is still elusive.

The lateral part of the bed nucleus of the stria terminalis (STL) and the central nucleus of the amygdala (CeA) form the core structures of EAc, and are connected by corridor of sublenticular cells along stria terminalis and ventral amygdalofugal pathway (Cassell et al. 1999). In both STL and CeA, multiple subdivisions exist but different nomenclatures have been used (McDonald 1982; Sun and Cassell 1993; Chieng et al. 2006).In the rodent brain, CeA has been divided into capsular (CeC), lateral (CeL) and medial divisions (CeM) (Cassell et al. 1999; Paxinos and Franklin 2012). In mouse, however, the border between CeC and CeL is more elusive and different delineations have been applied in different studies (Haubensak et al. 2010; Li et al. 2013; Kim et al. 2017), thus we refer them collectively as capsular and lateral CeA (CeL/C). On the other hand, the delineation of STL subdivisions is much less consensual (Alheid 2003; Dong et al. 2001a; Gungor and Pare 2016). In this study, we divided the middle STL level into dorsal part (STLD), ventral part (STLV) and posterior part (STLP), according to Franklin and Paxinos's mouse brain atlas (Paxinos and Franklin 2012).

CeA and STL display striking similarities in cytoarchitecture, neurochemistery and connectivity (Alheid 2003; Sun and Cassell 1993). For example, both STL and CeA are targeted by similar cortical, intraamygdaloid, thalamic and brainstem afferents, and they both project to the same hypothalamic and brainstem targets (McDonald et al. 1999; Alheid 2003; Davis and Shi 1999). In addition, STL and CeA are linked by subdivisions-specific interconnections and a directional bias in intrinsic EAc connections has been suggested from STLD and CeL/C to ventral STL (STLV) and CeM (Sun et al. 1991; Cassell et al. 1999).

GABAergic neurons constitutes the large majority of neurons in STL and CeA and they give rise to local inhibition (Sun and Cassell 1993; Cassell et al. 1999; Hunt et al. 2017), as well as mutual inhibitions between STL and CeA (Sun et al. 1991; Sun and Cassell 1993; Veinante and Freund-Mercier 1998) and long range projections (Moga et al. 1989; Sun and Cassell 1993). While tract-tracing and virus tracing clearly established GABAergic projections between STLD and CeL/C, as well as STLD or CeL/C to STLV/CeM (Ciocchi et al. 2010; Li

et al. 2013; Cai et al. 2014), it is still unclear which cell populations mediate such interactions. It is indeed well known that both STL and CeA contain mixed neuronal populations expressing different neuropeptides, such as somatostatin, corticotropin-releasing factor (CRF), neurotensin, enkephalin (Cassell et al. 1999; Li et al. 2013; Haubensak et al. 2010; Veinante et al. 1997), which pose a good challenge to dissect cell-type specific circuits in EAc.
Recent researches on mouse CeL/C revealed the existence of two non-overlapping neuronal groups expressing either protein kinase C delta type (PKCδ) or somatostatin (SOM), which together constitutes the majority of local GABAergic neurons (Haubensak et al. 2010). PKCδ+ and SOM+ neurons can form delicate disinhibitory circuit controlling fear learning (Ciocchi et al. 2010; Haubensak et al. 2010; Li et al. 2013; Fadok et al. 2017), anxiety (Botta et al. 2015), active defense (Yu et al. 2016), and feeding behavior (Cai et al. 2014; Campos et al. 2016). On the other hand, STL is also involved in fear response (Davis et al. 2009; De Bundel et al. 2016) and anxiety (Kim et al. 2013; Jennings et al. 2013; Mazzone et al. 2016), yet it is not clear whether STL shares some features of cell-type specific connectivity in CeA. Moreover, the involvement of PKCδ+ and SOM+ cells in projections from CeA to STL is unknown. Based on similar enrichment of PKCδ+ and SOM+ neuronal populations in STL and CeA (Lein and et al. 2007) and the idea that symmetric components of EAc can share similar organization, we hypothesize that, similar to CeA, microcircuits based on PKCδ+ or SOM+ neurons might also exist in STL and also contribute to intra-EAc circuitry.
Thus, in this study, we combined tract-tracing and immunofluorescence in mice to address the neuronal circuits of STL and CeA at three levels: long-range inputs, intrinsic EAc interconnectivity, and long-range outputs. Our results show that both PKCδ+ and SOM+ neuronal populations are involved in microcircuits similarly organized in CeL/C and STLD. In both CeL/C and STLD, PKCδ+ neurons are preferentially innervated by calcitonin gene-related peptide (CGRP)-positive inputs from the external lateral part of the parabrachial nucleus (LPBE), and can also integrate other long-range excitatory inputs, from insular cortex (InsCx) and posterior basolateral amygdala (BLP). This PKCδ+ population also provides the main inhibition within EAc, by projecting to CeM and STLV. On the other hand, mutual connections between STLD and CeL/C can be mediated by both cell-types. In comparison, SOM+ neurons provide the main outputs from STLD and CeL/C to extra-EAc targets, including LPBE and periaqueductal gray (PAG).

MATERIALS& METHODS

Animals

Adult male C57BL/6J mice of 6 - 9 weeks old (Charles River®, L'Arbresle, France) were purchased and housed in standard housing cages, allowing for ad libitum access to food and water (12/12-hour light/dark cycle). In total, 27 mice were used for this study. All the experimental procedures were carried out in accordance with the regulations from European Communities Council Directive and approved by the local ethical committee (CREMEAS under reference AL/61/68/02/13).

Stereotaxic tract-tracing

Individual animal (11-12 weeks old) was anesthetized by an intraperitoneal injection (i.p.) of a mixture of ketamine (87 mg/kg) and xylazine solution (13 mg/kg). Then the deep-anesthetized animal was treated with metacam (2 mg/kg, subcutaneous, or s.c.) to alleviate inflammatory response and bupivacaine (2 mg/kg, s.c.) was infiltrated on the scalp to induce local analgesia. After that, the mouse was mounted into a stereotaxic frame (Model 900, David Kopf Instrument). A small craniotomy was made with surgical drill allowing for passage of glass pipette.

Solution of tracers were loaded into a glass pipette (tip diameter 15-25 μm) that was pulled with a P-97 micropipette puller (Sutter Instrument) and was positioned according to the stereotaxic coordinates (Table 1)(Paxinos and Franklin 2012). The tracers were either passed to brain tissue under iontophoresis with a constant current source (Midgard Model 51595, Stoelting Co.) or by pressure injection (Picospritzer® III, Parker Hannifin Corp). Two different tracers were used for anterograde tracing. Biotin dextran amine, 10000 MW (BDA; 2% or 4% in phosphate buffer saline, PBS; cat. #D1956, Molecular Probe®) or *Phaseolus vulgaris* leucoagglutinin (PHA-L; 2.5% in phosphate buffer, PB; cat. #L-1110, Vector Laboratories®) were injected for 10-15 min (+3-5 μA, 7 s ON/OFF cycle). Three different tracers were used for retrograde tracing. First, hydroxystilbamidine methanesulfonate (cat. #A22850, Molecular Probes®) or aminostilbamidine (cat. #FP-T8135A, Interchim®) (indicated together as Fluorogold, or FG; 2% in 0.9% NaCl), was injected for 10 min (+2 μA, 3 s ON/OFF cycle). Secondly, cholera toxin B subunit (CTb; 0.25% in 0.1 M Tris buffer and 0.1% NaCl; cat. #C9903, Simga®) was injected for 15 min (+4-5 μA, 3 s ON/OFF cycle). The third tracer, red Retrobeads™ (50 -150 nl; Lumafluor Inc.) was injected into region of interest by Picrospritzer® III.

After the injection, the pipette was kept in place for 5 - 10 min before withdrawing. The scalp was then closed and one lidocaine spray (2%, Xylovet®) was infiltrated near the wound. The

animal was monitored by the experimenter until waking up and was placed in his home cage in the animal facility for 7 to 14 days to allow transport of the tracers.

Slices preparation

The animal was euthanized by a lethal dose of pentobarbital (273 mg/kg, i.p.) or Dolethal (300 mg/kg, i.p.). After checking the disappearance of toe-pinch reflex, the animal was transcardially perfused with ice-cold phosphate buffer for 1 min (PB; 0.1 M, pH 7.4; 10 ml) and then with fixative (2% paraformaldehyde, in 0.1 M PB, pH 7.4; 150 ml) for 15 min. The brain was removed and put for post-fixation in the fixative (4 °C) overnight. Then, brains were kept in phosphate-buffered saline (PBS, Cat. # ET300-A, Euromedex, France) (4 °C) for one week or in PBS-sodium azide (0.02%) for longer time before sectioning. Serial coronal sections (thickness 30 μm) were cut with a vibratome (VT1000S, Leica Biosystem). Slices were kept in PBS (4 °C) for use within one week or in sodium azide (0.02% in PBS) for longer time. Subsequent immunohistochemistry procedures were then carried out on selected brain slices (120 μm apart for adjacent slices) to for each animal. The procedures were carried out to simultaneously visualize PKCδ$^+$ and/or SOM$^+$ neurons together with the tracers and/or another cellular marker of interest (i.e. calcitonin gene-related peptide, or CGRP), through different combinations of primary and secondary antibodies.

Combined catalyzed reporter deposition (CARD) for somatostatin

In our hands, the traditional immunofluorescent staining of SOM revealed only a few cell bodies in STLD and CeL/C, probably due to the low content of SOM peptide in the soma of projection neurons. In order to get robust staining of SOM+ cell bodies in EAc, we thus applied a highly sensitive method known as the combined catalyzed reporter deposition (CARD) (Speel et al. 1997; Hunyady et al. 1996). With the catalytic power of horseradish peroxidase, the CARD method allows specific deposit of tyramide-conjugates nearby the antigen. The reaction can amplify the immunochemical signal up to a 10 to 100- fold, compared to that of general immunofluorescent staining (Hunyady et al. 1996). In this study, we use fluorochrome-conjugated tyramide (i.e. fluorescein-tyramide and Cy3-tyramide) to reveal SOM signal. All procedures were carried out in floating brain slices, at room temperature, unless specified otherwise. First, the intrinsic peroxidase activity of brain slices was inhibited by 1% H_2O_2 (in 50% ethanol) solution for 20 min. Then slices were washed with PBS (3 x 5 min), and blocked with the blocking buffer (Triton X-100 0.3% and donkey serum 5% in PBS) for 45 min. After that, slices were incubated overnight with rabbit anti-

somatostatin antibodies (Table 2) in dilution buffer (Triton X-100 0.3% and donkey serum 3% in PBS). Then, the slices were washed with PBS (3 x 5 min), and incubated with the HRP-conjugated donkey anti-rabbit antibody (1:300, in dilution buffer) for 3 hours. Slices were then washed in PBS (2 x 5 min) and then in PBS-imidazole buffer (100 mM, pH 7.6; 5 min). Finally, the CARD reaction was carried with fluorescein-tyramide or Cy3-tyramide (1:1000, a gift from Prof. Klosen, University of Strasbourg) in PBS-imidazole buffer and H_2O_2 (0.001%) for up to 30 min. The reaction was stopped by washing off the reaction buffer with PBS (3 x 5 min). The same CARD procedures were also used to reveal BDA labeled axons (i.e. Fig. 4 - 5) when the signal was weak with traditional immunofluorescent staining. In those cases, peroxidase was introduced by incubation of ABC-HRP system (1: 500; Cat. # PK-6100, Vector Laboratories™) for 1.5 hr (room temperature).

Immunofluorescent staining

General immunofluorescent staining of other antigens were carried out after CARD revelation of SOM when applicable. Thus, SOM immunoreactivities, together with another tracer (i.e. CTb, FG) or cellular marker of interest (i.e. PKCδ, CGRP), were simultaneously visualized with combinations of different primary antibodies (see Table 2) and secondary antibodies, following the general procedure below.

After finishing the CARD revelation of SOM, a combinations of other primary antibodies were applied overnight (room temperature) in dilution buffer. The combinations depended on the aim of each experiment, types of tracers and technical constraints. For example, we added PKCδ primary antibodies to show the spatial distribution of PKCδ+ and SOM+ neurons, but also used PKCδ and CGRP immunofluorescence to analyze the apposition of CGRP terminals in EAc.

Next, slices were washed in PBS (3 x 5 min) and incubated with corresponding secondary antibodies (1:300 in dilution buffer) for 3 hrs at room temperature. Diverse fluorophore-conjugated secondary antibodies were chosen for triple labeling of SOM, PKCδ and the third antigen, based on compatibility of fluorophore. Overall, the following secondary antibodies were used: donkey anti-mouse-Alexa-647 conjugates (Cat. #: A-31571, Invitrogen™), donkey anti-mouse-Cy3 conjugates (Cat. #: 715-165-151, Jackson Immunoresearch™), donkey anti-rabbit-Cy5 (Cat. #: 711-175-152, Jackson Immunoresearch™), donkey anti-rabbit-Alexa 488 (Cat. #: A-21206, Invitrogen™), donkey anti-goat-Alexa 488 (Cat. #: A-11055, Invitrogen™). Streptavidin-Alexa 488 conjugate (1: 750; Cat. #: S32354, Molecular Probe®) was used for visualization of BDA.

After washing in PBS (3 x 5 min), the slices were counterstained with DAPI (4',6-Diamidino-2-Phenylindole, Dihydrochloride; 300 nM, Cat.# D1306, Invitrogen™) for 3 - 5 min. The slices were arranged onto Superfrost® plus slides (Thermo Fisher Scientific™) and mounted in Fluoromount™ medium (Cat. #: F4680, Sigma-Aldrich™).

We observed that these procedures (details in the next section) make it possible to stain two kinds of antigens with two different primary antibodies from the same species (Hunyady et al. 1996). In this study, we used different rabbit antibodies for SOM, FG, and CGRP. For instance, to simultaneously visualizing of PKCδ, SOM, and CGRP, a low concentration of rabbit-anti-SOM (1: 5000) was used for CARD revelation, and a higher concentration of rabbit-anti-CGRP (1: 1000) antibody was subsequently applied. In this way, SOM and FG or CGRP can be revealed with sequential applications of primary antibodies from rabbit, without showing detectable cross-staining. The absence of cross-staining is determined by the separation of the staining pattern and negative control experiments in which CGRP primaries were omitted.

Imaging and analysis

For each animal, the location of injection core of tracer was examined on successive slices containing the injection sites and was evaluated according to salient anatomical features (i.e. fiber bundle) and neurochemical features (i.e. DAPI staining, $PKC\delta^{+}$ immunoreactivity). The delineation of subdivisions of EAc, LPB, PAG, among others, were done according to fourth edition of mouse brain atlas (Paxinos and Franklin 2012). Cases in which the injection sites spilled beyond the target over nearby regions were not included into the data analysis.

For illustrations of injection sites and neurochemical patterns, if not stated otherwise, epi-fluorescence images were acquired by an Axio Imager 2 (Carl Zeiss™) microscope equipped with a digital camera (ProgRes® CF*cool*, Jenoptik, GmbH, Germany), under 10x, or 20x objectives; or by a NanoZoomer S60 (Hamamatsu Photonics) under a 20x objective.

For demonstrating co-localization of markers and potential appositions between neurons and axonal processes, confocal imaging at the middle focal plane of the slice was taken with a Leica TCS SP5 II system (Leica Biosystem). Images were sampled to pixel resolution = 0.255 µm by 2.5-fold of Nyquist sampling, under 20x objective with 1 airy unit. To gain more details of axonal apposition, single plane or z-stack (1 µm) confocal images were taken under 63x objective, which was used to confirm structural appositions seen in images taken under 20x objectives.

For quantitative analysis of colocalization, epifluorescent imaging were taken with Axio Imager 2 (Carl Zeiss™) equipped with a digital microscope camera (ProgRes® CF*cool*, Jenoptik, GmbH, Germany), under 20x apochromatic objectives. A z-stack image (step size = 2.049 μm) was obtained in STLD (bregma +0.13 mm) or CeA (bregma -1.43 mm) for each animal. In principle, the colocalization of tracers with PKCδ+ or SOM+ neurons in epifluorescence was also confirmed by corresponding confocal images. Preprocessing of images, which are primarily for pseudo-coloring and adjusting contrast, and subsequent analysis including cell counting and colocalization was carried out manually on open software FIJI (Schindelin et al. 2012).

Statistics

For colocalization and apposition studies, mean value and standard error of the mean (SEM) are reported by injection group and brain areas. Unpaired two-sample Student's *t*-test was carried out in R program (©The R Foundation).

RESULTS

Distribution of PKCδ neurons and SOM neurons in STLD and CeL/C

We first examined the pattern of PKCδ and SOM imunoreactivities in subdivisions of the STL (n = 3) and the CeA (n = 3). PKCδ positive (PKCδ+) soma were detected mainly in the STLD and CeA, as well as in the lateral septum (Fig. 1a), the thalamus (Fig. 1d). In STL, well-stained PKCδ+ cell bodies were concentrated in the STLD of which they sharply defined its limits with surrounding STLP (Fig. 1a), while they were also present in CeL/C where they tend to be concentrated laterally with a reduced density medially at the limit with the CeM (Fig. 1d). Dense PKC δ+ neuropil was also obviously packed in STLD and CeL/C (Fig. 1a, d; see also Fig. 2c, e, f). SOM positive (SOM+) neurons were observed mainly in the STL, cerebral cortex, caudate-putamen, hypothalamus (Fig. 1b), and amygdala (Fig. 1e). While the staining of SOM+ interneurons filled the cell bodies in cerebral cortex and caudate-putamen, the SOM labeling of somas of STL and CeA was patchier and hardly defined the somatic contour, probably due to the low content of SOM in the soma of projection neurons. In the STL, SOM+ neurons and fibers were observed in all subdivisions, but appeared denser in the STLD (Fig. 1b) where their distribution overlaps with that of PKCδ+ neurons (Fig. 1c). In the CeA, a low density of SOM+ soma and processes occurred in the CeM, but a strong concentration was observed in the CeL/C (Fig. 1e). The distribution of SOM+ cell bodies overlapped with that of PKCδ+ neurons in the medial part (i.e. CeL), but decreased laterally

(i.e. CeC) where PKCδ+ neurons were abundant (Fig. 1f). Despite their similar regional distribution in STLD and CeL/C, PKCδ and SOM immunoreactivities remained segregated and were almost never observed in the same neurons (Fig. 1c, f; see also Fig2c, e). Finally, while PKCδ+ and SOM+ neurons were observed along the rostrocaudal extent of STLD (bregma +0.25 mm to +0.01 mm) and CeL/C (bregma -0.80 mm to -2.03 mm), their density appeared stronger in the caudal parts of STLD and CeL/C.

Thus, we confirmed the expression of the similar cellular markers, PKCδ and SOM, in segregated neuronal populations of STLD and CeL/C, in accordance with previous descriptions (Ciocchi et al. 2010; Li et al. 2013; Haubensak et al. 2010).

A majority of PKCδ+ neurons are surrounded by CGRP+ terminals

Having established the distribution of PKCδ+ and SOM+ neurons in STLD and CeL/C, we tested whether external inputs could target similar populations in both nuclei. The lateral parabrachial nucleus (LPB) is known to provide a dense input to STLD and CeL/C (Bernard et al. 1993; Alden et al. 1994). This LPB-EAc pathway is characterized by large basket-like pericellular terminals (Sarhan et al. 2005) co-releasing glutamate and neuropeptides, especially calcitonin gene-related peptide (CGRP) (Delaney et al. 2007; Salio et al. 2007). As the CGRP innervation to EAc has been shown to originate essentially from LPB in rats (Yasui et al. 1991b; D'Hanis et al. 2007) and as a recent study in mice suggested that the cells expressing CGRP receptor overlap with SOM and PKCδ populations (Han et al. 2015), we first examined the potential innervation of SOM and PKCδ by CGRP terminals using a triple immunofluorescence protocol (Fig. 2).

In accordance with previous descriptions, CGRP positive (CGRP+) terminals were observed in the STLD and the CeL/C. Their distribution largely overlapped with that of PKCδ+ cells and partially overlapped with that of SOM+ cells (Fig. 2b, d) and displayed characteristic perisomatic terminals (Fig. 2c, e).

Confocal analysis at cellular level showed that PKCδ+ somas were often surrounded by basket-like CGRP+ elements in STLD (Fig. 2c) and CeL/C (Fig. 2e). A close observation revealed the wrapping of soma, and proximal dendrites of PKCδ+ neurons by CGRP+ terminals (Fig. 2f). A Quantitative analysis (n=3) indicated that 84.4% and 80.6 % of PKCδ+ soma in STLD and CeL/C, respectively, were closely surrounded by CGRP+ perisomatic terminals (Fig. 2a). In addition, most of CGRP+ baskets-like structures either contact PKCδ+ neurons or PKCδ-/SOM- neurons.

By contrast, CGRP+ basket-like structures almost never surrounded SOM+ somas in STLD (Fig. 2c) or CeL/C (Fig. 2e, f). Yet, we cannot exclude that thinner single CGRP+ terminal which lacks the basket-like appearance, could contact SOM+ neurons, as such putative appositions were sometimes registered under high magnification (Fig. 2f). However, the incomplete staining of SOM+ soma did not allow to validate the existence of such contacts. Thus, these evidences support a dominant perisomatic CGRP+ innervation onto PKCδ+, but not SOM+, neurons in EAc, even though an underestimated number of SOM+ neurons in STLD and CeL/C were labeled in our study. In addition, non-perisomatic contacts between CGRP+ terminals and SOM+ neurons can be suggestive.

CGRP terminals from LPB target PKCδ neurons in EAc.

In order to further confirm the possibility that CGRP+ axonal terminals contacting EAc PKCδ+ neurons were derived from the LPB, we performed anterograde tracing from LPBE by BDA followed by subsequent triple fluorescent labeling.

BDA injection sites in LPB (n = 5) were centered in the LPBE (mainly from bregma -5.07 mm to -5.41 mm), with occasional expansion into its neighbouring central lateral and dorsal subnuclei (LPBcl, LPBd) but never extending to medial parabrachial nucleus or Kölliker-Fuse nucleus (Fig. 3a, f). In the ipsilateral EAc, BDA+ axons were primarily located in the oval-shaped STLD (Fig. 3b, g), putative fusiform nucleus of ventral STL (not shown), and CeL/C (Fig. 3d, i), with only a few axonal processes in STLP or CeM. At higher magnification, distinct BDA+ perisomatic arrangements were observed along with individual fibers (Fig. 3c, e, h, j). The comparison of BDA+ and CGRP+ signals showed that a substantial number of the BDA+ axons forming basket-like structures contained CGRP signal. Conversely, CGRP+ basket-like structures were often coincident with BDA+ labeling (Fig. 3c, e, h, j). However, some CGRP+ perisomatic formations appeared to be BDA negative (BDA-), and individual BDA+ axons only partially overlapped with CGRP immunoreactivity.

Triple labeling for PKCδ, CGRP and BDA (Fig. 3a - e) revealed that the large majority of the PKCδ+ somas in STLD (Fig. 3c) and CeL/C (Fig. 3e) were surrounded by CGRP+ baskets, as shown in the previous experiment, including most of the BDA+/CGRP+ baskets. In addition, a number of BDA+/CGRP- axonal segments were also found in close apposition with PKCδ+ somas. In sections processed for triple labeling for SOM, CGRP and BDA (Fig. 3f - j), perisomatic structures revealed by BDA and/or CGRP signals, very rarely contacted SOM+ cell bodies; albeit BDA+/ CGRP- terminals could be found in close proximity to SOM+ somas in STLD (Fig. 3h) and CeL/C (Fig. 3j).

Thus, the preferential perisomatic CGRP innervation onto PKCδ+, but not SOM+, neurons in STLD and CeL/C, is likely to derive, at least in part, from the LPBE. In addition, the BDA+/ CGRP- perisomatic terminals surrounding PKCδ+ neurons and individual axons found close to PKCδ+ or SOM+, suggest the existence of a non-CGRP input from LPBE to EAc.

PKCδ+ neurons in EAc integrate convergent signals

Beside inputs from the LPBE, both STL and CeA are strongly innervated by the basolateral nucleus of amygdala, especially the posterior subdivision (BLP) (Dong et al. 2001a; Pitkanen et al. 2003), and by the insular cortex (InsCx) (Saper 1982; Yasui et al. 1991a; Sun et al. 1994). Kim and her colleagues (Kim et al. 2017) recently showed that BLP strongly targeted PKCδ+ neurons in CeL/C, and a recent study using rabies virus tracing unveiled convergent inputs to CeL PKCδ+ neurons from multiple brain regions including InsCx, BLP and LPBE (Cai et al. 2014). However, it is not known if the same goes true for STLD PKCδ+ neurons and whether they can potentially integrate information from intra-amygdaloid (i.e. BLP) and extra-amygdaloid (i.e. LPB or InsCx) inputs. We thus injected the anterograde tracer BDA in BLP or in InsCx and carried out triple fluorescent labeling in STLD and CeL/C to look for the potential innervation of PKCδ+ neurons by CGRP+ baskets (potentially from LPBE) and BLP or InsCx afferents.

The BDA injection sites in BLP were largely confined to the lateral part of the caudal BLP (Fig. 4a, b; bregma -2.45 mm), with minor leak in the nearby piriform cortex and lateral nucleus of amygdala. In the ipsilateral STL, BDA+ axon terminals spread quite evenly in STLD and STLP (Fig. 4c). At higher magnification, BDA+ axonal varicosities (Fig. 4d) could be observed to form close appositions with PKCδ+ neurons, which were simultaneously surrounded by CGRP+ terminals. Similarly, the CeA was also densely innervated by BDA+ axons from BLP (Fig. 4e). At cellular level, these BDA+ axonal varicosities can also form close apposition with PKCδ+ neurons contacted by CGRP+ baskets (Fig. 4f).

The BDA injections in InsCx targeted the granular and dysgranular insular areas at middle level (bregma -0.23 mm), with some minimal extent dorsally in the secondary somatosensory cortex (S2) (Fig. 5a, b). Ipsilaterally, a moderate to strong projection was found in the STLD (Fig. 5c) and in the CeL/C (Fig. 5e) where intense CGRP+ axonal field and PKCδ+ neurons coexisted. Observation at high magnification confirmed the existences of simultaneous axonal appositions by BDA+ varicosities and CGRP+ varicosities onto a single PKCδ+ neuron in STLD (Fig. 5d) and in CeL/C (Fig. 5f).

Thus, these structural evidences support the notion that PKCδ+ neurons in EAc can mediate the integration of both viscero- and somato-sensory signals from LPBE and highly processed polymodal information from BLP and InsCx. However, it should be noted that these BLP and InsCx inputs to PKCδ+ neurons are not exclusive, as numerous BDA+ varicosities were observed without evident apposition to PKCδ+ neurons in STLD and CeL/C.

A majority of CeM-projecting or STLV-projecting neurons in STLD and CeL/C express PKCδ

After establishing the structural evidences for possible integration of sensory and polymodal pathways onto PKCδ+ neurons, we asked what the possible downstream targets of these neurons are in the EAc. Both STLV and CeM, which are considered as the main outputs subnuclei of the EAc, have long been known as important intrinsic targets of STLD and CeL/C (Dong et al. 2001b; Cassell et al. 1999). It has been shown that PKCδ+ neurons in the CeL/C project to CeM (Haubensak et al. 2010; Li et al. 2013), but the neurochemical organization of connections inside the STL and between CeA and STL is still elusive. We thus injected the retrograde tracer CTb into the CeM (Fig. 6) or the STLV (Fig. 7), followed by triple fluorescent labeling for neuronal markers.

CTb injections (n = 3) in rostral CeM (bregma level: -0.95/-1.07 mm) were centered in its ventral or dorsal portions (Fig. 6a), based on the cytoarchitectural features in DAPI staining (Fig. 6b) and the typical retrograde labeling in rostral lateral amygdala (LA) and InsCx. In these cases, a robust retrograde labeling was found in the CeL/C (Fig. 6f, g), while much fewer cells were labeled in STLD (Fig. 6d, e). Quantitative analysis of the colocalization between CTb and PKCδ or SOM immunoreactivity revealed that, among the CeM-projecting CeL/C neurons, 71.4 ± 1.3 % (Mean ± SEM) co-labeled with PKCδ and 13.9 ± 2.4 % with SOM (two sample *t*-test, p-value = 0.0009). In comparison, 60.8 ± 1.5 % of CTb+ cells in STLD were PKCδ+, but only 19.2 ± 2.6 % of them were SOM+ (two sample *t*-test, p-value = 0.002).

CTb injections (n = 3) into STLV area (possibly including the fusiform nuclei) (Fig. 7a,b) revealed a considerable number of labeled neurons in STLD and CeL/C. The injection cores were confined to STLV as judged by DAPI staining and few/no retrograde labeling occurred in the STMA and medial amygdaloid nucleus (MeA). In STLD, we found that 64.6 ± 4.1% (Mean ± SEM) of CTb+ neurons were PKCδ+, while only 5.1 ± 0.1% of them were SOM+, significantly less than previous group (two sample *t*-test, p-value = 0.011). In CeL/C,

48.1±0.6% of STLV-projecting neurons were PKCδ+, by contrast only 2.7 ± 0.2 % were SOM+ (two sample *t*-test, p-value = 0.048).

Taken together, our data suggest a significant role of PKCδ+ neurons in relaying information flow within EAc by connecting STLD and CeL/C with STLV and CeM. However, a sizeable part of the projections from STLD and CeL/C to STLV and CeM may originate in PKCδ-/SOM- neurons.

Both PKCδ+ and SOM+ neurons are involved in STLD-CeL/C reciprocal connections

Although STL and CeA have been known to be reciprocally connected to each other (Dong et al. 2001a; Gungor et al. 2015; Sun et al. 1994; Sun and Cassell 1993; Sun et al. 1991) , it remains not clear which cell types mediate the mutual connections between STLD and CeL/C. In mouse, rabies virus tracing from CeL PKCδ+ neurons revealed a dense neuronal labeling in dorsal STL (Cai et al. 2014), which arose an interesting speculation that PKCδ+ cells might serve as intrinsic projection neurons between STLD and CeL/C. To test this hypothesis, we carried out retrograde (Fig. 8) and anterograde (Fig. 9) tracings from STLD and CeL/C, followed by immunostaining of the tracers, PKCδ and SOM.

To determine if PKCδ+ and/or SOM+ neurons in CeL/C project to STLD, CTb injections were done in the STLD (n = 2; bregma level +0.13 mm). The injection sites were restricted to the PKCδ-expressing STLD (Fig. 8 b – c) and led to a large number of retrogradely labeled neurons in CeM and CeL/C, while labeling in medial amygdala was rarely seen (Fig. 8d). With confocal analysis, we found both CTb+/PKCδ+ and CTb+/SOM+ double labeled neurons in ipsilateral CeL/C (Fig. 8e). In a similar attempt, we labeled CeA-projecting neurons in STLD by injecting retrobeads into caudal CeL/C (n = 2; Fig. 8f, g). Here, the retrobeads were preferred to CTb to avoid any leakage in the CeM. Retrobeads indeed produced a local injection zone in CeL/C, without extension into CeM (Fig. 8g). Despite a leakage into the amygdalostriatal transition area (ASt) and globus pallidus (GP), we consider possible confounding retrograde labeling in STLD would be negligible as anterograde tracing from STLD rarely labeled neurons in ASt region. In this case, similar to that of CeL/C, the retrograde labeling could be found in both PKCδ+ neurons (Fig. 8j) and SOM+ neurons (Fig. 8i).

Thus, our evidences indicate that both PKCδ+ and SOM+ neurons contribute to intra-EAc connections, mediating mutual talks between the STLD and CeL/C. To further identify the possible neurochemical profile of the neurons that receive inputs from STLD or CeL/C, we

injected PHA-L in STLD or CeL/C and looked for potential appositions of anterogradely labeled axons with PKCδ+ and SOM+ neurons (Fig. 9).

Small PHA-L injections into STL (n = 1) produced a restricted labeling of neurons and processes which was confined to the PKCδ-expressing STLD (Fig. 9b). In caudal CeA, a moderate density of PHA-L+ axonal branches and terminals were found in CeM and CeL/C (Fig. 9c). Confocal images (z stack = 11.9 μm) at high magnification showed that PHA-L+ varicosities from single continuous axons ramifications could be found apposed to both PKCδ+ and SOM+ neurons (Fig. 9d). Similarly, PHA-L injection sites into caudal CeL/C were centered in CeL/C, without leakage in BLA or CeM (n = 1; Fig. 9f). Numerous PHA-L+ axons could be observed in STL, with the highest density in the STLD (Fig. 9 g). Apposition analysis following triple immunofluorescence staining revealed that many axon terminals formed close appositions with PKCδ+ and SOM+ neurons (Fig. 9h).

Thus, we concluded that projections from PKCδ+ and SOM+ neurons in STLD and CeL/C can target both PKCδ+ and SOM+ in the same subdivisions.

SOM+ neurons in STLD and CeL/C are the main sources of downstream projections to brainstem

Apart from the intra-EAc projection, neurons in STLD and CeL/C give rise to efferent to extra-EAc targets as well, including, the LPB and the PAG (Tokita et al. 2009; Dong et al. 2001b; Petrovich and Swanson 1997; Gray and Magnuson 1992; Moga and Gray 1985). Interestingly, brainstem-projecting neurons in STL and CeA share similar neuropeptidergic features in rats (Moga et al. 1989). In mice, it has been shown that SOM+ cells in CeL/C project to PAG (Penzo et al. 2014). In order to establish the neurochemical identity of neurons in STLD and CeL/C projecting to brainstem, we injected retrograde tracers into LPB and PAG.

Fluorogold (FG) injections in LPBE (n = 3; Fig. 10) usually resulted in minor lesion centered within LPBE (bregma -5.19 mm) and diffuse expansion into other subdivisions of LPB (Fig. 10b). The retrograde labeling in ST and amygdala was specifically restricted to STL and CeA, especially in STLD and CeL/C, with much sparser labeling in STLP and CeM. In STLD (Fig. 10d, e) as in CeL/C (Fig. 10f, g), numerous FG+ cells were SOM+ but very few were PKCδ+. Quantitative analysis (Fig. 10c) revealed that, SOM+ neurons accounted for 62.7± 0.4 % and 63.9± 0.7 % of the retrogradely labeled cells in STLD and CeL/C, respectively, whereas only 6.1± 0.4 % and 6.9±0.7 %; of FG+ neurons were PKCδ+ (two sample *t*-test, STLD p-value = 0.011, CeL/C p-value = 5.37e-06). To further examine the possibility that STLD and CeL/C

projections to LPBE can target CGRP+ neurons, we processed sections from animals with PHA-L injections into STLD (same case as in Fig. 9b) or into CeL/C (same case as in Fig. 9f), to label PHA-L and CGRP on LPB sections Consistent with the previous retrograde tracing, intense labeling of PHA-L+ axons was observed in LPB, especially dense in LPBE, following PHA-L injection in STLD (Fig. 11b) or CeL/C (Fig. 11d). CGRP+ neurons were concentrated in the ventrolateral part of the LPB, including the LPBE. Confocal analysis at high magnification revealed frequent, although not exclusive, appositions between PHA-L+ axonal varicosities, from STLD and CeL/C, and LBPE somas containing CGRP immunofluorescence. (Fig. 11b, d).

To investigate the EAc projection to PAG, we used retrograde tracers FG or CTb and performed triple immunofluorescence staining for the tracer, PKCδ and SOM. In order to achieve reasonable number of retrograde labeling in STLD and CeL/C (versus STLP or CeM), we produced large injection sites with tracer deposits extending into the lateral (LPAG) and ventrolateral (VLPAG) columns of the PAG and dorsal raphe nuclei (DR; bregma -4.47/-4.59 mm; Fig. 12b, c). Retrogradely labeled cells were found in STL and CeA, including STLD (Fig. 12d) and CeL/C (Fig. 12f). While no quantification has been done (one FG case and one CTb case), we observed that more than half of the retrogradely labeled neurons colocalized with SOM immunofluorescence in STLD (Fig. 12e) and in CeL/C (Fig. 12g), but almost never with PKCδ signal. These data indicate, in both STLD and CeL/C, SOM+ neurons, but not PKCδ+ ones, project to PAG/DR areas.

Taken together, these data supports a major role of STLD and CeL/C SOM+ neurons in mediating long range projections to LPB and PAG, while PKCδ+ neurons contribute very little in this direction.

DISCUSSION

In this study, we addressed the possibility of similar organization of cell-type specific neuronal circuits in STLD and CeA of mice, by combining retrograde and anterograde tract-tracing with immunofluorescent staining. Overall, we looked at three different aspects of neuronal circuit organizations of EAc, including the long-range inputs, intrinsic projections and long-range external outputs. We propose a model of cell-type specific parallel microcircuits in EAc, based on the connectivity of PKCδ+ and SOM+ neuronal populations (Fig. 13).

For the external excitatory inputs, our data support the hypothesis that multiple excitatory inputs can converge onto single neuronal populations in STLD and CeL/C. For instance,

excitatory sensory information from cortex or polymodal information from amygdala nuclei (i.e. BLP) can converge to PKCδ+ neurons which at the same time are innervated by excitatory CGRP+ sensory input from brainstem (i.e. LPB).

These excitatory drives onto distinct neuronal populations in EAc are then processed by intrinsic circuits, including local inhibition (i.e. SOM+ →SOM+ in CeL/C) (Hunt et al. 2017; Douglass et al. 2017) and long-range connection (i.e. PKCδ+ neurons in CeL/C →STLV). Because much less is known on local inhibitory circuits in STLD, we hypothesize that a similar configuration also exists there (dashed line, Fig. 13), which is featured with both homotypic (i.e. SOM+ → SOM+, not shown) and heterotypic (SOM+ → PKCδ+) connections (Fig. 13). For intrinsic long-range connections, we confirmed similar preferential innervations of STLV and CeM by PKCδ+ neurons in STLD and CeL/C, although sparse innervations from SOM+ populations are observed. The long-range, mutual connections between STLD and CeL/C can be carried out by both types of neurons.

Information from EAc are carried out mainly by SOM+ neurons in STLD and CeL/C, as well as undefined neuronal groups in STLV and CeM. Notably, we find that SOM+, not PKCδ populations, mediate the feedback to LPBE and PAG areas. Other downstream targets including lateral hypothalamus, can also possibly be mediated by SOM+ neurons, but further evidences are needed.

Technical considerations

In this study, the quality of injection sites are critical for reliable and accountable explanations that drawn from tract-tracing experiments. In total, we used FG/CTb and retrobeads for retrograde tracing, PHA-L/BDA for anterograde tracing. After checking the neuroanatomical localization of injection sites on successive coronal brain sections, we excluded those cases with confounding spillovers from our final report. When applied by iontophoresis, CTb, BDA and PHA-L reliably produced limited injection sites which usually confined to the nature shape of the target nucleus (i.e. see CTb injection into STLD, Fig. 8). Iontophoresis of FG into LPBE usually resulted in strong diffusive labeling in the other subdivisions of LPB, but we find minimal contaminations from these non-LPBE subdivision as suggested by minimal retrograde labeling in non-EAc subdivisions. In our hands, pressure injection of retrobeads in CeL/C usually resulted in deposits along the pipette passage, probably contaminating areas in ASt, GP or CPu, but none of these areas are innervated by STLD based on our retrograde tracing results and literature (Weller and Smith 1982; McDonald 1991).

We relied on antibodies to determine the cellular identity of PKCδ+ and SOM+ neurons. Due to unknown reasons, we observed that the immunofluorescent signal in STLD and CeL/C was weaker than the one in thalamic PKCδ+ neurons and cortical or striatal SOM+ neurons in the same brain sections. Nevertheless, the primary antibody for PKCδ we used was shown to detected most of the cre-positive neurons in a transgenic mouse line (Haubensak et al. 2010). The antibody against SOM gave a specific labeling of SOM-expressing neurons (Jhou et al. 2009) but seems to reveal much less neurons than what is observed in SOM-cre mouse line (Li et al. 2013). Finally, CGRP antibody revealed terminal fields in EAc that are consistent with previous reports (Dobolyi et al. 2005). Thus, we have a good confidence in showing the basket-like CGRP+ axon terminals and the appositions with PKCδ+ neurons in STLD and CeL/C, as PKCδ+ signal usually nicely traced out the whole cell body and proximal dendrites. We rarely observe these obvious basket-like terminals circle around SOM-expressing neurons. However, we cannot exclude other forms of CGRP+ terminals might exist and contact SOM+ neurons at soma or dendrites. We also likely underestimate the extent of CGRP+ contacts with PKCδ+ neurons as non-basket CGRP+ varicosity is not confirmable in our experimental conditions. Confirmation of CGRP+ synaptic contact by immunostaining of presynaptic markers (i.e. by vesicular glutamate transporter 2) or by synaptic ultra-structures with electronic microscopy are probably be good options for future studies.

Neurochemical features of EAc

Subdivisions of EAc have long been known to express a variety of neuropeptides and receptors, such as ENK, CRF, SOM, dopamine receptor, serotonin receptor 2a (Htr2a) (Cassell et al. 1986; Cassell et al. 1999; De Bundel et al. 2016; Douglass et al. 2017; Veinante et al. 1997). In this study, we focus on mapping the cellular connectivity of PKCδ+ and SOM+ neurons, primarily because these two neuronal populations are largely non-overlapping and constitute the majority of local GABAergic neurons in CeA (Haubensak et al. 2010; Li et al. 2013). In this study, we found a similar segregation and expression patterns of PKCδ and SOM in CeA as in previous reports on cre mouse line (Li et al. 2013) using double immunofluorescent staining. In addition, we describe for the first time a similar pattern was found in STLD. Even though immunofluorescent staining together with the highly sensitive CARD method (Hunyady et al. 1996) allows us to visualize many SOM+ and PKCδ+ neurons in EAc, the transgenic mouse lines might provide a more robust and reliable way to label these neurons (Li et al. 2013).

On the other hand, these two neuronal populations can intersect with other neuronal markers. For example, More than 70% of PKCδ neurons in CeLC and STLD are colabeled with dopamine receptor D2 (D2R) using Drd2-cre-EGFP mouse (De Bundel et al. 2016). PKCδ neurons do not overlap Htr2a-expressing cells in CeL, but more than half of Htr2a+ neurons coexpress SOM, a significant portion with CRF (Douglass et al. 2017). SOM+ neurons in both STL and CeA can also coexpress neuropeptide Y (NPY) (Wood et al. 2016). Thus, it is possible that some of the EAc PKCδ+ or SOM+ neurons revealed in this study can also belong to other specific neuronal populations.

Comparison with other studies on cell-type specific circuits in EAc

Long-range inputs

The identities of presynaptic inputs from extra-EAc sources have been studied in various ways and are in accordance with our study. Projection neurons from LPBE and BLP are the best studied compared to insular cortex.

CGRP+ neurons in LPBE have been shown project to CeL/C or STL by immunohistochemistry (Dobolyi et al. 2005), retrograde tract tracing (Carter et al. 2013), cell-type specific rabies tracing (Cai et al. 2014) and optogenetic mapping (Carter et al. 2013; Sato et al. 2015). Furthermore, CGRP receptor-expressing (CGRPR) CeL/C neurons were proved to be innervated by CGRP+ neurons in LPBE, using a double cre mouse line (Han et al. 2015), while the connectivity of CGRPR+ neurons in STL remains relatively unexplored. In our study, most of the CGRP+ terminals in CeL/C and STLD, as well as many of the axon terminals anterogradely labeled from LPBE, appear as basket perisomatic terminals, which are morphologically similar with those described in studies on rat (Sarhan et al. 2005; Dobolyi et al. 2005) and mouse (Campos et al. 2016). We found a preferential targeting of CGRP+ nerve terminals to PKCδ+ soma and proximal dendrites, not SOM+ ones. But we cannot exclude the synaptic or extra-synaptic influence of CGRP projection on SOM+ neurons, as a recent study indicates that only about half of calcitonin receptor-like (Calcrl) positive neurons coexpress PKCδ in CeC of mice (Kim et al. 2017).

On the other hand, projection from basolateral amygdala (BL) to CeA and STL, has been revealed by anterograde tract-tracing (Pitkanen et al. 1995; Dong et al. 2001a; Savander et al. 1996) and monosynaptic rabies virus tracing (Kim et al. 2017), optogenetic mapping (Li et al. 2013). It is worth noting that these CeA-projecting neurons are distributed differently along the rostral-caudal axis of BL. Most of CeA-projecting neurons situated in the posterior BLA (or BLP) and they are protein phosphatase 1 regulatory subunit 1B positive (Ppp1r1b+); while

less neurons are R-spondin 2 positive (Rspo2+) in BLA (Kim et al. 2017). In line with their findings, we found that CTb tracing from STLD and CeL/C resulted in dramatically more labeling in BLP than BLA. Insular cortex inputs to CeA and STL have also been previously described (Yasui et al. 1991a; McDonald et al. 1999; Sun et al. 1994) and have been shown to arise mainly from agranular and dysgranular areas. In this study, we further provide evidences that support a convergence of long-range pathways onto individual PKCδ+ neuron in both STLD and CeL/C, by showing a single PKCδ+ soma can be apposed by CGRP+ basket-like axonal terminal from LPBE, and BDA-labeled axonal varicosities from BLP or insular cortex. However, this connection is not exclusive as we also observed axon terminals from BLP or insular cortex apposed to PKCδ- soma, which could be also targeted by non-CGRP LPBE projections. It also important to note that, if we show that a number of given inputs can converge onto PKCδ+ population, other inputs might favor different populations. For example, afferents from the thalamic paraventricular nucleus target two times more the SOM+ neurons than PKCδ+ neurons in CeL/C (Penzo et al. 2015).

Intrinsic circuits

In this study, information on cell-type specificity of short range, local intrinsic connections are obscured by bulk tract-tracing method. But armed with advanced techniques like optogenetic mapping, electrophysiology and monosynaptic rabies tracing, recent works on CeA revealed complex disinhibitory circuit between PKCδ+ and SOM+ neurons (Ciocchi et al. 2010; Haubensak et al. 2010; Li et al. 2013; Janak and Tye 2015; Hunt et al. 2017; Douglass et al. 2017). Into the CeL/C, for example, PKCδ+ neurons can project to PKCδ-negative ones (Haubensak et al. 2010; Douglass et al. 2017) and non-PKCδ neurons project more to non-PKCδ cells (Hunt et al. 2017). By taking advantage of rabies virus tracing in multiple cre mouse lines, Kim and colleagues revealed surprising complexity in several neuronal populations in CeL, including PKCδ, SOM, CRF, neurotensin, and tachykinin 2 (Kim et al. 2017). Here again, information on STLD local circuits is still missing.

On the other hand, connectivity between EAc subdivisions, including short-range ones linking CeA or STL subdivisions and long-range ones between CeA and STL subdivisions, is well-resolved by restricted injection of retrograde tracer like CTb. Li and colleagues reported that about 15% of CeM-projecting neurons are SOM+ in CeL/C (Li et al. 2013), but that PKCδ+ ones project to CeM (Ciocchi et al. 2010; Li et al. 2013; Oh et al. 2014), which is consistent with the present findings. In comparison, limited information is available on STLV-projecting CeL/C or STLD neurons. In this study, we show that, similarly to the CeL/C-CeM pathway,

PKCδ+ neurons are the main source of projection from the STLD to STLV with only a small contribution of SOM+ neurons. In addition we also evidenced the fact that these neuronal populations contribute to long-range projection from CeL/C to STLV and from STLD to CeM. It would be interesting to verify whether a single CeL/C or STLD neuron can project to both CeM and STLV, as it has been suggested in rats for CeL neurons (Veinante and Freund-Mercier 2003).While PKCδ+ neurons are clearly involved in these intrinsic EAc connections, it is worth noting that, in our hands, only 80% of CeM-projecting neurons in STLD or CeL/C can be attributed to PKCδ and SOM population, while for STLV-projecting ones, about 30 – 50% were not labeled by either of the two markers. This suggests other neuronal populations can significantly contribute to the internal long-range projection, especially to STLV. Indeed, other neuronal populations have been shown to mediate mutual or unidirectional connection between STL and CeA by NPY+ (Wood et al. 2016), Htr2a+ (Douglass et al. 2017) and CRF+ populations (Pomrenze et al. 2015).

The cellular identity of STLD – CeL/C mutual connections is also elusive. In this study, we used retrograde tracing and anterograde tracing to reveal that both PKCδ+ and SOM+ neurons can be projection neurons and can be targeted (Fig. 9). We also observed that retrograde labeling in STLD is much weaker than that in CeL/C, and most of labeling is in STLP and STLV, which is partly due to a much weaker STLD → CeL/C projection than the other way around. Future investigation might as well take advantage of cell-type specific optogenetic tools to pinpoint the direct and indirect synaptic responses between CeL/C and STLD.

Long-range outputs

EAc neurons projecting to LPB has been suggested to contain several different neuronal markers such as CRF, neurotensin, ENK and SOM (Moga et al. 1989; Panguluri et al. 2009; Magableh and Lundy 2014; Moga and Gray 1985). While PKCδ+ neurons have been demonstrated to not, or faintly, project to LPBE by optogenetic mapping (Douglass et al. 2017; Oh et al. 2014), a strong terminal field from CeL/C PKCδ+ neurons was described in LPB (Cai et al. 2014). Our results indicate a preferential innervation of LPB by SOM+, not by PKCδ neurons in both STLD and CeL/C. Furthermore, with anterograde tracing, we reveal that the axonal varicosities from EAc can specifically target CGRP+ neurons in LPBE, as well as non-CGRP+ neurons.

Similarly, PAG-projecting neurons in STL and CeA have also been known to express multiple neuronal markers such as neurotensin, CRF, and SOM (Gray and Magnuson 1992). In CeL/C, SOM+ neurons, but not PKCδ ones, have been shown to project to PAG by tract-

tracing in SOM-cre mouse line (Penzo et al. 2014). So far, our findings on PAG/DR-projecting neurons are consistent with what has been reported for CeA and suggest that the same organization may exist in the STLD-PAG pathway. Besides LPB and PAG, CeL/C SOM+ neurons can also project to the solitary nucleus (Sol) (Higgins and Schwaber 1983; Gray and Magnuson 1987) and to the paraventricular thalamic nucleus (Penzo et al. 2014). Taken together, it is reasonable to hypothesize that SOM+ neurons, not PKCδ+ ones, are the major long-range projection neurons in STLD and CeL/C. However, SOM+ cells might not be the only populations involved in long range projections. Several neuropeptidic markers, including ENK, CRF and neurotensin, have been detected in brainstem-projecting neurons of CeL/C and STLD, but also in CeM and STLV (Gray and Magnuson 1992, 1987; Moga and Gray 1985; Moga et al. 1989; Magableh and Lundy 2014).

Functional implications of cell-type specific circuits in EAc

The pioneer studies of Cassell's group (Cassell et al. 1986; Sun et al. 1991; Sun and Cassell 1993; Sun et al. 1994; Cassell et al. 1999) established the notion that the rat CeL (and CeC) constitute an inhibitory interface between inputs and the outputs derived from CeM. The organization of this microcircuitry was later precised in mice to show that, in fear conditioning, a conditioned stimulus, previously associated to an unconditioned stimulus, activate in CeL/C a population of PKCδ negative cells, potentially SOM+, which then inhibits in turn a population of PKCδ+ cells projecting to CeM, leading thus to the disinhibition of CeM outputs neurons (Ciocchi et al. 2010; Haubensak et al. 2010). Subsequent studies have detailed the roles of CeL/C PKCδ+ and SOM+ cells, along with LPB CGRP input, in fear learning and memory, in fear generalization and anxiety (Li et al. 2013; Han et al. 2015; Botta et al. 2015; Penzo et al. 2015). The role of these CeA circuits in feeding has also been examined through elegant studies showing that LPB CGRP signaling to PKCδ+ CeL/C suppresses appetite, while other inputs, including from BL, can target other cell populations, including SOM+ and Htr2a+, that promote appetite (Carter et al. 2013; Cai et al. 2014; Campos et al. 2016; Douglass et al. 2017; Kim et al. 2017). The CeA circuit we described is consistent with the connectivity revealed in these studies. By contrast, this level of precision in microcircuits has not yet been reached for STL. The STL has been shown to be largely involved in contextual fear learning, anxiety and stress response (Zimmerman and Maren 2011; Goode et al. 2015; Daldrup et al. 2016; De Bundel et al. 2016; Davis et al. 2009). De Bundel and colleagues showed that fear generalization relays on coordinate action of STLD and CeL/C dopamine D2 receptor-expressing neurons, which mostly coexpress PKCδ (De

Bundel et al. 2016). Thus, considering the parallel circuits existing in CeL/C and STLD, it is possible that LPB →STLD pathway use a similar microcircuitry than CeL/C to support STL roles in associative learning and memory or in feeding.

Conclusions

Although the principle components of EAc are well-known to substantially share input/output connectivities and neurochemical features, comparative studies of STL and CeA neuronal circuits at cellular level are missing. In this study, we revealed a new depth of structural similarity between STLD and CeL/C by showing similar cell-type specific neuronal circuits in both nuclei. We showed that, like in CeA, the non-overlapping PKCδ+ and SOM+ neuronal populations also exist in STLD. In both nuclei, these two distinct neuronal groups form cell-type specific microcircuits integrating long-range inputs, mediating intrinsic connections, and sending long-range projections. In addition, these parallel microcircuits are, at the same time, integrated circuits, largely through interconnections within nuclei, between STLD and CeL/C and from STLD to CeM as well as from CeL/C to STLV.

ST and CeA are also known to be similarly involved in emotion, but with distinct roles. For instance, both structures have been implicated in fear and anxiety, with ST more involved in unconditioned/sustained fear response or anxiety-like behavior versus CeA being more implicated in conditioned/phasic fear response (Walker and Davis 1997; Walker et al. 2003; Davis et al. 2009; Lebow and Chen 2016). Similarly, CeA participates in both sensory and affective aspects of pain (Neugebauer et al. 2004; Carrasquillo and Gereau 2007; Neugebauer 2015; Veinante et al. 2013), while ST seems to contribute only to the affective component of pain (Deyama et al. 2008; Minami and Ide 2015). So far, it is not clear what kind of structural differences underlies such functional discrepancy in ST and CeA. One possibility could be the subtle differences in the inputs and outputs circuits of ST and CeA, as well as in local neuronal pools. For example, it is remain to be explored whether ST and CeA are innervated by different sets of neurons in LPB or InsCx, or whether different pools of PKCδ+ or SOM+ neurons are preferred in fear versus anxiety. Another possibility could be the asymmetric connections between STLD and CeA, where the projection from CeA to STL seems to be stronger than that of the reverse direction (Dong et al. 2001a; Oler et al. 2017). Again, the functional implications of these structural differences remain to be further explored.

So far, compared to STL, the structures and functions of CeA microcircuits have been better studied by cell-type/pathway specific genetic manipulation and behavior assays (Ciocchi et al. 2010; Haubensak et al. 2010; Cai et al. 2014; Han et al. 2015; Li et al. 2013). Our results

demonstrate that CeA-like microcircuits also exist in STLD, and that they contribute to a complex network linking the components of the EAc. Future studies on structures and functions of neuronal circuits of ST might benefit from considering previous researches of CeA microcircuits.

Acknowledgments

We thank Dr. Paul Klosen for helpful advices in CARD method and Dr. Alessandro Bilella for help in using NanoZoomer S60 platform. This work was supported by the Centre National de la Recherche Scientifique (contract UPR3212), the University of Strasbourg and the NeuroTime Erasmus Mundus Joint Doctorate Program.

Compliance with ethical standards

All applicable international, national, and/or institutional guidelines for the care and use of animals were followed.

Informed consent

No human subject were used in this study

Disclosure of potential conflicts of interest

The authors declare that they have no conflict of interest.

References

Alden M, Besson JM, Bernard JF (1994) Organization of the efferent projections from the pontine parabrachial area to the bed nucleus of the stria terminalis and neighboring regions: a PHA-L study in the rat. J Comp Neurol 341 (3):289-314. doi:10.1002/cne.903410302

Alheid GF (2003) Extended amygdala and basal forebrain. Ann N Y Acad Sci 985:185-205. doi:10.1111/j.1749-6632.2003.tb07082.x

Bernard JF, Alden M, Besson JM (1993) The organization of the efferent projections from the pontine parabrachial area to the amygdaloid complex: a Phaseolus vulgaris leucoagglutinin (PHA-L) study in the rat. J Comp Neurol 329 (2):201-229. doi:10.1002/cne.903290205

Botta P, Demmou L, Kasugai Y, Markovic M, Xu C, Fadok JP, Lu T, Poe MM, Xu L, Cook JM, Rudolph U, Sah P, Ferraguti F, Luthi A (2015) Regulating anxiety with extrasynaptic inhibition. Nat Neurosci 18 (10):1493-1500. doi:10.1038/nn.4102

Cai H, Haubensak W, Anthony TE, Anderson DJ (2014) Central amygdala PKC-delta(+) neurons mediate the influence of multiple anorexigenic signals. Nat Neurosci 17 (9):1240-1248. doi:10.1038/nn.3767

Campos CA, Bowen AJ, Schwartz MW, Palmiter RD (2016) Parabrachial CGRP Neurons Control Meal Termination. Cell Metab 23 (5):811-820. doi:10.1016/j.cmet.2016.04.006

Carrasquillo Y, Gereau RWt (2007) Activation of the extracellular signal-regulated kinase in the amygdala modulates pain perception. J Neurosci 27 (7):1543-1551. doi:10.1523/JNEUROSCI.3536-06.2007

Carter ME, Soden ME, Zweifel LS, Palmiter RD (2013) Genetic identification of a neural circuit that suppresses appetite. Nature 503 (7474):111-114. doi:10.1038/nature12596

Cassell MD, Freedman LJ, Shi C (1999) The intrinsic organization of the central extended amygdala. Ann N Y Acad Sci 877:217-241

Cassell MD, Gray TS, Kiss JZ (1986) Neuronal architecture in the rat central nucleus of the amygdala: a cytological, hodological, and immunocytochemical study. J Comp Neurol 246 (4):478-499. doi:10.1002/cne.902460406

Chieng BC, Christie MJ, Osborne PB (2006) Characterization of neurons in the rat central nucleus of the amygdala: cellular physiology, morphology, and opioid sensitivity. J Comp Neurol 497 (6):910-927. doi:10.1002/cne.21025

Ciocchi S, Herry C, Grenier F, Wolff SB, Letzkus JJ, Vlachos I, Ehrlich I, Sprengel R, Deisseroth K, Stadler MB, Muller C, Luthi A (2010) Encoding of conditioned fear in central amygdala inhibitory circuits. Nature 468 (7321):277-282. doi:10.1038/nature09559

D'Hanis W, Linke R, Yilmazer-Hanke DM (2007) Topography of thalamic and parabrachial calcitonin gene-related peptide (CGRP) immunoreactive neurons projecting to subnuclei of the amygdala and extended amygdala. J Comp Neurol 505 (3):268-291. doi:10.1002/ene.21495

Daldrup T, Lesting J, Meuth P, Seidenbecher T, Pape HC (2016) Neuronal correlates of sustained fear in the anterolateral part of the bed nucleus of stria terminalis. Neurobiol Learn Mem 131:137-146. doi:10.1016/j.nlm.2016.03.020

Davis M, Shi C (1999) The extended amygdala: are the central nucleus of the amygdala and the bed nucleus of the stria terminalis differentially involved in fear versus anxiety? Ann N Y Acad Sci 877:281-291

Davis M, Walker DL, Miles L, Grillon C (2009) Phasic vs sustained fear in rats and humans: role of the extended amygdala in fear vs anxiety. Neuropsychopharmacology 35 (1):105-135. doi:10.1038/npp.2009.109

De Bundel D, Zussy C, Espallergues J, Gerfen CR, Girault JA, Valjent E (2016) Dopamine D2 receptors gate generalization of conditioned threat responses through mTORC1 signaling in the extended amygdala. Mol Psychiatry 21 (11):1545-1553. doi:10.1038/mp.2015.210

de Olmos JS, Heimer L (1999) The concepts of the ventral striatopallidal system and extended amygdala. Ann N Y Acad Sci 877:1-32

Delaney AJ, Crane JW, Sah P (2007) Noradrenaline modulates transmission at a central synapse by a presynaptic mechanism. Neuron 56 (5):880-892. doi:10.1016/j.neuron.2007.10.022

Deyama S, Katayama T, Ohno A, Nakagawa T, Kaneko S, Yamaguchi T, Yoshioka M, Minami M (2008) Activation of the beta-adrenoceptor-protein kinase A signaling pathway within the ventral bed nucleus of the stria terminalis mediates the negative affective component of pain in rats. J Neurosci 28 (31):7728-7736. doi:10.1523/JNEUROSCI.1480-08.2008

Dobolyi A, Irwin S, Makara G, Usdin TB, Palkovits M (2005) Calcitonin gene-related peptide-containing pathways in the rat forebrain. J Comp Neurol 489 (1):92-119. doi:10.1002/cne.20618

Dong HW, Petrovich GD, Swanson LW (2001a) Topography of projections from amygdala to bed nuclei of the stria terminalis. Brain Res Brain Res Rev 38 (1-2):192-246

Dong HW, Petrovich GD, Watts AG, Swanson LW (2001b) Basic organization of projections from the oval and fusiform nuclei of the bed nuclei of the stria terminalis in adult rat brain. J Comp Neurol 436 (4):430-455

Douglass AM, Kucukdereli H, Ponserre M, Markovic M, Grundemann J, Strobel C, Alcala Morales PL, Conzelmann KK, Luthi A, Klein R (2017) Central amygdala circuits modulate food consumption through a positive-valence mechanism. Nat Neurosci 20 (10):1384-1394. doi:10.1038/nn.4623
Fadok JP, Krabbe S, Markovic M, Courtin J, Xu C, Massi L, Botta P, Bylund K, Muller C, Kovacevic A, Tovote P, Luthi A (2017) A competitive inhibitory circuit for selection of active and passive fear responses. Nature 542 (7639):96-100. doi:10.1038/nature21047
Goode TD, Kim JJ, Maren S (2015) Reversible Inactivation of the Bed Nucleus of the Stria Terminalis Prevents Reinstatement But Not Renewal of Extinguished Fear. eNeuro 2 (3). doi:10.1523/ENEURO.0037-15.2015
Gray TS, Magnuson DJ (1987) Neuropeptide neuronal efferents from the bed nucleus of the stria terminalis and central amygdaloid nucleus to the dorsal vagal complex in the rat. J Comp Neurol 262 (3):365-374. doi:10.1002/cne.902620304
Gray TS, Magnuson DJ (1992) Peptide immunoreactive neurons in the amygdala and the bed nucleus of the stria terminalis project to the midbrain central gray in the rat. Peptides 13 (3):451-460
Gungor NZ, Pare D (2016) Functional Heterogeneity in the Bed Nucleus of the Stria Terminalis. J Neurosci 36 (31):8038-8049. doi:10.1523/JNEUROSCI.0856-16.2016
Gungor NZ, Yamamoto R, Pare D (2015) Optogenetic study of the projections from the bed nucleus of the stria terminalis to the central amygdala. Journal of Neurophysiology 114 (5):2903-2911. doi:10.1152/jn.00677.2015
Han S, Soleiman MT, Soden ME, Zweifel LS, Palmiter RD (2015) Elucidating an Affective Pain Circuit that Creates a Threat Memory. Cell 162 (2):363-374. doi:10.1016/j.cell.2015.05.057
Haubensak W, Kunwar PS, Cai H, Ciocchi S, Wall NR, Ponnusamy R, Biag J, Dong HW, Deisseroth K, Callaway EM, Fanselow MS, Luthi A, Anderson DJ (2010) Genetic dissection of an amygdala microcircuit that gates conditioned fear. Nature 468 (7321):270-276. doi:10.1038/nature09553
Higgins GA, Schwaber JS (1983) Somatostatinergic projections from the central nucleus of the amygdala to the vagal nuclei. Peptides 4 (5):657-662
Hunt S, Sun Y, Kucukdereli H, Klein R, Sah P (2017) Intrinsic Circuits in the Lateral Central Amygdala. eNeuro 4 (1). doi:10.1523/ENEURO.0367-16.2017
Hunyady B, Krempels K, Harta G, Mezey E (1996) Immunohistochemical signal amplification by catalyzed reporter deposition and its application in double immunostaining. J Histochem Cytochem 44 (12):1353-1362
Janak PH, Tye KM (2015) From circuits to behaviour in the amygdala. Nature 517 (7534):284-292. doi:10.1038/nature14188
Jennings JH, Sparta DR, Stamatakis AM, Ung RL, Pleil KE, Kash TL, Stuber GD (2013) Distinct extended amygdala circuits for divergent motivational states. Nature 496 (7444):224-228. doi:10.1038/nature12041
Jhou TC, Geisler S, Marinelli M, Degarmo BA, Zahm DS (2009) The mesopontine rostromedial tegmental nucleus: A structure targeted by the lateral habenula that projects to the ventral tegmental area of Tsai and substantia nigra compacta. J Comp Neurol 513 (6):566-596. doi:10.1002/cne.21891
Kim J, Zhang X, Muralidhar S, LeBlanc SA, Tonegawa S (2017) Basolateral to Central Amygdala Neural Circuits for Appetitive Behaviors. Neuron 93 (6):1464-1479 e1465. doi:10.1016/j.neuron.2017.02.034
Kim SY, Adhikari A, Lee SY, Marshel JH, Kim CK, Mallory CS, Lo M, Pak S, Mattis J, Lim BK, Malenka RC, Warden MR, Neve R, Tye KM, Deisseroth K (2013) Diverging neural pathways assemble a behavioural state from separable features in anxiety. Nature 496 (7444):219-223. doi:10.1038/nature12018
Lebow MA, Chen A (2016) Overshadowed by the amygdala: the bed nucleus of the stria terminalis emerges as key to psychiatric disorders. Mol Psychiatry 21 (4):450-463. doi:10.1038/mp.2016.1
Lein ES, et al. (2007) Genome-wide atlas of gene expression in the adult mouse brain. Nature 445 (7124):168-176. doi:10.1038/nature05453
Li H, Penzo MA, Taniguchi H, Kopec CD, Huang ZJ, Li B (2013) Experience-dependent modification of a central amygdala fear circuit. Nat Neurosci 16 (3):332-339. doi:10.1038/nn.3322
Magableh A, Lundy R (2014) Somatostatin and corticotrophin releasing hormone cell types are a major source of descending input from the forebrain to the parabrachial nucleus in mice. Chem Senses 39 (8):673-682. doi:10.1093/chemse/bju038
Mazzone CM, Pati D, Michaelides M, DiBerto J, Fox JH, Tipton G, Anderson C, Duffy K, McKlveen JM, Hardaway JA, Magness ST, Falls WA, Hammack SE, McElligott ZA, Hurd YL, Kash TL (2016) Acute engagement of Gq-mediated signaling in the bed nucleus of the stria terminalis induces anxiety-like behavior. Mol Psychiatry. doi:10.1038/mp.2016.218
McDonald AJ (1982) Cytoarchitecture of the central amygdaloid nucleus of the rat. J Comp Neurol 208 (4):401-418. doi:10.1002/cne.902080409

McDonald AJ (1991) Topographical organization of amygdaloid projections to the caudatoputamen, nucleus accumbens, and related striatal-like areas of the rat brain. Neuroscience 44 (1):15-33
McDonald AJ, Shammah-Lagnado SJ, Shi C, Davis M (1999) Cortical afferents to the extended amygdala. Ann N Y Acad Sci 877:309-338
Minami M, Ide S (2015) How does pain induce negative emotion? Role of the bed nucleus of the stria terminalis in pain-induced place aversion. Curr Mol Med 15 (2):184-190
Moga MM, Gray TS (1985) Evidence for corticotropin-releasing factor, neurotensin, and somatostatin in the neural pathway from the central nucleus of the amygdala to the parabrachial nucleus. J Comp Neurol 241 (3):275-284. doi:10.1002/cne.902410304
Moga MM, Saper CB, Gray TS (1989) Bed nucleus of the stria terminalis: cytoarchitecture, immunohistochemistry, and projection to the parabrachial nucleus in the rat. J Comp Neurol 283 (3):315-332. doi:10.1002/cne.902830302
Neugebauer V (2015) Amygdala pain mechanisms. Handb Exp Pharmacol 227:261-284. doi:10.1007/978-3-662-46450-2_13
Neugebauer V, Li W, Bird GC, Han JS (2004) The amygdala and persistent pain. Neuroscientist 10 (3):221-234. doi:10.1177/1073858403261077
Oh SW, Harris JA, Ng L, Winslow B, Cain N, Mihalas S, Wang Q, Lau C, Kuan L, Henry AM, Mortrud MT, Ouellette B, Nguyen TN, Sorensen SA, Slaughterbeck CR, Wakeman W, Li Y, Feng D, Ho A, Nicholas E, Hirokawa KE, Bohn P, Joines KM, Peng H, Hawrylycz MJ, Phillips JW, Hohmann JG, Wohnoutka P, Gerfen CR, Koch C, Bernard A, Dang C, Jones AR, Zeng H (2014) A mesoscale connectome of the mouse brain. Nature 508 (7495):207-214. doi:10.1038/nature13186
Oler JA, Tromp DP, Fox AS, Kovner R, Davidson RJ, Alexander AL, McFarlin DR, Birn RM, B EB, deCampo DM, Kalin NH, Fudge JL (2017) Connectivity between the central nucleus of the amygdala and the bed nucleus of the stria terminalis in the non-human primate: neuronal tract tracing and developmental neuroimaging studies. Brain Struct Funct 222 (1):21-39. doi:10.1007/s00429-016-1198-9
Panguluri S, Saggu S, Lundy R (2009) Comparison of somatostatin and corticotrophin-releasing hormone immunoreactivity in forebrain neurons projecting to taste-responsive and non-responsive regions of the parabrachial nucleus in rat. Brain Res 1298:57-69. doi:10.1016/j.brainres.2009.08.038
Paxinos G, Franklin K (2012) Paxinos and Franklin's The mouse brain in stereotaxic coordinates. Fourth edition. edn. Academic Press, Amsterdam
Penzo MA, Robert V, Li B (2014) Fear conditioning potentiates synaptic transmission onto long-range projection neurons in the lateral subdivision of central amygdala. J Neurosci 34 (7):2432-2437. doi:10.1523/JNEUROSCI.4166-13.2014
Penzo MA, Robert V, Tucciarone J, De Bundel D, Wang M, Van Aelst L, Darvas M, Parada LF, Palmiter RD, He M, Huang ZJ, Li B (2015) The paraventricular thalamus controls a central amygdala fear circuit. Nature. doi:10.1038/nature13978
Petrovich GD, Swanson LW (1997) Projections from the lateral part of the central amygdalar nucleus to the postulated fear conditioning circuit. Brain Res 763 (2):247-254
Pitkanen A, Savander M, Nurminen N, Ylinen A (2003) Intrinsic synaptic circuitry of the amygdala. Ann N Y Acad Sci 985:34-49
Pitkanen A, Stefanacci L, Farb CR, Go GG, LeDoux JE, Amaral DG (1995) Intrinsic connections of the rat amygdaloid complex: projections originating in the lateral nucleus. J Comp Neurol 356 (2):288-310. doi:10.1002/cne.903560211
Pomrenze MB, Millan EZ, Hopf FW, Keiflin R, Maiya R, Blasio A, Dadgar J, Kharazia V, De Guglielmo G, Crawford E, Janak PH, George O, Rice KC, Messing RO (2015) A Transgenic Rat for Investigating the Anatomy and Function of Corticotrophin Releasing Factor Circuits. Front Neurosci 9:487. doi:10.3389/fnins.2015.00487
Salio C, Averill S, Priestley JV, Merighi A (2007) Costorage of BDNF and neuropeptides within individual dense-core vesicles in central and peripheral neurons. Dev Neurobiol 67 (3):326-338. doi:10.1002/dneu.20358
Saper CB (1982) Convergence of autonomic and limbic connections in the insular cortex of the rat. J Comp Neurol 210 (2):163-173. doi:10.1002/cne.902100207
Sarhan M, Freund-Mercier MJ, Veinante P (2005) Branching patterns of parabrachial neurons projecting to the central extended amgydala: single axonal reconstructions. J Comp Neurol 491 (4):418-442. doi:10.1002/cne.20697
Sato M, Ito M, Nagase M, Sugimura YK, Takahashi Y, Watabe AM, Kato F (2015) The lateral parabrachial nucleus is actively involved in the acquisition of fear memory in mice. Mol Brain 8:22. doi:10.1186/s13041-015-0108-z

Savander V, Go CG, Ledoux JE, Pitkanen A (1996) Intrinsic connections of the rat amygdaloid complex: projections originating in the accessory basal nucleus. J Comp Neurol 374 (2):291-313. doi:10.1002/(SICI)1096-9861(19961014)374:2<291::AID-CNE10>3.0.CO;2-Y

Schindelin J, Arganda-Carreras I, Frise E, Kaynig V, Longair M, Pietzsch T, Preibisch S, Rueden C, Saalfeld S, Schmid B, Tinevez JY, White DJ, Hartenstein V, Eliceiri K, Tomancak P, Cardona A (2012) Fiji: an open-source platform for biological-image analysis. Nat Methods 9 (7):676-682. doi:10.1038/nmeth.2019

Shackman AJ, Fox AS (2016) Contributions of the Central Extended Amygdala to Fear and Anxiety. J Neurosci 36 (31):8050-8063. doi:10.1523/JNEUROSCI.0982-16.2016

Speel EJ, Ramaekers FC, Hopman AH (1997) Sensitive multicolor fluorescence in situ hybridization using catalyzed reporter deposition (CARD) amplification. J Histochem Cytochem 45 (10):1439-1446

Sun N, Cassell MD (1993) Intrinsic GABAergic neurons in the rat central extended amygdala. J Comp Neurol 330 (3):381-404. doi:10.1002/cne.903300308

Sun N, Roberts L, Cassell MD (1991) Rat central amygdaloid nucleus projections to the bed nucleus of the stria terminalis. Brain Res Bull 27 (5):651-662

Sun N, Yi H, Cassell MD (1994) Evidence for a GABAergic interface between cortical afferents and brainstem projection neurons in the rat central extended amygdala. J Comp Neurol 340 (1):43-64. doi:10.1002/cne.903400105

Tokita K, Inoue T, Boughter JD, Jr. (2009) Afferent connections of the parabrachial nucleus in C57BL/6J mice. Neuroscience 161 (2):475-488. doi:10.1016/j.neuroscience.2009.03.046

Veinante P, Freund-Mercier MJ (1998) Intrinsic and extrinsic connections of the rat central extended amygdala: an in vivo electrophysiological study of the central amygdaloid nucleus. Brain Res 794 (2):188-198. doi:S0006-8993(98)00228-5 [pii]

Veinante P, Freund-Mercier MJ (2003) Branching Patterns of Central Amygdaloid Nucleus Efferents in the Rat: Single-Axon Reconstructions. Ann N Y Acad Sci 985:552-553. doi:10.1111/j.1749-6632.2003.tb07126.x

Veinante P, Stoeckel ME, Freund-Mercier MJ (1997) GABA- and peptide-immunoreactivities co-localize in the rat central extended amygdala. Neuroreport 8 (13):2985-2989

Veinante P, Yalcin I, Barrot M (2013) The amygdala between sensation and affect: a role in pain. J Mol Psychiatry 1 (1):9. doi:10.1186/2049-9256-1-9

Walker DL, Davis M (1997) Double dissociation between the involvement of the bed nucleus of the stria terminalis and the central nucleus of the amygdala in startle increases produced by conditioned versus unconditioned fear. J Neurosci 17 (23):9375-9383

Walker DL, Toufexis DJ, Davis M (2003) Role of the bed nucleus of the stria terminalis versus the amygdala in fear, stress, and anxiety. Eur J Pharmacol 463 (1-3):199-216. doi:S0014299903012822 [pii]

Weller KL, Smith DA (1982) Afferent connections to the bed nucleus of the stria terminalis. Brain Res 232 (2):255-270

Wood J, Verma D, Lach G, Bonaventure P, Herzog H, Sperk G, Tasan RO (2016) Structure and function of the amygdaloid NPY system: NPY Y2 receptors regulate excitatory and inhibitory synaptic transmission in the centromedial amygdala. Brain Struct Funct 221 (7):3373-3391. doi:10.1007/s00429-015-1107-7

Yasui Y, Breder CD, Saper CB, Cechetto DF (1991a) Autonomic responses and efferent pathways from the insular cortex in the rat. J Comp Neurol 303 (3):355-374. doi:10.1002/cne.903030303

Yasui Y, Saper CB, Cechetto DF (1991b) Calcitonin gene-related peptide (CGRP) immunoreactive projections from the thalamus to the striatum and amygdala in the rat. J Comp Neurol 308 (2):293-310. doi:10.1002/cne.903080212

Yu K, Garcia da Silva P, Albeanu DF, Li B (2016) Central Amygdala Somatostatin Neurons Gate Passive and Active Defensive Behaviors. J Neurosci 36 (24):6488-6496. doi:10.1523/JNEUROSCI.4419-15.2016

Zimmerman JM, Maren S (2011) The bed nucleus of the stria terminalis is required for the expression of contextual but not auditory freezing in rats with basolateral amygdala lesions. Neurobiol Learn Mem 95 (2):199-205. doi:10.1016/j.nlm.2010.11.002

Table 1. Stereotaxic coordinates used in this study.

Areas	Coordinates		
	AP (mm)	**ML** (mm)	**DV** (mm)
STLD	+0.20	+0.90	-3.30
STLV	+0.20	+0.90	-4.00
CeL/C	-1.43	+2.35	-3.75
CeM	-1.07	+2.20	-4.00
AI/DI	-0.23	+3.80	-2.10
BLP	-2.45	+3.30	-3.90
PAG	-4.47	+0.40	-2.70
LPBE	-5.19	+1.60	-3.60

Abbreviations: AP, Anterior – Posterior axis; ML, Medial - Lateral axis; DV, dorsal - ventral axis. The stereotaxic coordinates are taken from Paxinos and Franklin's mouse brain atlas (Paxinos and Franklin 2012), with the bregma point as the origin for AP and ML axis. The DV distance was referred to its cortical surface at the corresponding AP, ML location.

Table 2. Primary antibodies

Name	Species, Poly/mono-	Dilution	Antigen	Source, catalog etc.	Reference
CGRP	Rabbit, polyclonal	1:1500	Rat CGRP	Cat. #RPN1842, Amersham	(Franke-Radowiecka 2011)
CTb	Goat, antiserum	1:3000	choleragenoid	Cat. #703, List Biological Laboritories	(Thompson and Swanson 2010)
FG	Rabbit, polyclonal	1:1000	KLH-conjugated Fluorescent Gold	Cat. #AB153-I, Millipore	(Thompson and Swanson 2010
PHA-L	Goat, polyclonal	1:1000	pure lectin	Cat. #AS-2224, Vector Laboratories	(Thompson and Swanson 2010)
PKCδ	Mouse, monoclonal	1:1000	Human PKCδ aa. 114-289	Cat. #610398, BD Biosciences	(Haubensack et al; 2010)
SOM	Rabbit, antiserum	1:5000	KLH-conjugated synthetic somatostatin (AGCKNFFWKTFTSC)	Cat. #20067, Immunostar	(Jhou et al. 2009)

Abbreviations: see the list.

Legends

Fig 1. PKCδ and SOM expressing cells are concentrated in STLD and CeL/C. Double staining of PKCδ (**a, c, d, f**; red) and SOM (**b, c, e, f**; green) in coronal sections of STLD (**a - c**; bregma level +0.13mm) and CeL/C (**d - f**; bregma -1.55 mm) detected with epifluorescence. DAPI staining (blue) of cell nuclei is also shown (**c1, f1, c2, f2** and **a3 - f3**). The first column shows a full view of sections at the level of the STL (**a1 - c1**) and of the amygdala (**d1 – f1**), the second column shows a detailed view of STL (**a2 - c2**) and amygdala (**d2 - f2**) with delineation, corresponding to the boxed area in **a1-f1**, and the third column shows a magnification at cellular level in the STLD (**a3 - c3**) and in the CeL/C (**d3 - f3**) of the boxed area in **a2 - f2**. See list for abbreviations. Scale bars: **a1- f1**, 1.0 mm; **a2 - f2**, 500 μm; **a3 - f3**, 50 μm.

Fig. 2 Structural apposition of CGRP+ terminals with PKCδ+ neurons in STLD and CeL/C. Confocal imaging of triple labeling for PKCδ (cyan), SOM (green) and CGRP (red) in STLD (**b, c**) and CeL/C (**d - f**). **a** Percentages of PKCδ+ somas in putative contact with perisomatic CGRP+ terminals, for STLD (Mean = 84.4%, SEM = 0.031, n = 3) and CeL/C (Mean = 80.6%, SEM = 0.0005, n = 3). **b1 - b4; d1 - d4:** Low power view of STLD (**b1 – b4**) and CeL/C (**d1 - d4)** showing distribution of, PKCδ (**b1, d1),** SOM (**b2, d2**),CGRP (**b3, d3**) immunoreactivities and the three signals merged (**b4, d4**). **c1-c4; e1-e4:** Magnifications at cellular level of the boxed areas in **b4** (STLD) and **d4** (CeL/C) showing signals for PKCδ and SOM (**c1, e1**), CGRP and PKCδ (**c2, e2**), CGRP and SOM (**c3, e3**) and merge (**c4, e4**); the arrows point to PKCδ+ neurons and the arrowheads point to SOM+ neurons (same in **f1 - f4**). Note the absence of overlap between PKCδ+ and SOM+ somas (c.1,e.1), the frequent appositions of CGRP+ baskets around PKCδ+ somas (**c2, e2**) and the absence of such appositions onto SOM+ somas (**c3, e3**)..In **f1 - f4**, a further magnification in STLD leads to the same observations and shows that CGRP+ baskets wrapped around soma and primary dendrites of PKCδ+ somas. Abbreviations, see the list. Scale bars: **b.1-b4**, 100 μm; **c1 - c4**, 25 μm; **d1 - d4**, 200 μm; **e1- e4**, 25 μm; **f1 - f4**, 20 μm.

Fig. 3 Structural apposition of CGRP+ terminals anterogradely labeled from LPB with PKCδ+ neurons in STLD and CeL/C. Following BDA injection in the LPBE (**a, f**), triple labeling for BDA (green), CGRP (red) and PKCδ (cyan) (**b - e**) or for BDA (green), CGRP (red) SOM (cyan) along with DAPI (blue) (**g - j**) was performed on STLD (**b, c, g, h**) and

CeL/C (**d, e, i, j**). The injection (red outlines) were centered in LPBE (**a, f**). Dense cores of BDA labeled fibers were observed in STLD but not STLP (**b1, g1**) where they overlap with the distribution of CGRP+ and PKCδ+ (**b2**) or SOM+ (**g2**) somas and fibers. Similarly, BDA-labeled fibers were densest in CeL/C (**d1, i1**) and partially overlapping with the distribution of CGRP+ and PKCδ+ (**d2**) or SOM+ (i**2**) somas and fibers. In **c1 - c4** and **e1 - e4**, the higher magnifications of the boxed areas in **b2** and **d2**, respectively, show that BDA+ basket-like structures, either in CGRP+ or CGRP-, can be found in close apposition with PKCδ+ somas (arrows) in STLD (**c1 - c4**) and CeL/C (**e1 - e4**). In addition, BDA-/CGRP+ terminals can also contact PKCδ+ somas. In **h1 - h4** and **j1 - j4**, the higher magnifications of the boxed areas in **g2** and **i2**, respectively, show that BDA+ basket-like structures, either CGRP+ or CGRP- are rarely found in close apposition with SOM+ somas in STLD (**h1 - h4**) and CeL/C (**j1 - j4**). Abbreviations: see list. *Scale* bars: **b1 - b2**, 100 μm; **c1 - c4**, 25 μm; **d1 - d2**, 100 μm; **e1 - e4**, 25 μm; **g1 - g2**, 100 μm; **h1 - h4**, 25 μm; **i1 - i2**, 100 μm; **j1 - j4**, 25 μm.

Fig. 4 Projections from caudal BLP and from CGRP+ terminals can target the same PKCδ+ neuron in STLD and CeL/C. After anterograde tracing from the caudal BLP area (**a** – **b**; bregma level -2.45 mm), triple immunofluorescent labeling of BDA (green), CGRP (cyan) and PKCδ (red), together with nuclear counterstaining by DAPI (blue), was performed on STL (**c - d**) and CeA sections (**e - f**). BDA injection were located in lateral region of the caudal BLP, with minor leakage in in the nearby piriform cortex (Pir) and ventromedial part of the lateral nucleus of amygdala (LaVM) (**b1** – **b3**). BDA+ axon were present in almost the STL, and overlapped in STLD with PKCδ+ neurons and CGRP+ terminals. At high magnification, z-projection images (z stack = 5.43 μm) revealed close apposition of BDA+ axonal varicosities (**d1**, **d2**, **d4**; arrow heads) with CGRP-innervated PKCδ+ neurons (**d4**). Similarly, moderate to dense labeling of BDA+ axonal terminals were observed in CeL/C, which also overlaps with CGRP+ axonal field and PKCδ+ neuronal populations. z-projection images (z stack = 9.38 μm) showed close apposition of BDA+ axonal varicosities (**f1**, **f2**, **f4**; arrow heads) with PKCδ+ neurons that were innervated by CGRP+ axonal terminals. Abbreviations: see list. *Scale* bars: **a**, 1000 μm; **b**, 150 μm; **c1** – **c4**, 100 μm; **d1** – **d4**, 10 μm; **e1** – **e4**, 150 μm; **f1** – **f4**, 10 μm.

Fig. 5 Projections from insular cortex and from CGRP+ terminals can target the same PKCδ+ neuron in STLD and CeA. Following anterograde tracing from insular cortical area (**a** – **b**; bregma level -0.23 mm mm), triple immunofluorescent labeling of BDA (green),

CGRP (cyan) and PKCδ (red), together with nuclear counterstaining by DAPI (blue), was performed on STL (**c - d**) and CeA sections (**e - f**). BDA injections were restricted to in layer II/III of InsCx and largely confined to granular (GI) and dysgranular (DI) areas (**a** – **b**; epifluorescent images by NanoZoomer S60). The BDA+ axons spread in all the dorsal STL, including STLD where it overlapped with PKCδ+ neurons and CGRP+ terminals (**c1 - c4**; single confocal plane). With high magnification, z-projection images (z stack = 8.89 μm) revealed close apposition of BDA+ axonal varicosities (**d1**, **d2**, **d4**; arrow heads) with CGRP-innervated PKCδ+ neurons (**d4**). Similarly, BDA+ axonal terminals were also found in CeL/C, which again largely coincides with CGRP+ axonal field and PKCδ+ neuronal populations (**e1 – e4**; z stack = 5.93 μm). Higher magnification revealed close apposition of BDA+ axonal varicosities (arrow heads) with PKCδ+ neurons surrounded by CGRP+ basket-like terminals (**f1**, **f2**, **f4**; z stack = 9.38 μm). Abbreviations: see list. *Scale* bars: **a**, 1000 μm; **b**, 100 μm; **c1** – **c4**, 100 μm; **d1** – **d4**, 15 μm; **e1** – **e4**, 200 μm; **f1** – **f4**, 15 μm.

Fig. 6 Retrograde labeled CeM-projecting neurons in STLD and CeL/C express PKCδ. After injection of the retrograde tracer CTb into rostral CeM (**a - b**, bregma -0.95 mm), triple labeling of SOM (green), PKCδ (cyan) and CTb (red) was performed on STLD (**d - e**) and CeL/C sections (**f - g**). The injection sites (n = 3; **b1 – b2**) were confined to the rostral CeM, with minimal extension into nearby subdivisions. **c** Percentages of CTb+ somas positive for PKCδ and SOM in the STLD (PKCδ 60.8 ± 1.5 %; SOM 19.2 ± 2.6 %; two sample *t*-test, $p < 0.05$) and CeL/C (PKCδ 71.4 ± 1.3 %; SOM 13.9 ± 2.4 %; two sample *t*-test, $p < 0.001$). Confocal imaging in the STLD (**d**) and CeA (**f**) shows that retrogradely labeled CTb+ neurons were frequently PKCδ+ (**e1**, **e2**, **g1**, **g2**; arrowheads), but rarely SOM+ (**e1**, **e3**, **g1**, **g3;** short arrows). Abbreviations: see list. Scale bars: **b1**, 250 μm; **d**, 100 μm; **e1 – e3**, 25 μm; **f**, 100 μm; **g1 - g3**, 25 μm.

Fig. 7 Retrograde labeled STLV-projecting neurons in STLD and CeL/C express PKCδ. After injection of the retrograde tracer CTb into anterior STLV (**a – b**, bregma + 0.13 mm), triple labeling of triple labeling of SOM (green), PKCδ (cyan) and CTb (red) was performed on STLD (**d - e**) and CeL/C sections (**f - g**). The injection sites (n = 3; b1 – b2) were confined to the STLV with minimal extension to its neighbor areas. **c** Percentages of CTb+ somas positive for PKCδ and SOM in the STLD (PKCδ 64.6 ± 4.1 %; SOM 5.1 ± 0.1 %; two sample *t*-test, $p < 0.05$) and CeL/C PKCδ 48.1±0.6 %; SOM 2.7 ± 0.2 %; two sample *t*-test, $p < 0.05$). Confocal imaging in the STLD (**d**) and CeA (**f**) shows that retrogradely labeled CTb+ neurons

were frequently PKCδ+ (**e1**, **e2**, **g1**, **g2**; arrowheads), but rarely SOM+ (**e1**, **e3**, **g1**, **g3;** short arrows). Abbreviations: see list. Scale bars: **b1**, 200 μm; **d**, 100 μm; **e1 – e3**, 25 μm; **f**, 200 μm; **g1 - g3**, 25 μm.

Fig. 8 Retrogradely labeled STLD-projecting neurons or CeL/C-projecting neurons express PKCδ or SOM. Following by CTb injection in STLD (**b – c**, bregma level + 0.13 mm) and red retrobeads in CeL/C (**g**, bregma level – 1.43 mm), triple immunofluorescence labeling was carried out for CTb (red), PKCδ (cyan) and SOM (green), while intrinsic fluorescence from retrobeads was used. In STL, CTb injection site was limited to the PKCδ-expressing STLD (**b - c**). In ipsilateral caudal CeL/C (**c**), confocal image (z stack = 5.78 μm) identified CTb+/PKCδ+ colabeled neurons (arrowheads) and CTb+/SOM+ ones (short arrows) (**e1 – e4**). Pressure injection of red retrobeads resulted in dense deposit in CeL/C (**g1 – g2**). Subsequent colocalization analysis revealed double labeling from SOM+ populations (arrowheads) (**i1 - i3**) and PKCδ+ ones (short arrows) (**j1 – j3**). Abbreviations, see list. Scale bars: **b**, 1000 μm; **c1 - c3**, 100 μm ; **d**, 200 μm ; **e1 – e3**, 25 μm; **g1**, 1000 μm; **g2**, 250 μm**; h**, 100 μm; **i1 – i3**, 20 μm; **j1 – j3**, 20 μm.

Fig. 9 Anterogradely labeled STLD or CeL/C axonal projections can target both PKCδ+ and SOM+ neurons. Following by PHA-L injection in STLD (**b**, bregma level + 0.01 mm) and in CeL/C (**e**, bregma level – 1.55 mm), triple immunofluorescence labeling was carried out for PHA-L (red), PKCδ (cyan) and SOM (green). In STL, restricted PHA-L injection site was confined to the STLD (**b1 – b3**). In caudal level of CeL/C (**c**), confocal imaging (z stack = 11.9 μm) revealed PHA-L+ varicosities apposed to PKCδ+ (arrowheads) and SOM+ neurons (short arrows) (**d1 – d3**). In another case, PHA-L injection into CeL/C (**f1 – f3**) resulted in dense axonal projection in STL, especially in STLD (**g**). With high magnification confocal images (z stack = 10.9 μm), PHA-L+ varicosities formed close apposition with PKCδ+ (arrowheads) and SOM+ (short arrows) (**h1 – h3**). Abbreviations, see list. Scale bars: **b**, 150 μm; **c**, 150 μm ; **d1 – d3**, 15 μm ; **f1 – f3**, 200 μm; **g**, 150 μm; **h1 – h2**, 15 μm.

Fig. 10 LPBE-projecting neurons in STLD and CeL/C express mainly SOM. Triple labeling of FG (red), PKCδ (cyan) and SOM (green) in STLD (**d - e**) and CeA (**f - g**) was performed after FG retrograde tracing from LPBE (**a – b**, bregma level – 5.19 mm). The FG injection sites (n = 3) were centered in LPBE, with diffusion in other LPB subdivisions, but minor labeling in MPB areas (**b1 – b2**). **c** Percentage of FG+ somas positive for PKCδ and

SOM in STLD (PKCδ, 6.1± 0.4 %; SOM, 62.7± 0.4 %; p-value < 0.05) and in CeL/C (PKCδ, 6.9±0.7 %; SOM, 63.9± 0.7 %; p-value < 0.001). **d - g** Confocal images shows rare colabeling of PKCδ (arrowheads) with FG, whereas SOM+ neurons (short arrows) frequently contained FG, in both STLD (**d - e**) and CeL/C (**f – g**). Abbreviations, see list. Scale bars: **b1**, 250 μm; **d**, 100 μm; **e1 - e3**, 25 μm; **f**, 100 μm; **g1 - g3**, 25 μm.

Fig. 11 STLD and CeL/C projections can target CGRP+ neurons in LPBE. Double immunofluorescent labeling for PHA-L (red) and CGRP (green), together with DAPI (white) in LPB, after PHA-L injection in STLD (**a**) or CeL/C (**c**). A dense PHA-L+ axonal labeling was observed in LPB, especially LPBE where it overlapped with the presence of CGRP+ neurons (**b1, b2, d1, d2**). With high magnification confocal images, axonal apposition with CGRP+ soma (arrowheads) were frequently observed for projections from STLD (**b3**; z stack = 9 μm) and CeL/C (**d3;** z stack = 7.9 μm). Abbreviations, see list. Scale bars: **b1 – b2**, 50 μm; **b3**, 15 μm; **d1 – d2**, 50 μm; **d3**, 15 μm.

Fig. 12 PAG/DRN-projecting neurons in STLD and CeL/C express SOM. Triple labeling of CTb (red), PKCδ (cyan), and SOM (green) in STLD (**d, e**) and CeA (**f, g**), after CTb injection into PAG areas (**a-c**). **b** illustrates a CTb injection site. **c** The CTb or FG injection sites were covered lateral (LPAG), ventrolateral PAG (VLPAG) and dorsal raphe (DR). **d - g** Confocal images showed that most of the CTb+ neurons were colabeled by SOM (short arrows) in STLD (**e1, e3**; z-stack = 15.8 μm) and CeL/C (**g1, g3**; z-stack = 5.9 μm), but not PKCδ (arrowheads) in both areas (**e1 – e2**, **g1 – g2**). Abbreviations, see list. Scale bars: **b**, 1000 μm; **d**, 100 μm; **e1 – e3**, 25 μm; **f**, 200 μm; **g1 – g3**, 25 μm.

Fig. 13 A simplified model of parallel, cell-type specific, neuronal circuits in EAc. This model highlight the similar configuration of cell-type specific neuronal circuits in STL and CeA, which are featured by PKCδ+ neurons and SOM+ neurons in STLD and CeL/C. Excitations coming from insular cortex or principle amygdala nuclei, together with CGRP inputs from LPB, can converge onto PKCδ+ neurons in STLD and CeL/C, in a similar fashion. The internal inhibitory circuits are mediated by same type of neurons or different types of neurons in STLD or CeL/C. The internal long-range projections to STLV and CeM is primarily mediated by PKCδ+ neurons, while mutual connection between STLD and CeL/C can be mediated by both types, although the connection from CeL/C to STLD is stronger than

the reverse direction. The external inhibition to LPB and PAG can be mediated by SOM+ neurons in STLD or CeL/C, as well as undefined populations in STLV and CeM.

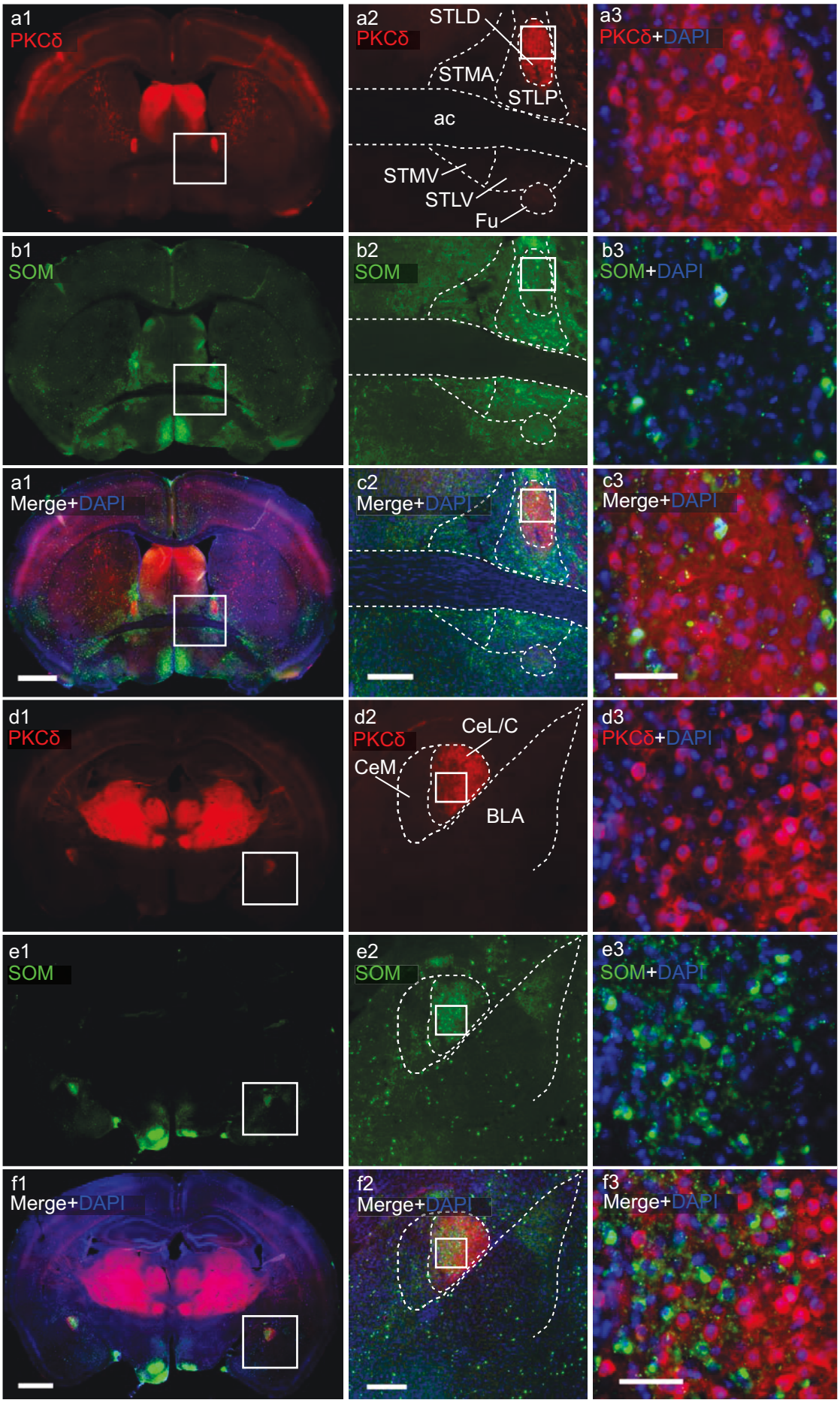
a1
PKCδ
a2
PKCδ
STLD
STMA
STLP
ac
STMV
STLV
Fu
a3
PKCδ+DAPI
b1
SOM
b2
SOM
b3
SOM+DAPI
a1
Merge+DAPI
c2
Merge+DAPI
c3
Merge+DAPI
d1
PKCδ
d2
PKCδ
CeL/C
CeM
BLA
d3
PKCδ+DAPI
e1
SOM
e2
SOM
e3
SOM+DAPI
f1
Merge+DAPI
f2
Merge+DAPI
f3
Merge+DAPI

Fig. 1

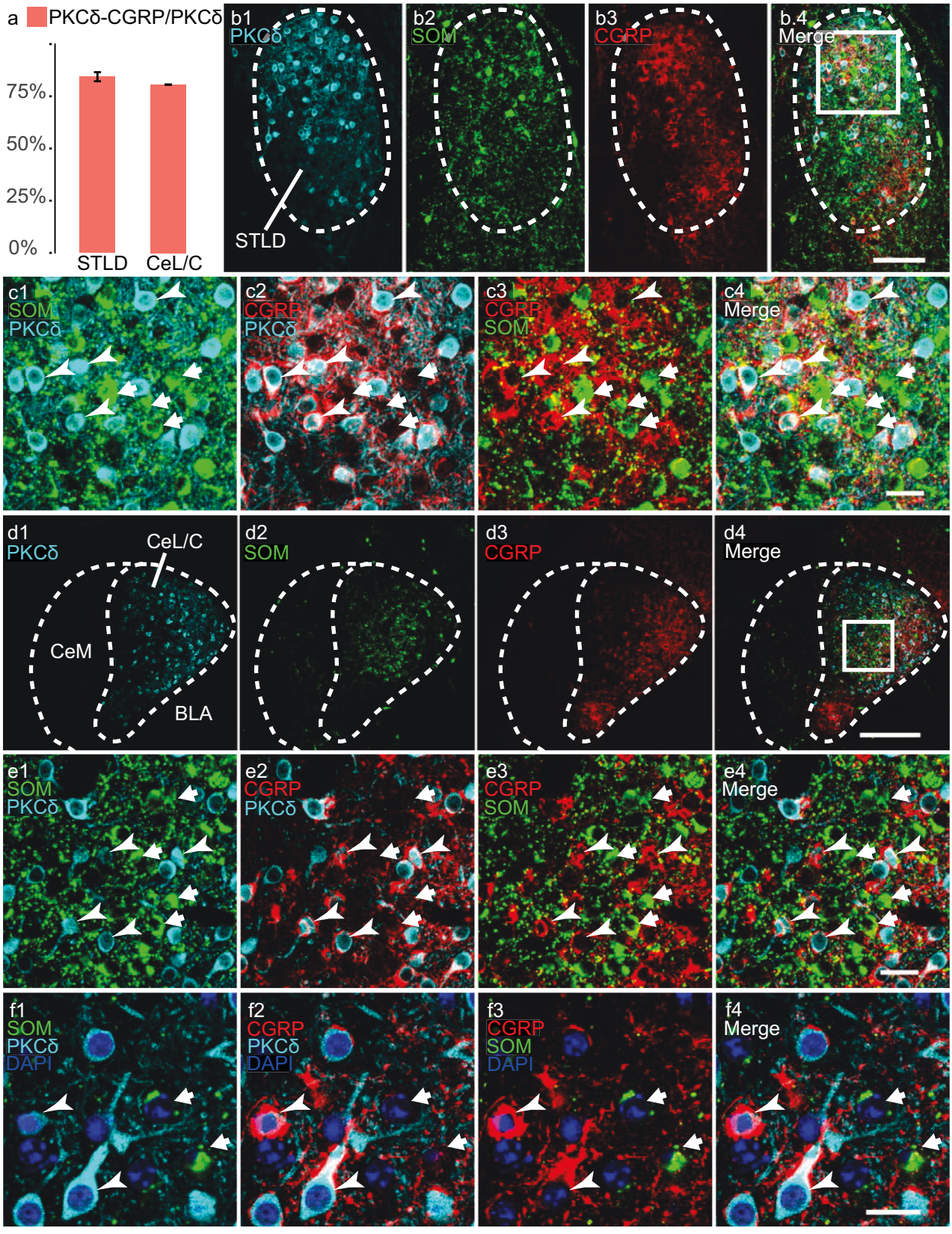
a
PKCδ-CGRP/PKCδ
75%
50%
25%
0%
STLD
CeL/C
b1
PKCδ
STLD
b2
SOM
b3
CGRP
b.4
Merge
c1
SOM
PKCδ
c2
CGRP
PKCδ
c3
CGRP
SOM
c4
Merge
d1
PKCδ
CeL/C
CeM
BLA
d2
SOM
d3
CGRP
d4
Merge
e1
SOM
PKCδ
e2
CGRP
PKCδ
e3
CGRP
SOM
e4
Merge
f1
SOM
PKCδ
DAPI
f2
CGRP
PKCδ
DAPI
f3
CGRP
SOM
DAPI
f4
Merge

Fig. 2

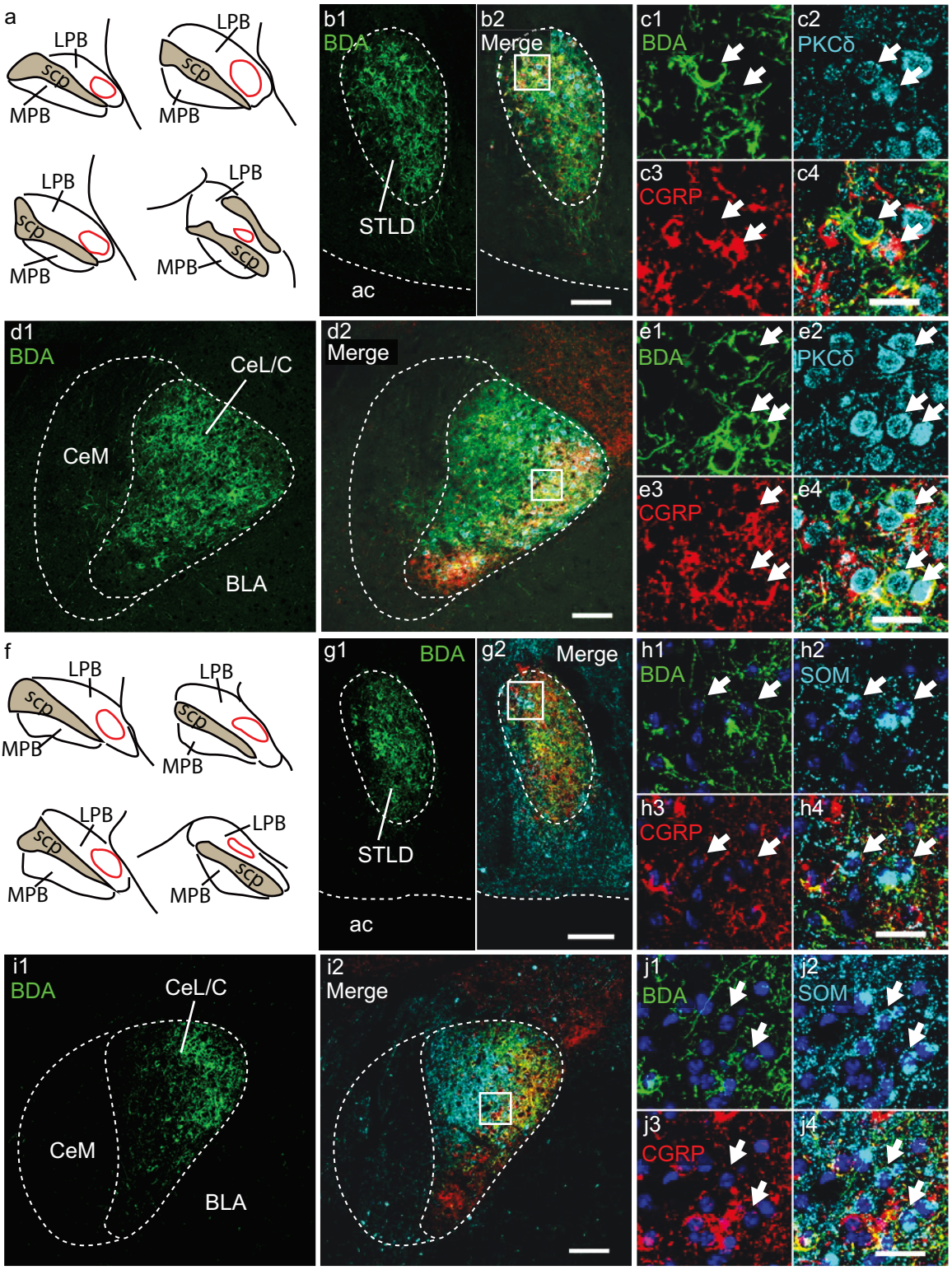
a
LPB
scp
MPB
b1
BDA
STLD
ac
b2
Merge
c1
BDA
c2
PKCδ
c3
CGRP
c4
d1
BDA
CeL/C
CeM
BLA
d2
Merge
e1
BDA
e2
PKCδ
e3
CGRP
e4
f
g1
BDA
STLD
ac
g2
Merge
h1
BDA
h2
SOM
h3
CGRP
h4
i1
BDA
CeL/C
CeM
BLA
i2
Merge
j1
BDA
j2
SOM
j3
CGRP
j4

Fig. 3

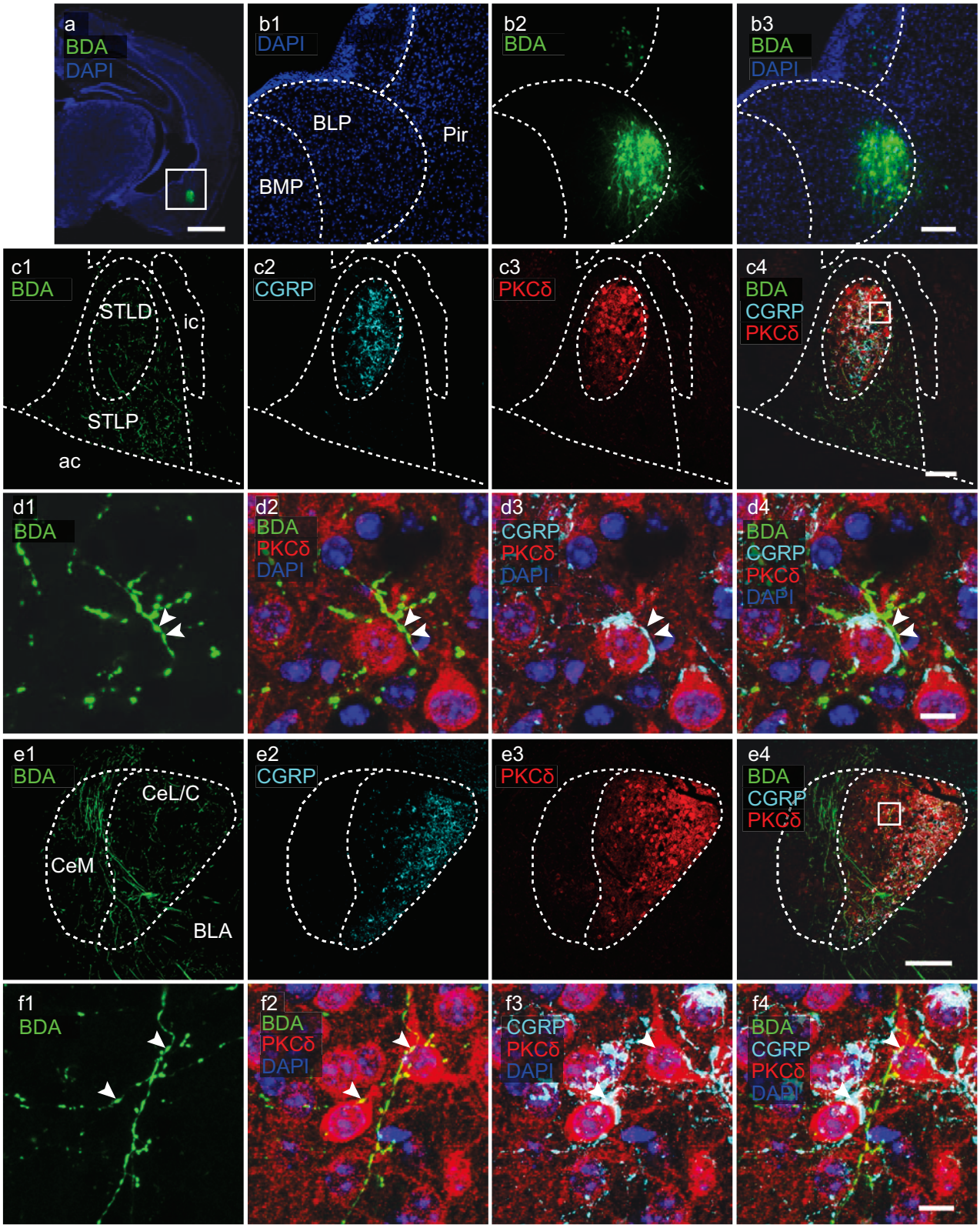
a
BDA
DAPI
b1
DAPI
BLP
Pir
BMP
b2
BDA
b3
BDA
DAPI
c1
BDA
STLD
ic
STLP
ac
c2
CGRP
c3
PKCδ
c4
BDA
CGRP
PKCδ
d1
BDA
d2
BDA
PKCδ
DAPI
d3
CGRP
PKCδ
DAPI
d4
BDA
CGRP
PKCδ
DAPI
e1
BDA
CeL/C
CeM
BLA
e2
CGRP
e3
PKCδ
e4
BDA
CGRP
PKCδ
f1
BDA
f2
BDA
PKCδ
DAPI
f3
CGRP
PKCδ
DAPI
f4
BDA
CGRP
PKCδ
DAPI

Fig. 4

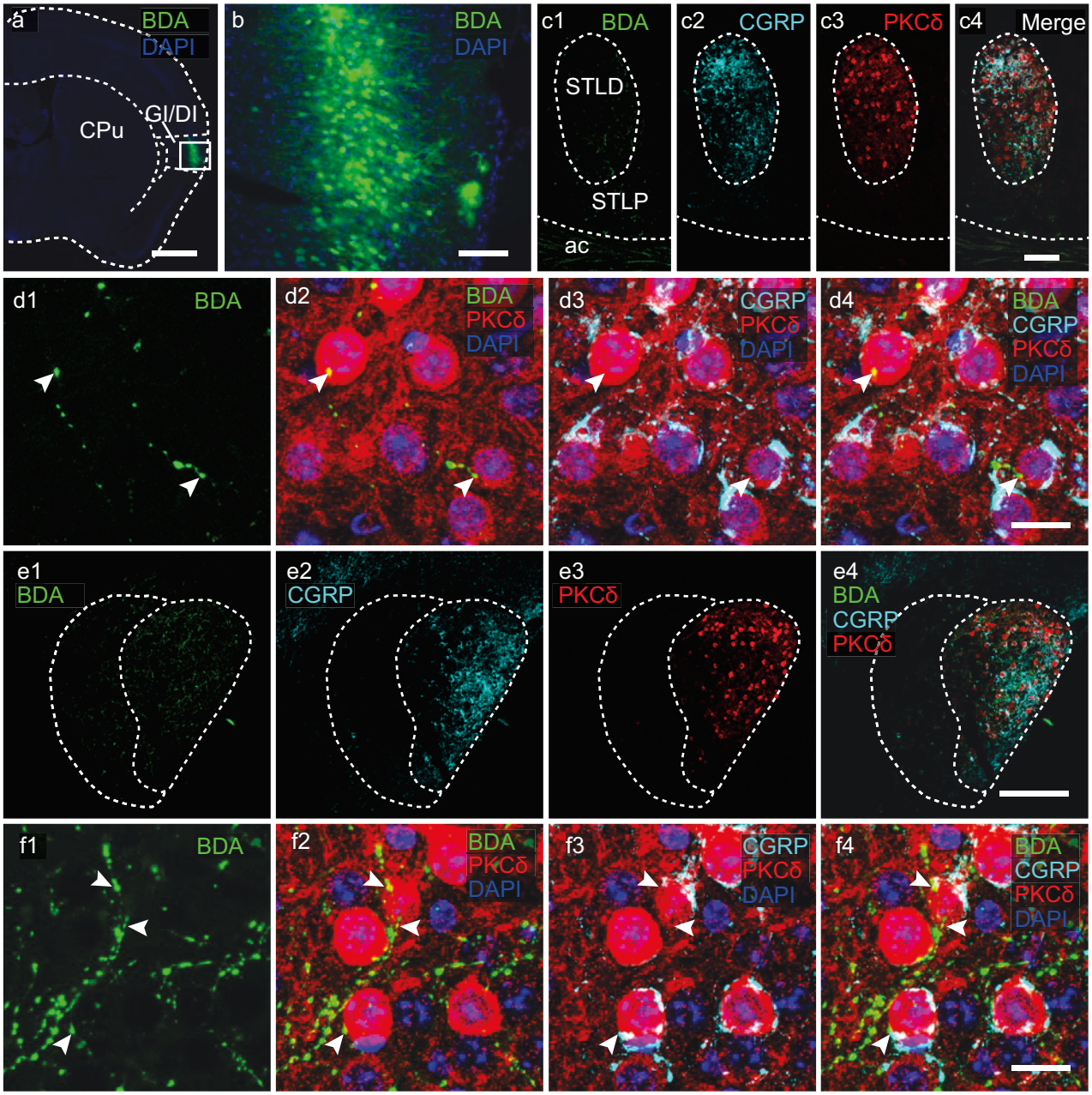
a
BDA
DAPI
CPu
GI/DI
b
BDA
DAPI
c1
BDA
STLD
STLP
ac
c2
CGRP
c3
PKCδ
c4
Merge
d1
BDA
d2
BDA
PKCδ
DAPI
d3
CGRP
PKCδ
DAPI
d4
BDA
CGRP
PKCδ
DAPI
e1
BDA
e2
CGRP
e3
PKCδ
e4
BDA
CGRP
PKCδ
f1
BDA
f2
BDA
PKCδ
DAPI
f3
CGRP
PKCδ
DAPI
f4
BDA
CGRP
PKCδ
DAPI

Fig. 5

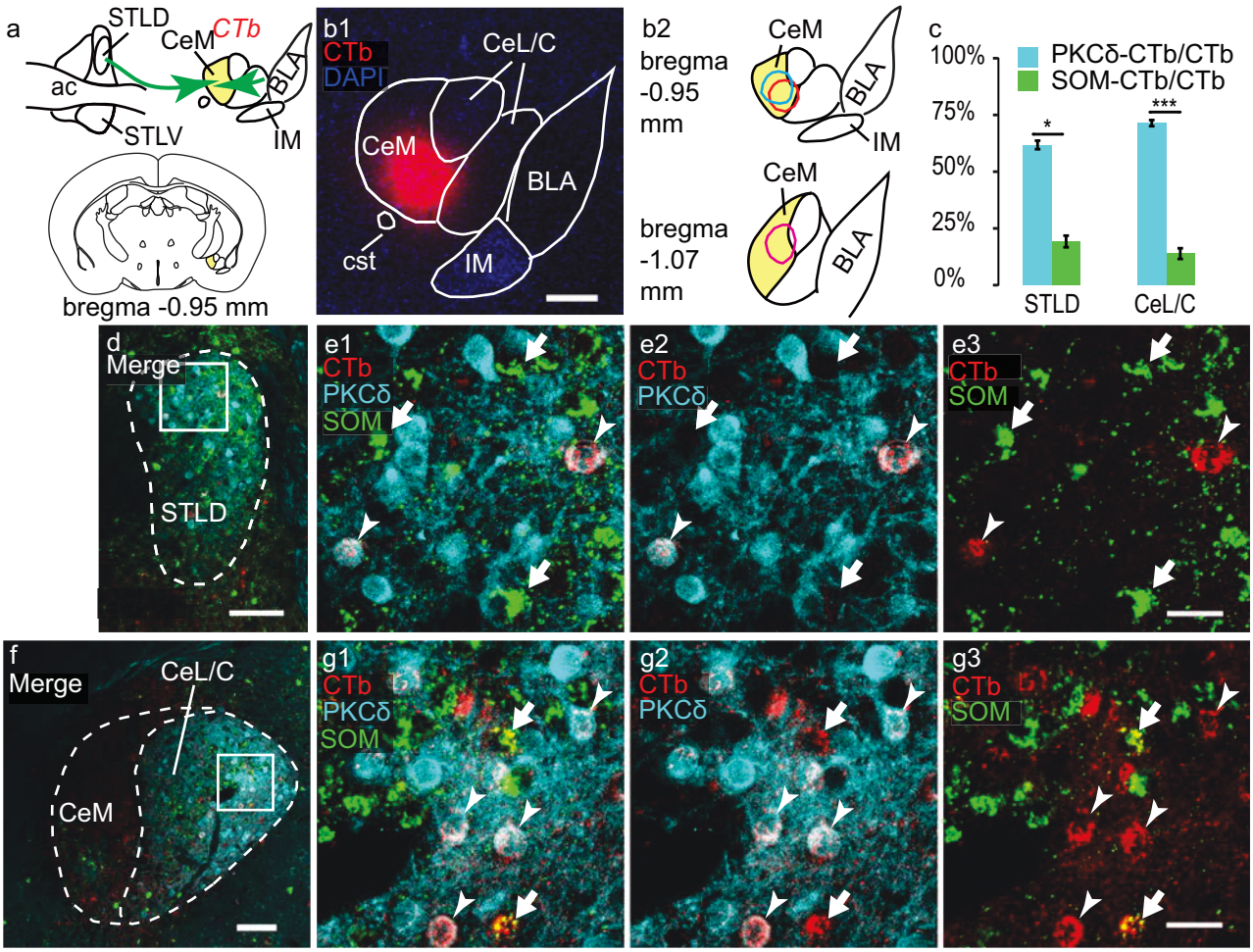
a
STLD
CeM
CTb
ac
BLA
STLV
IM
bregma -0.95 mm
b1
CTb
DAPI
CeL/C
CeM
BLA
cst
IM
b2
bregma
-0.95
mm
CeM
BLA
IM
bregma
-1.07
mm
CeM
BLA
c
100%
75%
50%
0%
PKCδ-CTb/CTb
SOM-CTb/CTb
*
***
STLD
CeL/C
d
Merge
STLD
e1
CTb
PKCδ
SOM
e2
CTb
PKCδ
e3
CTb
SOM
f
Merge
CeL/C
CeM
g1
CTb
PKCδ
SOM
g2
CTb
PKCδ
g3
CTb
SOM

Fig. 6

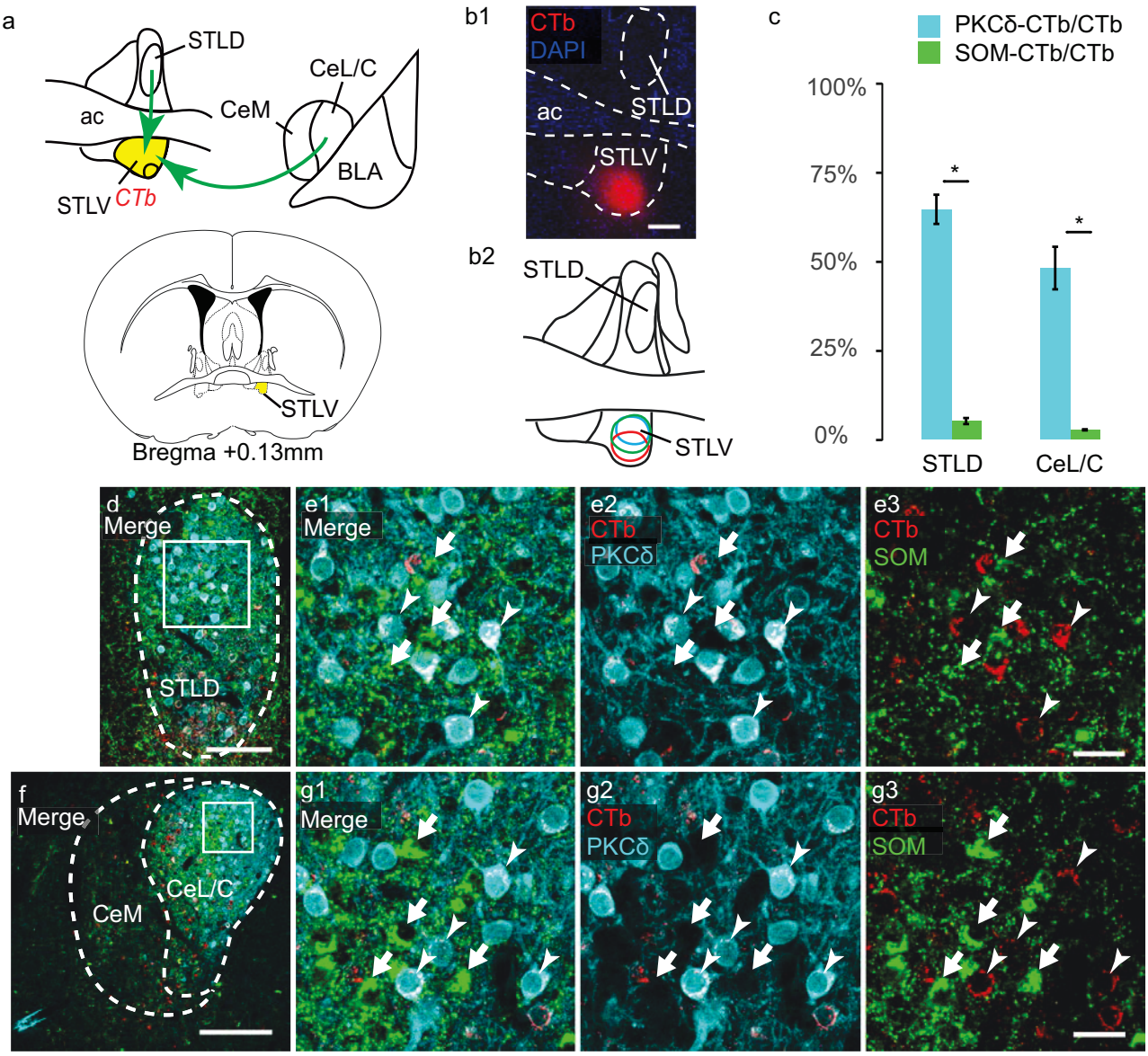
a
STLD
CeL/C
ac
CeM
BLA
STLV
CTb
Bregma +0.13mm
b1
CTb
DAPI
ac
STLD
STLV
b2
STLD
STLV
c
PKCδ-CTb/CTb
SOM-CTb/CTb
100%
75%
50%
25%
0%
*
*
STLD
CeL/C
d
Merge
STLD
e1
Merge
e2
CTb
PKCδ
e3
CTb
SOM
f
Merge
CeL/C
CeM
g1
Merge
g2
CTb
PKCδ
g3
CTb
SOM

Fig. 7

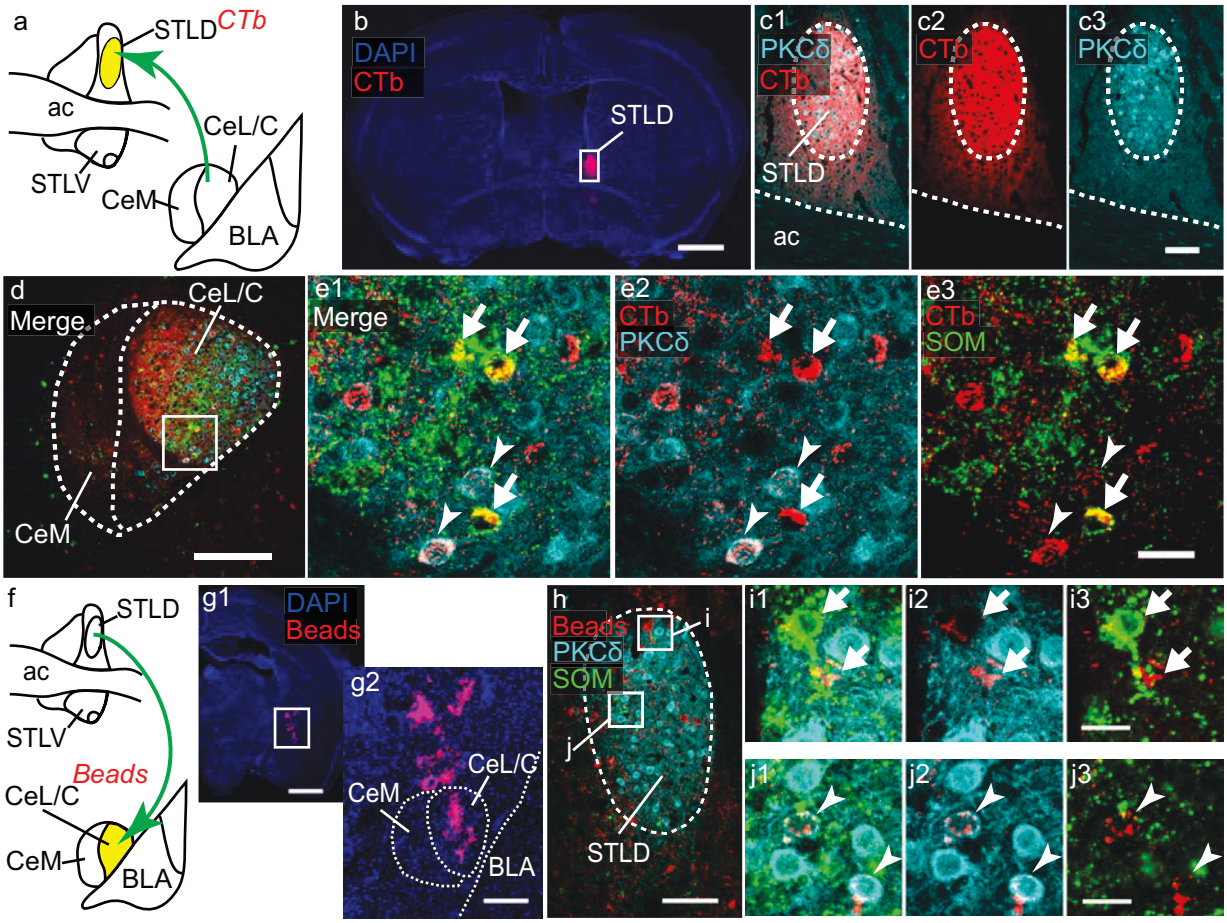
a
STLD
CTb
ac
CeL/C
STLV
CeM
BLA
b
DAPI
CTb
STLD
c1
PKCδ
CTb
STLD
ac
c2
CTb
c3
PKCδ
d
Merge
CeL/C
CeM
e1
Merge
e2
CTb
PKCδ
e3
CTb
SOM
f
STLD
ac
STLV
Beads
CeL/C
CeM
BLA
g1
DAPI
Beads
g2
CeL/C
CeM
BLA
h
Beads
PKCδ
SOM
i
j
STLD
i1
i2
i3
j1
j2
j3

Fig. 8

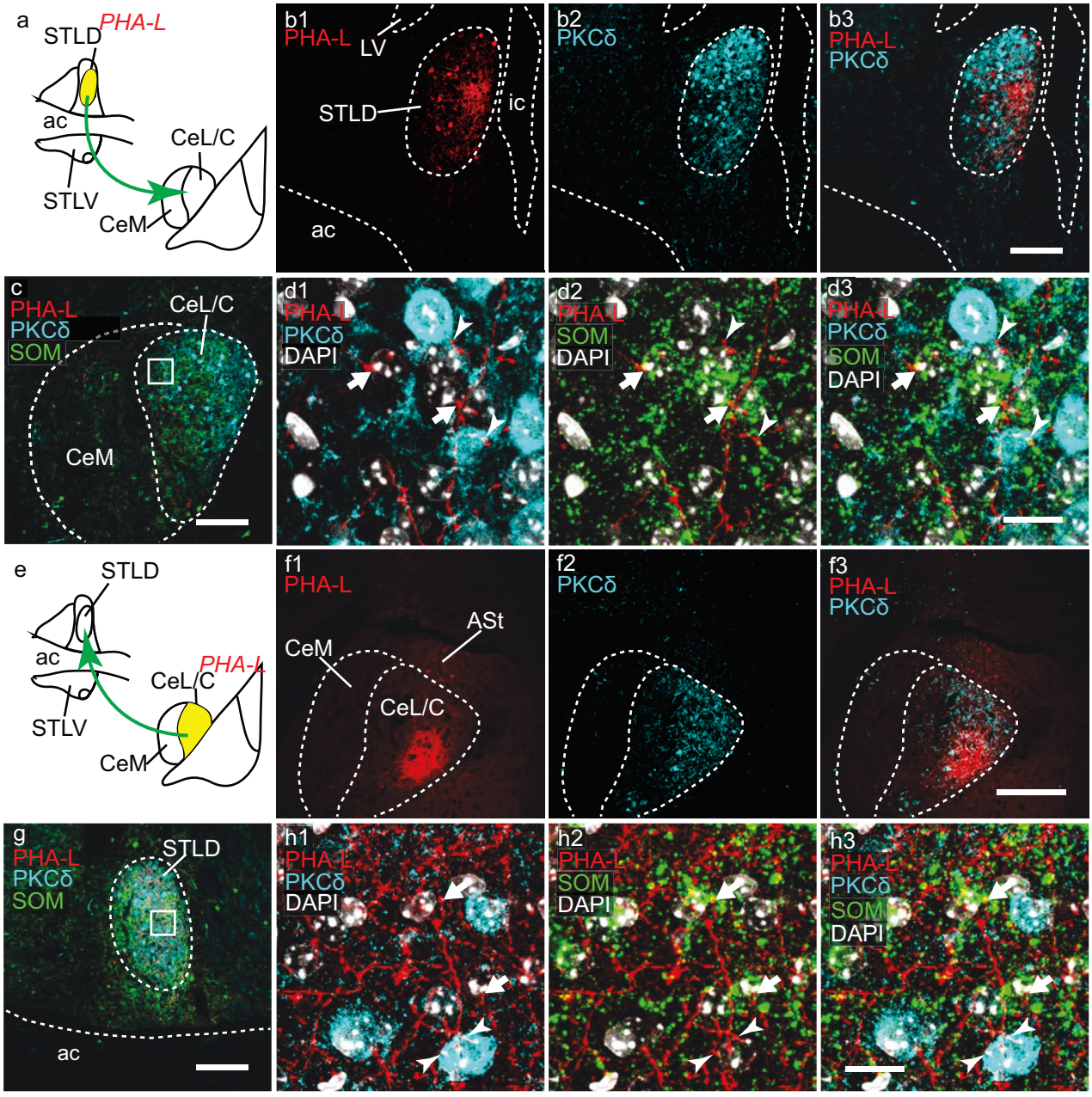
a
STLD
PHA-L
ac
CeL/C
STLV
CeM
b1
PHA-L
LV
STLD
ic
ac
b2
PKCδ
b3
PHA-L
PKCδ
c
PHA-L
PKCδ
SOM
CeL/C
CeM
d1
PHA-L
PKCδ
DAPI
d2
PHA-L
SOM
DAPI
d3
PHA-L
PKCδ
SOM
DAPI
e
STLD
ac
PHA-L
CeL/C
STLV
CeM
f1
PHA-L
ASt
CeM
CeL/C
f2
PKCδ
f3
PHA-L
PKCδ
g
PHA-L
PKCδ
SOM
STLD
ac
h1
PHA-L
PKCδ
DAPI
h2
PHA-L
SOM
DAPI
h3
PHA-L
PKCδ
SOM
DAPI

Fig. 9

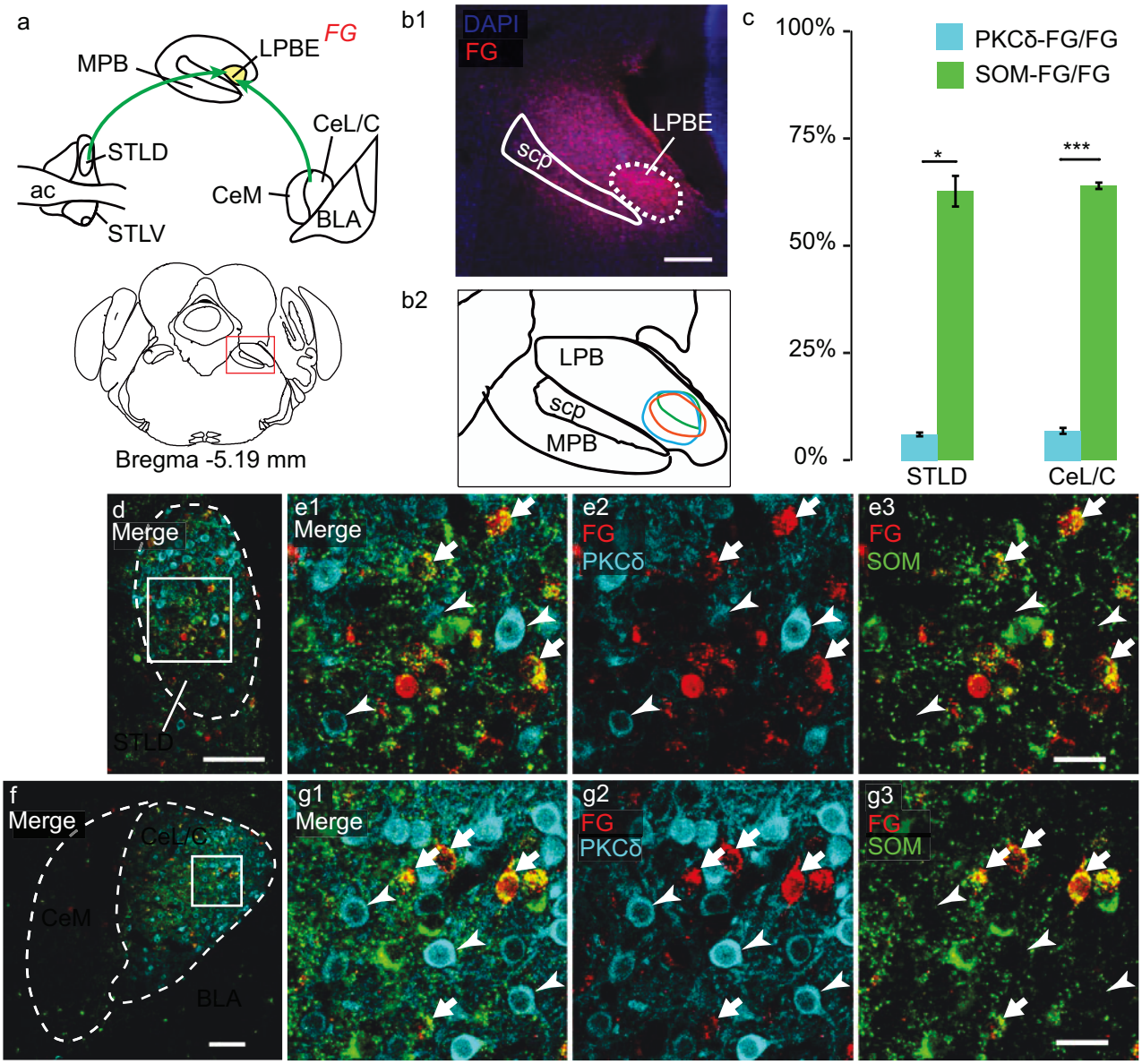
a
MPB
LPBE
FG
CeL/C
STLD
ac
CeM
STLV
BLA
Bregma -5.19 mm
b1
DAPI
FG
LPBE
scp
b2
LPB
scp
MPB
c
100%
75%
50%
25%
0%
PKCδ-FG/FG
SOM-FG/FG
*
***
STLD
CeL/C
d
Merge
STLD
e1
Merge
e2
FG
PKCδ
e3
FG
SOM
f
Merge
CeL/C
CeM
BLA
g1
Merge
g2
FG
PKCδ
g3
FG
SOM

Fig. 10

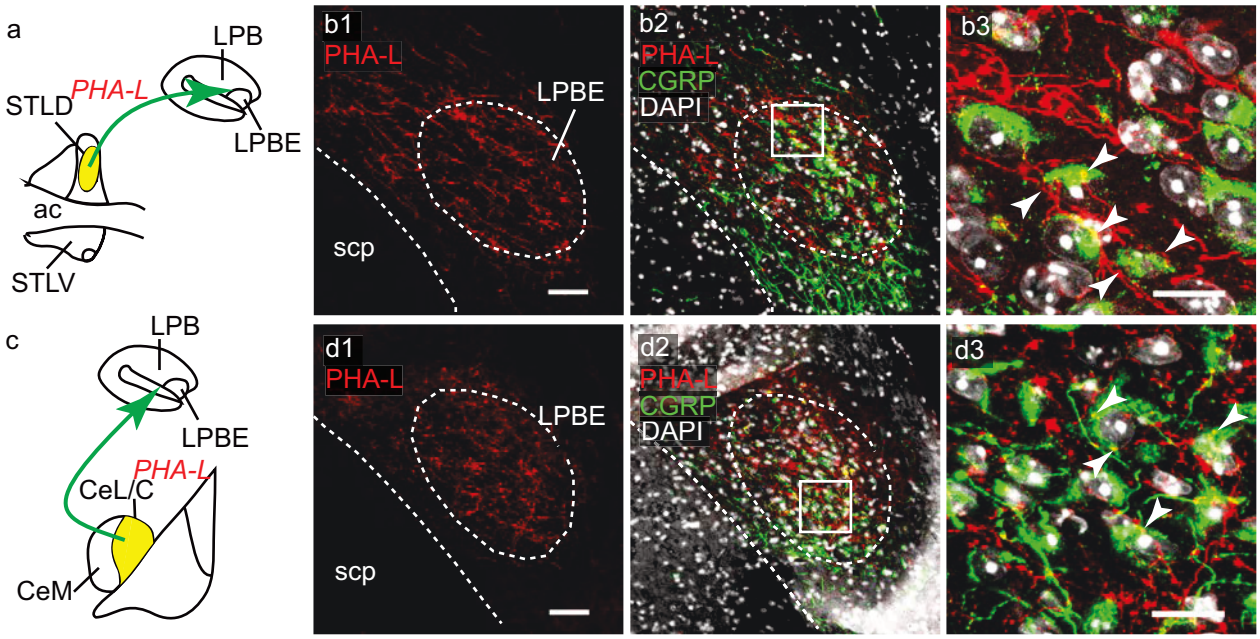
a
LPB
PHA-L
STLD
LPBE
ac
STLV
b1
PHA-L
LPBE
scp
b2
PHA-L
CGRP
DAPI
b3
c
LPB
LPBE
PHA-L
CeL/C
CeM
d1
PHA-L
LPBE
scp
d2
PHA-L
CGRP
DAPI
d3

Fig. 11

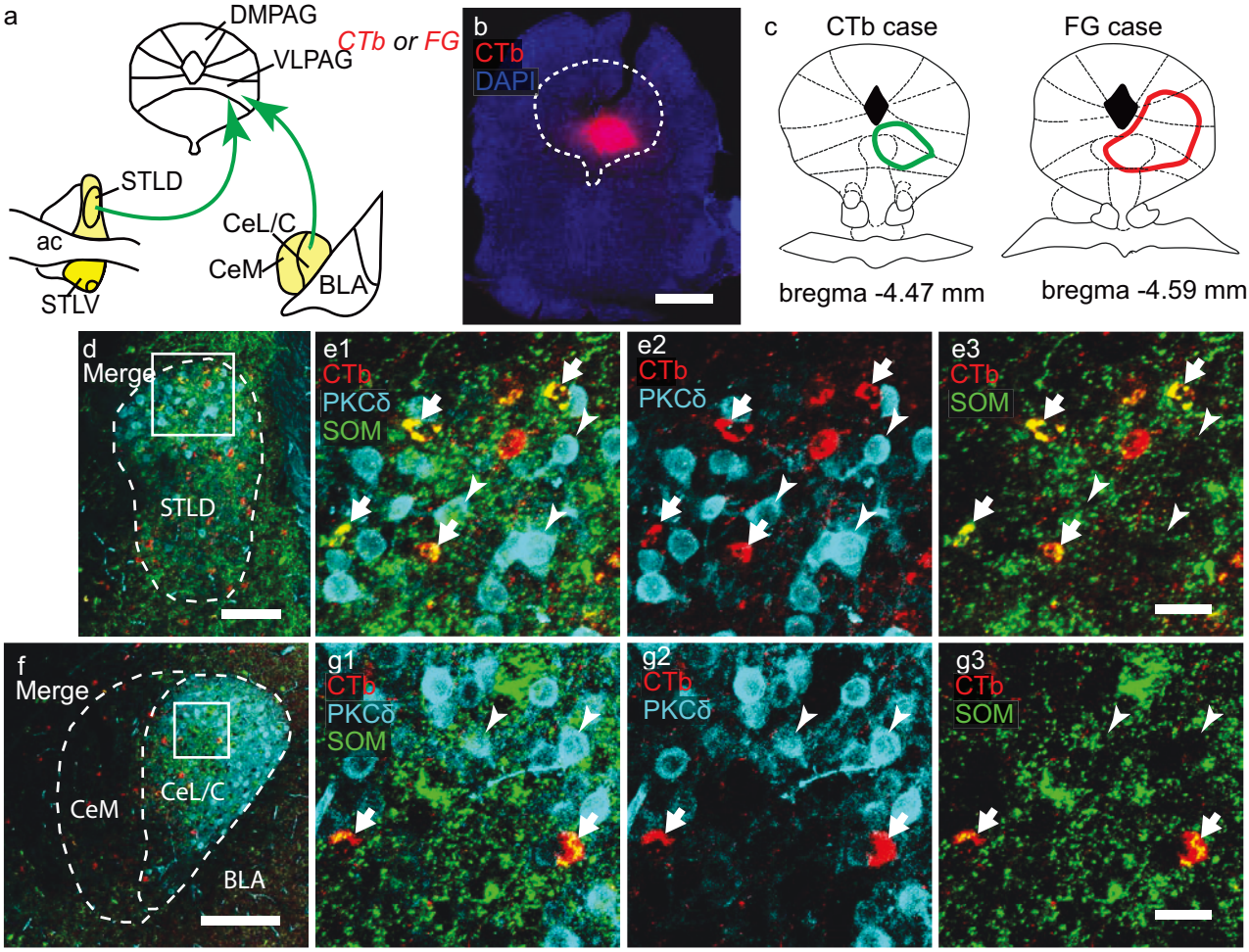
a
DMPAG
VLPAG
CTb or FG
STLD
ac
STLV
CeL/C
CeM
BLA
b
CTb
DAPI
c
CTb case
FG case
bregma -4.47 mm
bregma -4.59 mm
d
Merge
STLD
e1
CTb
PKCδ
SOM
e2
CTb
PKCδ
e3
CTb
SOM
f
Merge
CeM
CeL/C
BLA
g1
CTb
PKCδ
SOM
g2
CTb
PKCδ
g3
CTb
SOM

Fig. 12

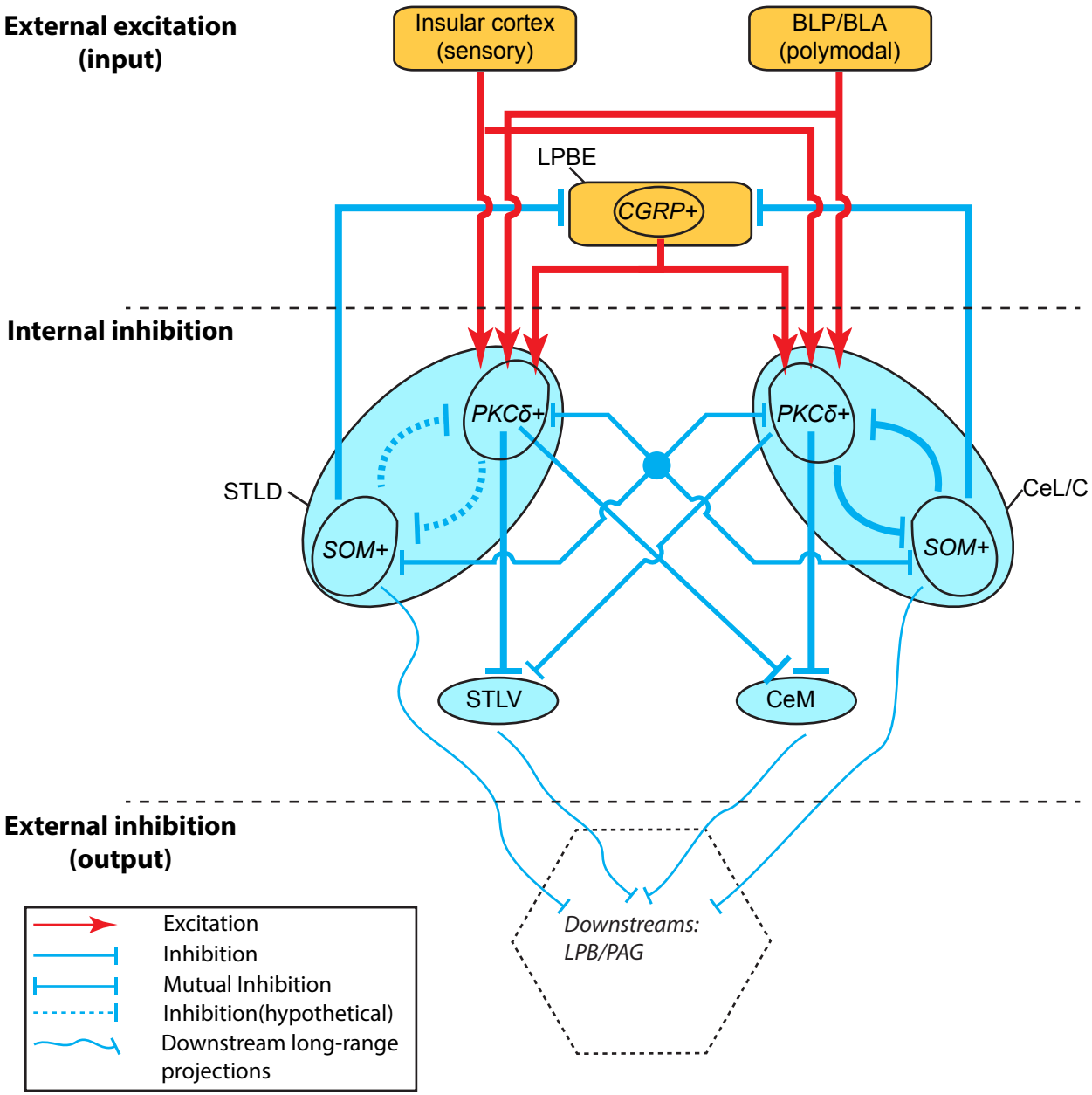
External excitation
(input)
Insular cortex
(sensory)
BLP/BLA
(polymodal)
LPBE
CGRP+
Internal inhibition
PKCδ+
PKCδ+
STLD
CeL/C
SOM+
SOM+
STLV
CeM
External inhibition
(output)
Downstreams:
LPB/PAG
Excitation
Inhibition
Mutual Inhibition
Inhibition(hypothetical)
Downstream long-range
projections

Fig. 13

4. Functional implications of PKCδ-expressing neurons in tonic pain

In this part, we will look at a possible functional involvement of PKCδ-expressing neurons in pain.

This part is merely primitive, therefore we will briefly present our main observations with different parts for a concise summary, background, experiment design, main results and discussion.

SUMMARY

The central nucleus of amygdala (CeA) has long been known to be involved in nociceptive transmission and modulation and pain-induced affective behavior (Neugebauer et al. 2004; Veinante et al. 2013; Neugebauer 2015). Nociceptive input activates neurons in the lateral/capsular part of CeA (CeL/C) (Carrasquillo and Gereau 2007) and prolonged pain can be associated to potentiation of the excitatory transmissions to CeL/C, especially that from lateral parabrachial nucleus (LPB) (Ren and Neugebauer 2010; Cheng et al. 2011). On the other hand, the lateral bed nucleus of stria terminalis (STL) has also been implicated in affective pain responses (Hagiwara et al. 2009; Hagiwara et al. 2013; Ide et al. 2013; Minami and Ide 2015).

However, it is not clear whether there are similar neuronal populations in CeL/C ad STL that involved in pain. In the CeL/C, the increased phosphorylation of extracellular signal-regulated kinase (pERK) has been associated to mechanical hyperalgesia during inflammatory pain, but the neurochemical identity of these neurons have not been determined. In our analysis of EAc circuits, we noticed that the CeL/C contains a high density of neurons expressing protein kinase C delta (PKCδ), and that a similar neuronal population is distributed in the dorsal STL (STLD). Therefore, considering the fact that PKCδ-positive (PKCδ+) neuronal population in ed to draw some clues regarding to whether there are parallel functionsome of the pERK-positive neurons recruited during pain might be PKCδ+.With our preliminary effort, we found that STLD and CeL/C similarly activated in tonic formalin pain model, and that many of these neurons expressed PKCδ. This indicates a possible functional role of EAc PKCδ-expressing neurons in pain behavior and possibly pain-induced emotional disorders.

ABBREVIATIONS

CeA: central nucleus of amygdala
CeL/C: lateral/capsular part of CeA (CeL/C
EAc: central extended amygdala
LPB: lateral parabrachial nucleus (LPB)
pERK : phosphorylated extracellular signal-regulated kinase
PKCδ: protein kinase C delta
STL: lateral bed nucleus of stria terminalis
STLD: lateral bed nucleus of stria terminalis, dorsal part

BACKGROUND

The STL and CeA have been implicated in both sensory-discriminative and affective aspects of pain (Neugebauer et al. 2004; Carrasquillo and Gereau 2007; Veinante et al. 2013; Hagiwara et al. 2009; Minami and Ide 2015). On one hand, pain activates EAc neurons, for example, by inducing pERK (phosphorylation of extracellular signal-regulated kinase) and neuronal plasticity related immediate-early genes like c-fos (Nakagawa et al. 2003; Carrasquillo and Gereau 2007; Cheng et al. 2011; Morland et al. 2016) and enhancing excitatory transmission (Ren and Neugebauer 2010; Cheng et al. 2011; Ji et al. 2017; Kaneko et al. 2016). On the other hand, functional manipulation of EAc nuclei can actively regulate pain-induced nociceptive behavior and/or affective behavior (Hagiwara et al. 2009; Ide et al. 2013; Minami and Ide 2015; Neugebauer et al. 2004; Veinante et al. 2013; Neugebauer 2015). The lateral bed nucleus of stria terminalis (STL) has also been implicated in pain behavior (Hagiwara et al. 2009; Hagiwara et al. 2013) and especially in pain-induced aversion (Deyama et al. 2008; Deyama et al. 2009; Minami and Ide 2015). The roles of EAc in pain behavior, however, have been relatively better studied in CeA than STL.

In CeA, robust induction of pERK in the capsular part of CeA (CeC) was observed in a formalin-induced pain model, and has been causally associated to the resulting mechanical hyperalgesia (Carrasquillo and Gereau 2007). The lateral/capsular part of CeA (CeL/C) has been characterized as the "nociceptive amygdala" due to its enrichment of nociceptive-responsive neurons (Neugebauer et al. 2004). CeL/C can integrate nociceptive information from multiple pathways, the more direct being the spino-parabrachio-amygdaloid pain pathway (Bernard and Besson 1990; Gauriau and Bernard 2002; Neugebauer et al. 2004). Interestingly, the functional role of STLD, which receives intense external LPB projection (Bourgeais et al. 2001), was not quite directly studied in pain models. In fact, like CeA, STLD can be similarly activated by systematic morphine treatment (Sarhan et al. 2013).

Here, we tried to draw some clues regarding to whether there are parallel functional elements in STLD that are involved in formalin pain model as that of CeA. We use the induction of pERK as a neuronal activity marker for EAc nuclei. Further, since there is a remarkable overlap between the pERK expression and protein kinase C delta (PKCδ) positive neurons in CeL/C (Carrasquillo and Gereau 2007; Haubensak et al. 2010; Amano et al. 2012), we hypothesize there some of these activated neurons might express PKCδ.

EXPERIMENT DESIGN

Formalin pain model

Male C57BL6J mice (8-9 weeks old, n = 33) was used for formalin pain model. The habituation of handling procedures started 4 weeks after the arrival of animal, followed by habituation of control procedures of formalin injection (without intraplantar injection).
On the day of formalin injection, the animal was allowed for 30 min for accommodation of environment in the test room. After that, mice were briefly anesthetized with isoflurane (4 %), and an intraplantar injection of 20 µl of vehicle (neutral PBS) or formalin (5 %, prepared in neutral PBS; Cat. #: 15714-S, Electron Microscopy Sciences™) was made into the left hind paw. Animals was placed back in their home cage immediately after injection. Spontaneous pain behavior (i.e. paw-licking) was observed without scoring, in the first hour after formalin injection.

pERK and PKCδ immunostaining

Animals were euthanized at 1.5 hrs after formalin injection and paraformaldehyde transcardiac perfusion was performed. Immunostaining of pERK and PKCδ were carried out with DAB immunohistochemistry or double immunofluorescent staining. A rabbit polyclonal anti-phospho-p44/42 MAPK (Erk1/2) antibody (1:10000 for IHC DAB, 1: 1000 for IHF; Cat: #4370, Cell Signaling Technology™), and a mouse monoclonal anti-PKCδ primary antibody (1: 1000 for IHF; Cat. #: 610398, BD Biosciences™) were used with biotin or fluorophore conjugated secondary antibodies.

Imaging

Brightfield images were taken with Neurolucida 10.0 software (MBF Bioscience ™) on a Nikon Eclipse 80i microscope equipped with a MBF CX9000 digital camera (MBF Bioscience ™). Epifluorescent images (20x objective) were acquired in the Axio Imager 2 system (Carl Zeiss™) equipped with optical filters for DAPI, FITC, Cy3 and Cy5.

RESULTS

As this experiment was performed on a small cohort of animals, no quantification has been done and only qualitative results are presented.
We sacrificed the animals 90 min after the intraplantar formalin injection into the left hind paw. With DAB immunohistochemistry, we found increased induction of pERK neurons in STLD (Fig. a - c) and CeL/C (Fig. d - f) after formalin injection, compared to vehicle or naïve control.

We further performed double labeling of pERK and PKCδ in formalin-treated animal. In both STLD and CeL/C, many of the pERK-expressing neuron were PKCδ positive (PKCδ+) (arrow heads) (Fig. 1 g - h).

DISCUSSION

In this pilot effort, we found similar activations of STLD and CeL/C in formalin-pain model, especially by PKCδ+ neurons. Due to several unsolved problems in establishing reliable formalin pain behavior test in our animal facilities, we did not get enough data to reach a statistically conclusion. However, it seems that an elevated neuronal activity of PKCδ+ populations in pain fit well with their known functional role in fear, anxiety and threat responses (Ciocchi et al. 2010; Haubensak et al. 2010; Cai et al. 2014; Han et al. 2015; De Bundel et al. 2016).

REFERENCE

Amano T, Amir A, Goswami S, Pare D (2012) Morphology, PKCdelta expression, and synaptic responsiveness of different types of rat central lateral amygdala neurons. J Neurophysiol 108 (12):3196-3205. doi:10.1152/jn.00514.2012

Bernard JF, Besson JM (1990) The spino(trigemino)pontoamygdaloid pathway: electrophysiological evidence for an involvement in pain processes. J Neurophysiol 63 (3):473-490

Bourgeais L, Gauriau C, Bernard JF (2001) Projections from the nociceptive area of the central nucleus of the amygdala to the forebrain: a PHA-L study in the rat. Eur J Neurosci 14 (2):229-255. doi:ejn1640 [pii]

Cai H, Haubensak W, Anthony TE, Anderson DJ (2014) Central amygdala PKC-delta(+) neurons mediate the influence of multiple anorexigenic signals. Nat Neurosci 17 (9):1240-1248. doi:10.1038/nn.3767

Carrasquillo Y, Gereau RWt (2007) Activation of the extracellular signal-regulated kinase in the amygdala modulates pain perception. J Neurosci 27 (7):1543-1551. doi:10.1523/JNEUROSCI.3536-06.2007

Cheng SJ, Chen CC, Yang HW, Chang YT, Bai SW, Yen CT, Min MY (2011) Role of extracellular signal-regulated kinase in synaptic transmission and plasticity of a nociceptive input on capsular central amygdaloid neurons in normal and acid-induced muscle pain mice. J Neurosci 31 (6):2258-2270. doi:10.1523/JNEUROSCI.5564-10.2011

Ciocchi S, Herry C, Grenier F, Wolff SB, Letzkus JJ, Vlachos I, Ehrlich I, Sprengel R, Deisseroth K, Stadler MB, Muller C, Luthi A (2010) Encoding of conditioned fear in central amygdala inhibitory circuits. Nature 468 (7321):277-282. doi:10.1038/nature09559

De Bundel D, Zussy C, Espallergues J, Gerfen CR, Girault JA, Valjent E (2016) Dopamine D2 receptors gate generalization of conditioned threat responses through mTORC1 signaling in the extended amygdala. Mol Psychiatry 21 (11):1545-1553. doi:10.1038/mp.2015.210

Deyama S, Katayama T, Kondoh N, Nakagawa T, Kaneko S, Yamaguchi T, Yoshioka M, Minami M (2009) Role of enhanced noradrenergic transmission within the ventral bed nucleus of the stria terminalis in visceral pain-induced aversion in rats. Behav Brain Res 197 (2):279-283. doi:S0166-4328(08)00473-7 [pii]

10.1016/j.bbr.2008.08.024

Deyama S, Katayama T, Ohno A, Nakagawa T, Kaneko S, Yamaguchi T, Yoshioka M, Minami M (2008) Activation of the beta-adrenoceptor-protein kinase A signaling pathway within the ventral bed nucleus of the stria terminalis mediates the negative affective component of pain in rats. J Neurosci 28 (31):7728-7736. doi:10.1523/JNEUROSCI.1480-08.2008

Gauriau C, Bernard JF (2002) Pain pathways and parabrachial circuits in the rat. Exp Physiol 87 (2):251-258. doi:EPH_2357 [pii]

Hagiwara H, Funabashi T, Akema T, Kimura F (2013) Sex-specific differences in pain response by dopamine in the bed nucleus of the stria terminalis in rats. Neuroreport 24 (4):181-185. doi:10.1097/WNR.0b013e32835d8540

Hagiwara H, Ishida M, Arita J, Mitsushima D, Takahashi T, Kimura F, Funabashi T (2009) The cAMP response element-binding protein in the bed nucleus of the stria terminalis modulates the formalin-induced pain behavior in the female rat. European Journal of Neuroscience 30:2379-2386. doi:10.1111/j.1460-9568.2009.07002.x

Han S, Soleiman MT, Soden ME, Zweifel LS, Palmiter RD (2015) Elucidating an Affective Pain Circuit that Creates a Threat Memory. Cell 162 (2):363-374. doi:10.1016/j.cell.2015.05.057

Haubensak W, Kunwar PS, Cai H, Ciocchi S, Wall NR, Ponnusamy R, Biag J, Dong HW, Deisseroth K, Callaway EM, Fanselow MS, Luthi A, Anderson DJ (2010) Genetic dissection of an amygdala microcircuit that gates conditioned fear. Nature 468 (7321):270-276. doi:10.1038/nature09553

Ide S, Hara T, Ohno A, Tamano R, Koseki K, Naka T, Maruyama C, Kaneda K, Yoshioka M, Minami M (2013) Opposing roles of corticotropin-releasing factor and neuropeptide Y within the dorsolateral bed nucleus of the stria terminalis in the negative affective component of pain in rats. J Neurosci 33 (14):5881-5894. doi:10.1523/JNEUROSCI.4278-12.2013

Ji G, Zhang W, Mahimainathan L, Narasimhan M, Kiritoshi T, Fan X, Wang J, Green TA, Neugebauer V (2017) 5-HT2C Receptor Knockdown in the Amygdala Inhibits Neuropathic-Pain-Related Plasticity and Behaviors. J Neurosci 37 (6):1378-1393. doi:10.1523/JNEUROSCI.2468-16.2016

Kaneko T, Kaneda K, Ohno A, Takahashi D, Hara T, Amano T, Ide S, Yoshioka M, Minami M (2016) Activation of adenylate cyclase-cyclic AMP-protein kinase A signaling by corticotropin-releasing factor within the dorsolateral bed nucleus of the stria terminalis is involved in pain-induced aversion. Eur J Neurosci 44 (11):2914-2924. doi:10.1111/ejn.13419

Minami M, Ide S (2015) How does pain induce negative emotion? Role of the bed nucleus of the stria terminalis in pain-induced place aversion. Curr Mol Med 15 (2):184-190

Morland Rh, Novejarque A, Spicer C, Pheby T, Rice Asc (2016) Enhanced c-Fos expression in the central amygdala correlates with increased thigmotaxis in rats with peripheral nerve injury. European Journal of Pain:n/a-n/a. doi:10.1002/ejp.839

Nakagawa T, Katsuya A, Tanimoto S, Yamamoto J, Yamauchi Y, Minami M, Satoh M (2003) Differential patterns of c-fos mRNA expression in the amygdaloid nuclei induced by chemical somatic and visceral noxious stimuli in rats. Neurosci Lett 344 (3):197-200. doi:S0304394003004658 [pii]

Neugebauer V (2015) Amygdala pain mechanisms. Handb Exp Pharmacol 227:261-284. doi:10.1007/978-3-662-46450-2_13

Neugebauer V, Li W, Bird GC, Han JS (2004) The amygdala and persistent pain. Neuroscientist 10 (3):221-234. doi:10.1177/1073858403261077

Ren W, Neugebauer V (2010) Pain-related increase of excitatory transmission and decrease of inhibitory transmission in the central nucleus of the amygdala are mediated by mGluR1. Mol Pain 6:93. doi:10.1186/1744-8069-6-93

Sarhan M, Pawlowski SA, Barthas F, Yalcin I, Kaufling J, Dardente H, Zachariou V, Dileone RJ, Barrot M, Veinante P (2013) BDNF parabrachio-amygdaloid pathway in morphine-induced analgesia. Int J Neuropsychopharmacol 16 (7):1649-1660. doi:10.1017/S146114571200168X

Veinante P, Yalcin I, Barrot M (2013) The amygdala between sensation and affect: a role in pain. J Mol Psychiatry 1 (1):9. doi:10.1186/2049-9256-1-9

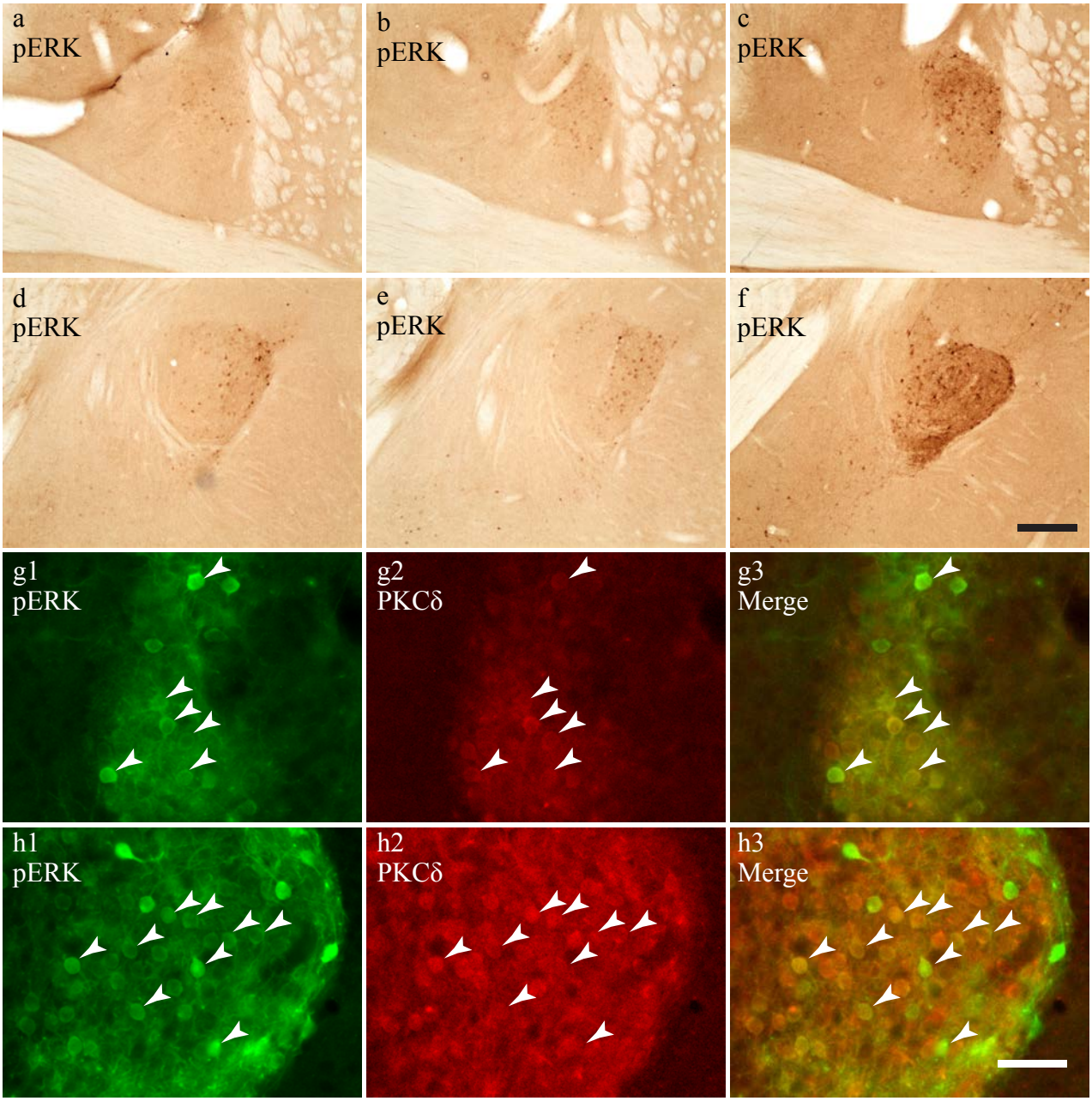

Fig. 1 Induction of pERK expression in PKCδ cells might be activated by chronic pain. DAB Immunohistochemistry of pERK-expressing soma (in brown) at contralateral STLD levels (**a** - **b**) and CeA (**d** - **f**) levels are performed in naive (**a**, **d**; case 15F04#03), vehicle (**b**, **e**; case 15F04#07) and formalin pain model (**c**, **f**; case 15F04#04). Double immunofluorescent staining of pERK (in green) and PKCδ (in red) were carried out at STLD (**g1** - **g3**) and CeA (**h1** - **h3**) of one formalin treated animal (case 15F04#04), with many colabeling neurons (indicated by arrow heads) were found in both nuclei. Scale bars: **a** - **f**, 250 μm; **g** - **h**, 50 μm.

CHAPTER III. DISCUSSIONS

1. Dissecting neuronal circuits: the best techniques wanted

Are there best techniques to dissect a neuronal circuit? The short answer is: probably not. With a specific research questions in mind, one can have many options for a combinations of different feasible techniques. New tools research have been being invented constantly to answer the old questions.

1.1 Methodology of this study: pros and cons

In this study, we rely on old techniques to answer old questions. To map the afferents and efferents of subdivisions of mouse central extended amygdala (EAc), we combined tract-tracing techniques and immunohistochemistry to label their distinctive and shared connections, as well as to identify their cellular identities.

The general pros and cons of tract-tracing techniques have been extensively discussed in the literatures (Kobbert et al. 2000; Lanciego and Wouterlood 2006; Lanciego and Wouterlood 2011). Here, we will briefly discuss the two sides of tract-tracing approach in the dissecting EAc neuronal circuits.

The pros

The main advantage of using traditional tract-tracing technique to study EAc neuroanatomical connectivity is the reproducibility. In our hands, we achieved a considerable consistence in the same neuroanatomical pathway with anterograde tracers and retrograde tracers. For example, most of the relative strengths and projection directions are well-conserved for intra-EAc pathways (see Fig. 16 of Results 1, and Fig. 13 of Results 2). Our method also works quite well for many of the long-range connections to EAc. For example, retrograde tracing from STLD and CeL/C resulted in strong labeling of LPBE projection neurons, consistently anterograde tracing from LPBE revealed comparable strong axonal projections in STLD and CeL/C. This reproducible connectivity mapping by tract-tracing also enabled us to make reliable comparisons of afferents and efferents between different EAc subnuclei.
Overall, the techniques employed in this study allowed for accurate targeting of individual EAc subdivisions and high quantity of somatic and axonal labeling by the tracers. These techniques are ready to be employed in mouse, but several limitations were observed.

The cons

Compared to STLD and CeA, the ventral division of STL in mouse is very difficult to be unequivocally targeted. This problem is likely contributed by many factors, including the small sizes of STLV and Fu, and a lack of clear neuroanatomical boundaries with the neighbouring basal forebrain subdivisions.

We also found it is difficult to label enough projection neurons in STLD and CeL/C to certain brain areas. For instance, we found retrograde tracing with FG and CTb from the ventrolateral periaqueductal gray (VLPAG) at best labeled several neurons in STLD and CeL/C, while intensively labeled neurons in the STLP, STLV, and CeM. Considering our anterograde tracing with BDA and PHA-L from STLD and CeL/C consistently produced strong axonal fibers in VLPAG area, the lack of retrograde labeling in STLD and CeL/C likely limited by the properties of tracers. A recent study reported VLPAG-projecting CeA neurons located exclusively in CeL/C, but not CeM, by rabies virus tracing in *Gad2-ires-Cre* mouse line (Tovote et al. 2016).

We also relies on the immunostaining to reveal the PKCδ+ and SOM+ cell populations in EAc. While our anti-PKCδ antibody can label almost all the PKCδ expressing neurons in the *PKCδ:GluClα-ires-Cre* mouse line (Haubensak et al. 2010), the anti-somatostatin antibody primarily resulted in somatic SOM+ labeling in patchy, making difficult to recognize cell bodies. This suboptimal labeling of SOM+ soma in EAc is likely region-specific, as somatic SOM+ signal quality is superb in many areas such as cortex and BLA. Thus, in this study, we likely underestimate the number of SOM+ neurons in STLD and CeL/C, especially when compared to the abundance of SOM+ neurons in the *SOM-ires-Cre* mouse line (Li et al. 2013a).

1.2 Hunting the cell-types of EAc in functions: the alternative methods

Apart from the structural connectivity, we are interested in the functions of these EAc microcircuits. Specifically, we want to know how EAc neurons involved in pain.

As PKCδ+ cells are concentrated in the CeL/C (Haubensak et al. 2010), which is also preferably activated by formalin-induced pain (Carrasquillo and Gereau 2007; Zaidi et al. 2000), we tried to correlate certain cell-types of CeL/C neurons with pain. Our primitive data indicates that PKCδ+ neurons from both STLD and CeLC are preferably activated by pain. But this immunohistochemistry-based approach has only limited power to resolve potential new cell-types. In order to have a less-biased view on functional cell-types in EAc, we turned to methods to qualify the gene expressions in EAc.

Becker and colleagues characterized the EAc-specific gene expressions in mouse by tissue dissection and microarray analysis (Becker et al. 2008). We also noticed that many EAc-specific genes from their study seems to have no known function in EAc. EAc, on the other hand, is well-known for its roles in pain and pain related emotion disorders (Ide et al. 2013; Minami and Ide 2015; Lebow and Chen 2016; Neugebauer et al. 2004; Veinante et al. 2013; Neugebauer 2015). Therefore, it would be interesting to assay mRNA changes in EAc areas in pain.

As different EAc nuclei and their neighbouring areas (i.e. EAm and BLA) might play differential or even opposing roles in pain responses (Crown et al. 2000; Ji et al. 2010; Li et al. 2013b), some mRNA expression levels might be assigned as unchanged false-positively due to tissue contaminations from functional different structures. There are also functional lateralization between left and right EAc. For instance, the right CeA, not its left counterpart, have been more implicated in pain behavior (Carrasquillo and Gereau 2007, 2008; Gonçalves and Dickenson 2012; Leite-Almeida et al. 2012; Neugebauer et al. 2004; Veinante et al. 2013). We therefore tried to reduce potential contaminations from confounding brain areas by laser capture microdissection.

To this end, we started with the cuff neuropathic model that has been well-established in our lab (Yalcin et al. 2014; Barthas et al. 2015) and tried to compared the gene expressions in SLTD and CeL/C in animals showing pain-induced depressive and anxiety-like behavior (Yalcin et al. 2011). We successfully employed the laser capture microdissection to dissect STLD (volume, about 0.02 mm^3 for an adult mouse) and CeL/C (volume, about 0.1 mm^3 for an adult mouse) in the right hemisphere from animals showing pain induced depressive behavior. We also extracted high quality total RNA of small quantity (total RNA = 5 – 10 ng, RIN > 7.5 for STLD; total RNA = 20 – 30 ng, RIN > 7.5 for CeL/C) which could be used for downstream assays of mRNA profiling by RNA-seq techniques that well established in Prof. Hein's lab.

We expected to see a group of EAc genes that specifically changed in the pain model. Then with complementary techniques including in situ mRNA hybridization and immunofluorescent staining, it would be possible to shed light on roles of new genes or new cell-types of EAc subdivisions in pain and pain-related emotion disorders.

2. Parallel and differential EAc neuronal circuits

In this study, our results reveal a rich repertoire of structural connectivity which parallel exist in EAc subdivisions. A comprehensive understanding of the impact of each subdivision and combined on behavior is obviously impossible unless future efforts are set in to dissect the functional roles of each element. In this section, however, we try to conjecture a synthetic picture of the structural organizations of EAc subdivisions, in particular the looped EAc – LPBE pathway, with some functional implications.

2.1 Towards a synthetic view of EAc circuits

Thus far, the structures of EAc neural circuits in mouse are quite complicated, such as in the intra-EAc (or intrinsic) connections and extra-EAc (or external) connections.

EAc intrinsic connections are usually strong between different EAc nuclei and are often of asymmetric strength. Overall, the intra-EAc connectivity favors information flow to STLV(Fu) and CeM, which contribute more extensive extra-EAc projections than STLD or CeL/C. In addition, STLV(Fu) and CeM shared many common external afferents and external efferents which are of similar strength. Taken together, this suggests STLV(Fu) and CeM are at a similar position in the EAc neural networks. While functions of CeM has been intensively studied, the STLV(Fu) remain elusive and can be a reasonable target for the future studies.

EAc external connections are also very likely to be shared between STLD and CeL/C, between STLV(Fu) and CeM. Because the analysis of external efferents is preliminary, we will focus on the external afferents. For the afferents, any two EAc nuclei has higher incidence of sharing inputs than to have preferential inputs. This is quite unexpected and puzzling. The pair of STLD and STLV(Fu), for example, have striking differences in their functions (Park et al. 2013; Daniel and Rainnie 2016) and efferents (Dong et al. 2001), one would more likely expect distinctive afferents to this two subdivisions. This surprising high coincidence of sharing inputs might be reconciled with the hidden layer of divergences from individual common input area. In our double tracing experiments, we showed STLD and CeL/C were rarely innervated by collateral neurons from some commonly shared input areas, but more likely by distinct neuronal groups. Two distinctive LPBE projection neuron pools, for example, innervate the STLD and CeL/C respectively. Thus, it is very likely LPBE → STLD and LPBE →CeL/C can have differential functional impact on EAc, even though we

found that LPBE CGRP+ neurons similarly innervate most of the PKCδ+ neurons in STLD and CeL/C.

Double retrograde tracing from CeA and STL, either in a whole structure or in a specific subdivision, have revealed consistently common and distinct inputs across the brain (Reynolds and Zahm 2005; Bienkowski and Rinaman 2013; Reichard et al. 2016; Dong et al. 2017). The divergence and convergence of afferents to different EAc subnuclei might be a common theme of EAc structural connectivity. They might indicate differential functions, and might further underlie the known dissociable functions between STL and CeA in such as fear and anxiety.

There are also distinct afferents and efferents to an EAc subdivision. These distinct connections display much higher strength of connectivity with one EAc subnuclei than with the rest three ones. For example, CeM has the strongest outputs to solitary nucleus (Sol) and the heaviest input from posterior thalamic nucleus. STLV(Fu) has the strongest inputs from hypothalamic areas, and strongest output to VTA.

Additionally, multiple areas including PSTh and VLPAG, bidirectionally connect with EAc nuclei. The cellular structural connections of such looped circuits, however, is not clear.

2.2 LPBE – EAc pathways

Structural feedback loops between LPB and EAc have been known in rat (Sarhan et al. 2013; Dobolyi et al. 2005; Carter et al. 2013; Moga and Gray 1985; Moga et al. 1989; Petrovich and Swanson 1997). Anterograde tract-tracing from LPB, especially LPBE, labeled specifically CeL/C and STLD, while retrograde tract-tracing from CeL/C specifically labeled neurons that confined the LPBE subdivision (Sarhan et al. 2013). Here, we piece together what we found in this study and literatures into one diagram (Fig. 4).

EAc neurons are mainly GABAergic and give rise to intrinsic and long-range projections (Cassell et al. 1999; Hunt et al. 2017). Specifically, here we focus on two non-overlapping neuronal populations which express PKCδ and SOM respectively. On the other hand, LPBE projections are glutamatergic and can be CGRPergic (Carter et al. 2013; Sugimura et al. 2016; Okutsu et al. 2017).

The descending LPBE glutamatergic projections target PKCδ+ neuronal populations of STLD and in parallel, of CeL/C. These LPBE projection neurons come from two distinct cell pools, which are composed of CGRP+ and CGRP- neurons. Then, information is propagated to the

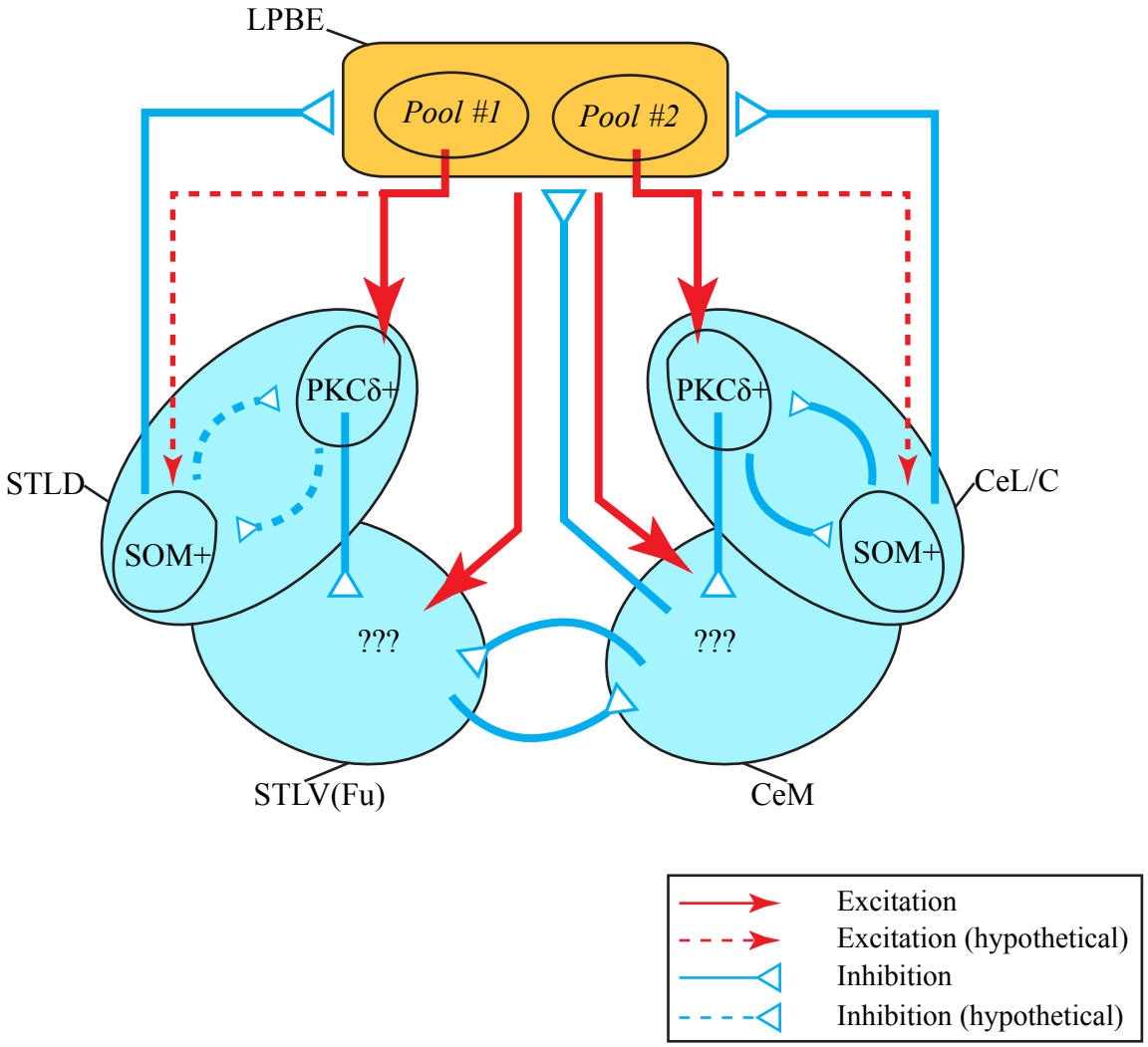

Fig. 4 A synthetic view of the looped neural circuits between LPBE and EAc. The connections are mainly mediated by excitatory LPBE neurons and inhibitory EAc neurons. At least two distinctive neuronal pools in the LPBE, each consisting of CGRP-positive neurons and CGRP-negative ones, drive the PKCδ+ neurons in STLD and CeL/C. The feedbacks from STLD and CeL/C SOM+ neurons likely innervate the LPBE neuronal pools indiscriminately. The STLV (Fu) received dense inputs from LPBE, but rarely project back; on the other hand, the CeM have mutual talks with LPBE. The STLV(Fu) and CeM can also have strong mutual connections, but it is still unknown which cell-types mediate these connections. We also highlight the hypothetic innervations from LPBE to EAc SOM+ neurons, and hypothetic mutual connections between PKC δ+ and SOM+ neurons in STLD. Abbreviations: see the list.

GABAergic neurons in STLV(Fu) and CeM, which are reciprocally connected. The feedback inhibitory inputs to LPBE mainly come from SOM+ neurons, which probably target all the LPBE neuron pools indiscriminately. The reciprocal inhibition between PKCδ+ neurons and SOM+ neurons exist in CeL/C, and presumably so in STLD.

In addition to the above descriptions, LPBE also projects to STLV(Fu) and CeM; CeM, but not STLV(Fu) projects back to LPBE. The LPBE might also directly innervate SOM+ neurons with non-basket fine axonal varicosities, which cannot be identified with our technique approaches.

Based on this model, activation of LPBE CGRP+ neurons can inhibit CeM and STLV(Fu) projection neurons via CeL/C and STLD, respectively. On the other hand, STLV(Fu) is under strong LPB excitation and inhibition reciprocally by CeM. Thus, a likely competence between LPBE →STLD →STLV(Fu) and LPBE→CeL/C→CeM might exist when both the two CGRP+ neuron pools are activated. Further, if the reciprocal inhibitions are not symmetric between STLV(Fu) and CeM, then a potential inhibitory pull-push control of either STLV(Fu) or CeM activity can be achieved. Thus, LPBE is capable of influencing STLV(Fu) and CeM, which mediate majority of EAc outputs, via direct and indirect pathways. The lack of feedback inhibition on LPBE from STLV(Fu), but not from CeM is also an interesting feature.

The finding of two distinct LPBE neuron pools to STLD and CeL/C is potentially important. It has been shown that LPBE – CeA pathway, which is also a part of the spino-parabrachio-amygdala pain pathway (Bernard and Besson 1990; Jasmin et al. 1997; Gauriau and Bernard 2002), plays critical roles in fear learning and affective pain response (Han et al. 2010; Han et al. 2015; Sato et al. 2015). The roles of LPBE – STLD pathway, however, remain largely elusive. It is likely that STLD-projecting neurons in LPBE are differentially activated by pain signal than CeL/C-projecting ones.

2.3 Convergent inputs to PKCδ+ neurons

Here we put them together into one model (Fig. 5) to illustrate potential convergence of multiple excitatory pathways onto a specific cell type in EAc. In our study, we have demonstrated axon – soma structural appositions between PKCδ+ soma and putative excitatory synapses (i.e. CGRP+, from amygdala and insular cortex). We also showed the

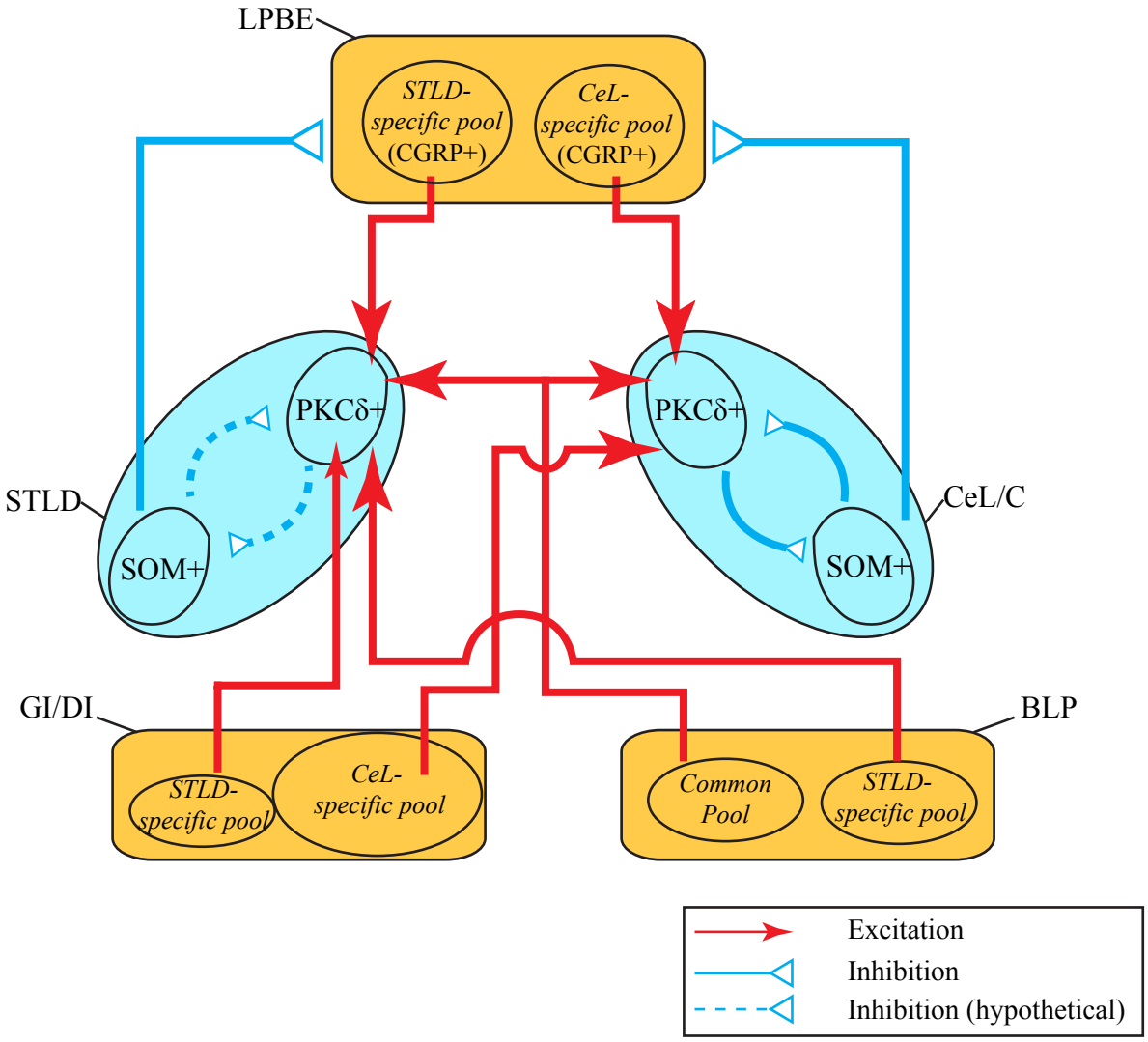

Fig. 5 Integration of multiple excitatory inputs onto PKCδ-expressing neurons. For each source area, there are three types of EAc-projecting neurons: STLD only (STLD-specific pool), to CeL/C only (CeL/C-specific pool) and to both (common pool). The size of projection-specific neuron pools are adjusted to reflect the relative strength of each category in each input area, except that the neuron pool of the smallest size is not shown. Note the excitatory innervations from LPBE, GI/DI and BLP can be converged to PKCδ-expressing (PKCδ+) neurons in STLD and CeL/C. Abbreviations: see the list.

differential portions of putative glutamatergic projection neurons in LPBE, GI/DI, and BLP to STLD and CeL/C. Currently, there is no direct evidence for such synaptic convergence onto PKCδ+ neurons, but a concurrent potentiation of nociceptive-specific LPB → CeL/C synapses and polymodal BLA → CeL/C synapses were reported in pain model and fear learning paradigm (Neugebauer et al. 2003; Watabe et al. 2013). However, it is not clear how this concurrent changes of two different pathways are induced. Simultaneous synaptic potentiations were observed between LPB→CeA pathway and BLA →CeA pathway, and they are dependent only on associative learning, not on electric shock, sensory cues or memory retrieval (Watabe et al. 2013). PKCδ+ neurons in STLD and CeL/C can also be activated simultaneously by D2R agonist and promote fear overgeneralization (De Bundel et al. 2016). It worth noting that optogenetic activation of LPBE → CeL/C pathway can replace electric shock as the unconditioned stimulus and it leads to significant associative fear learning when paired with a conditioned stimulus (Sato et al. 2015). Since LPBE:CGRP+ projection to CeL/C is important in transmitting pain signal caused by the electric shock (Han et al. 2015), it is possible that some kind of interactions might exist between LPB→CeA pathway and BLA →CeA pathway. Thus, the convergent structural appositions of LPBE CGRP+ terminals and BLP glutamatergic terminals onto the same PKCδ+ neuron possibly imply a functional interaction between the two pathways. Future studies might look at the fine synaptic structures (i.e. by staining presynaptic protein) and interactions between synaptic transmissions (i.e. by electrophysiological recording) of these excitatory inputs to PKCδ+ neuron.

3. Miscellanies

3.1 Cell types of EAc-projecting LPBE neurons: alternative cell types

According to the Allen Brain ISH database, the LPB regions seems to be dominated by excitatory neurons. The LPB areas are enriched with traditional glutamatergic neuronal markers including *CamK2α* (calcium/calmodulin dependent protein kinase II alpha) and the vesicular glutamate transporter vglut2+ (coded by gene *Slc17a6*) neurons, which is consistent with a previous report (Kudo et al. 2012) (Fig. 6). On the other hand, several GABAergic neuronal markers, such as GAD65 (by *GAD2*), GAD67 (by *GAD1*)), and Vgat (by *Slc32a1*) are largely missing. The LPB neurons also express different neuropeptides, including CGRP (by *Calca*), PACAP (by *Adcyap1*), Calretinin (by *Calb2*), and encephalin (by *Penk*, not shown). LPBE might also has a number of SOM+ neurons, while lacks of other classic cortical inhibitory neuronal markers including PV and VIP (from Allen Brain ISH database, not shown here).

In our studies, we focus mainly on CGRP+ and calretinin+ neuronal populations, partially due to the availability of the antibodies in our lab. Combined with tract-tracing and immunofluorescent staining, we revealed almost all EAc-projecting neurons express calretinin, of which a small proportion express CGRP. We also observed that LPBE axonal projections to STLD and CeL/C were only partially colocalized with CGRP. Thus, we conclude there are non-CGRP LPBE projection neurons innervating EAc.

Therefore, to better understand effect of LPBE – EAc pathway, we need to gain access to other EAc-projecting LPBE cell types. It worth noting that, PACAP-expressing LPBE neurons also project to CeL/C and STLD (Cho et al. 2012; Missig et al. 2014), but the PACAP+ axonal field only partially overlapped with that of CGRP+ in EAc (Missig et al. 2014). These PACAP projections can be functionally important. In a chronic neuropathic pain model, enhanced PACAP immunoreactivity and pERK induction were observed in CeL/C, while anxiety and hyperalgesia were heightened (Missig et al. 2017). Interestingly, acute local infusion of PACAP receptor antagonist block behavior changes in this chronic pain model (Missig et al. 2017).

3.2 CRF immunoreactivity: discrepancy in STLD and CeA

CRF-expressing neurons have long been known to be distributed in STL and CeA of mouse and rat (Swanson et al. 1983; Erb et al. 2001; Asan et al. 2005). In our study, we observed that a substantial portion of STLD and CeL/C projection neurons were not labeled by PKCδ and SOM, therefore we turned to CRF, which was reported to be a complementary cell

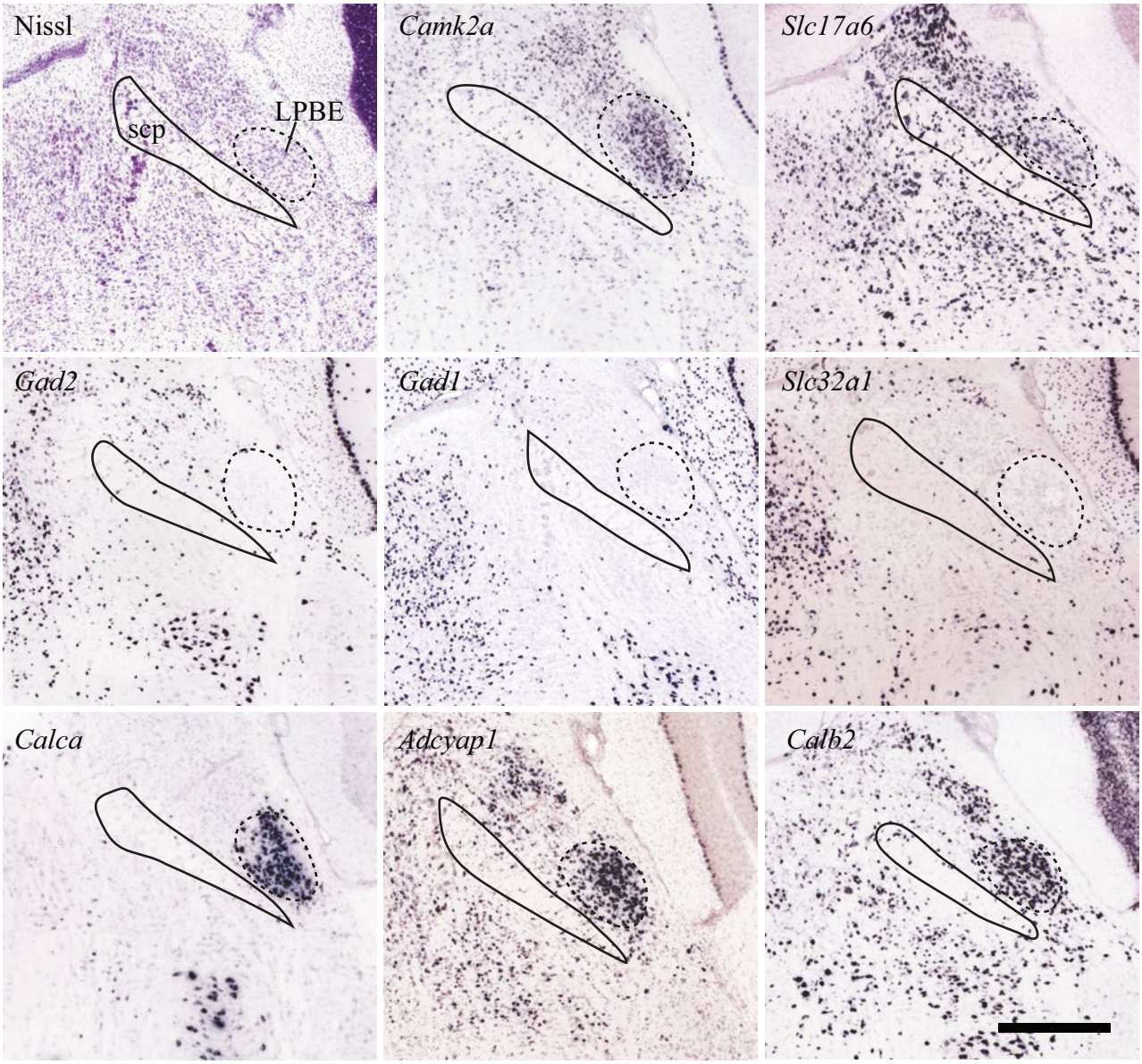

Fig. 6 Gene expressions in LPBE. ISH mRNA signals of different genes are enriched or absent from mouse LPBE. Nissl staining shows the cytoarchitecture, *Camk2a* and *Slc17a6* are glutamatergic neuronal markers; *Gad2*, *Gad1*, and *Slc32a1* are GABAergic neuronal markers; *Calca*, *Adcyap1*, *Calb2* are selected neuropeptidergic markers. Images are taken from the Allen Mouse Brain Atlas (Lein, E.S. et al., 2007), Scale bars: all are 500 μm, except for the unknown scale in *Gad1*.

populations in mouse CeL/C (Kim et al. 2017). We are lucky to get a gifted rabbit-anti-CRF antiserum (code PBL rC68) from Dr. P.Sawchenko of Salk Institute, but due to unknown reasons we could not identify CRF+ neurons in STLD (Fig. 7) and CeL/C (not shown). With confocal imaging, we can locate somatic colabeling of PKCδ and CTb (which we injected in the STLV area), but only perisomatic CRF+ signal (Fig. 7b – c) are observed, which could easily be mistaken as part of soma. Outside EAc, the antibody gave specific somatic labeling in areas such as cortex, basal amygdala, and paraventricular nucleus of hypothalamus (Swanson et al. 1983; Chen et al. 2015). But in STLD and CeL/C, we only observed very intense CRF+ fibers, not cell bodies as that reported by Chen and colleagues on wide-type mice and a *Crf-ires-Cre* mouse line (Chen et al. 2015). Considering the similar procedures for tissue processing and immunostaining, it is quite odd that we did not observed any CRF+ somatic staining in mouse STLD and CeL/C.

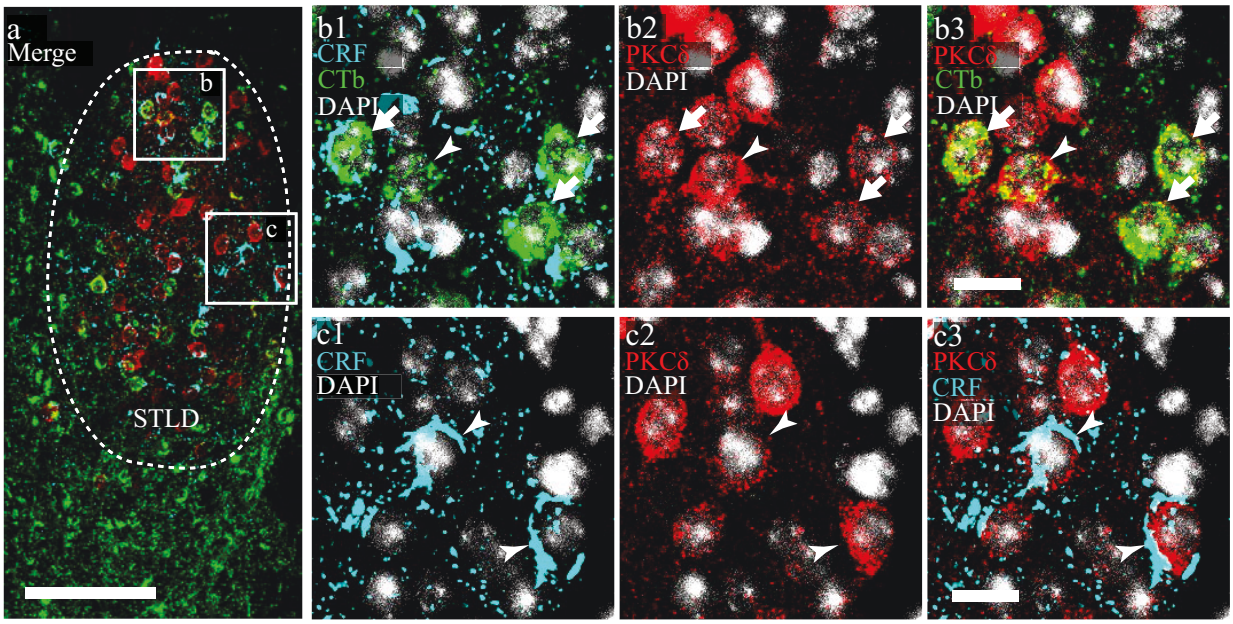

Fig. 7 CRF immunoreactivity in STLD. Triple labeling of CTb (green), CRF (cyan) and PKCδ (red) was performed after CTb injection into the STLV. **a** Confocal images shows specific enrichment of CRF signal in STLD. **b - c** Confocal images (20x objective, z-stack = 13.8 µm) showing the subcellular location of CRF. Note that the CTb and PKCδ well overlap within the somatic structures, while CRF mainly localizes peripherally against outer border of somatic CTb (short arrows) and PKCδ (arrow heads). Scare bars: **a**, 100 µm; **b1 - b3**, 15 µm; **c1 - c3**, 15 µm.

REFERENCE

Adams JC (1992) Biotin amplification of biotin and horseradish peroxidase signals in histochemical stains. J Histochem Cytochem 40 (10):1457-1463. doi:10.1177/40.10.1527370

Alden M, Besson JM, Bernard JF (1994) Organization of the efferent projections from the pontine parabrachial area to the bed nucleus of the stria terminalis and neighboring regions: a PHA-L study in the rat. J Comp Neurol 341 (3):289-314. doi:10.1002/cne.903410302

Alheid GF (2003) Extended amygdala and basal forebrain. Ann N Y Acad Sci 985:185-205. doi:10.1111/j.1749-6632.2003.tb07082.x

Alheid GF, Heimer L (1988) New perspectives in basal forebrain organization of special relevance for neuropsychiatric disorders: the striatopallidal, amygdaloid, and corticopetal components of substantia innominata. Neuroscience 27 (1):1-39

Amano T, Amir A, Goswami S, Pare D (2012) Morphology, PKCdelta expression, and synaptic responsiveness of different types of rat central lateral amygdala neurons. J Neurophysiol 108 (12):3196-3205. doi:10.1152/jn.00514.2012

Andero R, Daniel S, Guo JD, Bruner RC, Seth S, Marvar PJ, Rainnie D, Ressler KJ (2016) Amygdala-Dependent Molecular Mechanisms of the Tac2 Pathway in Fear Learning. Neuropsychopharmacology 41 (11):2714-2722. doi:10.1038/npp.2016.77

Apps R, Ruigrok TJ (2007) A fluorescence-based double retrograde tracer strategy for charting central neuronal connections. Nat Protoc 2 (8):1862-1868. doi:10.1038/nprot.2007.263

Asan E, Yilmazer-Hanke DM, Eliava M, Hantsch M, Lesch KP, Schmitt A (2005) Corticotropin-Releasing Factor (CRF)-system and monoaminergic afferents in the central amygdala: Investigations in different mouse strains and comparison with the rat. Neuroscience 131 (4):953-967. doi:10.1016/j.neuroscience.2004.11.040

Avery SN, Clauss JA, Blackford JU (2016) The Human BNST: Functional Role in Anxiety and Addiction. Neuropsychopharmacology 41 (1):126-141. doi:10.1038/npp.2015.185

Barthas F, Sellmeijer J, Hugel S, Waltisperger E, Barrot M, Yalcin I (2015) The anterior cingulate cortex is a critical hub for pain-induced depression. Biol Psychiatry 77 (3):236-245. doi:10.1016/j.biopsych.2014.08.004

Becker JA, Befort K, Blad C, Filliol D, Ghate A, Dembele D, Thibault C, Koch M, Muller J, Lardenois A, Poch O, Kieffer BL (2008) Transcriptome analysis identifies genes with enriched expression in the mouse central extended amygdala. Neuroscience 156 (4):950-965. doi:10.1016/j.neuroscience.2008.07.070

Bernard JF, Alden M, Besson JM (1993) The organization of the efferent projections from the pontine parabrachial area to the amygdaloid complex: a Phaseolus vulgaris leucoagglutinin (PHA-L) study in the rat. J Comp Neurol 329 (2):201-229. doi:10.1002/cne.903290205

Bernard JF, Besson JM (1990) The spino(trigemino)pontoamygdaloid pathway: electrophysiological evidence for an involvement in pain processes. J Neurophysiol 63 (3):473-490

Bienkowski MS, Rinaman L (2013) Common and distinct neural inputs to the medial central nucleus of the amygdala and anterior ventrolateral bed nucleus of stria terminalis in rats. Brain Struct Funct 218 (1):187-208. doi:10.1007/s00429-012-0393-6

Bienvenu TC, Busti D, Micklem BR, Mansouri M, Magill PJ, Ferraguti F, Capogna M (2015) Large intercalated neurons of amygdala relay noxious sensory information. J Neurosci 35 (5):2044-2057. doi:10.1523/JNEUROSCI.1323-14.2015

Bobrow MN, Moen PT, Jr. (2001) Tyramide signal amplification (TSA) systems for the enhancement of ISH signals in cytogenetics. Curr Protoc Cytom Chapter 8:Unit 8 9. doi:10.1002/0471142956.cy0809s11

Botta P, Demmou L, Kasugai Y, Markovic M, Xu C, Fadok JP, Lu T, Poe MM, Xu L, Cook JM, Rudolph U, Sah P, Ferraguti F, Luthi A (2015) Regulating anxiety with extrasynaptic inhibition. Nat Neurosci 18 (10):1493-1500. doi:10.1038/nn.4102

Brandt HM, Apkarian AV (1992) Biotin-dextran: a sensitive anterograde tracer for neuroanatomic studies in rat and monkey. J Neurosci Methods 45 (1-2):35-40. doi:0165-0270(92)90041-B [pii]

Bupesh M, Abellan A, Medina L (2011) Genetic and experimental evidence supports the continuum of the central extended amygdala and a mutiple embryonic origin of its principal neurons. J Comp Neurol 519 (17):3507-3531. doi:10.1002/cne.22719

Cai H, Haubensak W, Anthony TE, Anderson DJ (2014) Central amygdala PKC-delta(+) neurons mediate the influence of multiple anorexigenic signals. Nat Neurosci 17 (9):1240-1248. doi:10.1038/nn.3767

Cai L, Bakalli H, Rinaman L (2012) Yohimbine anxiogenesis in the elevated plus maze is disrupted by bilaterally disconnecting the bed nucleus of the stria terminalis from the central nucleus of the amygdala. Neuroscience 223:200-208. doi:10.1016/j.neuroscience.2012.08.008

Carrasquillo Y, Gereau RWt (2007) Activation of the extracellular signal-regulated kinase in the amygdala modulates pain perception. J Neurosci 27 (7):1543-1551. doi:10.1523/JNEUROSCI.3536-06.2007

Carrasquillo Y, Gereau RWt (2008) Hemispheric lateralization of a molecular signal for pain modulation in the amygdala. Mol Pain 4:24. doi:1744-8069-4-24 [pii]
10.1186/1744-8069-4-24
Carter ME, Soden ME, Zweifel LS, Palmiter RD (2013) Genetic identification of a neural circuit that suppresses appetite. Nature 503 (7474):111-114. doi:10.1038/nature12596
Cassell MD, Freedman LJ, Shi C (1999) The intrinsic organization of the central extended amygdala. Ann N Y Acad Sci 877:217-241
Cassell MD, Gray TS (1989) Morphology of peptide-immunoreactive neurons in the rat central nucleus of the amygdala. J Comp Neurol 281 (2):320-333. doi:10.1002/cne.902810212
Cassell MD, Gray TS, Kiss JZ (1986) Neuronal architecture in the rat central nucleus of the amygdala: a cytological, hodological, and immunocytochemical study. J Comp Neurol 246 (4):478-499. doi:10.1002/cne.902460406
Chen Y, Molet J, Gunn BG, Ressler K, Baram TZ (2015) Diversity of Reporter Expression Patterns in Transgenic Mouse Lines Targeting Corticotropin-Releasing Hormone-Expressing Neurons. Endocrinology 156 (12):4769-4780. doi:10.1210/en.2015-1673
Chieng BC, Christie MJ, Osborne PB (2006) Characterization of neurons in the rat central nucleus of the amygdala: cellular physiology, morphology, and opioid sensitivity. J Comp Neurol 497 (6):910-927. doi:10.1002/cne.21025
Cho JH, Zushida K, Shumyatsky GP, Carlezon WA, Jr., Meloni EG, Bolshakov VY (2012) Pituitary adenylate cyclase-activating polypeptide induces postsynaptically expressed potentiation in the intra-amygdala circuit. J Neurosci 32 (41):14165-14177. doi:10.1523/JNEUROSCI.1402-12.2012
Ciocchi S, Herry C, Grenier F, Wolff SB, Letzkus JJ, Vlachos I, Ehrlich I, Sprengel R, Deisseroth K, Stadler MB, Muller C, Luthi A (2010) Encoding of conditioned fear in central amygdala inhibitory circuits. Nature 468 (7321):277-282. doi:10.1038/nature09559
Crown ED, King TE, Meagher MW, Grau JW (2000) Shock-induced hyperalgesia: III. Role of the bed nucleus of the stria terminalis and amygdaloid nuclei. Behav Neurosci 114 (3):561-573
Daniel SE, Guo J, Rainnie DG (2017) A Comparative Analysis of the Physiological Properties of Neurons in the Anterolateral Bed Nucleus of the Stria Terminalis in the Mus musculus, Rattus norvegicus, and Macaca mulatta. J Comp Neurol. doi:10.1002/cne.24202
Daniel SE, Rainnie DG (2016) Stress Modulation of Opposing Circuits in the Bed Nucleus of the Stria Terminalis. Neuropsychopharmacology 41 (1):103-125. doi:10.1038/npp.2015.178
Davis M, Walker DL, Miles L, Grillon C (2009) Phasic vs sustained fear in rats and humans: role of the extended amygdala in fear vs anxiety. Neuropsychopharmacology 35 (1):105-135. doi:10.1038/npp.2009.109
De Bundel D, Zussy C, Espallergues J, Gerfen CR, Girault JA, Valjent E (2016) Dopamine D2 receptors gate generalization of conditioned threat responses through mTORC1 signaling in the extended amygdala. Mol Psychiatry 21 (11):1545-1553. doi:10.1038/mp.2015.210
de Olmos JS, Beltramino CA, Alheid G (2004) Amygdala and Extended Amygdala of the Rat: A Cytoarchitectonical, Fibroarchitectonical, and Chemoarchitectonical Survey. In: Paxinos G (ed) The Rat Nervous System. Elsevier Academic Press, Amsterdam, pp pp. 509-603
de Olmos JS, Heimer L (1999) The concepts of the ventral striatopallidal system and extended amygdala. Ann N Y Acad Sci 877:1-32
Deisseroth K (2015) Optogenetics: 10 years of microbial opsins in neuroscience. Nat Neurosci 18 (9):1213-1225. doi:10.1038/nn.4091
Dobolyi A, Irwin S, Makara G, Usdin TB, Palkovits M (2005) Calcitonin gene-related peptide-containing pathways in the rat forebrain. J Comp Neurol 489 (1):92-119. doi:10.1002/cne.20618
Dong HW, Petrovich GD, Swanson LW (2001a) Topography of projections from amygdala to bed nuclei of the stria terminalis. Brain Res Brain Res Rev 38 (1-2):192-246
Dong HW, Petrovich GD, Watts AG, Swanson LW (2001b) Basic organization of projections from the oval and fusiform nuclei of the bed nuclei of the stria terminalis in adult rat brain. J Comp Neurol 436 (4):430-455
Dong X, Li S, Kirouac GJ (2017) Collateralization of projections from the paraventricular nucleus of the thalamus to the nucleus accumbens, bed nucleus of the stria terminalis, and central nucleus of the amygdala. Brain Struct Funct. doi:10.1007/s00429-017-1445-8
Douglass AM, Kucukdereli H, Ponserre M, Markovic M, Grundemann J, Strobel C, Alcala Morales PL, Conzelmann KK, Luthi A, Klein R (2017) Central amygdala circuits modulate food consumption through a positive-valence mechanism. Nat Neurosci 20 (10):1384-1394. doi:10.1038/nn.4623
Dumont EC, Martina M, Samson RD, Drolet G, Pare D (2002) Physiological properties of central amygdala neurons: species differences. Eur J Neurosci 15 (3):545-552

Erb S, Salmaso N, Rodaros D, Stewart J (2001) A role for the CRF-containing pathway from central nucleus of the amygdala to bed nucleus of the stria terminalis in the stress-induced reinstatement of cocaine seeking in rats. Psychopharmacology (Berl) 158 (4):360-365. doi:10.1007/s002130000642

Fadok JP, Krabbe S, Markovic M, Courtin J, Xu C, Massi L, Botta P, Bylund K, Muller C, Kovacevic A, Tovote P, Luthi A (2017) A competitive inhibitory circuit for selection of active and passive fear responses. Nature 542 (7639):96-100. doi:10.1038/nature21047

Faget L, Hnasko TS (2015) Tyramide Signal Amplification for Immunofluorescent Enhancement. Methods Mol Biol 1318:161-172. doi:10.1007/978-1-4939-2742-5_16

Fox AS, Oler JA, Tromp do PM, Fudge JL, Kalin NH (2015) Extending the amygdala in theories of threat processing. Trends Neurosci 38 (5):319-329. doi:10.1016/j.tins.2015.03.002

Fox AS, Shackman AJ (2017) The central extended amygdala in fear and anxiety: Closing the gap between mechanistic and neuroimaging research. Neurosci Lett. doi:10.1016/j.neulet.2017.11.056

Freedman LJ, Cassell MD (1994) Distribution of dopaminergic fibers in the central division of the extended amygdala of the rat. Brain Res 633 (1-2):243-252

Garcia-Lopez M, Abellan A, Legaz I, Rubenstein JL, Puelles L, Medina L (2008) Histogenetic compartments of the mouse centromedial and extended amygdala based on gene expression patterns during development. J Comp Neurol 506 (1):46-74. doi:10.1002/cne.21524

Gauriau C, Bernard JF (2002) Pain pathways and parabrachial circuits in the rat. Exp Physiol 87 (2):251-258. doi:EPH_2357 [pii]

Gerfen CR, Paletzki R, Heintz N (2013) GENSAT BAC cre-recombinase driver lines to study the functional organization of cerebral cortical and basal ganglia circuits. Neuron 80 (6):1368-1383. doi:10.1016/j.neuron.2013.10.016

Gerfen CR, Sawchenko PE (1984) An anterograde neuroanatomical tracing method that shows the detailed morphology of neurons, their axons and terminals: immunohistochemical localization of an axonally transported plant lectin, Phaseolus vulgaris leucoagglutinin (PHA-L). Brain Res 290 (2):219-238

Gonçalves L, Dickenson AH (2012) Asymmetric time-dependent activation of right central amygdala neurones in rats with peripheral neuropathy and pregabalin modulation. European Journal of Neuroscience 36:3204-3213. doi:10.1111/j.1460-9568.2012.08235.x

Gorka AX, Torrisi S, Shackman AJ, Grillon C, Ernst M (2017) Intrinsic functional connectivity of the central nucleus of the amygdala and bed nucleus of the stria terminalis. Neuroimage. doi:10.1016/j.neuroimage.2017.03.007

Gungor NZ, Pare D (2016) Functional Heterogeneity in the Bed Nucleus of the Stria Terminalis. J Neurosci 36 (31):8038-8049. doi:10.1523/JNEUROSCI.0856-16.2016

Hammack SE, Mania I, Rainnie DG (2007) Differential expression of intrinsic membrane currents in defined cell types of the anterolateral bed nucleus of the stria terminalis. J Neurophysiol 98 (2):638-656. doi:10.1152/jn.00382.2007

Han JS, Adwanikar H, Li Z, Ji G, Neugebauer V (2010) Facilitation of synaptic transmission and pain responses by CGRP in the amygdala of normal rats. Mol Pain 6:10. doi:10.1186/1744-8069-6-10

Han S, Soleiman MT, Soden ME, Zweifel LS, Palmiter RD (2015) Elucidating an Affective Pain Circuit that Creates a Threat Memory. Cell 162 (2):363-374. doi:10.1016/j.cell.2015.05.057

Harris JA, Hirokawa KE, Sorensen SA, Gu H, Mills M, Ng LL, Bohn P, Mortrud M, Ouellette B, Kidney J, Smith KA, Dang C, Sunkin S, Bernard A, Oh SW, Madisen L, Zeng H (2014) Anatomical characterization of Cre driver mice for neural circuit mapping and manipulation. Front Neural Circuits 8:76. doi:10.3389/fncir.2014.00076

Haubensak W, Kunwar PS, Cai H, Ciocchi S, Wall NR, Ponnusamy R, Biag J, Dong HW, Deisseroth K, Callaway EM, Fanselow MS, Luthi A, Anderson DJ (2010) Genetic dissection of an amygdala microcircuit that gates conditioned fear. Nature 468 (7321):270-276. doi:10.1038/nature09553

Heimer L, Alheid GF, de Olmos JS, Groenewegen HJ, Haber SN, Harlan RE, Zahm DS (1997a) The accumbens: beyond the core-shell dichotomy. J Neuropsychiatry Clin Neurosci 9 (3):354-381. doi:10.1176/jnp.9.3.354

Heimer L, de Olmos JS, Alheid GF, Pearson J, Sakamoto N, Shinoda K, Marksteiner J, C.SwitzerIII R (1999) Chapter II - The human basal forebrain. Part II. In: Bloom FE, Björklund A, Hökfelt T (eds) Handbook of Chemical Neuroanatomy, vol 15. Elsevier BV, pp 57-226. doi:10.1016/s0924-8196(99)80024-4

Heimer L, Harlan RE, Alheid GF, Garcia MM, de Olmos J (1997b) Substantia innominata: a notion which impedes clinical-anatomical correlations in neuropsychiatric disorders. Neuroscience 76 (4):957-1006

Henckens MJ, Printz Y, Shamgar U, Dine J, Lebow M, Drori Y, Kuehne C, Kolarz A, Eder M, Deussing JM, Justice NJ, Yizhar O, Chen A (2016) CRF receptor type 2 neurons in the posterior bed nucleus of the stria terminalis critically contribute to stress recovery. Mol Psychiatry. doi:10.1038/mp.2016.133

Holstege G, Meiners L, Tan K (1985) Projections of the bed nucleus of the stria terminalis to the mesencephalon, pons, and medulla oblongata in the cat. Exp Brain Res 58 (2):379-391

Hsu SM, Raine L, Fanger H (1981) Use of avidin-biotin-peroxidase complex (ABC) in immunoperoxidase techniques: a comparison between ABC and unlabeled antibody (PAP) procedures. J Histochem Cytochem 29 (4):577-580. doi:10.1177/29.4.6166661
Hsu SM, Soban E (1982) Color modification of diaminobenzidine (DAB) precipitation by metallic ions and its application for double immunohistochemistry. J Histochem Cytochem 30 (10):1079-1082
Hunt S, Sun Y, Kucukdereli H, Klein R, Sah P (2017) Intrinsic Circuits in the Lateral Central Amygdala. eNeuro 4 (1). doi:10.1523/ENEURO.0367-16.2017
Hunyady B, Krempels K, Harta G, Mezey E (1996) Immunohistochemical signal amplification by catalyzed reporter deposition and its application in double immunostaining. J Histochem Cytochem 44 (12):1353-1362
Ide S, Hara T, Ohno A, Tamano R, Koseki K, Naka T, Maruyama C, Kaneda K, Yoshioka M, Minami M (2013) Opposing roles of corticotropin-releasing factor and neuropeptide Y within the dorsolateral bed nucleus of the stria terminalis in the negative affective component of pain in rats. J Neurosci 33 (14):5881-5894. doi:10.1523/JNEUROSCI.4278-12.2013
Isosaka T, Matsuo T, Yamaguchi T, Funabiki K, Nakanishi S, Kobayakawa R, Kobayakawa K (2015) Htr2a-Expressing Cells in the Central Amygdala Control the Hierarchy between Innate and Learned Fear. Cell 163 (5):1153-1164. doi:10.1016/j.cell.2015.10.047
Jasmin L, Burkey AR, Card JP, Basbaum AI (1997) Transneuronal labeling of a nociceptive pathway, the spino-(trigemino-)parabrachio-amygdaloid, in the rat. J Neurosci 17 (10):3751-3765
Jennings JH, Rizzi G, Stamatakis AM, Ung RL, Stuber GD (2013a) The inhibitory circuit architecture of the lateral hypothalamus orchestrates feeding. Science 341 (6153):1517-1521. doi:10.1126/science.1241812
Jennings JH, Sparta DR, Stamatakis AM, Ung RL, Pleil KE, Kash TL, Stuber GD (2013b) Distinct extended amygdala circuits for divergent motivational states. Nature 496 (7444):224-228. doi:10.1038/nature12041
Ji G, Sun H, Fu Y, Li Z, Pais-Vieira M, Galhardo V, Neugebauer V (2010) Cognitive impairment in pain through amygdala-driven prefrontal cortical deactivation. J Neurosci 30 (15):5451-5464. doi:10.1523/JNEUROSCI.0225-10.2010
Johnston JB (1923) Further contributions to the study of the evolution of the forebrain. J Comp Neurol 35 (5):337-481. doi:10.1002/cne.900350502
Jolkkonen E, Pitkanen A (1998) Intrinsic connections of the rat amygdaloid complex: projections originating in the central nucleus. J Comp Neurol 395 (1):53-72
Ju G, Swanson LW (1989) Studies on the cellular architecture of the bed nuclei of the stria terminalis in the rat: I. Cytoarchitecture. J Comp Neurol 280 (4):587-602. doi:10.1002/cne.902800409
Ju G, Swanson LW, Simerly RB (1989) Studies on the cellular architecture of the bed nuclei of the stria terminalis in the rat: II. Chemoarchitecture. J Comp Neurol 280 (4):603-621. doi:10.1002/cne.902800410
Katz LC, Iarovici DM (1990) Green fluorescent latex microspheres: a new retrograde tracer. Neuroscience 34 (2):511-520
Kaufling J, Girard D, Maitre M, Leste-Lasserre T, Georges F (2017) Species-specific diversity in the anatomical and physiological organization of the BNST-VTA pathway. Eur J Neurosci. doi:10.1111/ejn.13554
Kim CK, Adhikari A, Deisseroth K (2017a) Integration of optogenetics with complementary methodologies in systems neuroscience. Nat Rev Neurosci 18 (4):222-235. doi:10.1038/nrn.2017.15
Kim J, Zhang X, Muralidhar S, LeBlanc SA, Tonegawa S (2017b) Basolateral to Central Amygdala Neural Circuits for Appetitive Behaviors. Neuron 93 (6):1464-1479 e1465. doi:10.1016/j.neuron.2017.02.034
Kim SY, Adhikari A, Lee SY, Marshel JH, Kim CK, Mallory CS, Lo M, Pak S, Mattis J, Lim BK, Malenka RC, Warden MR, Neve R, Tye KM, Deisseroth K (2013) Diverging neural pathways assemble a behavioural state from separable features in anxiety. Nature 496 (7444):219-223. doi:10.1038/nature12018
Kobbert C, Apps R, Bechmann I, Lanciego JL, Mey J, Thanos S (2000) Current concepts in neuroanatomical tracing. Prog Neurobiol 62 (4):327-351. doi:S0301-0082(00)00019-8 [pii]
Kodani S, Soya S, Sakurai T (2017) Excitation of GABAergic neurons in the bed nucleus of the stria terminalis triggers immediate transition from non-rapid eye movement sleep to wakefulness in mice. J Neurosci. doi:10.1523/JNEUROSCI.0245-17.2017
Krawczyk M, Georges F, Sharma R, Mason X, Berthet A, Bezard E, Dumont EC (2011) Double-dissociation of the catecholaminergic modulation of synaptic transmission in the oval bed nucleus of the stria terminalis. J Neurophysiol 105 (1):145-153. doi:10.1152/jn.00710.2010
Krettek JE, Price JL (1978) Amygdaloid projections to subcortical structures within the basal forebrain and brainstem in the rat and cat. J Comp Neurol 178 (2):225-254. doi:10.1002/cne.901780204
Krukoff TL, Harris KH, Jhamandas JH (1993) Efferent projections from the parabrachial nucleus demonstrated with the anterograde tracer Phaseolus vulgaris leucoagglutinin. Brain Res Bull 30 (1-2):163-172

Kudo T, Uchigashima M, Miyazaki T, Konno K, Yamasaki M, Yanagawa Y, Minami M, Watanabe M (2012) Three types of neurochemical projection from the bed nucleus of the stria terminalis to the ventral tegmental area in adult mice. J Neurosci 32 (50):18035-18046. doi:32/50/18035 [pii]
10.1523/JNEUROSCI.4057-12.2012
Lanciego JL, Wouterlood FG (2006) Multiple Neuroanatomical Tract-Tracing: Approaches for Multiple Tract-Tracing. In: Zaborszky L, Wouterlood FG, Lanciego JL (eds) Neuroanatomical Tract-Tracing 3: Molecules, Neurons, and Systems. Springer US, Boston, MA, pp 336-365. doi:10.1007/0-387-28942-9_11
Lanciego JL, Wouterlood FG (2011) A half century of experimental neuroanatomical tracing. J Chem Neuroanat 42 (3):157-183. doi:10.1016/j.jchemneu.2011.07.001
Lebow MA, Chen A (2016) Overshadowed by the amygdala: the bed nucleus of the stria terminalis emerges as key to psychiatric disorders. Mol Psychiatry 21 (4):450-463. doi:10.1038/mp.2016.1
LeDoux JE, Iwata J, Cicchetti P, Reis DJ (1988) Different projections of the central amygdaloid nucleus mediate autonomic and behavioral correlates of conditioned fear. J Neurosci 8 (7):2517-2529
Lein ES, et al. (2007) Genome-wide atlas of gene expression in the adult mouse brain. Nature 445 (7124):168-176. doi:10.1038/nature05453
Leite-Almeida H, Cerqueira JJ, Wei H, Ribeiro-Costa N, Anjos-Martins H, Sousa N, Pertovaara A, Almeida A (2012) Differential effects of left/right neuropathy on rats' anxiety and cognitive behavior. Pain 153 (11):2218-2225. doi:10.1016/j.pain.2012.07.007
Lencer WI, Tsai B (2003) The intracellular voyage of cholera toxin: going retro. Trends Biochem Sci 28 (12):639-645. doi:10.1016/j.tibs.2003.10.002
Li H, Penzo MA, Taniguchi H, Kopec CD, Huang ZJ, Li B (2013a) Experience-dependent modification of a central amygdala fear circuit. Nat Neurosci 16 (3):332-339. doi:10.1038/nn.3322
Li Z, Wang J, Chen L, Zhang M, Wan Y (2013b) Basolateral amygdala lesion inhibits the development of pain chronicity in neuropathic pain rats. PLoS One 8 (8):e70921. doi:10.1371/journal.pone.0070921
Linley SB, Olucha-Bordonau F, Vertes RP (2017) Pattern of distribution of serotonergic fibers to the amygdala and extended amygdala in the rat. J Comp Neurol 525 (1):116-139. doi:10.1002/cne.24044
Lopez de Armentia M, Sah P (2004) Firing properties and connectivity of neurons in the rat lateral central nucleus of the amygdala. J Neurophysiol 92 (3):1285-1294. doi:10.1152/jn.00211.2004
Lu YC, Chen YZ, Wei YY, He XT, Li X, Hu W, Yanagawa Y, Wang W, Wu SX, Dong YL (2015) Neurochemical properties of the synapses between the parabrachial nucleus-derived CGRP-positive axonal terminals and the GABAergic neurons in the lateral capsular division of central nucleus of amygdala. Mol Neurobiol 51 (1):105-118. doi:10.1007/s12035-014-8713-x
Luppi PH, Fort P, Jouvet M (1990) Iontophoretic application of unconjugated cholera toxin B subunit (CTb) combined with immunohistochemistry of neurochemical substances: a method for transmitter identification of retrogradely labeled neurons. Brain Res 534 (1-2):209-224
Madisen L, Zwingman TA, Sunkin SM, Oh SW, Zariwala HA, Gu H, Ng LL, Palmiter RD, Hawrylycz MJ, Jones AR, Lein ES, Zeng H (2010) A robust and high-throughput Cre reporting and characterization system for the whole mouse brain. Nat Neurosci 13 (1):133-140. doi:10.1038/nn.2467
Majak K, Ronkko S, Kemppainen S, Pitkanen A (2004) Projections from the amygdaloid complex to the piriform cortex: A PHA-L study in the rat. J Comp Neurol 476 (4):414-428. doi:10.1002/cne.20233
Marcinkiewcz CA, Mazzone CM, D'Agostino G, Halladay LR, Hardaway JA, DiBerto JF, Navarro M, Burnham N, Cristiano C, Dorrier CE, Tipton GJ, Ramakrishnan C, Kozicz T, Deisseroth K, Thiele TE, McElligott ZA, Holmes A, Heisler LK, Kash TL (2016) Serotonin engages an anxiety and fear-promoting circuit in the extended amygdala. Nature 537 (7618):97-101. doi:10.1038/nature19318
Mazzone CM, Pati D, Michaelides M, DiBerto J, Fox JH, Tipton G, Anderson C, Duffy K, McKlveen JM, Hardaway JA, Magness ST, Falls WA, Hammack SE, McElligott ZA, Hurd YL, Kash TL (2016) Acute engagement of Gq-mediated signaling in the bed nucleus of the stria terminalis induces anxiety-like behavior. Mol Psychiatry. doi:10.1038/mp.2016.218
McDonald AJ (1982) Cytoarchitecture of the central amygdaloid nucleus of the rat. J Comp Neurol 208 (4):401-418. doi:10.1002/cne.902080409
McDonald AJ (1991) Topographical organization of amygdaloid projections to the caudatoputamen, nucleus accumbens, and related striatal-like areas of the rat brain. Neuroscience 44 (1):15-33
McDonald AJ (1998) Cortical pathways to the mammalian amygdala. Prog Neurobiol 55 (3):257-332
McDonald AJ, Shammah-Lagnado SJ, Shi C, Davis M (1999) Cortical afferents to the extended amygdala. Ann N Y Acad Sci 877:309-338
Minami M, Ide S (2015) How does pain induce negative emotion? Role of the bed nucleus of the stria terminalis in pain-induced place aversion. Curr Mol Med 15 (2):184-190
Missig G, Mei L, Vizzard MA, Braas KM, Waschek JA, Ressler KJ, Hammack SE, May V (2017) Parabrachial Pituitary Adenylate Cyclase-Activating Polypeptide Activation of Amygdala Endosomal Extracellular

Signal-Regulated Kinase Signaling Regulates the Emotional Component of Pain. Biol Psychiatry 81 (8):671-682. doi:10.1016/j.biopsych.2016.08.025
Missig G, Roman CW, Vizzard MA, Braas KM, Hammack SE, May V (2014) Parabrachial nucleus (PBn) pituitary adenylate cyclase activating polypeptide (PACAP) signaling in the amygdala: implication for the sensory and behavioral effects of pain. Neuropharmacology 86:38-48. doi:10.1016/j.neuropharm.2014.06.022
Moga MM, Gray TS (1985) Evidence for corticotropin-releasing factor, neurotensin, and somatostatin in the neural pathway from the central nucleus of the amygdala to the parabrachial nucleus. J Comp Neurol 241 (3):275-284. doi:10.1002/cne.902410304
Moga MM, Saper CB, Gray TS (1989) Bed nucleus of the stria terminalis: cytoarchitecture, immunohistochemistry, and projection to the parabrachial nucleus in the rat. J Comp Neurol 283 (3):315-332. doi:10.1002/cne.902830302
Montecucco C, Papini E, Schiavo G (1994) Bacterial protein toxins penetrate cells via a four-step mechanism. FEBS Lett 346 (1):92-98
Nagalakshmi U, Waern K, Snyder M (2010) RNA-Seq: a method for comprehensive transcriptome analysis. Curr Protoc Mol Biol Chapter 4:Unit 4 11 11-13. doi:10.1002/0471142727.mb0411s89
Neugebauer V (2015) Amygdala pain mechanisms. Handb Exp Pharmacol 227:261-284. doi:10.1007/978-3-662-46450-2_13
Neugebauer V, Li W, Bird GC, Bhave G, Gereau RWt (2003) Synaptic plasticity in the amygdala in a model of arthritic pain: differential roles of metabotropic glutamate receptors 1 and 5. J Neurosci 23 (1):52-63
Neugebauer V, Li W, Bird GC, Han JS (2004) The amygdala and persistent pain. Neuroscientist 10 (3):221-234. doi:10.1177/1073858403261077
Oh SW, Harris JA, Ng L, Winslow B, Cain N, Mihalas S, Wang Q, Lau C, Kuan L, Henry AM, Mortrud MT, Ouellette B, Nguyen TN, Sorensen SA, Slaughterbeck CR, Wakeman W, Li Y, Feng D, Ho A, Nicholas E, Hirokawa KE, Bohn P, Joines KM, Peng H, Hawrylycz MJ, Phillips JW, Hohmann JG, Wohnoutka P, Gerfen CR, Koch C, Bernard A, Dang C, Jones AR, Zeng H (2014) A mesoscale connectome of the mouse brain. Nature 508 (7495):207-214. doi:10.1038/nature13186
Okutsu Y, Takahashi Y, Nagase M, Shinohara K, Ikeda R, Kato F (2017) Potentiation of NMDA receptor-mediated synaptic transmission at the parabrachial-central amygdala synapses by CGRP in mice. Mol Pain 13:1744806917709201. doi:10.1177/1744806917709201
Oler JA, Tromp DP, Fox AS, Kovner R, Davidson RJ, Alexander AL, McFarlin DR, Birn RM, B EB, deCampo DM, Kalin NH, Fudge JL (2017) Connectivity between the central nucleus of the amygdala and the bed nucleus of the stria terminalis in the non-human primate: neuronal tract tracing and developmental neuroimaging studies. Brain Struct Funct 222 (1):21-39. doi:10.1007/s00429-016-1198-9
Park J, Bucher ES, Fontillas K, Owesson-White C, Ariansen JL, Carelli RM, Wightman RM (2013) Opposing catecholamine changes in the bed nucleus of the stria terminalis during intracranial self-stimulation and its extinction. Biol Psychiatry 74 (1):69-76. doi:10.1016/j.biopsych.2012.11.008
Partin AC, Hosek MP, Luong JA, Lella SK, Sharma SA, Ploski JE (2013) Amygdala nuclei critical for emotional learning exhibit unique gene expression patterns. Neurobiol Learn Mem 104:110-121. doi:10.1016/j.nlm.2013.06.015
Paxinos G, Franklin K (2012) Paxinos and Franklin's The mouse brain in stereotaxic coordinates. Fourth edition. edn. Academic Press, Amsterdam
Penzo MA, Robert V, Li B (2014) Fear conditioning potentiates synaptic transmission onto long-range projection neurons in the lateral subdivision of central amygdala. J Neurosci 34 (7):2432-2437. doi:10.1523/JNEUROSCI.4166-13.2014
Penzo MA, Robert V, Tucciarone J, De Bundel D, Wang M, Van Aelst L, Darvas M, Parada LF, Palmiter RD, He M, Huang ZJ, Li B (2015) The paraventricular thalamus controls a central amygdala fear circuit. Nature. doi:10.1038/nature13978
Petrovich GD, Swanson LW (1997) Projections from the lateral part of the central amygdalar nucleus to the postulated fear conditioning circuit. Brain Res 763 (2):247-254
Phelix CF, Liposits Z, Paull WK (1992) Monoamine innervation of bed nucleus of stria terminalis: an electron microscopic investigation. Brain Res Bull 28 (6):949-965
Pitkanen A, Savander V, LeDoux JE (1997) Organization of intra-amygdaloid circuitries in the rat: an emerging framework for understanding functions of the amygdala. Trends Neurosci 20 (11):517-523
Pomrenze MB, Millan EZ, Hopf FW, Keiflin R, Maiya R, Blasio A, Dadgar J, Kharazia V, De Guglielmo G, Crawford E, Janak PH, George O, Rice KC, Messing RO (2015) A Transgenic Rat for Investigating the Anatomy and Function of Corticotrophin Releasing Factor Circuits. Front Neurosci 9:487. doi:10.3389/fnins.2015.00487

Potter E, Sutton S, Donaldson C, Chen R, Perrin M, Lewis K, Sawchenko PE, Vale W (1994) Distribution of corticotropin-releasing factor receptor mRNA expression in the rat brain and pituitary. Proc Natl Acad Sci U S A 91 (19):8777-8781
Poulin JF, Arbour D, Laforest S, Drolet G (2009) Neuroanatomical characterization of endogenous opioids in the bed nucleus of the stria terminalis. Prog Neuropsychopharmacol Biol Psychiatry 33 (8):1356-1365. doi:10.1016/j.pnpbp.2009.06.021
Poulin JF, Castonguay-Lebel Z, Laforest S, Drolet G (2008) Enkephalin co-expression with classic neurotransmitters in the amygdaloid complex of the rat. J Comp Neurol 506 (6):943-959. doi:10.1002/cne.21587
Poulin JF, Chevalier B, Laforest S, Drolet G (2006) Enkephalinergic afferents of the centromedial amygdala in the rat. J Comp Neurol 496 (6):859-876. doi:10.1002/cne.20956
Ravinder S, Burghardt NS, Brodsky R, Bauer EP, Chattarji S (2013) A role for the extended amygdala in the fear-enhancing effects of acute selective serotonin reuptake inhibitor treatment. Transl Psychiatry 3:e209. doi:10.1038/tp.2012.137
Reichard RA, Subramanian S, Desta MT, Sura T, Becker ML, Ghobadi CW, Parsley KP, Zahm DS (2016) Abundant collateralization of temporal lobe projections to the accumbens, bed nucleus of stria terminalis, central amygdala and lateral septum. Brain Struct Funct. doi:10.1007/s00429-016-1321-y
Reynolds SM, Zahm DS (2005) Specificity in the projections of prefrontal and insular cortex to ventral striatopallidum and the extended amygdala. J Neurosci 25 (50):11757-11767. doi:10.1523/JNEUROSCI.3432-05.2005
Roberts GW, Woodhams PL, Polak JM, Crow TJ (1982) Distribution of neuropeptides in the limbic system of the rat: the amygdaloid complex. Neuroscience 7 (1):99-131
Rodriguez-Sierra OE, Turesson HK, Pare D (2013) Contrasting distribution of physiological cell types in different regions of the bed nucleus of the stria terminalis. J Neurophysiol 110 (9):2037-2049. doi:10.1152/jn.00408.2013
Roth BL (2016) DREADDs for Neuroscientists. Neuron 89 (4):683-694. doi:10.1016/j.neuron.2016.01.040
Sah P, Faber ES, Lopez De Armentia M, Power J (2003) The amygdaloid complex: anatomy and physiology. Physiol Rev 83 (3):803-834. doi:10.1152/physrev.00002.2003
Sandvig K, van Deurs B (2002) Transport of protein toxins into cells: pathways used by ricin, cholera toxin and Shiga toxin. FEBS Lett 529 (1):49-53
Sanford CA, Soden ME, Baird MA, Miller SM, Schulkin J, Palmiter RD, Clark M, Zweifel LS (2017) A Central Amygdala CRF Circuit Facilitates Learning about Weak Threats. Neuron 93 (1):164-178. doi:10.1016/j.neuron.2016.11.034
Saper CB, Loewy AD (1980) Efferent connections of the parabrachial nucleus in the rat. Brain Res 197 (2):291-317
Sarhan M, Pawlowski SA, Barthas F, Yalcin I, Kaufling J, Dardente H, Zachariou V, Dileone RJ, Barrot M, Veinante P (2013) BDNF parabrachio-amygdaloid pathway in morphine-induced analgesia. Int J Neuropsychopharmacol 16 (7):1649-1660. doi:10.1017/S146114571200168X
Sato M, Ito M, Nagase M, Sugimura YK, Takahashi Y, Watabe AM, Kato F (2015) The lateral parabrachial nucleus is actively involved in the acquisition of fear memory in mice. Mol Brain 8:22. doi:10.1186/s13041-015-0108-z
Schiess MC, Callahan PM, Zheng H (1999) Characterization of the electrophysiological and morphological properties of rat central amygdala neurons in vitro. J Neurosci Res 58 (5):663-673
Schmued LC, Fallon JH (1986) Fluoro-Gold: a new fluorescent retrograde axonal tracer with numerous unique properties. Brain Res 377 (1):147-154
Schwaber JS, Kapp BS, Higgins G (1980) The origin and extent of direct amygdala projections to the region of the dorsal motor nucleus of the vagus and the nucleus of the solitary tract. Neurosci Lett 20 (1):15-20
Shackman AJ, Fox AS (2016) Contributions of the Central Extended Amygdala to Fear and Anxiety. J Neurosci 36 (31):8050-8063. doi:10.1523/JNEUROSCI.0982-16.2016
Shammah-Lagnado SJ, Alheid GF, Heimer L (1999) Afferent connections of the interstitial nucleus of the posterior limb of the anterior commissure and adjacent amygdalostriatal transition area in the rat. Neuroscience 94 (4):1097-1123
Sugimura YK, Takahashi Y, Watabe AM, Kato F (2016) Synaptic and network consequences of monosynaptic nociceptive inputs of parabrachial nucleus origin in the central amygdala. J Neurophysiol 115 (6):2721-2739. doi:10.1152/jn.00946.2015
Sullivan GM, Apergis J, Bush DE, Johnson LR, Hou M, Ledoux JE (2004) Lesions in the bed nucleus of the stria terminalis disrupt corticosterone and freezing responses elicited by a contextual but not by a specific cue-conditioned fear stimulus. Neuroscience 128 (1):7-14. doi:10.1016/j.neuroscience.2004.06.015

Sun N, Cassell MD (1993) Intrinsic GABAergic neurons in the rat central extended amygdala. J Comp Neurol 330 (3):381-404. doi:10.1002/cne.903300308
Sun N, Roberts L, Cassell MD (1991) Rat central amygdaloid nucleus projections to the bed nucleus of the stria terminalis. Brain Res Bull 27 (5):651-662
Swanson LW, Sawchenko PE, Rivier J, Vale WW (1983) Organization of ovine corticotropin-releasing factor immunoreactive cells and fibers in the rat brain: an immunohistochemical study. Neuroendocrinology 36 (3):165-186
Taniguchi H (2014) Genetic dissection of GABAergic neural circuits in mouse neocortex. Front Cell Neurosci 8:8. doi:10.3389/fncel.2014.00008
Tovote P, Esposito MS, Botta P, Chaudun F, Fadok JP, Markovic M, Wolff SB, Ramakrishnan C, Fenno L, Deisseroth K, Herry C, Arber S, Luthi A (2016) Midbrain circuits for defensive behaviour. Nature 534 (7606):206-212. doi:10.1038/nature17996
Tovote P, Fadok JP, Luthi A (2015) Neuronal circuits for fear and anxiety. Nat Rev Neurosci 16 (6):317-331. doi:10.1038/nrn3945
Turesson HK, Rodriguez-Sierra OE, Pare D (2013) Intrinsic connections in the anterior part of the bed nucleus of the stria terminalis. J Neurophysiol 109 (10):2438-2450. doi:10.1152/jn.00004.2013
Veening JG, Swanson LW, Sawchenko PE (1984) The organization of projections from the central nucleus of the amygdala to brainstem sites involved in central autonomic regulation: a combined retrograde transport-immunohistochemical study. Brain Res 303 (2):337-357
Veinante P, Yalcin I, Barrot M (2013) The amygdala between sensation and affect: a role in pain. J Mol Psychiatry 1 (1):9. doi:10.1186/2049-9256-1-9
Walker DL, Davis M (1997) Double dissociation between the involvement of the bed nucleus of the stria terminalis and the central nucleus of the amygdala in startle increases produced by conditioned versus unconditioned fear. J Neurosci 17 (23):9375-9383
Walker DL, Davis M (2008) Role of the extended amygdala in short-duration versus sustained fear: a tribute to Dr. Lennart Heimer. Brain Struct Funct 213 (1-2):29-42. doi:10.1007/s00429-008-0183-3
Walker DL, Miles LA, Davis M (2009) Selective participation of the bed nucleus of the stria terminalis and CRF in sustained anxiety-like versus phasic fear-like responses. Prog Neuropsychopharmacol Biol Psychiatry 33 (8):1291-1308. doi:10.1016/j.pnpbp.2009.06.022
Walker DL, Toufexis DJ, Davis M (2003) Role of the bed nucleus of the stria terminalis versus the amygdala in fear, stress, and anxiety. Eur J Pharmacol 463 (1-3):199-216. doi:S0014299903012822 [pii]
Watabe AM, Ochiai T, Nagase M, Takahashi Y, Sato M, Kato F (2013) Synaptic potentiation in the nociceptive amygdala following fear learning in mice. Mol Brain 6:11. doi:1756-6606-6-11 [pii]
10.1186/1756-6606-6-11
Wessendorf MW (1991) Fluoro-Gold: composition, and mechanism of uptake. Brain Res 553 (1):135-148
Wood J, Verma D, Lach G, Bonaventure P, Herzog H, Sperk G, Tasan RO (2016) Structure and function of the amygdaloid NPY system: NPY Y2 receptors regulate excitatory and inhibitory synaptic transmission in the centromedial amygdala. Brain Struct Funct 221 (7):3373-3391. doi:10.1007/s00429-015-1107-7
Xiu J, Zhang Q, Zhou T, Zhou TT, Chen Y, Hu H (2014) Visualizing an emotional valence map in the limbic forebrain by TAI-FISH. Nat Neurosci 17 (11):1552-1559. doi:10.1038/nn.3813
Xu C, Krabbe S, Grundemann J, Botta P, Fadok JP, Osakada F, Saur D, Grewe BF, Schnitzer MJ, Callaway EM, Luthi A (2016a) Distinct Hippocampal Pathways Mediate Dissociable Roles of Context in Memory Retrieval. Cell 167 (4):961-972 e916. doi:10.1016/j.cell.2016.09.051
Xu X, Ikrar T, Sun Y, Santos R, Holmes TC, Francesconi W, Berton F (2016b) High-resolution and cell-type-specific photostimulation mapping shows weak excitatory vs. strong inhibitory inputs in the bed nucleus of the stria terminalis. J Neurophysiol 115 (6):3204-3216. doi:10.1152/jn.01148.2015
Yalcin I, Bohren Y, Waltisperger E, Sage-Ciocca D, Yin JC, Freund-Mercier MJ, Barrot M (2011) A time-dependent history of mood disorders in a murine model of neuropathic pain. Biol Psychiatry 70 (10):946-953. doi:10.1016/j.biopsych.2011.07.017
Yalcin I, Megat S, Barthas F, Waltisperger E, Kremer M, Salvat E, Barrot M (2014) The sciatic nerve cuffing model of neuropathic pain in mice. J Vis Exp (89). doi:10.3791/51608
Yu K, Garcia da Silva P, Albeanu DF, Li B (2016) Central Amygdala Somatostatin Neurons Gate Passive and Active Defensive Behaviors. J Neurosci 36 (24):6488-6496. doi:10.1523/JNEUROSCI.4419-15.2016
Zaidi AU, Enomoto H, Milbrandt J, Roth KA (2000) Dual fluorescent in situ hybridization and immunohistochemical detection with tyramide signal amplification. J Histochem Cytochem 48 (10):1369-1375. doi:10.1177/002215540004801007
Zimmerman JM, Maren S (2011) The bed nucleus of the stria terminalis is required for the expression of contextual but not auditory freezing in rats with basolateral amygdala lesions. Neurobiol Learn Mem 95 (2):199-205. doi:10.1016/j.nlm.2010.11.002

Zirlinger M, Kreiman G, Anderson DJ (2001) Amygdala-enriched genes identified by microarray technology are restricted to specific amygdaloid subnuclei. Proc Natl Acad Sci U S A 98 (9):5270-5275. doi:10.1073/pnas.091094698

Jiahao Ye

Etude anatomique de l'amygdale étendue centrale chez la souris : Connectivité générale et circuits cellule-spécifiques ; implications fonctionnelles dans la douleur.

Résumé

L'amygdale centrale (EAc) est un macrosystème du cerveau antérieur qui joue un rôle important dans la peur, l'anxiété et la douleur. Les deux composants clés, le noyau latéral du lit de la strie terminale (STL) et l'amygdale centrale (CeA), possèdent des caractéristiques neurochimiques, hodologiques et fonctionnelles très similaires. En dépit de cette vision simplifiée du STL et du CeA, de nombreuses questions résident quant à l'organisation mésoscopiques des entrées et des sorties des subdivisions de l''EAc chez la souris. En outre, il reste à déterminer si ces similitudes de connexion sont également partagées au niveau cellulaire. Dans ce travail, nous avons abordé ces questions de manière comparative chez la souris. Nous avons trouvé de richesafférences et efférences préférentielles pour les différentes subdivisions de l'EAC, ainsi que des afférences convergentes et divergentes. Nous avons également mise en évidence deux groupes distincts de cellules exprimant la protéine kinase C delta (PKCδ) ou la somatostatine (SOM) qui sous-tendent des circuits neuronaux spécifiques parallèles dans le STL et le CeA, ainsi qu'entre les deux structures. Enfin, des données préliminaires suggèrent que les neurones exprimant la PKCδ dans le STL et le CeA pourraient être impliqués dans la douleur tonique. Ces organisations structurales parallèles, mais aussi différentielles, des circuits neuronaux dans le EAc pourraient sous-tendre des aspects fonctionnels similaires et dissociables de l'anxiété, de la peur et de la douleur.

Mots-clés :

Amygdale étendue centrale, noyau central de l'amygdale, Noyau du lit de la strie terminale, neurocircuits,

Abstract

Central extended amygdala (EAc) is a forebrain macrosystem that plays important roles in fear, anxiety and pain. The two key components, the lateral bed nucleus of stria terminalis (STL) and central nucleus of amygdala (CeA), are highly similar in their neurochemical, connectional, and functional features. Despite this simplified view of STL and CeA, much remains elusive of the mesoscopic inputs and outputs of EAc subdivisions in mouse model. Also, it is not known whether the connectional similarities are also shared at cellular level. Here, we addressed these question in comparative ways in mice. We found rich preferential inputs and outputs to different subdivisions of EAc, as well as convergent and divergent inputs. We also found two non-overlapping cell groups expressing either protein kinase C delta (PKCδ) or somatostatin (SOM) organize the parallel cell-type specific neuronal circuits in STL and CeA. Finally, preliminary data suggest that PKCδ in STL and CeA might be implicated in tonic pain. These parallel but also differential structural organizations of neuronal circuits in EAc might underlie similar and dissociable functional aspects of anxiety, fear and pain.

Key words:

central extended amygdala, central nucleus of the amygdala, bed nucleus of the stria terminalis, neurocircuit, protein kinase C delta, somatostatin